



03095  
1

## UNIVERSIDAD NACIONAL AUTONOMA DE MEXICO

POSGRADO EN CIENCIAS DE LA TIERRA  
INSTITUTO DE GEOFISICA

### ANÁLISIS DE DATOS SÍSMICOS DE BANDA ANCHA REGISTRADOS EN EL VOLCÁN POPOCATÉPETL, MÉXICO.

TESIS CON  
FALLA DE ORIGEN

T E S I S  
PARA OBTENER EL GRADO DE:  
D O C T O R E N C I E N C I A S  
(SISMOLÓGIA Y FÍSICA DEL INTERIOR DE LA TIERRA)  
P R E S E N T A:

MARIA ALEJANDRA ARCINIEGA CEBALLOS

DIRECTOR  
BERNARD CHOUE



**UNAM – Dirección General de Bibliotecas**

**Tesis Digitales**  
**Restricciones de uso**

**DERECHOS RESERVADOS ©**  
**PROHIBIDA SU REPRODUCCIÓN TOTAL O PARCIAL**

Todo el material contenido en esta tesis está protegido por la Ley Federal del Derecho de Autor (LFDA) de los Estados Unidos Mexicanos (Méjico).

El uso de imágenes, fragmentos de videos, y demás material que sea objeto de protección de los derechos de autor, será exclusivamente para fines educativos e informativos y deberá citar la fuente donde la obtuvo mencionando el autor o autores. Cualquier uso distinto como el lucro, reproducción, edición o modificación, será perseguido y sancionado por el respectivo titular de los Derechos de Autor.

## ÍNDICE

<b>Resumen . . . . .</b>	<b>5</b>
<b>Abstract . . . . .</b>	<b>6</b>
<b>Introducción . . . . .</b>	<b>7</b>
<b>Sismicidad en Volcanes Activos</b>	<b>13</b>
<b>Introducción . . . . .</b>	<b>13</b>
<b>Volcán KILAUEA, Hawaii . . . . .</b>	<b>17</b>
<b>Volcán STROMBOLI, Italia . . . . .</b>	<b>21</b>
<b>Volcán ASO, Japón . . . . .</b>	<b>23</b>
<b>Volcán EREBUS, Ross Island, Antártida . . . . .</b>	<b>24</b>
<b>Otros Volcanes . . . . .</b>	<b>26</b>
<b>Volcán POPOCATÉPETL . . . . .</b>	<b>29</b>

índice	2
Características Temporales y Espectrales de la Sismicidad Observada en el Volcán Popocatépetl (1994-1995) 34	
Abstract . . . . .	34
Introduction . . . . .	35
Temporal and Spectral Characteristics of Seismicity . . . . .	36
Observed Data vs. Crack Model Predictions . . . . .	42
Discussion . . . . .	46
Conclusions . . . . .	50
Eventos de Periodo Largo y Tremor Registrados en el Volcán Popocatépetl (1994-2000) y sus Características de Banda Ancha 54	
Abstract . . . . .	54
Introduction . . . . .	56
Data . . . . .	59
Observed eruptive activity and seismicity . . . . .	61
Description of LP events and tremor . . . . .	65
Discussion . . . . .	77
Conclusions . . . . .	83

<b>Señales de Periodo muy Largo Asociadas con Explosiones Vulcanianas en el Popocatépetl</b>	<b>88</b>
Abstract . . . . .	88
Introduction . . . . .	89
Data and analysis . . . . .	91
Conclusions . . . . .	99
<b>Experimento Sísmico de Banda Ancha en el Volcán Popocatépetl</b>	<b>102</b>
Introduction . . . . .	102
Instrumentation . . . . .	107
Short-period seismicity and eruptive behavior . . . . .	109
Crack model . . . . .	117
Spectral peaks and crack dimensions . . . . .	120
Far-field radiation patterns . . . . .	126
Discussion . . . . .	131
Very-long period seismic observations . . . . .	133
Very-long period signals . . . . .	144

<b>índice</b>	<b>4</b>
<b>Discussion and conclusions . . . . .</b>	<b>159</b>
<b>Agradecimientos</b>	<b>167</b>
<b>Apéndices</b>	<b>168</b>
A. Semblance . . . . .	168
B. Modelo de fractura . . . . .	171
<b>Referencias</b>	<b>188</b>

## Resumen

Se investigó la sismicidad generada por el volcán Popocatépetl y su relación con la actividad eruptiva observada a partir de Diciembre de 1994. En virtud de que los volcanes activos generan señales sísmicas con una amplia y variada gama de amplitudes y frecuencias, se muestran las ventajas de estudiar la sismicidad de un volcán activo con instrumentos de banda ancha. Se instaló y operó una red instrumental de 22 sismógrafos de banda ancha (0.04-100 s) como parte del Programa Internacional de Investigación de Volcanes Activos en colaboración con el Centro de Geociencias en Potsdam, Alemania, el Servicio Geológico de Estados Unidos en Menlo Park y el Instituto de Geofísica de la UNAM. El análisis muestra la relación entre el tipo de erupción observada y la firma que caracteriza las diferentes señales sísmicas. Se analizan señales de periodo largo (LP), de periodo muy largo (VLP) y tremor, y su relación con el posible mecanismo que las produce. Los eventos LP y tremor se caracterizan por un contenido de frecuencias similar y su relación con procesos eruptivos como son emisiones de gases y cenizas. Se demuestra que la distribución de los picos del espectro de potencia son compatibles con los modos de resonancia de un mecanismo de fuente superficial (< 2 km debajo del cráter) representado por un 'crack' relleno de fluidos. Los resultados del análisis de señales VLP las asocia con el transporte de fluidos debajo del volcán. Estos eventos VLP se identificaron en diversos periodos de actividad (*e.g.*, durante el emplazamiento de domos, explosiones, emisiones de gas). Las características y forma de onda de las señales VLP indican la presencia de un proceso de fuente que actúa repetidamente y por lo tanto no se destruye. Del análisis, se infiere que este proceso identificado en los registros símicos de banda ancha a lo largo de 5 años sugiere dos fuentes; una superficial (< 2 km) en la parte Este del cráter del volcán, y otra más profunda aproximadamente 6 km debajo del cráter. La identificación de eventos VLP con características quasi-idénticas en espacio y tiempo sugieren un mecanismo que involucra movimiento magmático en el conducto volcánico. Futuros estudios contemplan la estimación del mecanismo de fuente asociado aplicando técnicas de inversión de onda.

## **Abstract**

The goal of this work is to document the seismicity recorded at Popocatepetl volcano since December 1994. The benefits of recording the seismicity of active volcanoes with broadband instruments are discussed. A broadband seismic experiment was carried out at Popocatepetl volcano as part of the international cooperation program for the study of active volcanoes between GeoForschungsZentrum in Potsdam, Germany (GFZ-Potsdam), the U.S. Geological Survey (USGS) in Menlo Park, California, and the Institute of Geophysics at UNAM, Mexico City (IGF-UNAM). The broadband seismic network deployed at different elevations and distances from the crater recorded a wide variety of seismic signals in the frequency range 0.04-100 s allowing the observation of seismic energy propagating through various sections of the volcanic edifice. The seismicity of Popocatepetl presents a wide range of signals. Our analyses focus on long-period (LP) signals, tremor and very-long-period (VLP) signals. LP and tremor signals are characterized by similar frequency content and their relationships to gas and ash emissions are discussed. We demonstrate that the distribution of dominant spectral peaks of LP signals are consistent with a source mechanism represented by shallow (< 2 km) fluid-filled cracks beneath the crater. VLP signals were identified in association with several types of activity, including dome emplacement, vulcanian explosions, and degassing. Our results suggest that VLP signals are related to fluid transport beneath Popocatepetl. VLP waveforms with almost identical shapes suggest that a shallow non-destructive source mechanism acts repeatedly. Particle motions analyses using broadband data recorded during 5 years point to a shallow source located in the top 2 km beneath the eastern sector of the crater, and deeper source approximately 6 km beneath the crater. The VLP waveforms will allow us to estimate source mechanisms by means of a waveform inversion technique.

## Introducción

Uno de los más ambiciosos propósitos en ciencias de la tierra es el entender el comportamiento de los sistemas dinámicos terrestres, entre ellos el sistema hidrológico, el sistema meteorológico, la tectónica, volcanismo, gravedad e isostasia, etc. Los volcanes representan uno de los sistemas terrestres dinámicos de mayor complejidad y requiere para su comprensión y estudio de la participación de geocientíficos de diferentes disciplinas (geológicos, geofísicos, geoquímicos, vulcanólogos etc). La sismología volcánica es una de las ramas de la sismología que ha tomado fuerte impulso en los últimos años gracias a la introducción de nuevas tecnologías en materia de instrumentación y cómputo. Uno de los propósitos de la sismología volcánica es inferir el comportamiento volcánico, esto es, conocer cómo funcionan y en dónde se originan las fuentes sismicas y la relación que guardan con los procesos eruptivos.

El monitoreo en volcanes activos históricamente ha involucrado redes de sismómetros de periodo corto, frecuentemente acompañados por inclinómetros y otros sensores geodésicos. El análisis de riesgo volcánico se ha visto ampliamente beneficiado de esta combinación de redes de periodo corto e información geodésica, un ejemplo son las acertadas alertas de prevención previas a la erupción del Monte Pinatubo en Filipinas [Wolfe and Hoblitt, 1996]. Sin embargo, al evaluar la dirección que en el futuro debe tomar el monitoreo de volcanes en materia de sismicidad e investigación, está claro que existe un vacío muy importante en nuestro conocimiento en sismología volcánica entre las mediciones estáticas y los periodos de 1 s. El surgimiento de sensores portátiles de banda ancha, el desarrollo de tecnología de grabación digital y poderosos recursos de computo así como la aplicación de nuevas técnicas de análisis han empezado a llenar ese vacío. En los últimos 10 años algunos volcanes activos han sido instrumentados con sismómetros de banda ancha, a saber, los volcanes Sakurajima y Aso, Japón [Kawakatsu *et al.*, 1992; Kaneshima *et al.*, 1996], Satsuma-Iwojima, Japón [Ohminato and Eridato, 1997; Ohminato, 1998], Strom-

boli, Italia [Neuberg *et al.*, 1994; Chouet *et al.*, 1999], Kilauea, Hawaii [Dawson *et al.*, 1998; Ohminato *et al.*, 1998], y Erebus, Antarctica [Rowe *et al.*, 1998, 2000]. Señales de periodo muy largo ( $> 10$  s) han sido observadas por sismómetros de banda ancha en los volcanes Sakurajima y Aso y han sido atribuídas a procesos de transferencia de masa [Kawakatsu *et al.*, 1992, 2000]. Neuberg *et al.*, (1994) realizó un experimento con un arreglo de instrumentos de banda ancha en el volcán Stromboli y documentó la presencia de señales de periodo muy largo ( $> 10$  s) en los registros asociadas con explosiones de tipo Stromboliano. Las señales de periodos muy largos (VLP) registradas en volcanes con periodos de más de unos cuantos segundos son comúnmente asociadas con magma y/o transporte hidrotermal. Recientemente el nuevo desarrollo de funciones de Green para medios complejos incluyendo topografías en tres dimensiones [Ohminato y Chouet, 1997], y el mejoramiento en los métodos de inversión de forma de onda, están permitiendo la cuantificación de los mecanismos de fuente generadores de señales VLP [Ohminato *et al.*, 1998]. Desde los trabajos pioneros realizados en 1935 en el Aso [Kawakatsu *et al.*, 2000] hasta los estudios recientes mencionados se ha demostrado la utilidad de la sismología de banda ancha en el estudio de procesos de transferencia de masa en sistemas volcánicos, mismos que sirvieron de ímpetu para este trabajo.

El origen de las señales sísmicas en volcanes activos es de naturaleza diversa; fracturamiento, colapso de cavidades, explosiones de gas, fluctuaciones de presión en flujos de fluido no estacionario de magma y/o gas, degasamiento, etc. En consecuencia las señales sísmicas presentan una amplia y variada gama de amplitudes y anchos de banda. En este trabajo se presenta las características de los diferentes tipos de sismicidad generada por la actividad eruptiva del volcán Popocatépetl. Las señales sísmicas presentan características bien definidas que las particularizan. Las señales de origen volcánico se han clasificado de diferentes formas, llegando a darse el caso de que casi cada volcán podría tener su propia nomenclatura. Para evitar confusiones a lo largo de este trabajo usamos la terminología propuesta por Lahr *et al.*, (1994). Esta nomenclatura se ha usado en estudios de varios volcanes (v.g. Stromboli, Redoubt, Kilauea, Galeras) dado que se basa en las

diferencias que involucran los procesos físicos que dan lugar a mecanismos generadores de ondas elásticas en un medio como el volcánico. Esta clasificación ofrece una clara visión de la conexión entre el transporte de fluidos y la sismicidad. De tal manera que la enorme variedad de señales sísmicas observadas en los volcanes es meramente un reflejo de los efectos que la extrema heterogeneidad de la estructura y la pronunciada topografía de los edificios volcánicos ejercen sobre las señales originando básicamente dos tipos de procesos: uno que asocia a las fuentes volumétricas en la cual los fluidos participan activamente en la generación de ondas elásticas. En estas fuentes los gases, líquidos y sólidos están dinámicamente acoplados de tal modo, que la radiación elástica es el resultado del proceso de flujos de fluidos por conductos y fracturas; tal es el caso de los eventos de periodo largo (LP), eventos de periodo muy largo (VLP), el tremor y las explosiones. El segundo tipo, es el que comprende aquellas fuentes que involucran procesos de fracturamiento frágil y procesos puramente elásticos, como son los eventos volcano-tectónicos. El registro sísmico en el Popocatépetl incluye la diferenciación de señales, de periodo largo y de muy largo periodo, tremor y los eventos volcano tectónicos. Asimismo, se diferencian los eventos explosivos que generan señales sísmicas que varían en duración y amplitud de acuerdo a su intensidad y a las características eruptivas que las acompañan.

En este proyecto se estudió la sismicidad con énfasis en el análisis de señales LP, tremor y señales VLP. Estas señales están asociadas con emisiones de ceniza y de gases así como con explosiones como las ocurridas durante la crisis de 1998 (fotos 4.1, 5.1). Los datos de banda ancha utilizados en los capítulos II-IV provienen de los registros obtenidos en la estación de banda ancha (PPIG) diseñada para la detección de sismos regionales (fig 1.1). Por tratarse de una sola estación que opera en modo de disparo y que está localizada a 5 km del cráter, el análisis y técnicas aplicables se ven seriamente limitadas. Para estudiar las características de la sismicidad generada en volcanes activos en el rango de 1 a 120 s y mejorar nuestra compresión del comportamiento eruptivo y su relación con las señales observadas se llevó a cabo un experimento sísmico como parte del programa de cooperación internacional entre el Centro de Geociencias de Potsdam,

Alemania (GeoForschungsZentrum), el Servicio Geológico de Estados Unidos (USGS) y el Instituto de Geofísica de la UNAM. Este experimento permitió que la red instrumental de observación se incrementara de una sola estación a 22 instrumentos instalados en el volcán y sus alrededores (Fig 5.1). De esta manera se logró registrar y analizar la actividad sísmica en un amplio ancho de frecuencias alrededor del volcán.

Este trabajo comprende 5 capítulos y dos apéndices. Cada capítulo consta de introducción, desarrollo, discusión, conclusiones y referencias. Las referencias citadas en la introducción y en los apéndices se listan al final de la tesis.

El capítulo I se divide en dos partes; en la primera se presenta un breve resumen que muestra la sismicidad registrada en volcanes activos. Principalmente se mencionan los estudios relacionados con las señales que están en la categoría de señales de periodos largos ( $> 1$  s), como es el caso de los volcanes Kilauea, Stromboli, Aso y Erebrus. Se mencionan los volcanes Galeras y Redoubt por su similitud con la actividad eruptiva que ha presentado el Popocatépetl en los últimos cinco años y las características de los eventos LP, aunque no se han realizado estudios de banda ancha para identificar señales VLP. La selección de los volcanes se basa en el criterio de tipo de actividad eruptiva y su sismicidad asociada con la idea de resumir el estado del arte en cuanto a estudios en sismología volcánica. La segunda parte versa sobre el volcán Popocatépetl; brevemente se describe la actividad eruptiva que ha presentado en el pasado y se menciona en general el comportamiento eruptivo que hemos presenciado a partir de diciembre de 1994.

En el capítulo II se presentan las características típicas de las señales sísmicas LP y tremor registradas durante los primeros 100 días de actividad del volcán a partir del 21 diciembre de 1994, se discuten los resultados del análisis en frecuencia de las señales observadas y su variación en el tiempo, similitudes entre los datos observados y las predicciones del modelo de fractura [Chouet, 1988]; y la localización de señales LP y eventos

volcano-tectónicos. Los datos usados en este trabajo fueron recabados con un sismómetro Guralp CMT 40T, de 30 s y un sismógrafo Ref-Tek, este equipo operó en modo continuo del 5 de enero de 1995 al 7 de abril del mismo año.

El capítulo III contiene una descripción exhaustiva de las señales LP y tremor registradas a partir de la instalación de la estación de banda ancha PPIG, equipada con un sensor de 120 s y un sismógrafo Quanterra. Se describen la ocurrencia de las señales LP y tremor con relación a la actividad eruptiva a partir de diciembre de 1994 a marzo de 1999. Se analizan las características de banda ancha del tremor y de los eventos LP y su relación con señales de muy largos períodos.

El capítulo IV comprende un análisis de la ocurrencia de los eventos VLP en particular, y su asociación con los eventos eruptivos de carácter explosivo (foto 4.1). Los eventos explosivos varían en intensidad y en las características eruptivas que las acompañan. Haciendo distinción y atendiendo las características eruptivas, el grado de viscosidad de los magmas es indicativo del grado de explosividad que pueden presentar; entre más viscoso es el magma, por lo general, mayor es el comportamiento explosivo. Los fenómenos explosivos se deben a los procesos de separación de la masa de volátiles tanto de origen magmático como procedentes de la incorporación de agua al magma [Araña-Saavedra y Ortiz, 1984]. Los volcanes con magmas de baja viscosidad, de composición básica, se les clasifica como Hawaiianos porque presentan un comportamiento efusivo semejante al que presentan los volcanes en Hawaii como el Kilauea. Los volcanes con magmas de mayor viscosidad con actividad moderadamente explosiva se les denomina Strombolianos por su semejanza con el comportamiento explosivo que presenta el volcán de este nombre. Este tipo de actividad se considera intermedia entre las manifestaciones explosivas vulcanianas y las Hawaiianas. Los volcanes con magmas de alta viscosidad como el Sakurajima o el Galeras son volcanes con comportamiento explosivo tipo vulcaniano. Este tipo de actividad recibe su nombre del volcán Vulcano que presentó en tiempos históricos una actividad explosiva comparable a la del Sakurajima. A este tipo de actividad pertenecen

las explosiones que ha producido el Popocatépetl en el lapso estudiado en este trabajo.

En el capítulo V se describen las características del experimento sísmico que comprendió la instalación y operación de 22 equipos de banda ancha en los flancos y en las cercanías del volcán Popocatépetl, de Noviembre de 1999 a Julio del 2000. Se discuten los resultados del análisis de los datos y su relación con procesos eruptivos como son la emisión de gases y cenizas así como el emplazamiento de un domo de lava en el cráter (fotos 5.1, 5.2). El análisis de datos se realizó en dos partes; la primera contempla el análisis de las señales de periodo corto y su relación con las características eruptivas que se observan en superficie. La segunda muestra las características en espacio y tiempo de las señales de periodos muy largos identificadas alrededor del volcán. Se muestra el potencial, la importancia y utilidad de estudiar volcanes con equipos de banda ancha para entender mejor los procesos que dan lugar a las erupciones volcánicas. En cuyo caso se contribuye a ampliar el conocimiento influyendo de manera directa y positiva en futuros análisis y caracterizaciones de la sismicidad del volcán Popocatépetl.

Finalmente se presentan, los agradecimientos, apéndices y la bibliografía usada en la introducción, capítulo I y los apéndices. En la sección de apéndices se presentan el método de localización semblance y el modelo de "fluid-driven crack", éste último se usó para explicar las características de las señales observadas.



## Capítulo I

# Sismicidad en Volcanes Activos

### Introducción

El conocer y comprender las causas detrás de la sismicidad generada por los volcanes activos representa un gran reto debido a la complejidad de la fuente, en la cual los fluidos involucrados juegan un papel determinante. Además la pronunciada topografía puede distorsionar las señales generando mayor incertidumbre en la localización de la fuente.

Tradicionalmente el monitoreo sísmico en volcanes se ha basado en la operación de redes con sismómetros de periodo corto en combinación con inclinómetros y medidores de deformación. Estudios recientes con instrumentos sísmicos de banda ancha en algunos volcanes activos han permitido observar un ancho de banda en frecuencias abajo de 1 s. Los registros de sismos volcánicos y tremor de periodo corto describen la acumulación de esfuerzos cerca de donde se encuentra el magma ó el flujo de fluidos a través de conductos, y los instrumentos y técnicas de deformación registran principalmente la deformación quasi-

estática asociada con las respuestas más lentas de las fuentes de presión tales como las cámaras magmáticas. La investigación en el rango de 0.01 a 1 Hz, ha permitido ampliar el conocimiento de las fuentes de presión y de la dinámica de advección de masa durante una erupción. De estas investigaciones se presenta un breve resumen de los estudios realizados y sus resultados en volcanes como el Kilauea, el Stromboli y el Aso.

El estudio de las erupciones volcánicas mediante el análisis de su sismicidad asociada indican que éstas manifiestan características similares independientemente de la intensidad de los procesos eruptivos. Aunque presentan diferencias en el tipo de erupción (*e.g.*, hawaiana, stromboliana y vulcaniana) la energía elástica generada es indicativa de que existen procesos comunes o comparables. Estos procesos son el objeto a decifrar en sismología volcánica dada su relación con la actividad eruptiva. Las señales sísmicas generadas por diferentes volcanes se pueden clasificar bajo un esquema unificado dado que se producen siguiendo un proceso físico similar: aquellas que involucran fracturamiento puro (eventos volcano-tectónicos) y las que involucran cambio volumétrico debido a que los fluidos son determinantes en la dinámica del proceso, a saber eventos de periodo largo (LP), tremor, eventos de periodo muy largo (VLP) y explosiones [Lahr *et al.*, 1994; Chouet, 1996].

La variedad de fuentes elásticas solamente ocurre en sistemas magmáticos y geotérmicos, en los cuales los fluidos están involucrados. Las señales observadas son diversas. Por ejemplo: persistente tremor armónico como el observado en el Lascar o Arenal [Hellweg, 2000; Hagerty *et al.*, 1997; Garcés *et al.*, 1998] y tremor persistente o intermitente, observado en varios volcanes en el mundo caracterizado por picos espectrales estables [Mc Nutt, 1989; Chouet, 1996; Benoit y Mc Nutt, 1997; Hagerty *et al.*, 1997; Chouet *et al.*, 1997, 1998], así como el tremor espasmódico del Karimsky [Johnson and Lees, 2000]. Las señales de periodo largo (LP) parecen estar intimamente relacionadas con emisiones de ceniza y han sido igualmente observadas en una diversidad de volcanes como Redoubt [Chouet *et al.*, 1994], Galeras, [Gil-Cruz y Chouet, 1997], Stromboli [Chouet *et al.*, 1997] entre

muchos otros. Las señales de periodo muy largo (VLP) también han sido identificadas en el Kilauea [Dawson *et al.*, 1998; Ohminato *et al.*, 1998], en el Aso [Kaneshima *et al.* 1996; Legrand *et al.*, 2000; Kawakatsu *et al.*, 2000], en el Erebus [Rowe *et al.*, 2000] y Merapi [Hidayat, 2000], entre otros estudios.

En la creciente literatura en sismología volcánica, los estudios encaminados a interpretar los procesos asociados con eventos de periodo largo y muy largo coinciden en que las fuentes sismicas relacionandas con estos eventos LP y VLP son superficiales. La fuente activa en el Stromboli se estima entre 100 m y 660 m [Neuberg *et al.*, 19994; Chouet *et al.*, 1997, 1998]. En el Arenal se encontraron profundidades similares [Hagerty *et al.*, 1997]. La rápida atenuación de la amplitud de las señales de periodo largo y el tremor conforme la distancia al volcán aumenta es evidencia de que las fuentes son superficiales. De lo anterior se derivan los requerimientos de instalar los instrumentos lo más cercanos al cráter y con la mayor cobertura azimutal. Es importante mencionar que las técnicas rutinariamente usadas en sismología, por ejemplo el caso de técnicas de localización deben aplicarse cuidadosamente porque pueden producir resultados no confiables o irreales debido a que el edificio volcánico presenta relieve y puede inducir distorsiones importantes en las formas de onda. Además las señales presentan arribos emergentes y esta característica dificulta el proceso de lectura de primeros arribos. El efecto topográfico se debe remover para calcular las funciones de Green e invertir la forma de onda y definir el proceso involucrado con mayor certidumbre [Ohminato y Chouet, 1997]. Las técnicas de localización que se usan básicamente son el método clásico en el que se calculan los mínimos residuales de tiempo de trayectoria de la fuente, movimiento de particula, inversión de mecanismo focal, decomposición de ondeleta y el método semblance y sus variantes [Neidel y Tarner, 1971; Matsubayashi, 1995; Kawakatsu *et al.*, 2000; Almendros, 2002].

Numerosos autores explican la sismicidad observada por medio de conductos llenos de fluido, se trate de modelos acústicos [Garcés, 2000], de inversión de forma de onda o del tensor de momentos. Algunos consideran una fuente isotrópica puntual y una

fractura [Yamamoto *et al.*, 1999], otros el modelo de fractura en tres dimensiones aplicando diferencias finitas [Chouet, 1988; Apéndice B]. Hasta ahora se ha investigado con éxito que un conducto o fractura rellena de fluidos se ajusta, dentro de márgenes aceptables de incertidumbre dado el nivel de conocimiento en la materia, tanto a las observaciones en superficie como a la sismicidad observada.

Mediante las investigaciones y técnicas mencionadas, entre muchas otras, la sismología volcánica ha ido ganando terreno en el camino aún largo por recorrer con miras a entender el mecanismo de la fuente elástica y su relación con los procesos eruptivos que en su conjunto con estudios de otras disciplinas y de riesgo incrementan la posibilidad de comprender el comportamiento volcánico, mejorando así las condiciones de vigilancia y la posible prevención de un desastre en caso de una erupción mayor.

## Volcán KILAUEA, Hawaii

La erupción históricamente más voluminosa y aún activa en la zona Este del rift del Kilauea es la erupción Puu Oo-Kupaianaha. Esta erupción se ha dividido en tres fases cada cual consistió de multiples episodios. La primera fase se inició el 3 de Enero de 1983, se caracterizó por la actividad de fuentes de lava y grandes flujos "aa". De marzo de 1983 a julio de 1986, 44 vigorosos episodios construyeron un cono de 255 m de alto llamado Puu Oo, la altura de las fuentes de lava llegó hasta 370 m.

La segunda fase se inició en julio de 1986, cuando la actividad se movió de la fisura de Puu Oo a uno nuevo localizado 3 km hacia abajo del rift. Esta fase se caracterizó por la formación de estanques de lava y actividad efusiva la cual construyó el cono Kupaianaha. Los flujos de esta última fisura alcanzaron el océano en diciembre de 1986. En noviembre de 1991, se iniciaron las erupciones a lo largo de las fisuras entre el Puu Oo y el Kupaianaha, el volumen eruptado por este declinó en febrero 6 de 1992.

La fase actual corresponde a la tercera fase y se inició con la apertura de una fisura de 150 m de largo en la base del rift de Puu Oo el 17 de febrero de 1992. Esta fase se caracteriza por la emisión efusiva continua a través de multiples fisuras. Desde la erupción de 1983 la lava ha cubierto más de 54 km cuadrados. El volumen de lava emitido se estima en cerca de 2 mil millones de metros cúbicos.

En noviembre de 1994 una red de 10 estaciones digitales telemétricas se instaló en el volcán Kilauea, Hawaii [Dawson *et al.*, 1998]. Su objetivo fué probar el uso de sensores de banda ancha para investigar el proceso de transferencia de masa inestable dentro del volcán Kilauea. Las estaciones fueron equipadas con sensores Guralp CMG-3T y Guralps 3-ESP con respuesta plana entre 0.01-25 Hz. Dichos autores observaron que

existe un ruido de fondo entre los 2 y 7 s debido a la microsismosidad producida por el océano. En el estudio se demostró la aplicabilidad del método semblance (Apéndice A) para localizar eventos de origen volcánico, dado un arreglo de sismómetros alrededor del cráter. Dawson *et al.* (1998) identificaron señales de entre 12 y 30 s asociadas con la inflación de la caldera ocurrida en un periodo de 4 hrs. Analizaron eventos LP típicos (1-3 s) y eventos VLP, señales entre 12 y 30 s de periodo. Las técnicas usadas son análisis de polarización, movimiento de partícula y aplicación de la técnica de semblance. Para estimar el mecanismo de la fuente se invirtió la forma de onda de señales de periodos largos usando inversión del tensor de momentos [Ohminato *et al.*, 1998].

En la Fig 1.1 se muestra un ejemplo de los datos de la estación GU9, donde se presenta el registro de velocidad original de la componente vertical y diferentes filtros aplicados a la misma. En la figura pueden observarse las señales de periodo corto y su correspondiente evento de periodo largo. La localización de la fuente según todas las estaciones es consistente: todas apuntan hacia el cráter (Fig 1.2). El mismo resultado se encontró para las componentes horizontales usando señales LP. El movimiento de partícula asociado con estos pulsos es lineal y están dominados por movimiento compresional en todos los receptores, mismos que apuntan hacia una fuente fija, para la que se infiere una profundidad de 1 km debajo del cráter Halemaumau. El patrón de radiación de los pulsos y la inversión del tensor de momentos de los datos son consistentes con un mecanismo de transporte pulsante que opera en una fractura inclinada conectando el reservorio con el rift este del Kilauea [Dawson *et al.*, 1998].

Los datos de señales VLP asociadas con la inyección de magma debajo del volcán Kilauea se usaron para invertir la forma de onda (Fig 1.1) y cuantificar el mecanismo asociado con el flujo transitorio de magma que alimenta el rift este del volcán. El flujo transitorio de magma está marcado por una rápida inflación de la cima del Kilauea alcanzando  $22 \mu\text{rad}$  4.5 horas después del inicio del evento, seguido por una lenta deflación por un periodo de 3 días. Para cuantificar el mecanismo de la fuente Ohminato *et al.* (1998)

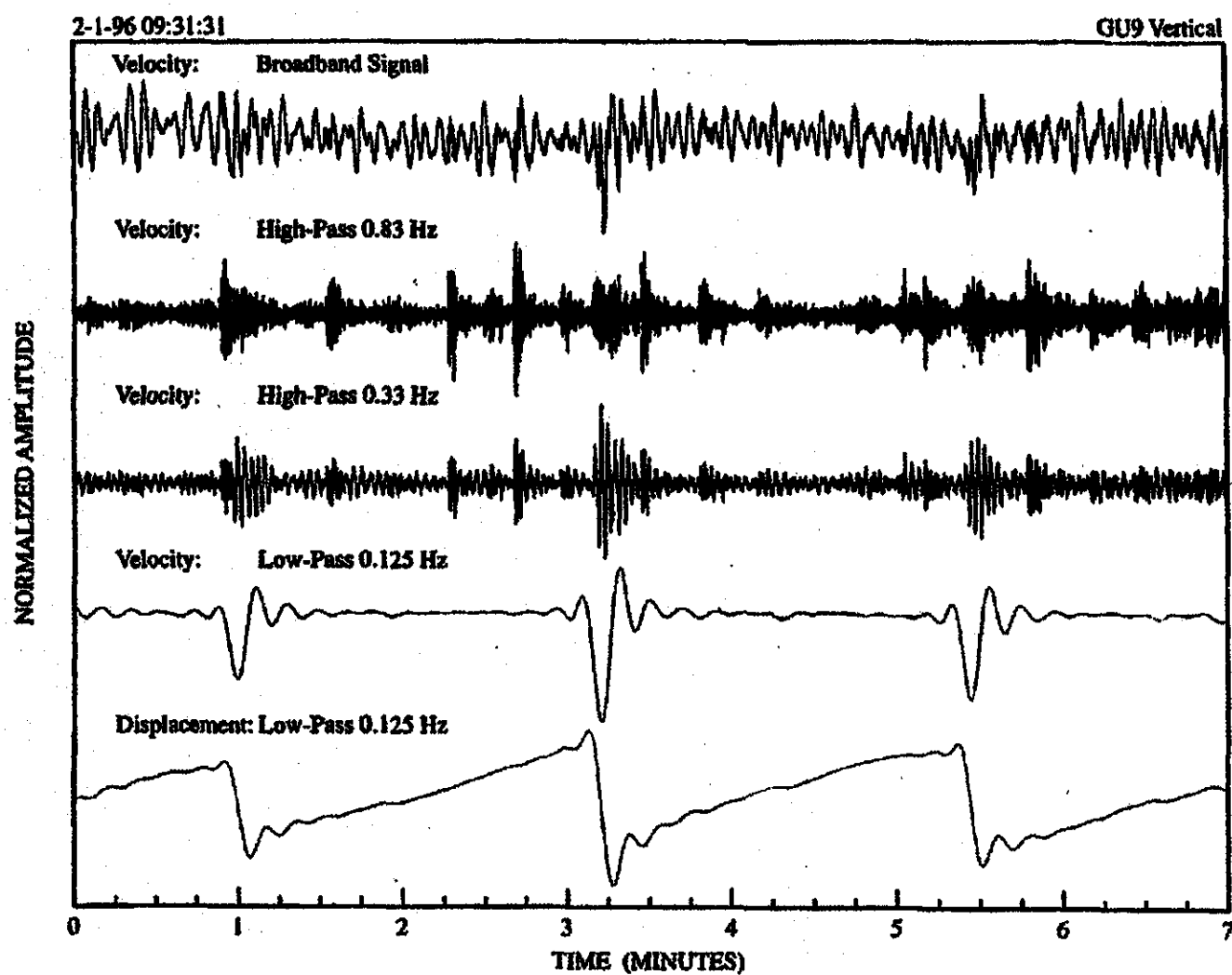


**Fig. 1.1** Diferentes bandas de frecuencia para la misma serie de tiempo, componente vertical. Todas las trazas están normalizadas. La primera muestra la traza de velocidad original. La segunda traza, muestra la misma señal filtrada con un pasa altas a 0.83 Hz. La tercera, es la señal filtrada con un pasa altas a 0.33 Hz. La cuarta traza es la señal filtrada con un pasa bajas a 0.125 Hz. La quinta traza es el desplazamiento de la cuarta. Puede observarse la forma de onda diente de sierra de cada pulso de desplazamiento y su coincidencia con los pulsos de periodo largo en el registro filtrado con 0.33 Hz. (Reproducida de Dawson *et al.*, 1997).

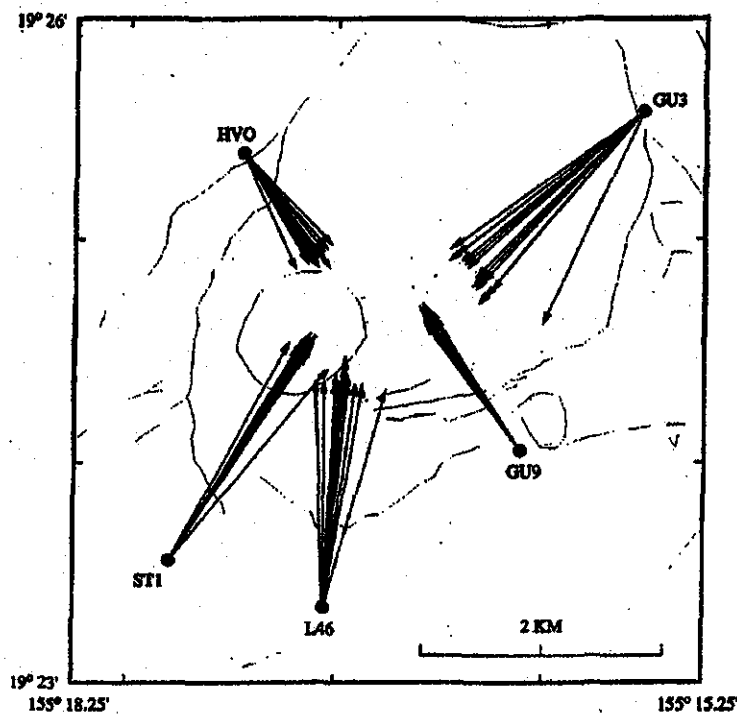


**Fig. 1.2** Vectores obtenidos en 5 estaciones con 18 pulsos usando movimiento de partícula. La magnitud de los vectores es arbitraria. (Reproducida de Dawson *et al.*, 1997).

aplicaron inversión del tensor de momentos a la forma de onda de señales VLP asumiendo una fuente puntual enterrada en un semiespacio homogéneo con una velocidad promedio para ondas compresionales y de cortante representativa según las propiedades del medio debajo del Kilauea. Sus resultados son congruentes con una fuente en forma de grieta ó ‘crack’ que actua como un amortiguador entre el flujo de magma que va hacia el rift Este. Calcularon que aproximadamente de 1000 a 4000 metros cúbicos son inyectados hacia el ‘crack’ durante la fase lenta, de acumulación, que dura de 1 y 3 min, y expulsados hacia fuera del ‘crack’ en la fase rápida, de deflación, durante 5 y 10 s, lo cual en conjunto produce las señales de desplazamiento de los eventos VLP en forma de diente de sierra mostrados en la Fig 1.1. [Ohminato *et al.*, 1998; Dawson *et al.*, 1997].

## Volcán STROMBOLI, Italia

El volcán Stromboli presenta condiciones de actividad explosiva constante y dadas las condiciones de acceso ha facilitado la realización de numerosos estudios para investigar el campo radiado por la actividad Stromboliana. Inicialmente la investigación estuvo concentrada en estudiar la sismicidad entre 0.1 y 10 s [Chouet *et al.* 1997; 1998; Sacarrotti *et al.*, 1998]. Los estudios de banda ancha realizados por Neuberg *et al.* (1994) demostraron que las erupciones strombolianas producen señales con periodos de más de 10 s. En 1997 se realizó un experimento sísmico de banda ancha con 21 sismómetros CMG-40T (0.02-60 s) instalados en los flancos del volcán. El objetivo pimordial fué investigar las propiedades de la fuente sísmica asociada a las explosiones strombolianas [Chouet *et al.*, 1999]. La mediciones demostraron claramente las características de banda ancha de cierto tipo de actividad volcánica.

En el Stromboli típicamente ocurren de 3 a 10 explosiones por hora. Ocasionalmente se presentan enjambres alcanzando 20 a 30 eventos por hora. La Fig 1.3 muestra un ejemplo de la sismicidad registrada durante una hora de actividad. En la Fig 1.3 (a) los datos originales de velocidad, en la Fig 1.3 (b) los datos filtrados entre 2 y 50 s. En el estudio encontraron los dos tipos de forma de onda mostrados en la Fig 1.3 (c) y (d). La acción repetitiva del tipo de señales en la Fig 1.3 (a) en todas las estaciones se muestra en la Fig 1.3 (e). Estas señales son características de las erupciones que se presentan en la parte norte-este del volcán. Los eventos VLP mantienen su forma de onda casi idéntica entre evento y evento con períodos menores a 20 s, lo cual sugiere la existencia de un proceso que se activa repetidamente sin destruir el mecanismo que lo genera. Estos eventos se presentan esencialmente debajo de Saciara del Fuoco al noroeste del cráter a profundidades someras (300 a 620 m). Para localizar los eventos se usó la técnica de semblance (Apéndice A) y análisis de movimiento de partículas. El efecto topográfico relacionado con el edificio volcánico fué estudiado por Ohminato y Chouet (1997). Estos

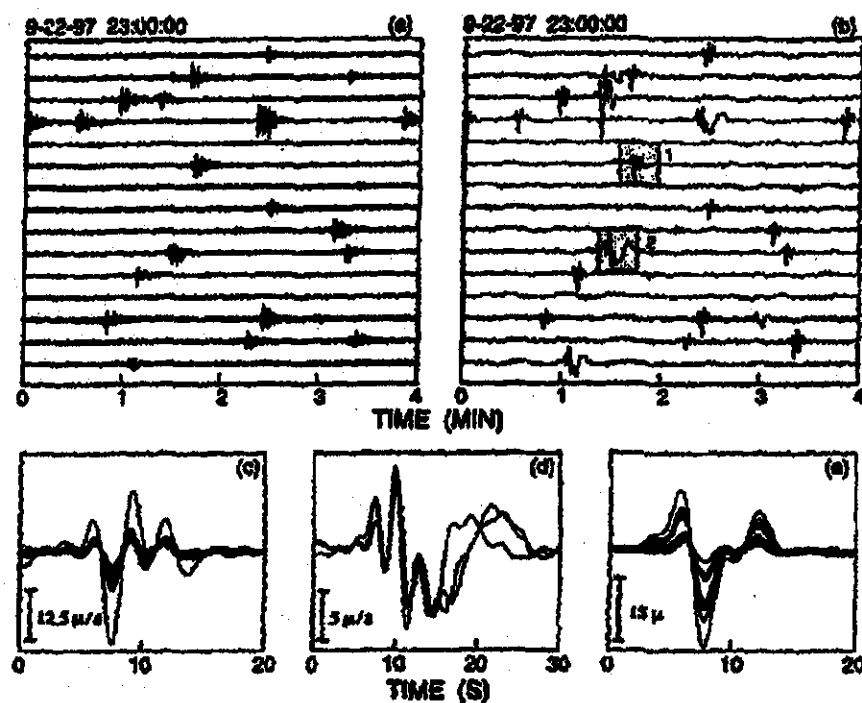


**Fig. 1.3** (a) Registros de banda ancha de velocidad componente vertical. (b) los mismos registros filtrados con un pasa banda (2-50 s). (c) registros de velocidad de 16 eventos en forma de pulsos quasi-idénticos registrados en la misma estación. (d) igual que (c) para tres eventos de un tipo diferente. (e) registros de desplazamiento vertical obtenidos en todas las estaciones para el tipo de señal mostrado en (c). (Reproducida de Chouet *et al.*, 1999).

autores encontraron que sistemáticamente las formas de onda son distorsionadas por la topografía, lo cual puede producir un sesgo en la localización de las fuentes.

Las características de las señales VLP asociadas con las explosiones strombolianas indican que pueden ser generadas por una secuencia de procesos en los que se presenta un estado de presurización y dilatación del conducto asociado con el ascenso de gas; seguido por un proceso de depresurización y deflación del conducto en respuesta a la remoción de masa. El conducto nuevamente se represuriza y dilata debido a la realimentación de la fuente con magma.

## Volcán ASO, Japón

La actividad eruptiva en el Volcán Aso es variable en el tiempo, y en general se espera una erupción Stromboliana cada 5 o 10 años. La actividad eruptiva que presenta la mayor parte del tiempo consiste de emisiones de gas, ceniza y vapor de agua. Este volcán se estudió con instrumentos de banda ancha en 1935 por Sassa [Sassa, 1935], quien realizó uno de los trabajos pioneros, instaló un sismógrafo horizontal Wiechert de 10 s y uno vertical de 4.6 s. Desde entonces se hizo patente la importancia de estudiar volcanes activos con instrumentos de banda ancha. En 1994 se operaron 10 sismómetros alrededor del cráter (STS2 or CMG-3T) [Kaneshima *et al.*, 1996; Kawakatsu *et al.*, 2000]. Durante el periodo de estudio, que abarcó un año de observaciones, se presentaron erupciones freáticas (consistentes de vapor de agua, gas y cenizas) precedidas unos cuantos minutos por desplazamientos evidenciados por señales VLP de periodos de más de 100 s [Kaneshima *et al.*, 1996].

Al igual que en Kilauea y Stromboli las señales de VLP son quasi-idénticas en espacio y tiempo y presentan periodos de 7.5 y 15 s. La Fig 1.4 muestra un ejemplo de las señales de banda ancha estudiadas por Kawakatsu *et al.* (2000) y Legrand *et al.* (2000). Las características observadas sugieren que también se trata de un mecanismo de fuente no destructivo que actúa repetidamente de evento a evento. La localización de la fuente apunta a una región somera en la parte sur-oeste del cráter. La profundidad se estima entre 1.1 km y 1.5 km debajo del cráter principal, según resultados de la inversión de la forma de onda. Durante el experimento también se observó tremor de muy largo periodo, que fué localizado aplicando semblance en la misma región. Los modelos de fuente investigados para explicar la sismicidad observada en el Aso contempla fuentes esféricas, como el modelo de Mogi (1958) y el modelo de fractura [Chouet, 1986].

Kawakatsu *et al.* (2000) enfatizan la importancia de monitorear el Aso vigilando la

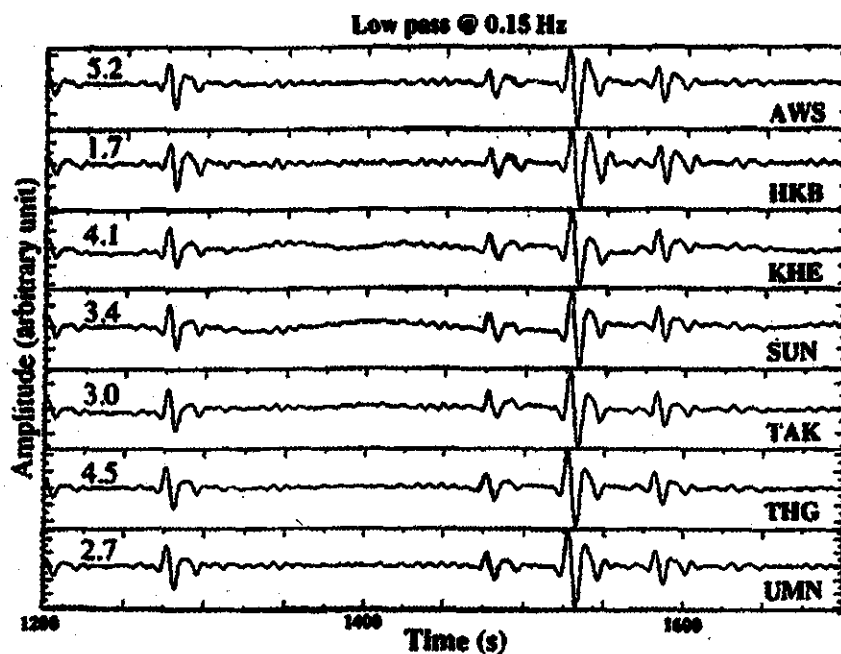


**Fig. 1.4** Sismograma de velocidad componente vertical registrado en siete diferentes estaciones filtrado con un pasa bajas (0.15 hz). Se puede apreciar la similitud de las trazas. El valor de amplitud pico-a-pico esta en  $\mu m$  a la izquierda. (Reproducida de Kawakatsu *et al.*, 2000)

sismicidad de LP y VLP puesto que han observado que las fuentes se activan aún cuando no haya manifestación eruptiva superficial. Esto lo explican considerando que la presión es suficiente para excitar la región de la fuente de las señales de bajas frecuencias pero no es suficiente para provocar una erupción superficial.

## Volcán EREBUS, Ross Island, Antártida

La actividad eruptiva del Monte Erebus está dominada por erupciones dentro de un lago de lava en el cráter. La actividad eruptiva varía desde emisiones de gas hasta explosiones

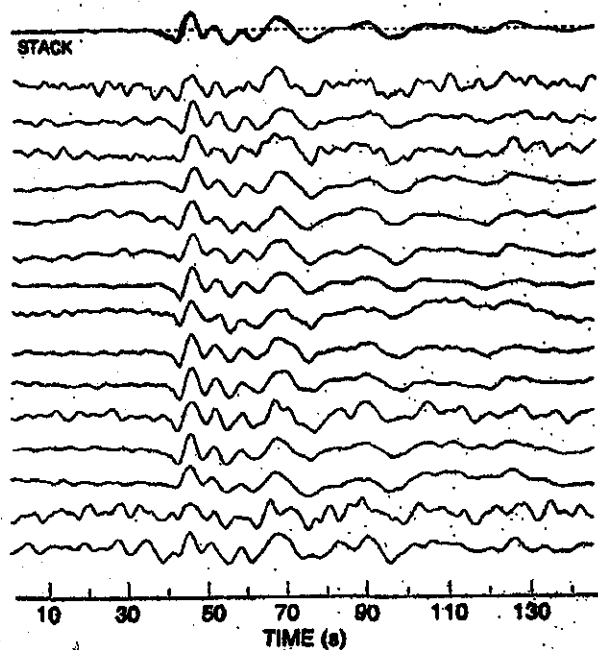


**Fig. 1.5** Registros de desplazamiento de explosiones ocurridas en el lago de lava. Se ilustra la repetitividad de las señales entre las diferentes explosiones registradas en una sola estación. La señales se normalizaron para facilitar la comparación. (Reproducida de Rowe *et al.*, 2000)

strombolianas. Las explosiones pueden ocurrir como varios eventos aislados en un día o en enjambres de hasta 900 eventos en un día [Giggenbach *et al.*, 1973; Kyle, 1994].

Se ha documentado la ocurrencia de señales de VLP con períodos de 20, 12 y 7 s que generalmente preceden explosiones superficiales por aproximadamente 1.5 s [Rowe *et al.*, 1998]. La forma de onda sugiere una fuente deflacionaria y una posiblemente inflacionaria que no se logró definir debido a que los instrumentos instalados están equipados con sensores de 30 s [Rowe *et al.*, 2000]. La Fig 1.5 muestra señales VLP de desplazamiento para 15 eventos diferentes registrados en una sola estación. La repetitividad de la forma de onda indica la existencia de un mecanismo fijo el cual esta asociado a un conducto magmático. En este conducto la presencia de una concreción donde los gases liberados se concentran formando una capa espumosa la cual eventualmente se consolida en una gran masa de gas que migra a la superficie y explota.

Rowe *et al.* (2000) localizaron la región donde ocurre la actividad VLP encontrándola concentrada en la zona superficial aproximadamente 800 m debajo del lago de lava. A diferencia de otros volcanes en el Erebus el tremor es muy raro y en los cinco años que se ha monitoreado se han detectado sólo algunos episodios de tremor monocromático y otros de tremor armónico.

Varias posibles explicaciones a las observaciones de señales de VLP consideran que para que se genere resonancia de señales VLP se requieren velocidades de fase muy lentas [Biot, 1952], como las de ondas de cortante acopladas en un medio parcialmente fundido en un conducto [Rowe *et al.*, 1998] o la excitación de 'crack waves' [Chouet, 1986; Ferrazini y Aki, 1987]. Por otro lado también se les liga a procesos en un sistema de recarga en equilibrio que actua seguido de una explosión [Julian, 1994].

## Otros Volcanes

### Volcán GALERAS, Colombia

La actividad eruptiva del volcán Galeras típicamente consiste de emisiones de vapor, gas y ceniza, acompañadas de construcción y destrucción de domos de lava en el cráter donde ocasionalmente ocurren explosiones vulcanianas. La sismicidad asociada con la actividad eruptiva principalmente consiste de eventos de periodo largo y tremor. A la fecha de este trabajo no se han reportado estudios explícitamente para investigar la sismicidad de muy bajas frecuencias. Sin embargo, de las características de la sismicidad de periodo corto se puede suponer que debe haberlas. Los eventos de periodo largo al igual que los observados en los volcanes mencionados en la sección anterior presentan características

repetitivas de evento a evento con periodos entre 0.2 y 1 s. Estos eventos son superficiales aproximadamente a 1 km debajo del cráter.

Gil-Cruz y Chouet, (1997) modelaron las características espectrales de los eventos LP usando el modelo de Chouet (1988, 1992). Encontraron las dimensiones de una fractura de entre 240-360 m de largo por 130-150 m de ancho situada justo debajo del domo. El conducto entra en resonancia en respuesta a las variaciones de presión liberando energía elástica dando origen a las señales LP. Los parámetros en combinación con información geológica y termodinámica sugieren que el proceso involucra un mecanismo de liberación de gas. En este proceso, el colapso de una capa de burbujas de gas, atrapada en la parte de arriba de la columna de magma pero subyacente al domo, libera el gas presurizado el cual, al escapar a la superficie produce dilatación en el sistema de fracturas. La exitación del conducto es atribuida a la rápida emisión y aceleración de los fluidos producto del colapso de la capa de espuma. Esta interpretación explica la repetitividad de la sismicidad observada [Gil-Cruz y Chouet, 1997].

## **Volcán REDOUBT, Alaska**

El episodio eruptivo presentado por el volcán Redoubt de 1989 a 1990 fué evaluado por los científicos exitosamente. El volcán Redoubt ha presentado erupciones caracterizadas por grandes y violentas emisiones de tefra, flujos piroclásticos, lahares, flujos de escombro y episodios de emplazamiento y destrucción de domos. El Redoubt entró en una nueva fase eruptiva en diciembre de 1989. Las erupciones iniciales de diciembre de 1989 fueron precedidas por intensos enjambres de eventos de periodo largo con características repetitivas. La presencia de erupciones menores seguidas por la extrusión y crecimiento de un domo de lava y el crecimiento y enfriamiento del mismo domo eventualmente sellaron el sistema. La sismicidad nuevamente reflejó acumulación de presión a través de otro

enjambre de eventos LP. Despues se presentó la consecuente destrucción del domo de lava produciéndose grandes columnas de ceniza que tapizaron casi todo el sur de Alaska. Este patrón eruptivo de emplazamientos y destrucción de domos fué característico de la actividad eruptiva del Redoubt hasta abril de 1990 produciendo la mayor erupción en febrero 13. La identificación de los enjambres de periodo largo permitió a los científicos alertar a las autoridades [Chouet *et al.*, 1994; Power *et al.*, 1994]. Los estudios de la distribución de picos espectrales demostró que la sismicidad repetitiva de periodo largo del Redoubt es compatible con los modos de vibrar de una fractura rellena de fluidos que se abre y se cierra en respuesta a los cambios de presión [Chouet *et al.*, 1994].

Otros ejemplos de sismicidad de eventos LP que precedieron erupciones sucedieron en el volcán Asama en 1958 y 1983 [Minakami, 1974; Kagiyama *et al.*, 1985; Shimozuru y Kagiyama, 1989]; en le volcán Meakan-dake [Usu Volcano Observatory, 1988]; en las erupciones de 1988-1989 del Tokachidake, Japón [Okada *et al.*, 1990]; en 1985 en el Nevado del Ruiz [Gil-Cruz *et al.*, 1987; Martinelli, 1990]; en 1982 en el volcán Chichonal [Havskov *et al.*, 1983]. La eventos LP y tremor se presentaron antes de eventos los explosivos en el St Helens durante mayo a octubre de 1980 [Malone *et al.*, 1981; Weaver *et al.*, 1981; Swanson *et al.*, 1985]. El ejemplo más relevante son los eventos que se registraron hasta 300 km de distancia previos a la erupción mayor del Pinatubo en junio 14, 1991 [Pinatubo Volcano Observatory Team, 1991].

## Volcán POPOCATÉPETL

### Actividad eruptiva en el pasado

El volcán Popocatépetl está situado a 65 km al SE de la Ciudad de México y a 50 km al W de la ciudad de Puebla. Forma parte de la Faja Volcánica que atraviesa el país de W a E. Se ubica en las coordenadas 19°03" N y 98°35" W, y tiene una altura de 5452 m s.n.m. (Fig. 1.6) Es un gran cono truncado que define un cráter externo elíptico cuyos ejes son aproximadamente 800 x 650 m [Carrasco *et al.*, 1986]. El volcán cubre actualmente un área de aproximadamente 500 km<sup>2</sup>, aunque algunos depósitos se han localizado a más de 30 km de radio a partir del cráter [Robin y Boudal, 1987; Siebe *et al.*, 1996]. El edificio volcánico muestra claramente dos estructuras, el cono actual del Popocatépetl y los restos de un antiguo estratovolcán sobre el cual se ha formado el actual edificio.

La historia del volcán Popocatépetl (ó cerro que humea en náhuatl) se puede dividir en dos periodos principales separados por un evento de tipo Bezymianny o St Helens. En el primer periodo se tiene la formación de un volcán primitivo de 3600 m de alto cuyos depósitos cubren un área de aproximadamente 30 km de ancho. En el segundo periodo se construyó el cono moderno de entre 6 y 8 km de diámetro y de 1700 m de altura [Robin y Boudal, 1987]. La actividad del volcán primitivo era escencialmente efusiva e inició en el último millón de años; este tipo de actividad se mantuvo cientos de miles de años. Este volcán era similar a otros volcanes de la Faja Volcánica como el Nevado de Toluca o el Pico de Orizaba. El segundo periodo comprende la construcción del volcán moderno Popocatépetl que data de 23000 años [Siebe *et al.*, 1995]. La actividad eruptiva durante la construcción del edificio volcánico moderno se caracterizó por etapas de flujos de lava intercalados con períodos que promedian de 1000 a 2000 años de actividad

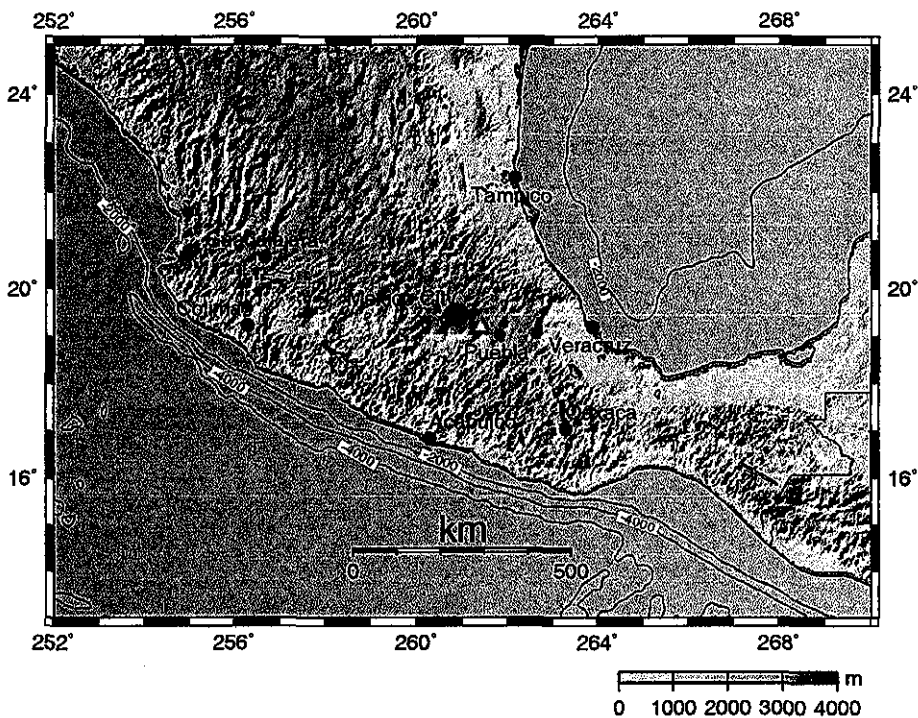


Fig. 1.6 Mapa de localización del volcán Popocatépetl.

efusiva alternada con actividad explosiva. El volcán experimentó en el pasado tres etapas marcadas por erupciones explosivas mayores con caída de piroclásticos, productos de magma heterogéneos y gruesas caídas de ceniza y escoria. La primera etapa data de más de 10000 años y la última de entre 5000 y 3800 años. Estos períodos muestran episodios alternados de flujos de lava en ciclos de varios cientos de años de duración [Boudal y Robin, 1988].

El periodo de construcción del cono se estima en 4000 años. La apertura de grandes cráteres se debe a la actividad explosiva que destruyó la parte superior del volcán. Hubo aproximadamente 2500 años de períodos de construcción mediante flujos de lava de entre 3800 y 1200 años. Durante este periodo la actividad del volcán fue principalmente efusiva. El último evento con producción de flujos piroclásticos se registró justo antes de la conquista española. Esta erupción se considera de tipo St. Vincent y cubre un área de aproximadamente 100 km<sup>2</sup> hacia las planicies de Atlixco. Desde entonces el Popocatépetl

ha presentado actividad alternada de tipo efusiva y pliniana [Boudal y Robin, 1988]. En esta etapa resaltan tres episodios de actividad piroclástica; el primer episodio consta de una capa uniforme de pómez amarillas de entre 0.3 y 1 m de espesor que datan de  $965 \pm 60$  años según Heide y Heide-Weise (1973) y de  $880 \pm 80$  años según Robin (1984); el segundo episodio es un horizonte gris de pómez de la misma edad y espesor que el anterior; y el tercer y último episodio está constituido de productos de la erupción tipo St Vincent, que incluye por lo menos cuatro flujos piroclásticos situados en el flanco norte sobreyacendo de las pómez grises que datan de  $1000 \pm 60$  años. Debido a estos datos se pueden dividir los últimos 1200 años de la actividad del Popocatépetl en tres partes: un primera etapa en la que las series de flujos de lavas se acumularon en un espesor de más de 150 m en la parte más baja del cráter. Una segunda que consiste de un periodo destructivo en el que se emitieron las capas de pómez grises y amarillas hace aporximadamente 900 a 1000 años. La tercera etapa que inició hace 900 años durante la cual se acumularon aproximadamente 100 m de espesor de flujos de lavas alternadas con depósitos de tipo pliniano [Robin y Boudal, 1987].

Estudios relizados por Siebe *et al.*(1996) muestran que las dos erupciones plinianas catastróficas ocurridas en tiempos históricos datan de  $800 \pm 135$  y  $822 \pm 65$  a nos A.C. la más vieja, y la más joven probablemente ocurrió apoximadamente 822-823 años D.C. Estas erupciones comprenden el periodo Clásico de la cultura mesoamericana.

La última manifestación de actividad eruptiva en tiempos históricos data de la época de la colonia en la que se cuenta que se subía al volcán con el objetivo de extraer azufre del cráter. La actividad fumarólica caracteriza el comportamiento eruptivo del volcán y es por ello que recibió del náhuatl el nombre de Popocatépetl que significa montaña que humea. La más reciente erupción, que antecedió el comportamiento eruptivo que estamos presenciando, sucedió en los años 20s. Esta etapa eruptiva se caracterizó por intensas emisiones de vapor de agua y cenizas, llegándose a contar hasta 50 en un día, y la formación de un domo en el interior del cráter [De la Cruz *et al.*, 1995].

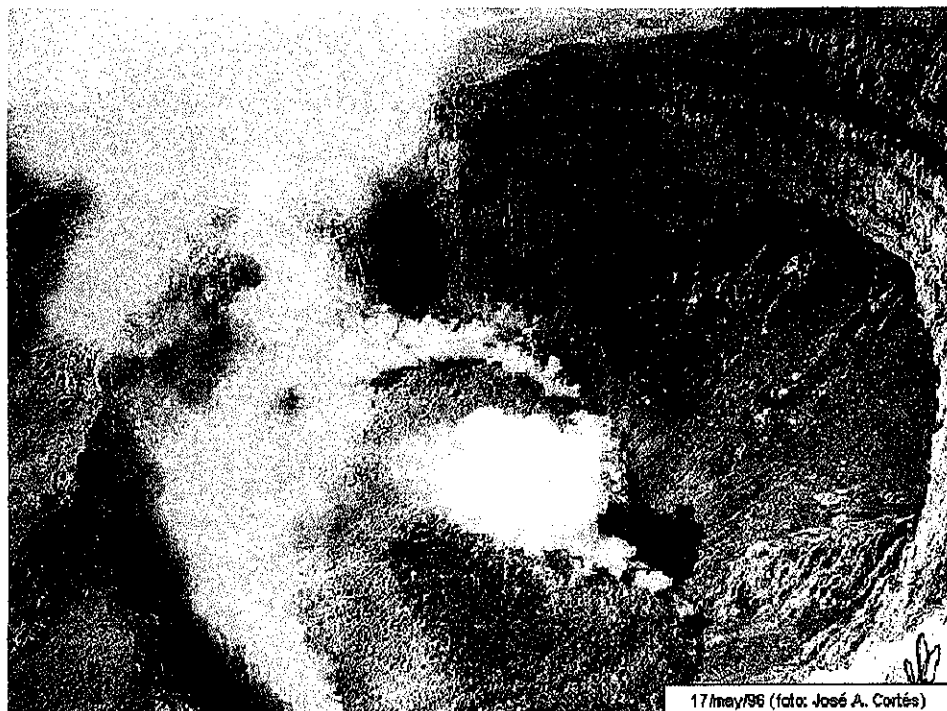


Foto. 1.1 Vista del cráter y del primer domo identificado en marzo de 1996.

Pasaron aproximadamente 70 años de relativa quietud en el volcán Popocatepetl, hasta el año de 1994 cuando comenzó una nueva etapa de actividad eruptiva que ha sido monitoreada sísmicamente. Esta etapa de actividad fué registrada desde sus inicios por una estación sismológica (PPM) de periodo corto localizada en el flanco norte aproximadamente 5 km del cráter. En el mes de octubre de 1994 la sismicidad observada caracterizada por 3 o 5 eventos al día se duplicó anunciando la reactivación y el comienzo de una fase eruptiva más intensa. El 21 de diciembre de 1994 un enjambre de eventos y tremor volcánico marcaron el inicio de la presente etapa de actividad en el volcán Popocatépetl. En general, de diciembre de 1994 a la fecha el Popocatépetl ha presentado consistentemente emisiones de gas y cenizas, emitiendo grandes cantidades de  $SO_2$  a la atmósfera [Delgado *et al.*, 2001]. Y se han presentado etapas de construcción y destrucción de domos de lava en el interior del cráter. Estos domos son destruidos total o parcialmente ocasionalmente por explosiones de tipo vulcaniano de diferente intensidad [ver Foto 1.1; Capítulos III y IV].

A partir de diciembre de 1994 el volcán se instrumentó con el fin de vigilar el desarrollo de la actividad eruptiva. Desde los diferentes punto de monitoreo se miden diferentes aspectos como: deformación usando inclinómetros (EDM) y sistemas de posicionamiento global (GPS); gases mediante mediciones con COSPEC y espectrometría; magnetometría y gravimetría; análisis geoquímicos y sismicidad entre otras. La sismicidad es una herramienta muy útil debido a que su continuidad en tiempo real permite observar los cambios importantes casi en el mismo instante en que ocurren siendo una herramienta fundamental en la labor de vigilancia.

## Capítulo II

# Características Temporales y Espectrales de la Sismicidad Observada en el Volcán Popocatépetl (1994-1995)

### Abstract

Popocatepetl volcano entered an eruptive phase from December 21, 1994 to March 30, 1995, which was characterized by ash and fumarolic emissions. During this eruptive episode the observed seismicity consisted of volcano-tectonic (VT) events, long-period (LP) events and sustained tremor. Precursory seismicity, mainly consisting of LP events, increased in October 1994. Before the initial eruption on December 21, VT seismicity exhibited no increase in number until a swarm of VT earthquakes was observed at 01:31

hours local time. Visual observations of the eruption occurred at dawn the next morning. LP activity increased from an average of 7 events a day in October, 1994 to 22 events per day in December, 1994. At the onset of the eruption, LP activity peaked at 49 events per day. LP activity declined until mid-January, 1995 when no events were observed. Tremor was first observed about one day after the initial eruption and averaged 10 hrs per episode. By late February, 1995 tremor episodes became more intermittent, lasting less than 5 minutes, and the number of LP events returned to pre-eruption levels (7 events per day). Using a spectral ratio technique, low-frequency oceanic microseismic noise with a predominant peak around 7 s was removed from the broadband seismic signal of tremor and LP events. Stacks of corrected tremor episodes and LP events show that both tremor and LP events contain similar frequency features with major peaks around 1.4 Hz. Frequency analyses of LP events and tremor suggest a shallow extended source with similar radiation pattern characteristics. In general LP and VT events do not coexist. VT events are distributed between 2.5 and 10 km depth. Tremor and LP events are located in the first 2500 m beneath the crater. Under the assumption that the frequency characteristics of the signals are representative of an oscillator we used a fluid-filled-crack model to infer the length of the resonator.

## Introduction

Popocatepetl is an andesitic composite volcano (5452 m a.s.l.) located in the central region of the Mexican Volcanic Belt (Fig. 2.1). Over the last 70 years the eruptive activity of Popocatepetl has been dominated by fumarolic emissions [Carrasco, 1986; Siebe *et al.*, 1996]. Seismic monitoring of Popocatepetl began in 1989, and until the fall of 1994 seismicity was characterized by low seismicity rates. In October 1994 LP seismicity showed a twofold increase. On December 21, 1994 a swarm of volcano-tectonic events, followed by eruption tremor accompanying a large ash plume, signaled a new episode in

the eruptive history of Popocatepetl volcano. Since December, 1994 Popocatepetl has presented distinct eruptive episodes with associated seismic activity. In this study we analyze data recorded between December 1994 and March 1995. During this period the eruptive activity of Popocatepetl volcano was restricted to emissions of fine ash, mostly non-juvenile material, and large amounts of volatiles (water vapor and other gases).

Seismic activity associated with this eruptive episode consisted of three types of signals: volcano-tectonic earthquakes (VT), long-period events (LP) and tremor [Valdes *et al.*, 1995]. These signals are identified according to their duration and dominant spectral peaks. In volcano seismology the term VT refers to short-period signals near 0.1s while the terms LP and tremor refer to long-period signals near 1s [Chouet, 1996]. We follow this terminology in this paper. The purpose of this work is to analyze the temporal and spectral characteristics of the VT, LP and tremor signals during the initial eruptive stage of Popocatepetl. We show that the LP events and tremor share similar frequency characteristics, which suggests a link in the generation process of tremor and LP events with a common source mechanism which involves a shallow resonator.

## Temporal and Spectral Characteristics of Seismicity

Seismic monitoring of Popocatepetl was initiated in 1989 when a three-component short-period (1 Hz) seismometer was installed at Cerro Tlamacas (PPM), 5 km North of the summit (Fig. 2.1). This station, operated by UNAM (National University of Mexico), has provided a continuous record of seismic activity since 1989. In October-November 1994, stations PPX and PPC were installed by CENAPRED-UNAM (National Disaster Prevention Center and National University of Mexico), and after the eruptive crisis stations PPB and PPP were deployed in January 1995. These four stations were initially

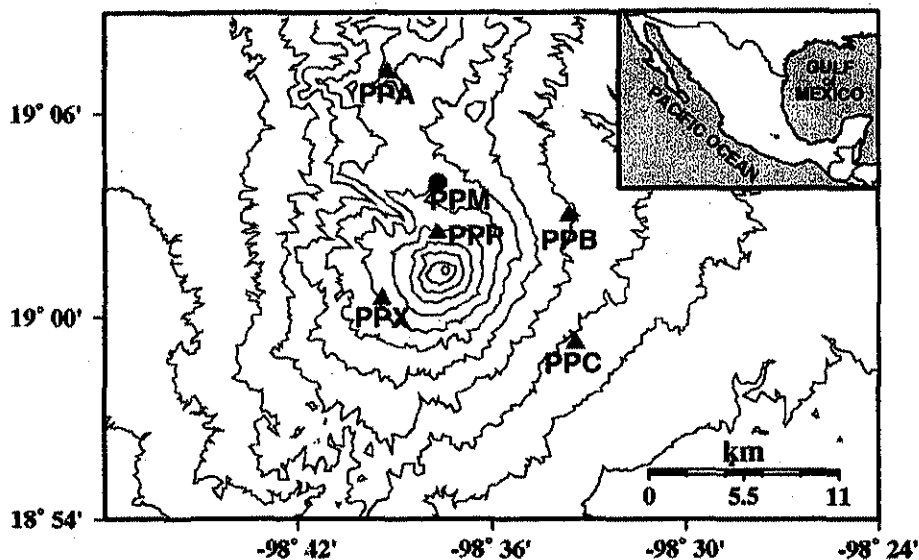


**Fig. 2.1** Map of Popocatepetl Volcano, Mexico. Solid triangles represent short-period seismic stations. The solid circle shows the location of PPM broadband seismometer. Inset shows the location of Popocatepetl.

equipped with vertical component (Mark products L4C 1s) sensors, and analog and digital recording systems. In addition, at PPM site a broadband three-component seismometer (Guralp CMG-40T 0.02-30 s) was operated from January 5 to March 30, 1995 (Fig. 2.1).

For the analysis of tremor and LP events we only use data from the single three-component broadband station because the short-period stations had operational problems after their initial deployment. For instance: 1) for a few months after deployment the single component stations were run with various filters, gain, and sensors, and as there is no record of the changes, proper calibration is not possible, 2) the digital stations were on trigger mode so only VT and large LP events were recorded, 3) the records were frequently saturated because of the low dynamic range of the recording system, 4) records of tremor episodes were as short as 80 s, too short a duration for our analysis, and many of the tremor episodes were not recorded, and 5) the frequency content of these signals below 1 Hz can not be seen in the short-period records due to the response of the sensors (1 Hz).

The seismic rate for VT events before December 21, 1994 typically averaged one event per day. The forty seven VT events (Fig. 2.2), which occurred between December 21, 1994 and March 1995, were located with HYPOCENTER [Lienert *et al.*, 1986] using a velocity model with 3 flat-layers for P-velocity and thickness of 3.5 km/s, 5.5 km; 4.5 km/s, 0.5 km; 5.0 km/s, 6.0 km, respectively [Valdes *et al.*, 1995]. The maximum error for plotted events is 1 km. In the velocity model we take into account available geologic information of Popocatepetl and velocity models from other stratovolcanos [Lahr *et al.*, 1994]. At least three stations were used in the locations and the S-P times were used to constrain the depth. At the beginning of the network operation the VT events were located using analog records as well. The VT events are restricted to depths of 2.5 to 10 km below the summit crater and no apparent trend in epicentral location or depth is observed with time. Another 136 VT events which occurred from April 1995 to November 1996 are also plotted in Figure 2.2 and these events also do not exhibit any change in the distribution of hypocenters. This distribution describes a dense sub-vertical zone approximately 3.5 km wide.

Typical LP seismicity rates before October, 1994 showed an average of 7 events per day and a maximum of 10 events per day. From October until early December the number of events slowly increased with an average rate of 22 events per day observed a few days prior to the December 21, 1994 eruption. The LP events had a maximum duration of 70 s and exhibit very emergent arrivals. At the onset of the eruption the maximum number of LP events was 49 events/day. The rate of occurrence decreased until early January, 1995 when observed rates were about 5 events per day and LP activity ceased by about mid-January, 1995 (Fig. 2.3). In late February, 1995 LP activity resumed with an average rate of about 5 events per day.

Tremor at Popocatepetl volcano started 22 hours after the eruptive crisis of December 21, 1994. From December to March, 198 episodes of tremor with duration of more than 10 minutes were identified in the analog record of station PPM. These tremor episodes

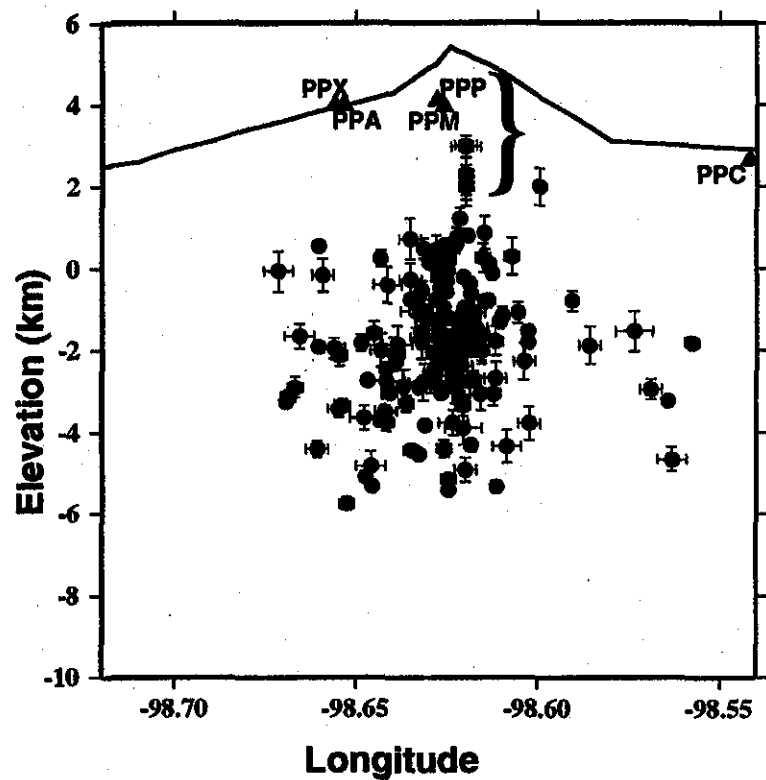


**Fig. 2.2** Hypocentral distribution of 183 VT events which occurred between December, 1994 and November, 1996 plotted as depth versus longitude. Solid circles represent hypocenters with maximum errors of 1 km (errors shown as bars). Solid triangles are stations. Large bracket shows the possible source region of the LP events and tremor.

**TESIS CON  
FALLA DE ORIGEN**

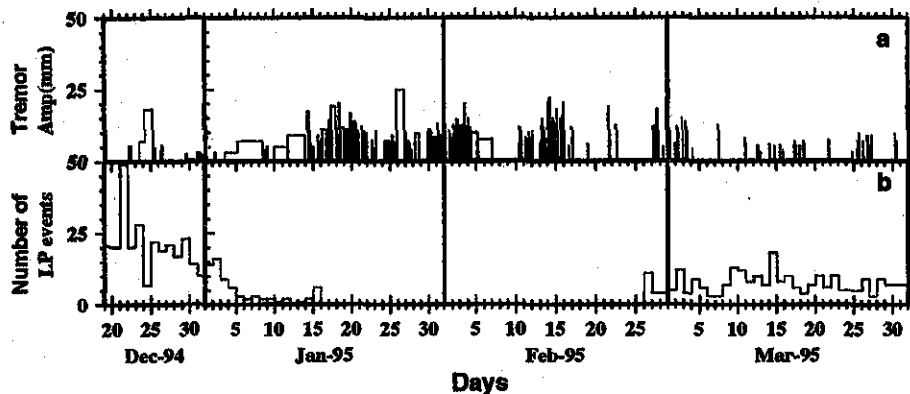


**Fig. 2.3** Tremor episodes and LP events versus time measured on analog records of station PPM (NS component). a) Tremor amplitude measured peak to peak and the duration of each episode. b) The maximum number of LP events per day.

became more intermittent with time and their duration decreased from hours to minutes. As the duration decreased the amplitude increased by a factor of three with respect to an episode of sustained tremor observed in early January, 1995 (Fig. 2.3a). The longest tremor episode lasted 72 hours with an average peak-to-peak amplitude of 7 mm and period between 0.8 and 1.5 Hz. At PPM, the minimum signal level was at least twice as large as the noise level. As shown in Figure 2.3, an inverse relationship between LP activity and tremor is observed. As tremor episodes increased the LP activity decreased. By the end of February, 1995 tremor episodes decreased and an increase in the occurrence of LP events was observed.

In early January 1995, a TV camera was installed at station PPA (Fig. 1), which provided a visual monitoring system to CENAPRED (65 km away). Both LP and tremor events were visually correlated with emissions of gas and ash from the summit crater. This suggests that the source of this seismicity is located at shallow depths beneath the summit. The LP waveforms are generally emergent, and phase picks are difficult to

determine. We attempted to locate one LP event using phase picks determined from five stations as well as using the semblance technique, a measure of multi-channel coherency (Ohminato et al., 1998; Dawson et al., 1998). Both techniques provide a location of the LP event at a depth of approximately 1 km beneath the crater floor. In both cases the error estimates are large ( $\pm 1$  km) due to the emergent first arrivals for this event. Nevertheless, the suggested source depth is quite shallow and in harmony with the correlation of vent emissions.

To investigate whether the LP events and tremor share a similar frequency content, spectrograms with a 2.56 s moving window offset by 0.64 s were calculated using the broadband data from station PPM. In Figure 2.4 an example of a typical LP event and tremor episode are shown. Both present similar waveforms and frequency content, with most of the energy concentrated between 0.5 and 5 Hz. This frequency content is similar to that observed at Arenal, Costa Rica [Benoit and McNutt, 1997], Galeras, Colombia [Gil-Cruz and Chouet, 1997] and Redoubt, Alaska [Chouet et al., 1994] among many other volcanos [McNutt, 1992]. We analyzed episodes of continuous tremor from the broadband seismometer in the frequency range 0.03-25 Hz to quantify the frequency content as a function of time. At low frequencies, energy between 0.12 and 0.18 Hz dominates the signals. This energy corresponds to the oceanic microseismic noise and has been well documented by among others, Longuet-Higgins (1950), Pomeroy et al. (1969) and Aki and Richards (1980). Since the oceanic microseismic noise is continuous and masks the tremor signals, we applied a spectral ratio technique to minimize the effects of this noise. First, we extract a section of signal which contains only the average ocean microseismic noise selected immediately before each tremor episode. A second section containing each tremor episode is then extracted. Both sections were tapered with a 5% cosine taper and the amplitude spectra calculated. Spectral ratios of each episode of tremor and background noise were then calculated, both with the same window length. Therefore, the spectral ratio represents the frequency content of the tremor signal free of site effect and ocean microseismicity. From this analysis, it was found that the average shape for

different tremor episodes is constant for the vertical and horizontal components. We observed that at a given frequency the relative amplitude of spectral ratios changed when comparing different windows of the same tremor episode, which suggests that these peaks are not due to path effects but represent a source effect involving a resonator. In this paper, the term source refers to the composite LP and tremor source region consisting of a driving mechanism and a resonator as described in Chouet (1988). Further observations of tremor episodes show temporal changes in the maximum peaks of the tremor spectrum which correlate with temporal variations in volcanic eruptive activity, and such behavior cannot be attributed to path effects [Chouet, 1992]. Only minor temporal changes were observed between different tremor episodes.

Selected LP events were analyzed using the same procedure as tremor episodes. In order to emphasize the dominant spectral peaks the three largest LP spectral ratios and thirteen tremor spectral ratios were stacked separately. A comparison between the frequency peaks of the tremor and LP events shows that there is an average difference of  $\pm 0.05$  Hz for vertical and horizontal components, with the maximum peaks of both spectra coinciding at 1.42 Hz (Figs. 2.5 and 2.6, Table 2.1). These similar frequency characteristics of the tremor and LP events suggest that they are generated by a similar physical mechanism in which magmatic fluids actively participate.

## Observed Data vs. Crack Model Predictions

Several models with a different of geometries including cracks [Aki *et al.*, 1977; Chouet, 1986], pipes [Chouet, 1985; Garces and McNutt, 1997]], spheres [Crosson and Bame, 1985], have been proposed to explain the generation mechanism and spectral features observed in tremor and LP signals. We interpret the frequency characteristics of the tremor and

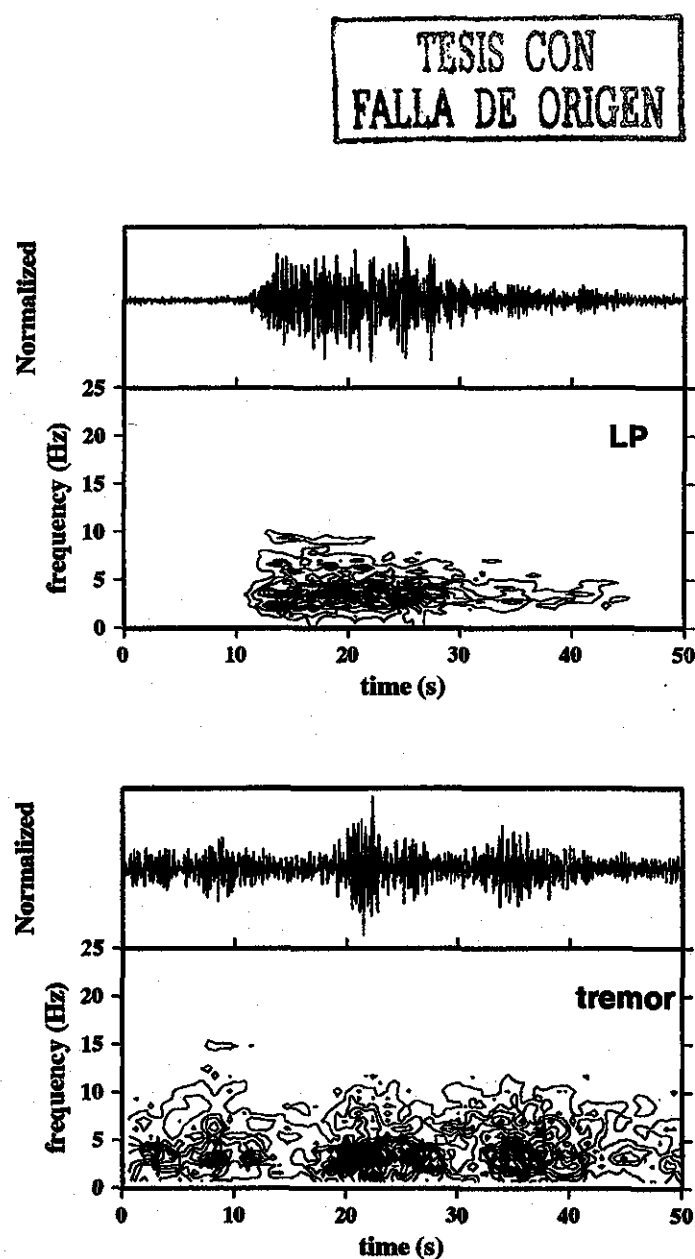
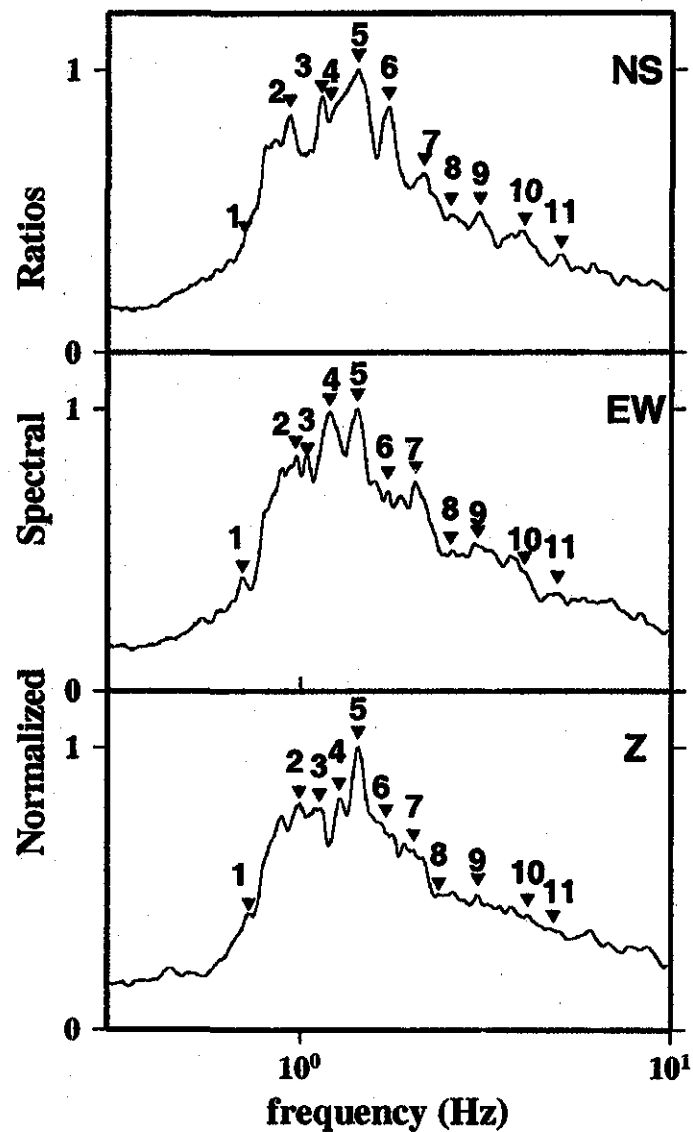


Fig. 2.4 Seismograms of the vertical component of motion for a typical LP event and tremor episode and the corresponding amplitude spectrograms of ground velocity versus time calculated with a 2.56 s moving window.

LP spectral ratios observed at Popocatepetl using the fluid-filled-crack model [Aki *et al.*, 1977; Chouet, 1986; Appendix B] considering the following: a) the LP and tremor events are manifestations of a transient or sustained pressure disturbance of any origin occurring within a fluid-filled cavity [Chouet, 1986; 1988; 1992]; b) the fluid-filled-crack model is appropriate for mass transport conditions beneath a volcano, and c) extensive studies of the crack model by Chouet (1986, 1988, 1992, 1994) show that the fluid-filled crack model generates a very slow wave which gives realistic estimates of the size of the resonator [Kumagai and Chouet, 1999].

We compare the observed spectral modes from tremor and LP events to those predicted by a given crack model making two assumptions concerning: 1) the velocity of the fluid is known and constant, and 2) the choice of the lowest spectral peak as the fundamental mode. In order to determine the length ( $L$ ) of the resonator, we fit the spectral peaks of Figures 2.4 and 2.5 (listed in Table 2.1) with the wavelength of the longitudinal modes of resonance given by the fluid-filled crack model of Chouet (1986) and Chouet *et al.* (1994). In this model the crack stiffness controls the speed of the crack wave [Aki *et al.*, 1977; Chouet, 1986], and dispersion curves are calculated for different values of crack stiffness for a variety of models with parameters consistent with the known or inferred rock and fluid properties in the crack [Chouet *et al.*, 1994]. We calculate the phase velocity  $v$  of the crack wave in km/s taking from the dispersion curves the velocity ratio  $v/v_f$  (phase velocity of the crack wave versus the acoustic velocity of the fluid) for stiffnesses  $C = 100, 200$  and  $500$  [Chouet *et al.*, 1994, Fig. 16; Appendix B] and  $v_f$  ranging from  $0.8$  to  $1.3$  km/s. The value of  $v_f$  was selected based on values for water-steam mixtures [Kieffer, 1977] and magmatic gases of various compositions [Chouet *et al.*, 1994] because volcanic activity at Popocatepetl from December, 1994 to April, 1995 was characterized by phreato-magmatic eruptions (S de la Cruz personal comm. 1996).

Eleven spectral peaks are selected in Figures 2.5 and 2.6. We observe that these peaks do not occur in a regular sequence as expected for a fluid-filled sphere [Crosson and Bame,



**Fig. 2.5** Normalized and stacked spectral ratios of 15 episodes of tremor. The numbers correspond to the frequencies shown in Table 2.1.

1985] or a fluid-filled cylinder [Chouet, 1985]. However, there is a semi-regular spacing (0.25 Hz) between the maximum peak (number 5) and peaks 4 and 6, and there is almost three times the space (0.71) between the maximum peak (number 5) and peaks 1 and 7 (Table 2.1). The sequence of spectral peaks roughly represents the eigen-frequencies of a free oscillator system and a constant physical length at the source is supported by the consistency of the spectral peaks for the wide range of LP events and tremor [Fehler, 1983].

The phase velocity  $v$  in km/s range from 0.08 to 0.585 for  $C = 100$ , range from 0.056 to 0.416 for  $C = 200$ , and from 0.04 to 0.26 for  $C = 500$ . Using those values of  $v$  and the lowest frequency  $f_0 = 0.71$  Hz (Table 2.1) we calculated the minimum and maximum wavelength for each stiffness as  $\lambda = v/f_0$  yielding;  $\lambda_{C=100} = 112$  to 824 m,  $\lambda_{C=200} = 78$  to 586 m,  $\lambda_{C=500} = 56$  to 367 m. Other frequencies listed in Table 2.1 match with the wavelengths of the model; for example the maximum peak (1.42 Hz) the wavelength is  $\lambda = L/2$  (mode 3) and so on (see Table 2.1). Since we are assuming  $f_0 = 0.71$  Hz as mode 1 the possible resonator lengths are  $L = \lambda$  depending on the contrast of the model parameters. Therefore, the observed modes are roughly consistent with a crack length of about 100 to 600 m given the assumptions above.

## Discussion

Surrounding Popocatepetl are several outcrops of Cretaceous limestone rocks between 300 to 1000 m a.s.l., which were correlated with borehole data from the basin of Mexico at Tulyehualco and Mixhuca [PEMEX, 1988; Perez-Cruz, 1988]. From those data we infer a contact between the limestone and volcanics at  $1000 \pm 500$  m a.s.l. beneath the volcano edifice. This contact defines the lower bound where the volcanic edifice rests and

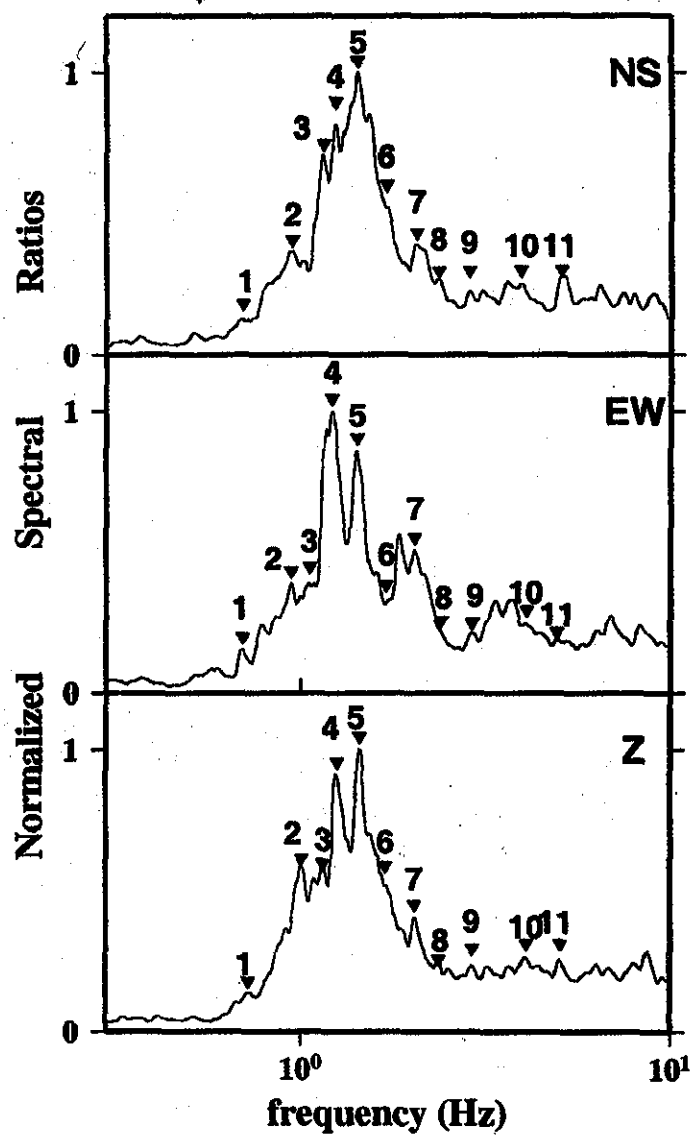


Fig. 2.6 Normalized and stacked spectral ratios of LP events. The numbers correspond to the common frequencies shown in Figure 2.4 and Table 2.1.

No Peak	Tremor N-S	LP N-S	Tremor E-W	LP E-W	Tremor Z	LP Z	$\lambda$
1	0.71716	0.69580	0.69732	0.69885	0.72631	0.72631	L
2	0.93078	0.94909	0.97656	0.94605	0.99639	1.01013	2L/3
3	1.13525	1.14746	1.04065	1.18103	1.12610	1.15662	—
4	1.20001	1.23596	1.20010	1.21460	1.27563	1.25732	—
5	1.42822	1.42212	1.42822	1.41907	1.43280	1.44348	L/2
6	1.71967	1.70288	1.71967	1.70593	1.70097	1.70593	2L/5
7	2.14233	2.05688	2.04010	2.03857	2.02179	2.04468	L/3
8	2.53754	2.35901	2.04010	2.40173	2.36206	2.38647	2L/7
9	3.03192	2.86560	3.00140	2.92969	3.00446	2.93274	L/4
10	4.00124	3.95508	4.00124	4.08936	4.09088	4.10461	2L/11
11	5.00565	5.07507	4.91562	4.97437	4.80003	5.06592	L/7

**Table 2.1** Common peaks of Figures 2.5 and 2.6, for tremor and LP events and the corresponding wavelength  $\lambda$  (see text for details).

coincides with a region marked by a relative paucity of VT earthquakes (Fig. 2.2). It is in this region that a resonator might be located, in the first 2500 m beneath the crater. The dynamic conditions required to generate tremor and LP events may be originating through a physical mechanism of flow instability as proposed by Chouet et al. (1994) for Redoubt volcano. A downward first motion is clearly identified in the largest LP events recorded at the stations shown in Figure 2.1. This feature implies that the excitation began with a pressure decrease in a resonator [Nakano et al., 1998]. This triggering mechanism is discussed in detail in Morrissey and Chouet (1997).

The hypocenters of VT events represent the fractured region through which fluids travel toward the surface or the region of stress readjustment in response to inflation or deflation [Benz et al., 1996]. As LP events and tremor were visually correlated with fumarolic emissions, this seismicity can be directly associated with the movement of fluids

at shallow depths. We infer that the triggering of the tremor and LP events is strongly related to pressure changes associated with magmatic fluids. This interpretation is supported by the ascent of magma and the eventual emplacement of a lava dome within the crater about one year and three months later (March 1996). The magma probably originated from depths greater than 6000 m b.s.l. as the deepest VT hypocenters with maximum errors of 1 km (Fig. 2.2) indicate that magmatic fluid pressure induced fracturing of rocks at these depths. This depth could possibly represent the brittle-ductile transition zone, therefore the magma reservoir could be deeper.

Water, vapor and other gases were the first fluids to appear at shallow depths on December 21, 1994. The transport of these fluids is the likely source of the tremor and LP events at depths shallower than 1000 m a.s.l. This observation is consistent with the definition of volcanic signals, where LP and tremor events are related to fluid flow through cracks and conduits [Chouet, 1996]. Although the location is poorly constrained, the depth of the LP event located with phase picks and the semblance technique is consistent with a source about 1 km below the summit crater. The observed inverse relationship between the occurrence of LP events and tremor episodes is in agreement with the idea that tremor is composed of many LP earthquakes that occur over a given period [Fehler, 1983; Chouet *et al.*, 1994]. This relationship between LP and tremor events is in harmony with the interpretation that tremor is the response to sustained pressure fluctuations and LP events are the response of the generating system to sudden pressure transients [Chouet, 1996]. The transition from LP events to tremor could be gradual or sudden, possibly corresponding to a flow regime changes.

Because we do not observe any frequency changes for the LP and tremor spectra during the period of study, the geometric characteristics of the resonator and the fluid properties were not significantly modified with time [Nakano *et al.*, 1998]. The observed spectral modes suggest that the resonator system appears to be common for both tremor and LP sources, and that the length of the resonator is about 100 to 600 m when compared to

the fluid-filled crack model [Chouet, 1986; Chouet, 1988]. The presence of strong tremor related with tephra emission probably indicates a reaming process of the conduit and intermittent tremor episodes may be related to pressure readjustments in the system. In response to the loss of pressure in the tremor generating system, the last tremor episode observed was a short transient with duration of less than 5 min and average amplitude of 2 mm (twice the noise of the station). After this crisis tremor was not observed and the seismic activity (VT and LP) returned to levels similar to before December 1994.

## Conclusions

This paper describes the seismicity observed from December 1994 to March, 1995, a new eruptive episode in the history of Popocatepetl. The seismic activity consisted of three types of signals, VT earthquakes, LP events and tremor episodes. 183 VT events were located, 47 of which occurred during the period of study. The VT occurrence is restricted to depths of 2.5 km to 10 km below the summit crater, but it is important to take into account that the number of stations and their distribution do not permit good depth constraint. The LP events and tremor episodes present an inverse correlation with time and exhibit common spectral characteristics suggesting that these signals share a similar source process. Spectra associated with the genesis of LP events and tremor is consistent with a crack-like resonator approximately 0.1-0.6 km in length. This origin process can be associated with a shallow mechanism due to the correlation of long-period seismicity and visual observations of emissions of ash, water vapor and other gases. A shallow source for the LP events, about 1 km below the crater floor, is also indicated using semblance and phase picks. Finally, using data from a single good-quality instrument recording for limited amount of time, *i.e.* 3 months, provides valuable insight into the generation process of tremor and LP events.

### Reference

- Aki K., Fehler M. and Das S. (1977). Source mechanism of volcanic tremor: fluid-driven crack models and their application to the 1963 Kilauea eruption. *J. Volcanol. Geotherm. Res.* 2, 259-287.
- Benoit J., and S. McNutt. (1977). New constraints on source processes of volcanic tremor at Arenal Volcano, Costa Rica, using broadband seismic data. *Geophys. Res. Lett.* 24, 449-452.
- Benz H, Chouet B, Dawson P., J. Lahr, R. Page and J. Hole. (1996). Three-dimensional P and S wave velocity structure of Redoubt Volcano, Alaska. *J. Geophys. Res.* 101, 8111-8128.
- Carrasco G., S. Mora, H. Delgado, and J. Urrutia. (1986). Geología y paleomagnetismo del Popocatepetl. Serie de Investigación, Instituto de Geofísica, UNAM.
- Chouet B. (1985) Excitation of a buried magmatic pipe: a seismic source model for volcanic tremor. *J. Geophys. Res.* 90, 1881-1893.
- Chouet B. (1986). Dynamics of a fluid-driven crack in three dimensions by the finite difference method. *J. Geophys. Res.* 91, 13967-13992.
- Chouet B. (1988). Resonance of a fluid-driven crack: radiation properties and implications for the source of long-period events and harmonic tremor. *J. Geophys. Res.* 93, 4375-4400.
- Chouet B. (1992). A seismic model for the source of long-period events and harmonic tremor. In *Volcanic Seismology*, pp 133-156, Eds. Gasparini, P Scarpa R & Aki K., Spring Verlag, Berlin.
- Chouet B., R. A. Page, C. D. Stephens, J. Lahr and J. A. Power. (1994). Precursory swarms of long-period events at Redoubt Volcano (1989-1990), Alaska; their origin and use as a forecasting tool. In: T P Miller and Chouet B (edit). *The 1989-1990 eruptions of Redoubt Volcano*. *J. Geophys. Res.* 62, 95-135, 1994.
- Chouet B. (1996). Long-period volcano seismicity: its source and the use in eruption forecasting. *Nature* 380, 309-316.
- Crosson R. S. and D. Bame. (1985). A spherical source model for low-frequency volcanic earthquakes. *Geophys. Res. Lett.* 90, 10237-10247.
- Dawson, P. B., C. Dietel, B. A. Chouet, K. Honma, T. Ohminato, and P. Okubo. (1998). A digitally telemetered broadband seismic network at Kilauea Volcano, Hawaii. *U. S. Geol. Surv. Open-File Rep.* 98-108, 121p.
- Garces, M and S. McNutt. (1997). Theory of the airborne sound field generated in a resonant magma conduit. *J. Volcanol. Geotherm. Res.* 78, 155-178.
- Gil-Cruz F. and B. Chouet. (1997) Long-Period events, the most characteristic seismicity accompanying the emplacement and extrusion of a lava dome in Galeras Volcano, Colombia, in 1991. *J. Volcanol. Geotherm. Res.* 77, 121-128.
- Fehler M. (1983). Observations of volcanic tremor at Mount St. Helens Volcano. *J. Geophys. Res.* 88, 3476-3484.
- Kieffer S. W. (1977). Sound speed in liquid-gas mixtures: water-air and water-steam. *J. Geophys. Res.* 82, 2895-2904.

- Kumagai, H and B. Chouet. (1999). The complex frequencies of long-period seismic events as probes of composition beneath volcanos. *Geophys. J. Int.*, 138, F7-F12.
- Lahr J.C., B.A. Chouet, C.D. Stephens., J.A. Power and R.A. Page. (1994). Earthquake classification, location and error analysis in a volcanic environment; implications for the magmatic system of the 1989-1990 eruptions at Redoubt Volcano, Alaska. *J. Geophys. Res.* 62, 137-151, 1994
- Lienert B., E. Berg and L. Frazer. (1986). HYPOCENTER an earthquake location method using centered, scaled and adaptively damped least squares. *Bull. Seism. Soc. Am.* 76, 771-783.
- Longuet-Higgins, M. S. (1950). A theory of the origin of microseism. *Philos. Trans. R. Soc. London, Ser. A* 423, 1-35.
- McNutt (1992). *Encyclopedia of Earth System Science*, Academic Press San Diego v. 4, p. 417-425.
- Morrissey M., and B. Chouet. (1997) A numerical investigation of choked flow dynamics and its application to the triggering mechanism of long-period events at Redoubt Volcano, Alaska. *J. Geophys. Res.* 102, 7965-7983.
- Nakano M., H. Kumagai, M. Kumazawa, K. Yamaoka and B. Chouet. (1998). The excitation and the characteristic frequency of the long-period volcanic event: An approach based on an inhomogeneous autoregressive model of a linear dynamic system. *J. Geophys. Res.* 103, 10,031-10,046.
- Ohminato, T., B. Chouet, P. Dawson, and S. Kedar. (1998). Waveform inversion of very long period impulsive signals associated with magmatic injection beneath Kilauea Volcano, Hawaii. *J. Geophys. Res.* 103, 23,839-23,862.
- PEMEX (1988). Cortes litológicos y registros geofísicos de los pozos profundos exploratorios Roma-1, Mixhuca-1, Tulyehualco-1 y Copilco-1. Fundación Barros Sierra. A.C.
- Perez-Cruz G. (1988). Estudio sismológico de reflexión del subsuelo de la Ciudad de México. M.A. Thesis Facultad de Ingeniería U.N.A.M.
- Pomeroy P., G. Hade, J. Savino and R. Chander. (1969) Preliminary results from high-gain wide-band long-period electromagnetic seismograph systems. *J. Geophys. Res.* 74, 3295-3298.
- Siebe C., M. Abrams, J.L. Macias, and J. Obenholzner. Repeated volcanic disasters in Prehispanic time at Popocatepetl central Mexico; Past key to the future ?. *Geology*, 24, 399-402, 1996.
- Valdes C., G. Gonzalez, A. Arciniega, E. Nava, M. Santoyo. (1995) Sismicidad del volcán Popocatépetl a partir del 21 de diciembre de 1994 al 30 de marzo de 1995. In: Volcán Popocatépetl, estudios realizados durante la crisis de 1994-1995, CENAPRED and • UNAM, pp 129-138.



Foto 2.1 Proyectil (foto A. Arciniega.).

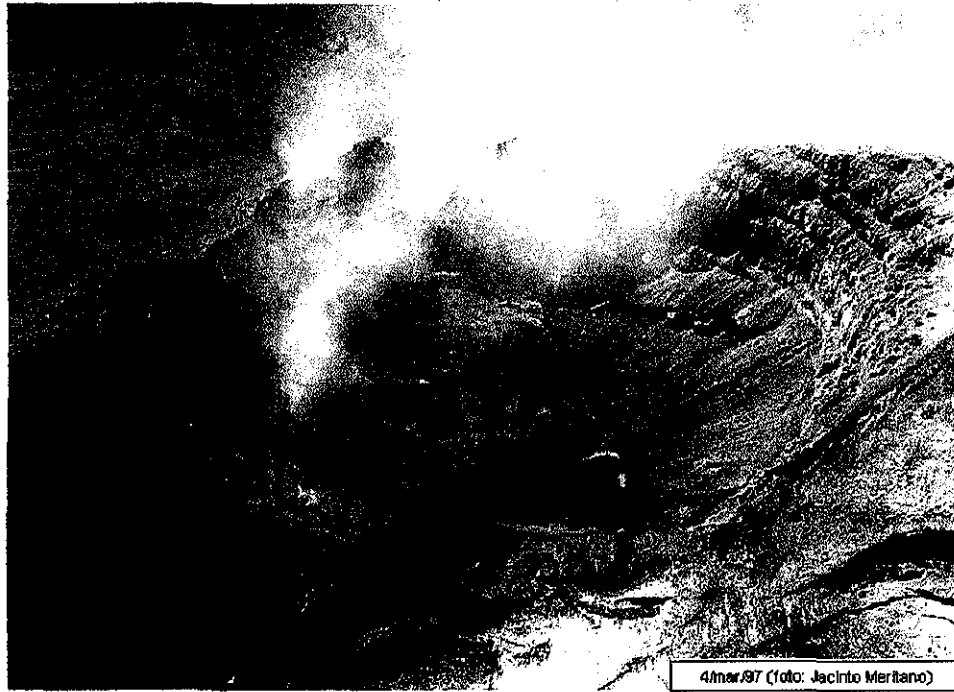


Foto 2.2 Interior del cráter marzo, 1997.

## Capítulo III

# Eventos de Periodo Largo y Tremor Registrados en el Volcán Popocatépetl (1994-2000) y sus Características de Banda Ancha

### Abstract

Following an initial phreatic eruption on 21 December 1994, activity at Popocatepetl has been dominated by fumarolic emissions interspersed with more energetic emissions of ashes and gases. A phase of repetitive dome-building and dome-destroying episodes began in March, 1996 and is still ongoing at present. We describe the long-period (LP) seismicity accompanying eruptive activity at Popocatepetl from December 1994 through May

2000 using data from a three-component broadband seismometer located 5 km from the summit crater. The broadband records display a variety of signals with periods ranging over the band 0.04–90 s. Long-period events and tremor with typical dominant periods in the range 0.3–2.0 s are the most characteristic signals observed at Popocatepetl. These signals appear to reflect volumetric sources driven by pressure fluctuations associated with the unsteady transport of gases beneath the crater. Very-long-period (VLP) signals are also observed in association with LP events and tremor. The VLP signals that accompany LP events display Ricker-like wavelets with periods near 36 s, while VLP signals associated with tremor waveforms typically show sustained oscillations at periods ranging up to 90 s. The spectra and particle motion patterns remain similar from event to event for the majority of LP and tremor signals analyzed during the time span of this study, suggesting a repeated non-destructive activation of a common source. Hypocenters determined by phase pick analyses of selected LP events recorded by the 7-station permanent Popocatepetl short-period network suggest that the majority of these events are confined to a source region in the top 1.5 km below the crater floor. The repetitive occurrences of VLP signals with closely matched waveform characteristics are consistent with a non-destructive reactivation of at least two sources. One source appears to coincide with the main source region of LP seismicity, while the second is a deeper source whose activity appears to be intimately linked with episodes of monochromatic tremor.

**Key words** Volcanic eruption, volcanic seismic signals, long-period events, tremor, very-long period signals, Popocatepetl.

## Introduction

Popocatepetl is a large, partly glacier clad composite andesitic volcano. With a summit elevation of 5452 m, Popocatepetl is located 60 km southeast of Mexico City on the volcanic front of the central Mexican magmatic arc. Since December 1994, eruptive activity at Popocatepetl has been dominated by passive fumarolic emissions interrupted by more energetic emissions of ash and gas through vents in the summit crater and passive lava effusions leading to the formation of lava domes within the crater. The first dome associated with the current eruptive phase was observed in March 1996. This dome was subsequently destroyed in a vulcanian explosion on April 30, 1996. Since then, eruptive activity has been marked by a sequence of repetitive dome-building and dome-destroying episodes that is still ongoing today.

The most common eruptive activity consists in emissions of steam and ash including both old and juvenile materials. These emissions can range in intensity from small short-lived plumes rising a few hundred meters above the crater rim, to larger events producing plumes that may reach up to 5,000 m above the crater and blanket the entire summit area with ejecta. These emissions are referred to as "exhalations" (S. de la Cruz, personal comm.) and may occur as isolated events or as sequences of discrete events with overall durations of venting lasting up to 600 s.

We classify the seismic signals observed at Popocatepetl according to a scheme first proposed by Lahr *et al.*, [1994] and Chouet [1996]. This scheme is based on the physics of the source process and includes two fundamental families of events. The first family consists of volcano-tectonic (VT) earthquakes representing the brittle response of volcanic rocks to stresses induced by fluid movements within the volcanic edifice. The second

family includes long-period (LP) events and tremor, collectively grouped under the common appellation of LP seismicity and representing volumetric sources driven by pressure disturbances associated with the flow of magmatic and/or hydrothermal fluids [Chouet, 1996].

In the seismic records from Popocatepetl, "exhalations" are observed to correlate in time with LP events and tremor and are usually characterized by very emergent onsets. While individual LP events never exceed 3-min in duration, tremor may last from 3-15 min to several days. Observations from many volcanoes around the world indicate that LP and tremor share similar spectral features with typical periods in the range 0.2-2 s [Chouet, 1996]. A common generation mechanism of acoustic resonance in a fluid-filled conduit excited by a pressure disturbance in the fluid has been invoked to explain these features [Chouet, 1985, 1986, 1988, 1992, 1996; Chouet *et al.*, 1994; Gil-Cruz and Chouet, 1997; Garces and McNutt, 1997].

Different features of tremor are commonly associated with different types of volcanic activities [*e.g.*, McNutt, 1992]. At Stromboli, Italy, tremor originates in the disruption of the fluid column resulting from bubble oscillations and bubble bursts during steady degassing [Chouet *et al.*, 1997] and is present as a persistent background signal that may last for weeks or months [Falsaperla *et al.*, 1998]. At Redoubt, Alaska, tremor was observed to result from the merging of individual events in the intense LP event swarm that preceded the December 14, 1989 eruption of this volcano [Chouet *et al.*, 1994]. At Merapi, tremor is commonly associated with lava-dome building phases [Seidl *et al.*, 1990]. Features similar to those seen in tremor at Redoubt and Merapi have also been observed in tremor at Popocatepetl depending on the eruptive behavior of the volcano. Persistent tremor was first observed 22 hours after the onset of the eruptive activity that marked the reawakening of Popocatepetl on 21 December 1994. From December 1994 through

March 1995, sustained tremor was observed to persist for weeks before eventually breaking into a pattern of intermittent discrete episodes. During times of tremor intermittence, swarms of LP events were also observed to merge into sustained tremor [Arciniega *et al.*, 2000]. This particular type of tremor was noted during several episodes of activity over the past five years. Sustained tremor also occurred during the emplacement of lava domes in March 1996 and February 2000. Another distinct kind of tremor seen at Popocatepetl is a sporadic tremor displaying a quasi-monochromatic spectrum. This type of tremor has occurred both before and after large ash emissions and explosive events.

Recent broadband observations at Sakurajima and Aso, Japan [Kawakatsu *et al.*, 1992, 1994, 2000; Kaneshima *et al.*, 1996; Legrand *et al.*, 2000], Satsuma-Iwojima, Japan [Ohminato and Ereditato, 1997; Ohminato, 1998], Iwate, Japan [Nishimura *et al.*, 2000], Miyake Island, Japan [Kumagai *et al.*, 2001], Stromboli, Italy [Neuberg *et al.*, 1994; Chouet *et al.*, 1999], Merapi, Indonesia [Hidayat *et al.*, 2001], Kilauea, Hawaii [Dawson *et al.*, 1998; Ohminato *et al.*, 1998], and Mount Erebus, Antarctica [Rowe *et al.*, 1998], demonstrate the ubiquitous nature of VLP signals under a variety of volcanic conditions. Put together, LP and VLP seismicities provide the most accurate and complete view of mass transport dynamics under a volcano.

At Popocatepetl, VLP signals have been observed to systematically accompany vulcanian explosions [Arciniega *et al.*, 1999]. VLP signals accompanying LP events were also reported by Arciniega *et al.* [1999]. However, a more complete study of VLP signals associated with LP events at Popocatepetl has yet to be done and is the purpose of the present paper. As broadband data from Popocatepetl are limited to a single three-component station, quantitative modeling of these data cannot be performed. Accordingly, we restrict our presentation to a description of two fundamental aspects of seismic activity at Popocatepetl. First, we provide a detailed description of the temporal sequence of the LP

events, tremor episodes, and other relevant signals accompanying volcanic phenomena observed at the surface, and second, we describe the spectral properties and particle motion characteristics of LP events and tremor together with the properties of their associated VLP signals. Phase pick locations obtained for a few of the most commonly observed LP events recorded on the Popocatepetl short-period network provide rough estimates of the hypocentral locations of LP seismicity, which are compared to locations based on VLP particle motions obtained with the broadband station.

## Data

The broadband data used in this study were recorded on a single three-component station (PPIG) featuring a Streckheisen STS-2 seismometer (0.05–120 s) and Quanterra Q680 LT/G 24-bit digital data acquisition system providing a dynamic range of up to 140 dB. The station is located at Cerro Tlamacas on the north flank of Popocatepetl at an altitude of 4000 m and distance of 5 km from the active crater (Fig. 3.1). Data are radio transmitted to the campus of the Universidad Nacional Autonoma de Mexico (UNAM) in Mexico City, where they are automatically recorded both in continuous mode at 1 sps and in triggered mode at 80 sps. The latter sampling frequency provides a useful signal bandwidth of 0.01–20 Hz. Also, continuous records at 20 sps can be obtained if needed. Station PPIG is part of the national broadband network and is primarily configured in trigger mode for earthquake monitoring purposes. Therefore, most of the Popocatepetl data readily available from this site since August 1996 consists of triggered records at 80 samples/s.

Also installed at Cerro Tlamacas is a digital three-component short-period station

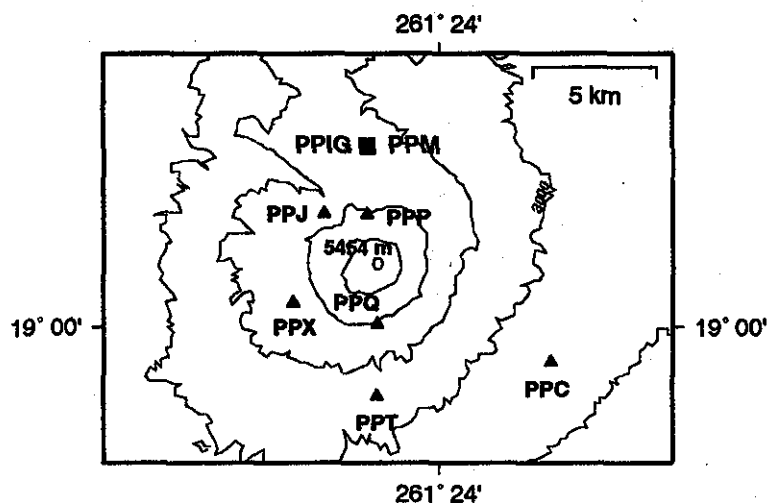


**Fig. 3.1** Map of Popocatepetl Volcano, Mexico. Solid triangles mark stations of the short-period seismic monitoring network. A solid square identifies the broadband seismic station PPIG, which is co-located with station PPM. Contours represent 600 m elevation intervals.

(PPM) in operation since 1989 and belonging to the permanent seismic network of Popocatepetl. Records from PPM provide another source of information from which a quick overview of seismic activity at Popocatepetl can be obtained. Analog records from PPM were used to estimate the daily rate of occurrence of seismic events and to discriminate between LP events, VT earthquakes, volcanic tremor, and explosions.

A third source of information is from the permanent short-period Popocatepetl monitoring network, which features seven Mark Products L-4C seismometers with natural periods of 1 s (Fig. 3.1). Data from this network are transmitted by radio telemetry to the Centro Nacional de Prevencion de Desastres (CENAPRED) in Mexico City. This network was primarily designed to locate deep (2-10 km depth) VT seismicity with clear impulsive P-wave arrivals at each station. Monitoring LP seismicity with this network is, however, hampered by several limitations. First, the number of stations within 5 km of the crater

is limited to five, which is only marginally sufficient to accurately document emergent signals accompanying ash and gas emissions. Second, in general horizontal-components are saturated so that accurate identification of shear phases can not be guaranteed. And third, there is no station coverage on the east flank, which makes the location of shallow events even more problematic. Because of these limitations only marginal use is made of data from the short-period network. Among the hundreds of events recorded on this network, we selected a subset of on-scale LP signals with good signal-to-noise ratios to estimate their source locations using a standard phase pick procedure.

## Observed eruptive activity and seismicity

Figure 3.2 summarizes the eruptive and seismic activities observed at Popocatepetl during the period September 1994 through May 2000. The graphs show the details of the activities of different types of events and provide an overview of the eruptive behavior at Popocatepetl. Figure 3.2a shows daily counts of LP events (in blue) and total duration of tremor per day (in red) based on horizontal-component records obtained at PPM. Episodes of harmonic tremor are indicated by green stars, and visually observed domes and explosions are indicated by arrows above the plot. Figure 3.2b shows the cumulative numbers of LP events (solid line) and cumulative number of VT events (dotted line) versus time. Different phases of activity can be identified based on the common occurrence of seismic signals together with visual observations of ash and gas emissions. Is notorious, the persistent low activity of VT events contrasting the high rates of LP event production. All the VT activity observed at Popocatepetl originates at depths of 2-10 km beneath the crater [Arciniega *et al.*, 2000]. The cumulative number of VT event production is characterized by smooth changes interrupted by four slopes, while no less than six distinct

gradients are distinguishable in the cumulative number of LP events. The latter higher slopes correlate closely with changes in eruptive activity as discussed in more detail below.

The first distinct eruptive phase begins on 21 December 1994 and ends on 30 March 1995. This phase is characterized by an average rate of 0.9 VT events per day (Fig. 3.2b) and by tremor initially of sustained character but which eventually breaks into intermittent episodes of tremor resembling sequences of closely spaced LP events. The latter tremor episodes are intimately linked to intermittent ash and fumarolic emissions. The previous average rate of LP event occurrence remains at 5 events per day between early September and early October, 1994, then increases to an average rate of 22 events per day by mid October, 1994. This LP activity is accompanied by mild fumarolic emissions. On 21 December 1994 a phreato-magmatic eruption (S de la Cruz, pers. comm.) marks the initial of a new stage in Popocatepetl eruptive history.

From April 1995 through February 1996, the seismicity consists of a low background of VT activity (0.14 event per day), low levels of LP activity (averaging 7.3 event per day), and a complete absence of tremor.

From early March through mid-September 1996, eruptive activity is dominated by the emplacement of a lava dome in the crater. This effusion of lava is accompanied by 4.05 days of sustained tremor in early March. Following this tremor episode, high rates of LP event production occur, averaging 130 events per day and reaching a peak of 237 events on August 16, 1995. VT activity increases slightly to 0.5 event per day in mid July.

By September 14, 1996, sustained tremor episodes lasting up to 15 hours begin again. LP events average 40 events per day through December 1997, while the rate of VT event

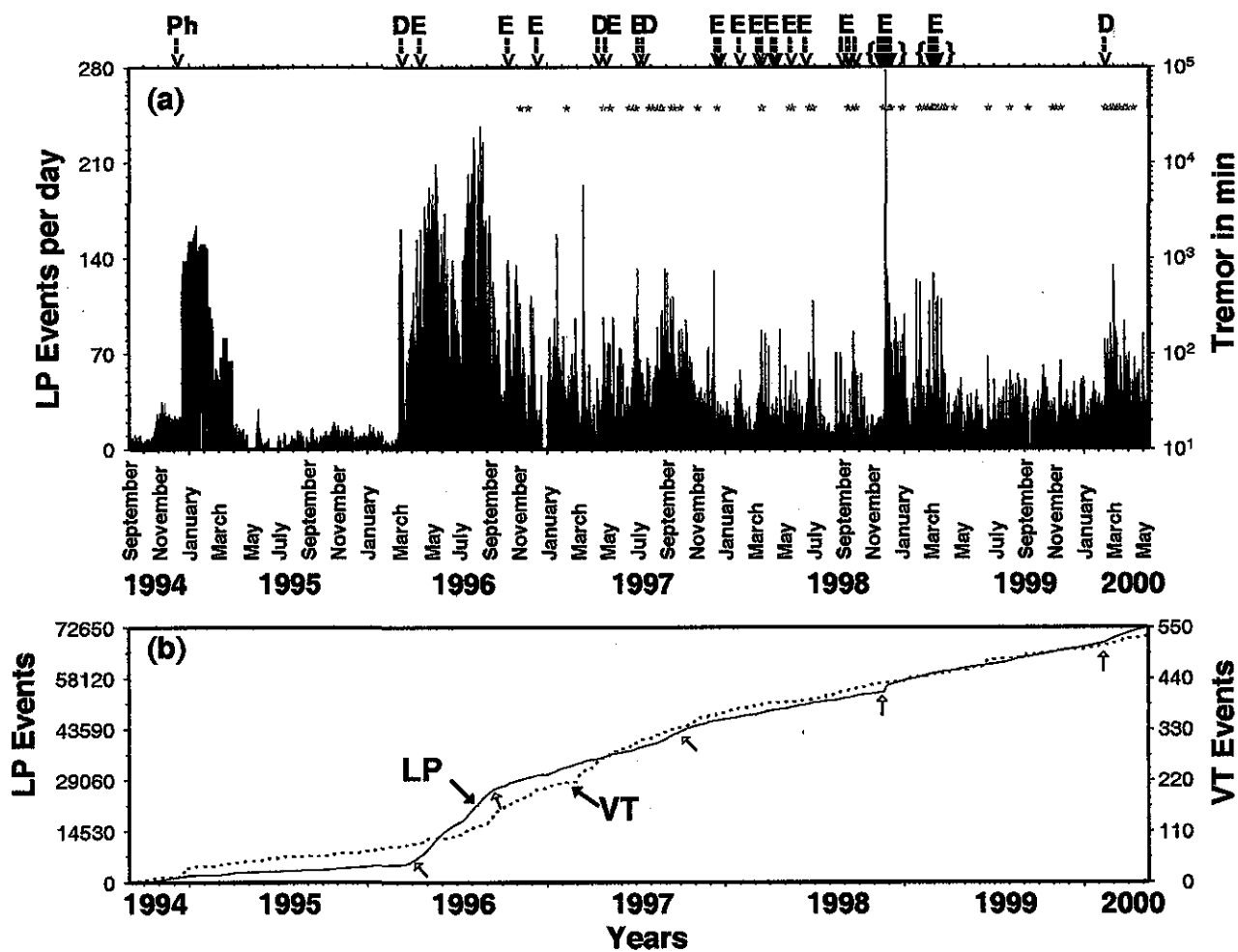


**Fig. 3.2** Seismicity observed at Popocatepetl from September, 1994 through May, 2000.

(a) Number of LP events per day (in blue) and total duration of tremor episodes per day (in red). Arrows above the plot mark vulcanian explosions (E), phreatic explosions (Ph), and visual observations of new domes (D) in the crater. Green stars indicate the presence of monochromatic tremor episodes. (b) Cumulative number of LP events (solid line) and VT events (dotted line). Transparent arrows mark some changes in slope.

production remains essentially unchanged. A second dome growth episode start. Sporadic episodes of quasi-monochromatic tremor are observed for the first time in early November. Eruptive activity is dominated by large sustained emissions of ashes and gases. The largest ash plume occurs on 30 June 1997 and reaches an altitude in excess of 12,000 m.

From late December 1997 through late October 1998, explosive events accompanied by large tephra eruptions become more frequent. This time interval is marked by a decrease in LP activity (averaging 30 event per day), sporadic episodes of harmonic and non-harmonic tremor, and a decrease in VT activity (averaging 0.19 event per day).

Between November 1998 and March 1999, seismic activity is dominated by strong episodes of harmonic tremor and explosions marking the destruction of lava domes. As many as 24 vulcanian explosions occur during a three-week interval in late November and early December 1998. Ash eruptions accompanied by strong bursts of tremor increase in size and number throughout this phase. A sustained background of harmonic tremor is also present. LP activity averages 34 events per day during the first 45 days, and peaks at 278 events on November 23. By mid-April 1999, LP activity decreases to 29 events per day and then remains stable at this rate during the next 10 months. VT activity remains comparatively low.

The next phase of activity starts in early February 2000 and runs through the end of the reporting period. LP activity increases in early February and then remains roughly constant with an average of 43 events per day throughout this interval. Frequent episodes of harmonic tremor are also observed, and eruptive activity is dominated by steam and ash emissions reaching altitudes up to 10,000 m.a.s.l. The presence of a new lava dome is visually confirmed by CENAPRED on February 25, 2000. No changes in the rate of VT occurrence are noted.

The data in Figure 3.2 indicate that the majority of LP events and tremor episodes observed at Popocatepetl are related to gas and ash emissions and dome growth episodes. Figure 3.2 also shows that eruptive activity becomes more explosive with time through March 1999, suggesting the involvement of more viscous magma and/or a faster rate of magma production. Following a high rate of explosive activity in late 1998 and early 1999, vulcanian explosions cease to occur and a long interval of repose ensues, interrupted by occasional emissions of steam and ash. This quiet phase persists through the end of the period reported in this study. A new lava dome, first observed in the crater in February 2000, points to a resumption of more pronounced eruptive activity and suggests that other vulcanian explosions are likely to occur at Popocatepetl in the near future.

## Description of LP events and tremor

LP events at Popocatepetl are characterized by emergent onsets and harmonic signatures with dominant frequencies below 5 Hz. A few events display quasi monochromatic signatures and another few are characterized by exponentially decaying coda. These features are quite similar to those seen in LP events at other active volcanoes [Chouet *et al.*, 1994; Kumagai and Chouet, 1999]. Using digital broadband data from PPIG available after August 1996, we selected LP signals based on the following three criteria: (1) the events display the characteristic features of LP signals described above; (2) visual observations indicate that the seismic signals are associated with fumarolic activity and/or more energetic emissions of gas and ash; and (3) the signals have a signal-to-noise ratio of at least 3.

Figure 3.3 illustrates three types of LP signatures commonly observed at Popocatepetl

## Broadband characteristics of LP and tremor

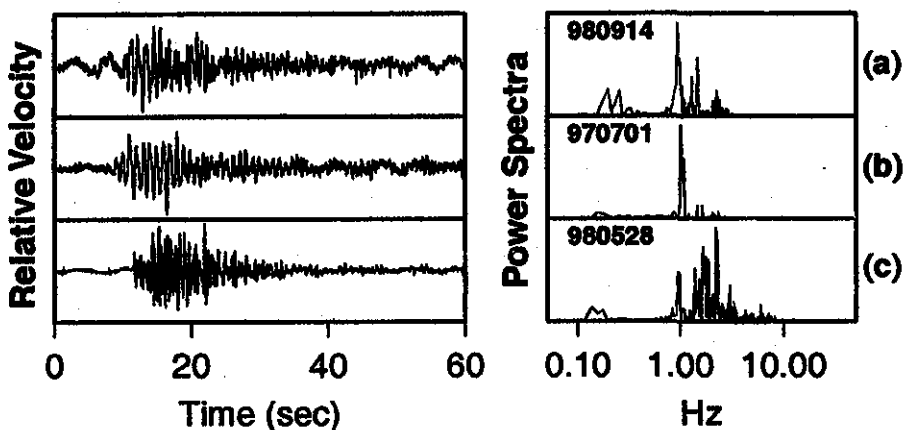
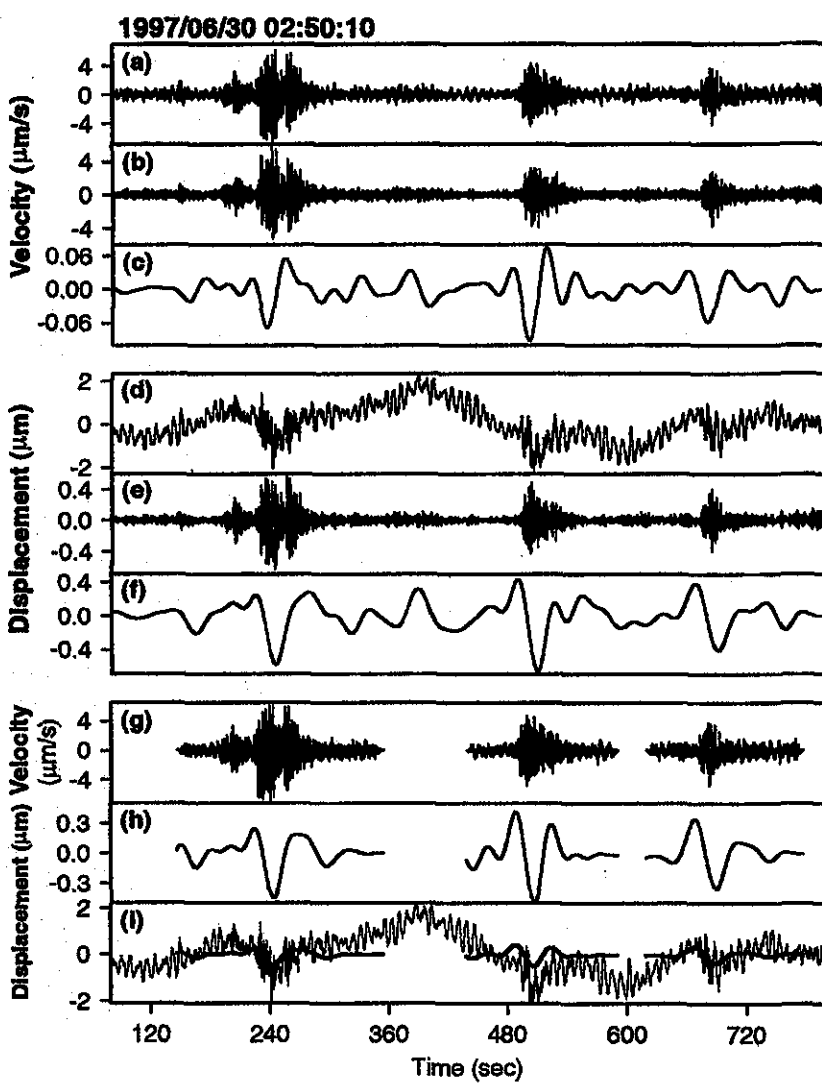


Fig. 3.3 Typical signatures (vertical velocity component) of LP events associated with ash and/or gas emissions, and corresponding normalized power spectra calculated over the same 60-s-long window. The date of each record is indicated at the upper left corner of the corresponding spectrum. (a) Features of most common LP events observed at Popocatepetl. (b) Example of monochromatic LP signal. (c) Example of event displaying a higher frequency content.

along with their associated power spectra. Spectral peaks below 0.5 Hz represent oceanic microseismic noise [Arciniega *et al.*, 1999, 2000], and spectral peaks in the 0.5-3.0 Hz band represent the volcanic signal. The LP signals can be characterized according to their frequency content. The first type of LP event (Fig. 3.3a) displays dominant spectral peaks in the 0.5-3.0 Hz band and is the most common LP event observed at Popocatepetl. The second type is characterized by a harmonic signature and quasi-monochromatic spectrum with a dominant peak near 1 Hz (Fig. 3.3b). The third type (Fig. 3.3c) is marked by sustained higher frequencies near the signal onset, and is also dominated by spectral peaks in the 0.5-3.0 Hz band. Common spectral peaks are observed among these events, particularly in events of type 1 and type 3. The amplitudes of the common peaks varies for different events, suggesting these may represent different excitations of a common source.

A broadband record and filtered versions of this record obtained at station PPIG on 30 June 1997, shown in Fig. 3.4, illustrate the broadband characteristics of the signals associated with LP events. The top three panels show, from top to bottom, the vertical component of raw velocity data (Fig. 3.4a), the short-period record obtained after filtering the broadband record with a 1-Hz high-pass filter (Fig. 3.4b), and the VLP record obtained after band-pass filtering the raw signal in the band 0.01-0.04 Hz (Fig. 3.4c). Figures 3.4d, 3.4e, and 3.4f show the displacement records obtained by integrating the velocity records in Figures 3.4a, 3.4b, and 3.4c, respectively. The 0.01-0.04 Hz band-pass filter allows the removal of energy due to the oceanic microseismic noise, as well as energy contained in the LP band. Although VLP energy was not readily identified in the spectra of Figure 3.3 due to the short length (60 s) of the window used to generate these spectra, the presence of VLP signals is clear in Figures 3.4c and 4f. Both VLP velocity and displacement records display a repetitive Ricker-like wavelet with period near 36 s that provides a clear indication of the repeated action of a non-destructive source.

When station PPIG is configured in trigger mode, data are digitized at 80 samples/s and records of individual LP events are mostly limited to 200 s in length, although tremor sections of up to 10-min duration can be obtained. While the duration of the triggered time series of LP events are not long enough to accurately quantify the energy contained in the VLP band, VLP energy is still clear in all the triggered records. To demonstrate this, we show in Figure 3.4g the triggered records for the LP events displayed in Figure 3.4a. Figure 3.4h shows the 0.01-0.04 Hz band-passed records of ground displacements obtained from the 200-s-long records displayed in Figure 3.4g, and Figure 3.4i compares the continuous broadband displacement record in Figure 3.4d with the VLP displacements in Figure 3.4h. Although the Ricker-like wavelets in Figures 3.4f and 3.4h differ in details, the periods of the dominant pulses are the same in both figures and, as shown in Figure 3.4i, the VLP displacements calculated from the shorter windows match the VLP components



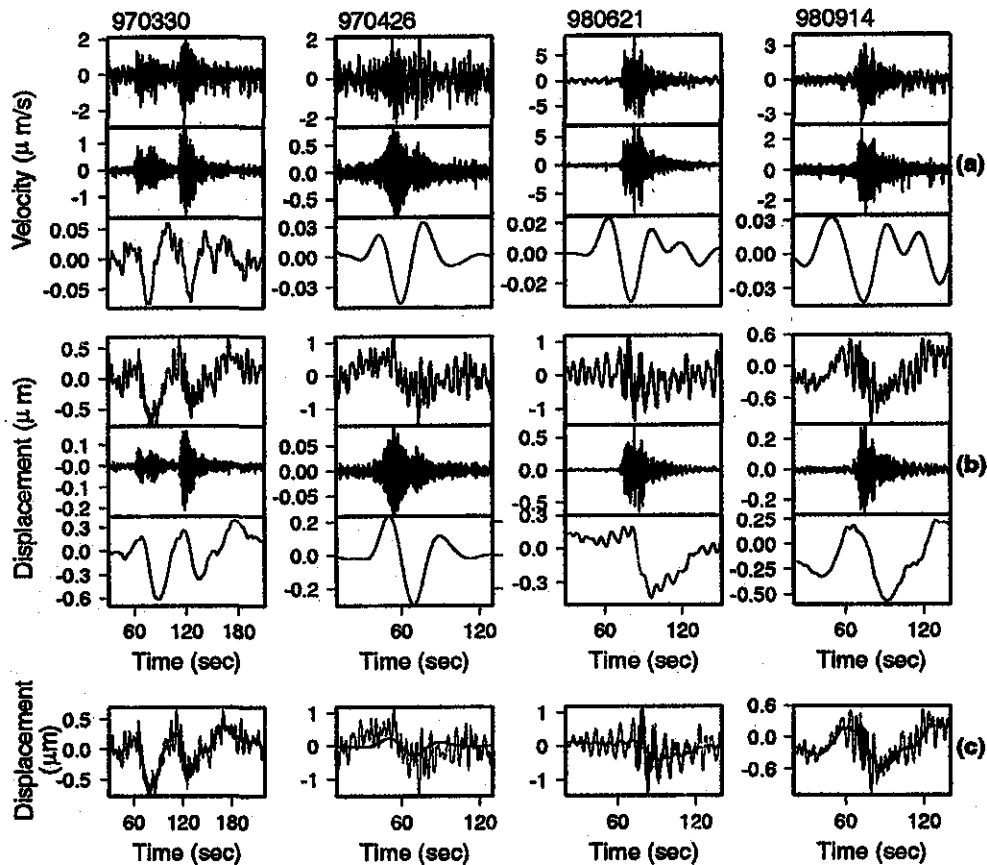
**Fig. 3.4** (a) Sample of vertical component of velocity obtained in continuous recording mode at 20 samples/s, showing a sequence of LP events on June 30, 1997. (b) short-period record (analogous to that written by a short-period seismograph) obtained after filtering the raw record in (a) with a 1-Hz high-pass filter. (c) Very-long period record obtained after applying a 0.01-0.04 Hz band-pass Butterworth filter to the raw record in (a). (d), (e), (f) Displacement records obtained by integrating the traces displayed in (a), (b), (c). (g) Vertical records of raw velocity obtained in trigger recording mode at 80 samples/s for the LP events displayed in (a). (h) Band-pass filtered (0.01-0.04 Hz) ground displacements obtained from the records in (g). (i) Comparison of band-pass filtered displacements in (h) (solid line) with the continuous broadband record of displacement displayed in (d) (dotted line).

of each individual event in the raw displacements calculated from the continuous record. Therefore, VLP records derived from the shorter triggered windows adequately reproduce the overall characteristics of the VLP signals extracted from the continuous record, giving us confidence in the VLP results derived from triggered data.

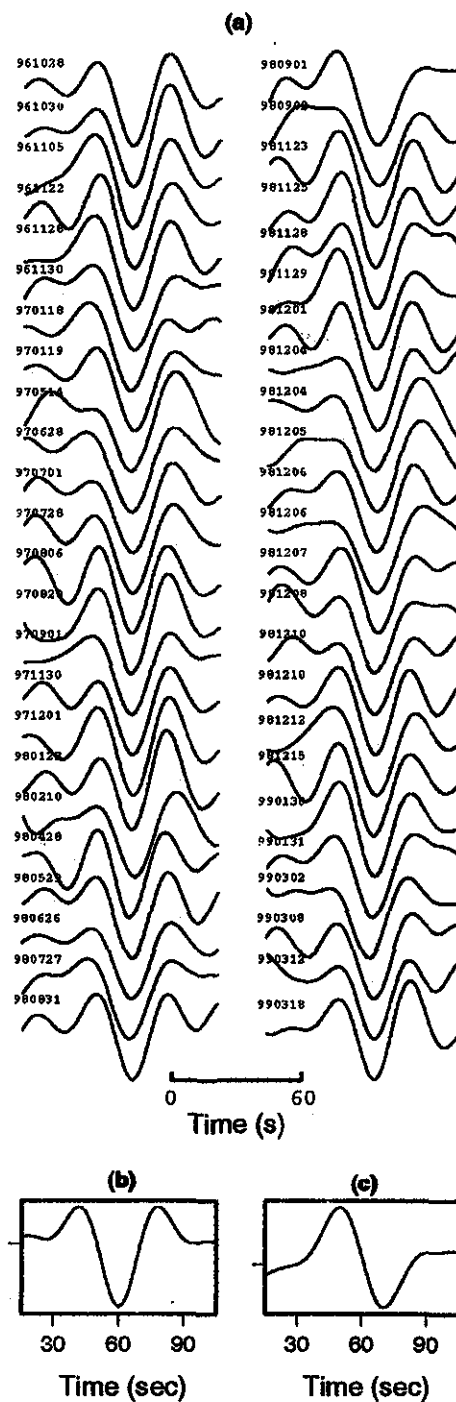
Triggered records of LP events were analyzed using the procedure illustrated in Figure 3.4. Figures 3.5 *a-c* shows examples of LP events considered in our analyses. Figures 3.5*a*, and 3.5*b*, respectively, show the vertical components of velocity and displacement for each triggered record, with each panel displaying from top to bottom, the broadband signal, short-period signal obtained by filtering the broadband signal with a 1-Hz high-pass filter, and VLP signal obtained by filtering the broadband signal with a 0.01–0.04 Hz band-pass filter. Figure 3.5*c* compares the broadband and VLP displacement traces, demonstrating that the VLP waveforms faithfully track the gross features of the raw data and underlying the suitability of the filter used to identify VLP signals.

The record on 30 March 1997 shows two LP events occurring in rapid succession (Fig. 3.5), each accompanied by a VLP wavelet. Similar VLP waveforms are observed to accompany other LP events in Figure 3.5. Notice that although the LP event on 26 April 1997 is completely buried in microseismic noise in the raw data trace, this event contains a clear VLP signal whose magnitude is comparable to those of the VLP signals accompanying the other LP events shown in the figure. These results show that the VLP signals are intimately related to these LP events.

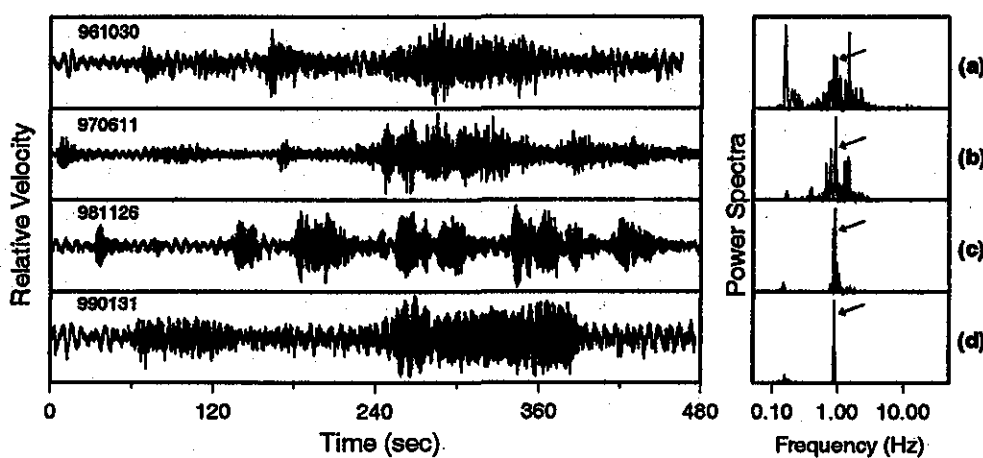
Using the same filtering method, we analyzed several hundred LP events sampling the period 1994–2000. The results from these analyses match those displayed in Figures 3.4 and 3.5 and consistently demonstrate that LP and VLP signals are closely related. The VLP velocity waveforms extracted from these data all show periods near 36 s (Fig 3.6a).



**Fig. 3.5** Samples of vertical-component records of LP events, together with filtered traces obtained from these records. The date of each record is indicated above the left upper corner of the top panel displaying the event. (a) Velocity records showing broadband data (*top*), 1-Hz high-pass filtered traces (*middle*), and 0.01-0.04 Hz band-pass filtered traces (*bottom*). (b) Displacement records obtained by integrating the records shown in (a). (c) Comparison between the raw displacement records (*top traces in (b)*) and the corresponding band-pass filtered traces (*bottom traces in (b)*). High levels of noise in the raw data traces are due to the oceanic microseismicity.



**Fig. 3.6** (a) 48 VLP signals associated with LP events. The traces are filtered in the 0.01-0.04 Hz band and individually normalized in amplitude. The date of occurrence is indicated at the upper left of each signal. (b) Stack of the 48 velocity records. (c) Stack of the corresponding displacement records.



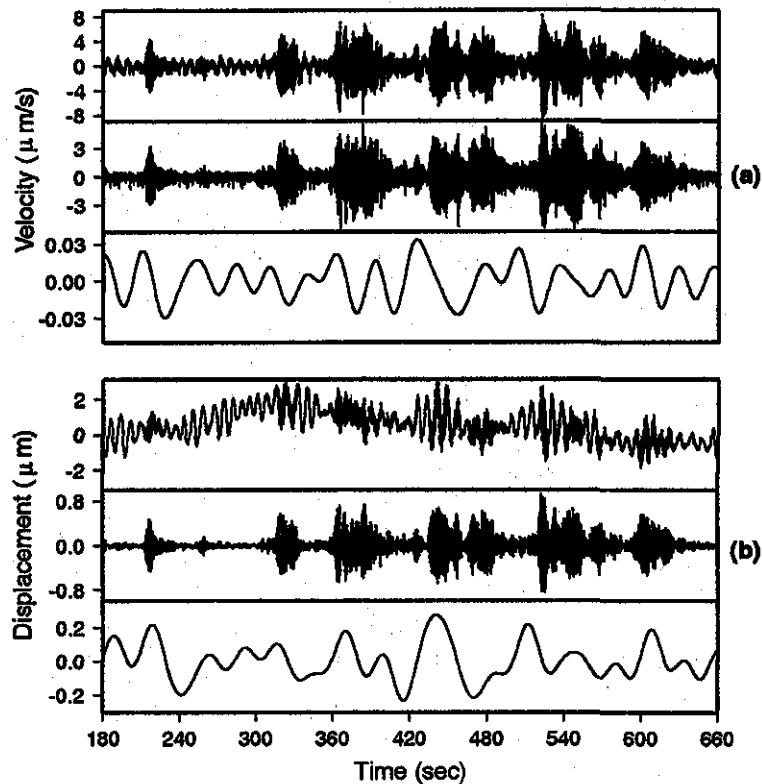
**Fig. 3.7** Seismograms of typical tremor episodes and corresponding normalized power spectra. Both seismograms and spectra are obtained over an 8-min-long window. The date of each record is indicated at the upper left of each seismogram. The vertical velocity records illustrate a variety of tremor signals; (a) and (b) show examples of tremor with several overtones; (c) illustrates a swarm of LP events leading to sustained tremor with quasi monochromatic characteristics; and (d) shows monochromatic tremor. The arrows in the spectra point to a common peak shared by the different tremor episodes. This spectral peak is suggestive of the presence of a common source.

Figure 3.6*b* shows the stack of the 48 VLP velocity wavelets, and Figure 3.6*c* shows the corresponding VLP displacement stack. The velocity stack clearly shows a Ricker-like wavelet with dominant period of 36 s, and the displacement stack roughly mimics a sawtooth waveform.

The criteria used to select LP events (see above) were also applied to select tremor episodes for analysis. Figure 3.7 shows examples of broadband records for different tremor episodes. Figures 3.7*a* and 3.7*b* show samples of harmonic tremor with distinct overtones, Figure 3.7*c* displays a swarm of LP events producing a tremor-like signal with a quasi monochromatic spectrum, and Figure 3.7*d* illustrates a burst of monochromatic tremor.

The noisy background is due to the oceanic microseism. As observed for LP events in Figure 3.3, two distinct bands of energy are apparent in the tremor spectra. The first band extends over the range 0.5-3.0 Hz and contains multiple narrow-band spectral peaks associated with volcanic tremor, while the second contains spectral peaks in the range 0.1-0.5 Hz representing oceanic microseismic noise [Longuet-Higgins, 1950]. Although present, VLP energy is not emphasized in these spectra because of its small spectral amplitude relative to those of the oceanic and/or short-period components of the signal. Most tremor at Popocatepetl appears in the form of either sustained or sporadic signals, or rapid-fire LP events producing a tremor-like signal with characteristics similar to those displayed in Figure 3.7. As in LP events (Fig. 3.3), the amplitude fluctuations of the stationary dominant spectral peak of tremor observed at frequency near 1 Hz are strongly suggestive of the repeated non-destructive excitation of a fixed source beneath the crater of Popocatepetl.

VLP signals were also observed in association with tremor. The filtering technique used for LP events (Fig. 3.4) was applied to tremor episodes having a minimum sustained amplitude of 3 microns/s peak-to-peak in the raw velocity records and lasting at least 400 s. Figures 3.8 and 3.9 show two examples of tremor records together with filtered versions of these records. Figure 3.8 illustrates a 480-s-long record displaying a swarm of LP events merging into tremor, and Figure 3.9 shows of 480-s-long burst of monochromatic tremor. In both figures the signal of volcanic origin is greatly enhanced by filtering out the oceanic microseism, which represents the dominant component of background noise. A sustained VLP signal with periods of 30-90 s is observed along with both types of tremor. Although individual VLP pulses are not readily identified, probably because of the rapid-fire bursts of energy observed in the short-period records, larger VLP amplitudes are observed to coincide with at least some of these energy bursts. These features of the VLP signals are most obvious in the displacement records. In Figure 3.8, for example, the



**Fig. 3.8** Tremor episode displayed in Figure 3.7(c) plotted together with filtered traces obtained from this record. (a) Vertical velocity records showing broadband data (*top*), 1-Hz high-pass filtered trace (*middle*), and 0.01-0.04 Hz band-pass filtered trace (*bottom*). (b) Displacements obtained by integrating the records in (a).

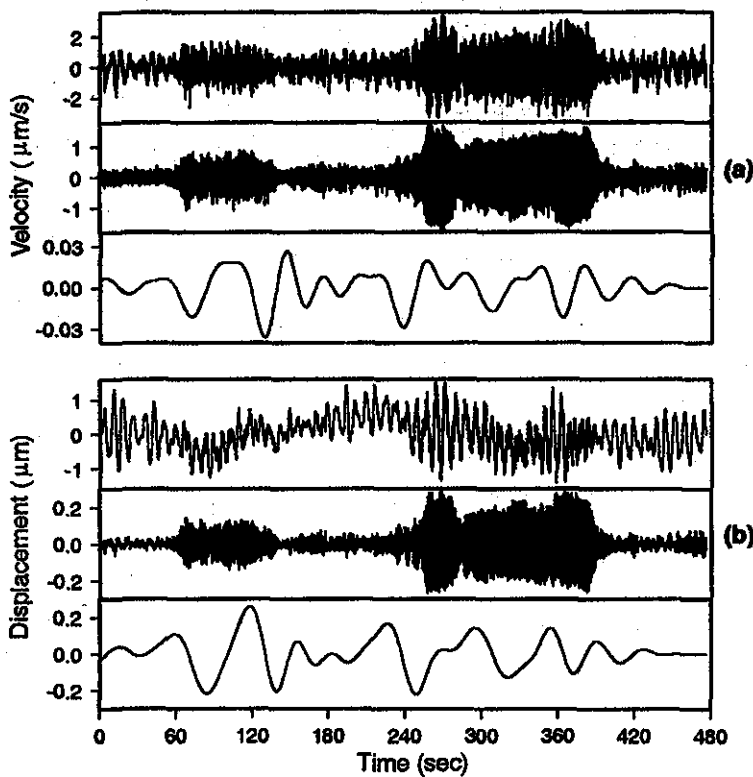


Fig. 3.9 Same as Figure 3.8 for the monochromatic tremor displayed in Figure 3.7(d).

largest VLP displacement amplitudes appear to coincide with the first three LP events displayed in the broadband record and also with the most intense burst of LP activity in the second half of this record. The same characteristics are observed in Figure 3.9 where the largest VLP displacements are roughly synchronous with the two bursts of short-period monochromatic tremor. Except for weak volcanic signals, whose lack of energy did not allow their extraction from the microseismic noise, VLP signals were found to be consistently present in all the tremor and LP events analyzed since August 1996.

Particle motion analyses were also carried out for VLP signals. Figure 3.11 shows the particle motion trajectories of displacement obtained in the band 0.01-0.04 Hz for the signals displayed in Figure 3.10. The trajectories in the vertical-radial plane are domi-

nated by nearly linear motions, while trajectories in the horizontal plane display a more complicated pattern. The patterns in Figure 3.11a appear to point to a source east of Popocatepetl at a depth of about 1 km below the crater floor. In contrast, the VLP signals in Figures 3.11b and 11c consistently point in the direction of Popocatepetl. The data in Figure 3.11b suggest a source location 1 km beneath the crater, and the data in Figure 3.11c suggest a deeper source, perhaps as deep as 6 km below the crater. Interestingly, the patterns of particle motions shown in Figures 3.10c and 3.11 c are intimately linked with episodes of monochromatic tremor (see Figs. 3.7d and 3.9), suggesting a deeper source origin for monochromatic tremor compared to other LP and tremor signals. Unfortunately, as our broadband data are limited to a single station, VLP source locations can not be further constrained and neither can we derive a more detailed physical model of the source based on these data.

## Discussion

The essential spectral features of LP events and tremor displayed in Figures 3.3 and 3.7 have remained unchanged since the onset of eruptive activity at Popocatepetl in December 1994. Oceanic microseismic noise typically dominates the signal in the 0.1–0.5 Hz band, while spectral peaks above 0.5 Hz are commonly associated with volcanic activity. Both tremor and LP events display dominant spectral peaks near 1 Hz with overtones near 1.5 and 2 Hz. The peak frequencies remain stable with time while the peak spectral amplitudes are observed to vary for different LP events and for distinct tremor episodes. These results are consistent with a generation mechanism involving a non-destructive resonant excitation of a stable fluid-filled cavity beneath the crater of Popocatepetl [Chouet, 1996]. The observed stability of the resonant frequencies further suggests that the fluid composition controlling the acoustic properties of the resonator also remains stable with time. Accordingly, the observed variations in the spectral amplitudes of the resonant peaks may be explained by variations in the spatio-temporal properties of the pressure disturbances triggering the excitation of the fluid-filled resonator [Chouet *et al.*, 1994; Morrissey and Chouet, 1997; Kumagai and Chouet, 2000].

No peaks are apparent at frequencies below 0.10 Hz in the spectra of Figures 3.3 and 3.7, in part because the energy content of the VLP signals is small in comparison to the energy contained in both microseismic noise and short-period components of the signal, and also because the triggered windows used to generate these spectra are too short to emphasize the energy contained in the VLP band. Although of small amplitudes compared to the microseismic and short-period signals, the VLP signals become obvious once the former signal components are removed by filtering. The VLP signals identified in this manner are correlated with LP and tremor signals, and thus are clearly of volcanic

origin (see Figs. 3.4, 3.5, 3.8 and 3.9).

The similarities in spectral characteristics shared by LP events and tremor are strongly suggestive of a common source. This idea is further supported by particle motion analyses, which show similar particle trajectories for LP and tremor signals. Figures 3.10a and 3.10b illustrate typical patterns of particle motions exhibited by the majority of LP and tremor signals within the 0.5-5 Hz band. Particle motions observed at PPIG in both vertical-radial and horizontal planes define narrow elliptical trajectories with coincident patterns and main axis orientations dipping to the southeast. Only a few events do not fit this common pattern shared by LP events and tremor (Fig. 3.10c). These exceptional events appear to have a distinct source origin deeper beneath Popocatepetl as discussed below.

The repeating elliptical trajectory of the particle motions seen in Figure 3.10 requires a source that radiates sustained harmonic *SH* and *SV* waves [Nuttli, 1961; Chouet *et al.*, 1997] and provides constraints on the geometry and position of the source. A vertical pipe can only radiate *P* and *SV* waves, and a spherical source can only produce *P* waves. In contrast, a vertical crack is an excellent radiator of *P*, *SV* and *SH* waves, and acoustic resonance of a fluid-filled vertical crack will naturally generate sustained harmonic waves of these types [Chouet, 1988; Chouet *et al.*, 1997]. For example, Chouet *et al.* [1997] made a detailed comparison of particle motions observed during a Strombolian explosion with synthetic particle motion trajectories produced at the free surface by the excitation of a vertical fluid-filled crack embedded in a homogeneous half space. In this model the elliptical trajectory of particle motion results from the interaction of incident *SH* and *SV* waves radiated by the sustained vertical and horizontal modes of resonance of the source. The optimum conditions leading to this free surface effect occur within a narrow angular range of wave incidences. At PPIG, this situation is best satisfied for a shallow source beneath the crater of Popocatepetl.

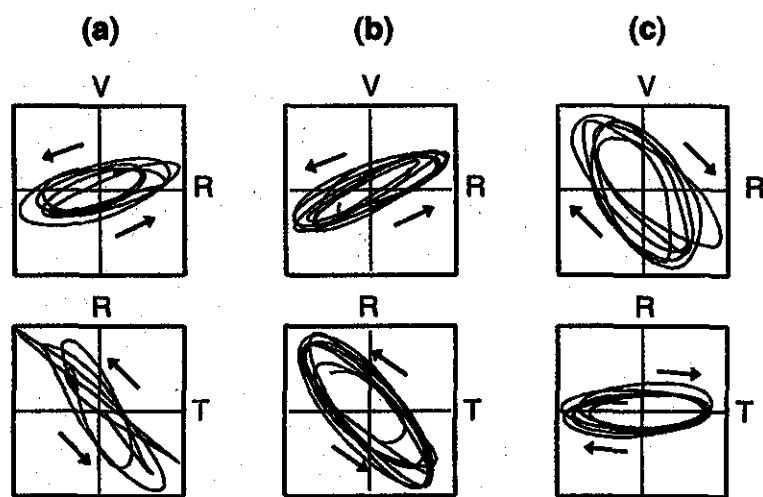


**Fig. 3.10** Particle trajectories of displacement obtained in the 0.5-5 Hz band for a LP event on March 26, 1997 (a), and tremor episodes on November 26, 1998 (b) and February 2, 1999 (c). The trajectories are plotted in the radial-vertical and horizontal planes in which the radial and transverse directions represent the N-S and E-W directions (see Fig. 3.1). Arrows indicate the direction of motion; (a) and (b) illustrate typical particle motion trajectories observed in the majority of LP events and tremor signals recorded at Popocatepetl; (c) shows an exceptional event which does not fit the pattern observed for the majority of LP and tremor events.

Using data from the short-period network to supplement the broadband data from PPIG we can obtain additional rough constraints on the source locations of LP signals. The emergent characteristics of these signals prevent the consideration of more than a few LP events for location. We used a standard phase pick procedure and location routine *gloc* [Julian, in preparation] to estimate the hypocenters of 65 LP events representing a sample of the most commonly observed LP signals at Popocatepetl. Figure 3.12 shows the hypocentral locations determined with a velocity model consisting of three flat layers with compressional wave velocities and thicknesses of 3.5 km/s, 5.5 km; 4.5 km/s, 0.5 km; and 5.0 km/s, 6.0 km, from top to bottom respectively. The scatter in individual event locations is the result of poor station coverage, uncertainties in velocity structure, and emergent characteristics of first arrivals detected by the receivers. Although location errors are quite large (on the order of 1 km), the source region outlined by hypocenters is confined within a restricted zone at shallow depths beneath the crater of Popocatepetl with a majority of hypocenters occurring in the depth range 0-2 km below the crater floor. Taking into account the uncertainty in event locations, it is reasonable to view these LP events as representative of the shallow seismicity associated with degassing activity in the crater and dome emplacement. These events have signatures that exhibit a broader range of frequencies similar to the signature illustrated in Figure 3.3a. Events with signatures similar to that shown in Figure 3.3b tend to locate at greater depths ranging down to 4-5 km below the crater floor. These depths are comparable to those of some of the sources inferred from VLP particle motions (see Fig. 3.11c).

The similar frequency characteristics of LP events and tremor (Figs. 3.3a-c and 3.7a-d), almost identical particle motion patterns shared by these signals (Figs. 3.10a-b), and common hypocentral locations (Fig. 3.12), all suggest that the bulk of LP seismicity originates within a common source region located in the top 1.5 km below the crater of Popocatepetl. The features of VLP particle motions seen in Figures 3.11a-b are consistent

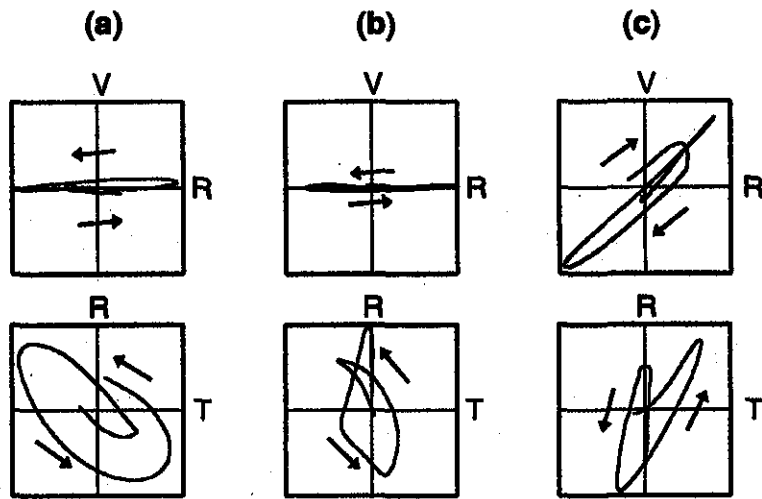


**Fig. 3.11** Particle trajectories of displacement obtained in the 0.01-0.04 Hz band for the events displayed in Figure 3.10 (see Figure 3.10 for details). Note the quasi horizontal motion of the VLP signals in (a) and (b), and steeply-dipping southward-trending (toward Popocatepetl) particle trajectories in (c).

with this picture. The observed stationarity of these features with time further suggests that a repeatable source is involved. The only viable mechanism that can explain such a repeating non-destructive source process is one involving the active participation of fluids [Chouet, 1996]. Acoustic resonance of a crack-like conduit containing magmatic and/or hydrothermal fluids provides a reasonable mechanism that can naturally explain such common properties in the LP event and tremor generation processes [Chouet *et al.*, 1994; Morrissey and Chouet, 1997; Gil Cruz and Chouet, 1997]. Unsteady mass transport provide a natural source of VLP signals, while short-term pressure disturbances associated with the transport process provide the required triggers for the generation of LP seismicity [Chouet, 1996; Dawson *et al.*, 1998]. The shallowness of the source region and close relationship observed between LP and VLP seismicity and steam and ash emissions provide strong qualitative evidence of a hydrothermal origin for most of this seismicity.

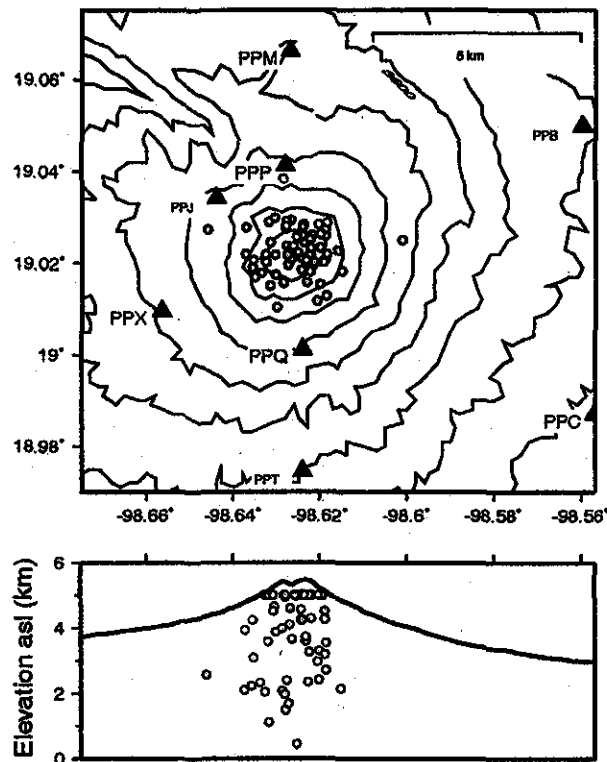


**Fig. 3.12** Hypocentral distribution (black circles) of 65 LP events recorded by the short-period seismic network. East-west cross section (2x vertical exaggeration) passing through the summit. Triangles indicate seismic stations. Contours represent 300 m elevation intervals.

## Conclusions

The main goal of this study was to document the broadband characteristics of signals associated with LP seismicity recorded at Popocatepetl. The recorded signals reveal that volcanic processes contain energy over a very wide band and thus demonstrate unequivocally the importance of monitoring volcanoes with broadband instruments. The bulk of LP seismicity observed in the 0.5-5.0 Hz band originates in a shallow source region located within the top 1.5 km below the crater of Popocatepetl. This LP seismicity is intimately linked to surficial processes of fluid transport such as fumarolic or more energetic emissions of gas and ash. VLP signals with energy extending below 0.1 Hz appear to point to two distinct sources beneath the volcano. One VLP source is located 1 km below the crater and overlaps the source region inferred for the dominant LP seismicity, while the second VLP source appears to be linked to deeper mass transport under the volcano.

## References

- Arciniega-Ceballos A, Chouet BA, Dawson P (1999) Very long-period signals associated with vulcanian explosions at Popocatepetl Volcano, Mexico. *Geophys. Res. Lett.* 26:3013-3016
- Arciniega-Ceballos A, Valdes C, Dawson P (2000) Temporal and spectral characteristics of seismicity observed at Popocatepetl volcano, central Mexico. *J. Volcanol. Geotherm. Res.* 102:207-216
- Chouet B (1985) Excitation of a buried magmatic pipe: A seismic source model for volcanic tremor. *J. Geophys. Res.* 90:1881-1893
- Chouet B (1986) Dynamics of a fluid-driven crack in three dimensions by the finite difference method. *J. Geophys. Res.* 91:13967-13992
- Chouet B (1988) Resonance of a fluid-driven crack: Radiation properties and implications for the source of long-period events and harmonic tremor. *J. Geophys. Res.* 93:4375-4400
- Chouet B (1992) A seismic model for the source of long-period events and harmonic tremor. In: *Volcanic Seismology*, Gasparini P, Scarpa R, Aki K (eds) Springer-Verlag, New York, pp. 133-156
- Chouet BA, Page RA, Stephens CD, Lahr JC, Power JA (1994) Precursory swarms of long-period events at Redoubt Volcano (1989-1990), Alaska: Their origin and use as a forecasting tool. *J. Volcanol. Geotherm. Res.* 62:95-135
- Chouet B (1996) Long-period volcano seismicity: its source and use in eruption forecasting. *Nature* 380:309-316
- Chouet B, Saccorotti G, Martini M, Dawson P, De Luca G, Milana G, Scarpa R (1997) Source and path effects in the wave fields of tremor and explosions at Stromboli Volcano, Italy. *J. Geophys. Res.* 102:15129-15150
- Chouet B, Saccorotti G, Dawson P, Martini M, Scarpa R, De Luca G, Milana G, Cattaneo M (1999) Broadband measurements of the sources of explosions at Stromboli Volcano, Italy. *Geophys. Res. Lett.* 26:1937-1940
- Dawson PB, Dietel C, Chouet BA, Honma K, Ohminato T, Okubo P (1998) A digitally telemetered broadband seismic network at Kilauea Volcano, Hawaii. U.S. Geol. Surv. Open-File Rep. 98-108 pp. 121
- Falsaperla S, Langer H, Spampinato S (1998) Statistical analyzes and characteristics of volcanic tremor on Stromboli Volcano (Italy). *Bull Volcanol* 60:75-88
- Falsaperla S, Privitera E, Chouet B, Dawson P (2001) Analysis of long-period events recorded at Mount Etna (Italy) in 1992, and their relationship to eruptive activity. *J. Volcanol. Geotherm. Res.* in press
- Garces M, McNutt S (1997) Theory of the airborne sound field generated in a resonant magma conduit. *J. Volcanol. Geotherm. Res.* 78:155-178
- Gil Cruz F, Chouet BA (1997) Long-Period events, the most characteristic seismicity accompanying the emplacement and extrusion of a lava dome in Galeras Volcano, Colombia, in 1991. *J. Volcanol. Geotherm. Res.* 77:121-158

- Hidayat D, Chouet BA, Voight B, Dawson P, Ratdomopurbo A (2001) Source mechanism of very-long-period signals accompanying dome growth activity at Merapi Volcano, Indonesia. *Geophys. Res. Lett.* submitted
- Julian B (2001) *gloc*, a general earthquake location computer program. U S Geol Surv Open-File Rep in preparation.
- Kaneshima S, Kawakatsu H, Matsubayashi H, Sudo Y, Tsutsui T, Ohminato T, Ito H, Uhira K, Yamasato H, Oikawa J, Takeo M, Iidaka T (1996) Mechanism of phreatic eruptions at Aso volcano inferred from near-field broadband seismic observations. *Science* 273:642-645
- Kawakatsu H, Ohminato T, Ito H, Kuwahara Y (1992) Broadband seismic observation at Sakurajima Volcano, Japan. *Geophys. Res. Lett.* 19:1959-1962
- Kawakatsu H, Ohminato T, Ito H (1994) 10-s-period volcanic tremors observed over a wide area in southwestern Japan. *Geophys. Res. Lett.* 21:1963-1966
- Kawakatsu H, Kaneshima S, Matsubayashi H, Ohminato T, Sudo Y, Tsutsui T, Uhira K, Yamasato H, Ito H, Legrand D (2000) Aso94: Aso seismic observation with broadband instruments. *J. Volcanol. Geotherm. Res.* 101:129-154
- Kumagai H, Chouet BA (1999) The complex frequencies of long-period events as probes of fluid compositions beneath volcanoes. *Geophys. J. Int.* 138:F7-F12
- Kumagai H, Chouet BA (2000) Acoustic properties of a crack containing magmatic or hydrothermal fluids. *J. Geophys. Res.* 105:25493-25512
- Kumagai H, Ohminato T, Nakano M, Ooi M, Kubo A, Inoue H (2001) Very-long-period seismic signals and the caldera formation at Miyake Island, Japan. *J. Volcanol. Geotherm. Res.* submitted
- Lahr JC, Chouet BA, Stephens CD, Power JA, Page RA (1994) Earthquake classification, location, and error analysis in a volcanic environment: Implications for the magmatic system of the 1989-1990 eruptions at Redoubt Volcano, Alaska. *J. Volcanol. Geotherm. Res.* 62:137-151
- Legrand D, Kaneshima S, Kawakatsu H (2000) Moment tensor analysis of broadband waveforms observed at Aso Volcano, Japan. *J. Volcanol. Geotherm. Res.* 101: 155-169
- Longuet-Higgins MS (1950) A theory of the origin of microseism. *Philos Trans R Soc London Ser A* 423:1-35
- McNutt SR (1992) Title of paper, Encyclopedia of Earth System Science. Academic Press, San Diego, v. 4 pp. 417-425.
- Morrissey MM, Chouet BA (1997) A numerical investigation of choked flow dynamics and its application to the triggering mechanism of long-period events at Redoubt Volcano, Alaska. *J. Geophys. Res.* 102:7965-7983
- Neuberg J, Luckett R, Ripepe M, Braun T (1994) Highlights from a seismic broadband array on Stromboli volcano. *Geophys. Res. Lett.* 21:749-752
- Nishimura T (2000) Source process of very long period seismic events associated with the 1998 activity of Iwate Volcano, northeastern Japan. *J. Geophys. Res.* 105:19135-19145
- Nuttli O (1961) The effect of the Earth's surface on the S wave particle motion, *Bull.*

Seismol. Soc. Am. 51:237-246

Ohminato T, Ereditato D (1997) Broadband seismic observations at Satsuma-Iwojima Volcano, Japan. Geophys. Res. Lett. 24:2845-2848

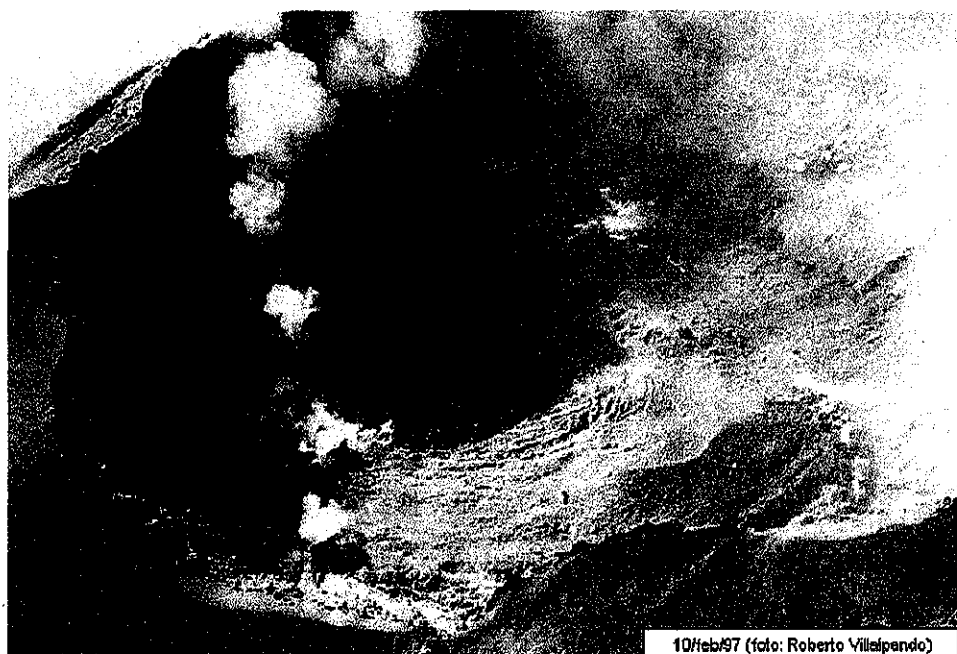
Ohminato T, Chouet BA, Dawson P, Kedar S (1998) Waveform inversion of very-long-period impulsive signals associated with magmatic injection beneath Kilauea Volcano, Hawaii. J. Geophys. Res. 103:23839-23862

Ohminato T (1998) Broadband analysis of seismic signals observed in and around active volcanoes. Ph. D. Thesis, University of Tokyo, Japan. pp. 114

Rowe CA, Aster RC, Kyle PR, Schlue JW, Dibble RR (1998) Broadband recording of Strombolian explosions and associated very-long-period seismic signals on Mount Erebus Volcano, Ross Island, Antarctica. Geophys. Res. Lett. 25:2297-2300

Seidl S, Kirbani SB, Brustle W (1990) Maximum entropy spectral analysis of volcanic tremor using data from Etna (Sicily) and Merapi (central Java). Bull Volcanol 52:460-474

Wessel P, Smith WHF (1995) New version of the Generic Mapping Tools released (abstract). Eos Trans AGU 76(33)-329



10 feb 97 (foto: Roberto Villalpando)

Foto. 3.1 Vista del cráter febrero 1997



Foto. 3.2 Interior del cráter abril 2000 (foto A. Arciniega).

## Capítulo IV

# Señales de Periodo muy Largo Asociadas con Explosiones Vulcanianas en el Popocatépetl

### Abstract

Very long period (VLP) seismic signals associated with large summit eruptions of Popocatepetl volcano in the last four years are investigated using data from a broadband seismometer (0.04–120 s) deployed on the north flank of the volcano at a radial distance of 5 km from the active crater. The VLP signals associated with individual eruptions share similar waveforms. Discrete VLP signals accompanying long-period (LP) events also share similar signatures and have dominant periods that are nearly identical to those observed

in the VLP waveforms of explosions. The VLP particle motions for eruption onsets consistently point to a source located a few km beneath the crater. The VLP ground displacement response to each explosion is marked by a compression, followed by a dilatation and terminating with another compression, suggesting a sequence of pressurization-depressurization-repressurization of the conduit. The repetitive nature of the waveforms points to a non-destructive source process which has remained active in the magmatic system of Popocatepetl at least since April 1997.

## Introduction

Popocatepetl is a large andesitic composite volcano, 5452 m high, located in the central region of the Mexican Volcanic Belt (Fig. 4.1). Its last major Plinian eruption occurred in historical time circa 822-823 A.D. [Siebe *et al.*, 1996]. Eruptive activity over the past 70 years has been characterized by mild fumarolic emissions through vents in the crater. Fumarolic activity increased in 1993, heralding renewed unrest. Seismic activity, initially monitored with a single three-component short-period (1 Hz) seismometer located at site PPM 5 km north of the crater (see Fig. 4.1), showed a marked increase starting in October 1994. A swarm of volcano-tectonic (VT) earthquakes, followed by sustained tremor accompanying a large ash plume, marked the reawakening of Popocatepetl on 21 December 1994.

Since December 1994 the eruptive activity of Popocatepetl has been characterized by intermittent production of ash and sustained emission of magmatic gases. A lava dome was first observed in the crater at the end of March 1996. This dome was partly

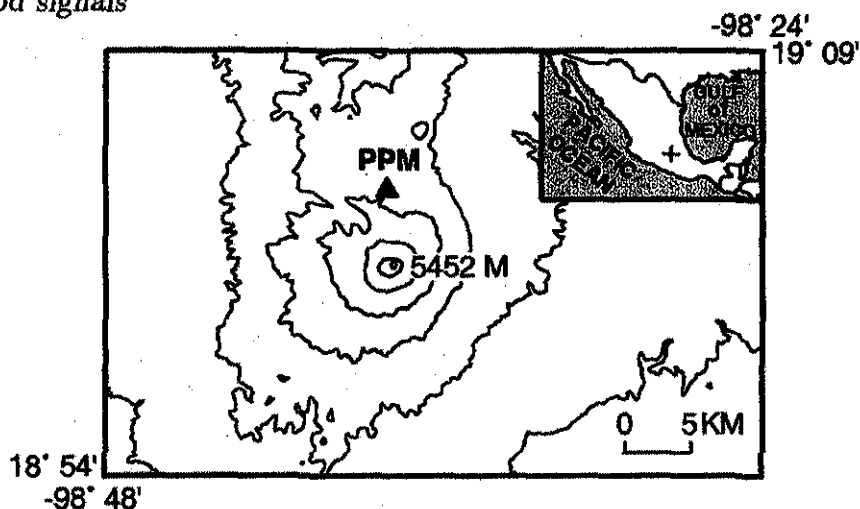


Fig. 4.1. Map of Popocatepetl Volcano, Mexico. Contours represent 500 m elevation intervals. Solid triangle marks the location of the broadband seismic station PPM. Inset shows a map of Mexico with the location of Popocatepetl indicated by a cross.

destroyed by a vulcanian explosion on April 1996, following which repeated episodes of dome emplacement and destruction began, and are still ongoing at present. A variety of seismic signals have been observed accompanying this activity. These signals are dominated by long-period (LP) events, sporadic harmonic and non-harmonic tremor episodes, and explosions.

Following the December 1994 eruptive crisis, five telemetered three-component short-period (1 Hz) seismometers were installed around the volcano and operated jointly by the Centro Nacional de Prevencion de Desastres (CENAPRED) and the Universidad Nacional Autonoma de Mexico (UNAM). In September 1996 this network was supplemented by a digitally telemetered broadband station deployed at PPM (see Fig. 4.1). The station is operated by UNAM and consists of a three-component Streckheisen STS-2 sensor with bandwidth of 0.04-120 s. Data from this station are digitized continuously at 1 sample/s, and in triggering mode at 80 samples/s.

Recent broadband observations at Sakurajima and Aso Volcanoes, Japan [Kawakatsu *et al.*, 1992; Kawakatsu *et al.*, 1994; Kaneshima *et al.*, 1996], Satsuma-Iwojima, Japan [Ohminato and Ereditato, 1997; Ohminato, 1998], Stromboli, Italy [Neuberg *et al.*, 1994; Chouet *et al.*, 1999], Kilauea, Hawaii [Dawson *et al.*, 1998; Ohminato *et al.*, 1998], and Mount Erebus, Antarctica [Rowe *et al.*, 1998] indicate that VLP signals with periods longer than a few seconds are commonly associated with magma and/or hydrothermal transport in volcanoes. Concurrently, new developments in the computation of Green's functions for complicated media including 3D topography [Ohminato and Chouet, 1997], and improvements in waveform inversion methods are now allowing the quantification of the source mechanisms producing VLP signals [Ohminato *et al.*, 1998], thus offering powerful new insights into volcanic processes. The goal of the present study is to document the characteristic features of the VLP waveforms associated with eruptive activity at Popocatepetl. Our analysis focuses on VLP signals accompanying large vulcanian explosions that have occurred at Popocatepetl since 1997. We address the relevance of VLP signals for mass transport beneath the volcano.

## Data and analysis

The broadband data recorded at PPM display a variety of signatures including short-period ( $T < 0.2$ s) VT earthquakes occurring at depths of 2.5 to 10 km beneath the crater, shallow (<3 km depth) LP events and tremor ranging in periods between 0.2 and 2 s, and explosions with typical periods in the range 0.1-50 s. LP events are the most common events observed at Popocatepetl and their rate of production varies from a few events per day to hundreds of events per day. Tremor is closely related to LP events and reflects the

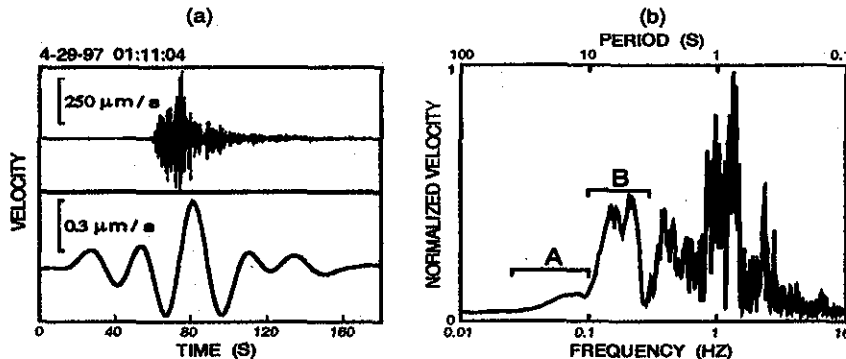


**Fig. 4.2(a).** Vertical component of velocity for an eruption signal; (*top*) signal in the 0.2–2 s band, and (*bottom*) signal in the 25–100 s band. The date and local time at the start of the record are indicated at the upper left. (*b*) Normalized spectrum of the vertical component of velocity for the eruption signal depicted in (*a*). Bracket (*A*) marks the identifiable portion of the VLP signal associated with the explosion, and bracket (*B*) marks the spectral components due to the oceanic microseismic noise.

response of fluid-filled conduits to sustained pressure fluctuations, whereas LP events are manifestations of short-term pressure disturbances in these conduits [Chouet, 1996]. Both types of activities are commonly associated with ash and gas emissions and with dome growth episodes. Vulcanian explosions occasionally occur, resulting in total or partial destruction of the lava dome capping the vent. These explosions launch incandescent debris as far as 3 km from the crater and release large quantities of ash and gas into the atmosphere.

The top trace in Figure 4.2a shows the vertical component of ground velocity in the band 0.2–2 s for an explosion which occurred on April 29, 1997. The bottom trace in that figure shows the same record bandpass filtered between 25 and 100 s, in which a VLP signal with dominant period near 28 s is clearly seen. This waveform is associated with

the first vulcanian explosion recorded on the broadband seismometer at PPM after the onset of eruptive activity in 1994. The explosion partly destroyed a lava dome emplaced in the crater. The onset of the VLP signal occurs roughly 45 s before the onset of the short period signal which coincides with the actual eruption. This suggests that the hypocenter of the vulcanian explosion is located at a depth significantly deeper than the crater floor. Similar observations have been made for vulcanian explosions occurring at Sakurajima Volcano, Japan [Uhira and Takeo, 1994]. Note that the peak-to-peak amplitude of the VLP signal from this explosion is roughly three orders of magnitude smaller than the peak-to-peak amplitude of the corresponding short period signal. We discuss these signal features in more detail below.

Figure 4.2b shows the spectrum of the vertical component of velocity calculated over a 300 s window bracketing the event. The spectrum is dominated by energy in the band 0.5-3 s associated with the volcanic signal, and by a series of peaks in the 3-10 s band reflecting the oceanic microseism. All seismic records include a high-amplitude component with periods between 3 and 10 s attributed to the oceanic microseismic noise [Longuet-Higgins, 1950]. Analyses of particle motion indicate that the energy of the oceanic microseismicity is incident at PPM from all directions. The VLP signal associated with the explosion appears as a small-amplitude broad bump in the period range of 10-50 s. A comparison of these spectral features with those obtained over the same period range for the radial (N-S) and transverse (E-W) components of velocity indicates that the amplitude of the vertical component is roughly twice as large as either radial or transverse components in the 10-25 s band, while the radial component is five times larger than either vertical or transverse components in the 30-100 s band. Another weaker source of noise is also apparent in the records in the period range 10-25 s. This noise is characterized by the same random pattern of particle motion as observed in the 3-10 s band and may represent the so-called primary period microseism thought to originate

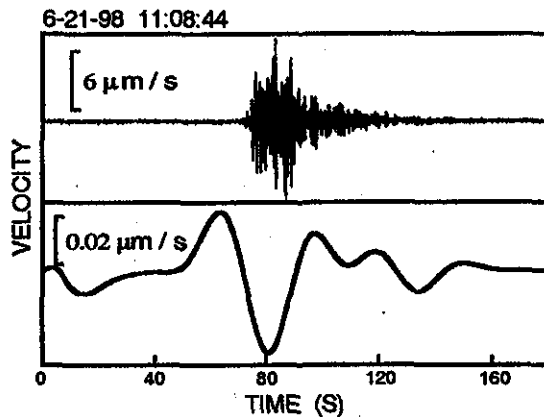


**Fig. 4.3.** Vertical component of velocity for a LP signal obtained from the broadband record using a 2-s high-pass filter (*top*), and associated VLP signal using a 25-100 s band-pass filter (*bottom*). The date and local time at the start of the record are indicated at the upper left.

primarily in shallow water above the continental shelf [Babcock *et al.*, 1994]. To emphasize the VLP signals originating from the volcano and avoid any possible phase and amplitude contaminations from microseismic noise we bandpass filtered the records of PPM over the 25-100 s band running a Butterworth filter over the data.

Both VLP and LP activities were noted to occur simultaneously with eruptions and to increase before and after large eruptive events. An example of VLP signal associated with a LP event on June 6, 1998, is shown in Figure 4.3. The LP event has a dominant period between 1 and 2 s and the VLP signal displays a dominant period near 28 s similar to the period of the VLP signal observed in the explosion of April 29, 1997 (see Fig. 4.2*a*). Notice, however, that the VLP waveforms associated with the two types of events are different. The VLP signal associated with the explosion displays a wave-packet-like waveform with clear dominant oscillation (Fig. 4.2*a*), while the VLP signal associated with the LP event shows a more pulse-like waveform (Fig. 4.3). These features are suggestive of differences

in the mechanisms underlying explosions and LP events. VLP signals with dominant period near 28 s were consistently observed in all the seismic records associated with either strong degassing or vulcanian explosions at Popocatepetl.

Figure 4.4 shows the VLP signals associated with each of the 26 vulcanian explosions that have occurred at Popocatepetl since the onset of eruptive activity in 1994. The first twelve traces in the left panel in this figure illustrate explosions which occurred between April 29, 1997 and September 23, 1998, while the bottom trace in this panel and thirteen traces in the right panel show explosions which occurred within a three-week period between November 25 and December 15, 1998. Visual observations suggest that each event marked the destruction of some portion of the lava dome present in the crater at the time. The waveforms in Figure 4.4 are similar from explosion to explosion and differ only in amplitude, with the largest difference amounting to a factor of 8 in scale.

Examples of seismograms for the VLP signals recorded at PPM during the explosion of April 29, 1997 are shown in Figure 4.5a. The three components of displacement display a characteristic sequence marked by an initial compression, followed by a larger-amplitude dilatation, and terminating with another compression of roughly equal amplitude to the preceding dilatation. These signal features resemble the waveforms associated with Strombolian eruptions [Chouet *et al.*, 1999], although the period of the signal is much longer and the relative amplitudes of the compression, dilatation, compression phases are different at Popocatepetl compared to Stromboli.

The peak-to-peak displacement amplitude produced by the explosion of April 29, 1997 is about 3 microns at PPM. In comparison, the largest explosion observed at Stromboli by Chouet *et al.* (1999) has a peak-to-peak displacement amplitude of 30 microns at a distance of 500 m from the source. Scaling the Stromboli data to the hypocentral

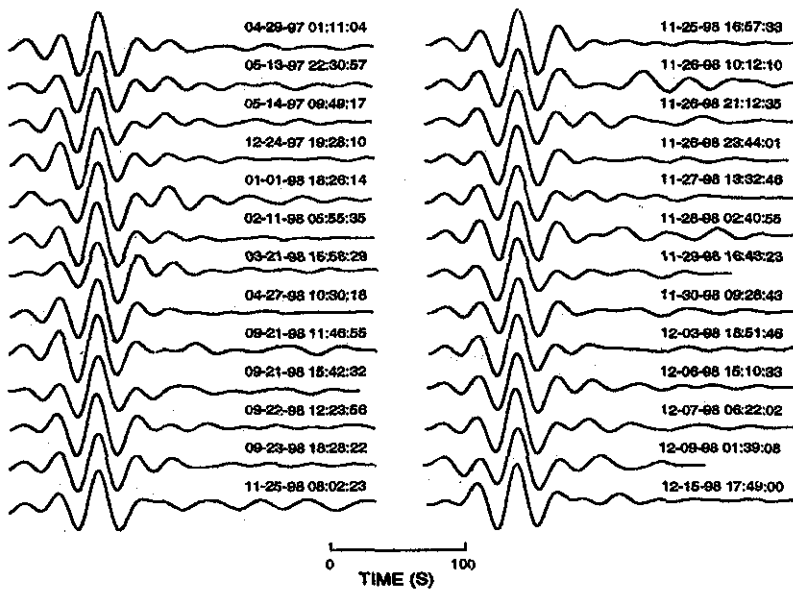


**Fig. 4.4.** Vertical component of velocity for VLP signals in the 25-100 s band associated with 26 vulcanian explosions at Popocatepetl. The date and local time at the start of each record are indicated at the upper right of the record. The amplitude scale is arbitrary.

distance  $R = 5.4$  km corresponding to PPM and assuming a near field decay proportional to  $1/R^{*3}$ , the corresponding displacement amplitude for Stromboli is 0.03 microns, which is 100 times smaller than the Popocatepetl explosion of 04/29/97. Comparing the Stromboli explosion to other explosions at Popocatepetl, we find that vulcanian explosions may be 10 to 100 times larger than Strombolian explosions.

It is also of interest to compare the size of the April 29, 1997 explosion at Popocatepetl with a typical explosion observed at Sakurajima Volcano. The peak-to-peak displacement amplitude of the vertical component of the VLP seismogram recorded at the KOME station located 4.4 km from the crater of Sakurajima is 20 microns for an explosion on October 30, 1986 [Uhira and Takeo, 1994]. Assuming again a near field decay proportional to  $1/R^{*3}$ , we find that the explosion of 04/27/97 at Popocatepetl is about three times smaller than the 10/30/86 explosion at Sakurajima. As the explosions observed in 1997-

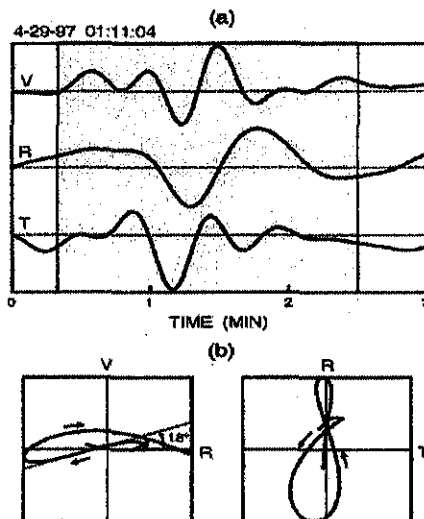


**Fig. 4.5.** (a) Three components of ground displacement in the 25-100 s band (shown with arbitrary amplitude scale) recorded at station PPM for the eruption displayed in Figure 4.2. Shading marks the interval over which particle motions in (b) are obtained. (b) Particle trajectories for the records in (a). The trajectories are plotted in the radial vertical and horizontal planes in which the radial and transverse directions represent the N-S and E-W directions. An arrow indicates the direction of particle motion, and a dotted line identifies the quasi-linear dilatational motion associated with the initial downgoing branch of the VLP signal in the radial vertical plane. Motion in the horizontal plane shows a clear trend in the radial (crater) direction.

1998 at Popocatepetl produced a displacement amplitude two times larger than that observed in the explosion of April 29, 1997, we may conclude that the sizes of vulcanian explosions at Popocatepetl and Sakurajima are roughly similar.

Figure 4.5b displays the particle motion for the explosion signal depicted in Figure 4.5a. In the vertical-radial plane, the motion associated with the dominant phase from the explosion shows a clear dilatational pulse whose initial swing is nearly linear and tilted 18° counterclockwise from the horizontal. Although not linear, the general trend of horizontal motion remains essentially radial (N-S) throughout the entire duration of the explosion

record. If one assumes a point source located vertically beneath the crater floor, then these features are consistent with a source located approximately 2.8 km beneath the crater. The clockwise loop described by particle motion in the vertical-radial plane during the dominant phase of the VLP signal suggests a shallowing of the source during the course of the eruption. The orientation of the VLP particle motions associated with other explosions point consistently to the same source region beneath the crater of Popocatepetl.

The repetitive nature of the signals (see Fig. 4.4) suggest a non-destructive source process, indicating that the source of the VLP signals is not affected by the details of the surficial destruction of the lava plug capping the vent a few km above the hypocentral source region. Interestingly, the inferred depth of the source of explosions at Popocatepetl is comparable to the depth of the source of vulcanian explosions observed at Sakurajima Volcano (Uhira and Takeo, 1994), and the compression-dilatation-compression sequence in the ground displacement response to explosions is similar at both volcanoes, suggesting common features in the dynamics of explosions in these two vulcanian systems. As noted by Uhira and Takeo (1994) and Chouet *et al.*(1999), these VLP signal characteristics appear to be consistent with the response of the volcanic conduit to a pressurization associated with the release and ascent of gases from the source, followed by a depressurization and deflation of the conduit in response to mass withdrawal during the eruption, and terminating with a repressurization and dilation of the conduit associated with replenishment of the source with fluid. The recoil from the eruption jet may contribute a significant component to the ground displacement response as well.

## Conclusions

VLP seismic signals identified at Popocatepetl are consistent with observations made at other volcanoes in which VLP activity has been clearly linked to mass transport [e.g., Ohminato *et al.*, 1998]. The VLP pulses display almost identical shapes, suggesting that the source mechanisms generating these signals share similar characteristics independent of time for all explosions recorded between April 1997 and December 1998. These features point to a mechanism involving the repetitive non-destructive activation of a fixed source. Of the 26 explosions analyzed, which occurred over a period of 19 months, the last 14 occurred in just over 20 days, suggesting a marked increase in vulcanian activity probably associated with an increased production of very viscous magma.

Although the location of the source can not be accurately constrained due to the lack of broadband receiver coverage of the volcano, particle motion analyses performed at PPM point to a source located a few km beneath the crater of Popocatepetl. A denser spatial coverage of broadband receivers around Popocatepetl will be required to further quantify the source mechanism of vulcanian explosions and map the geometry of the magma/gas transport system under this volcano.

## References

- Babcock, J. M., B. A. Kirkendall, and J. A. Orcutt, Relationships between ocean bottom noise and the environment, *Bull. Seismol. Soc. Am.*, **84**, 1991–2007, 1994.
- Chouet B. Long-period volcano seismicity: its source and the use in eruption forecasting. *Nature*, **380**, 309–316, 1996.
- Chouet, B., G. Saccorotti, P. Dawson, M. Martini, R. Scarpa, G. De Luca, G. Milana, and M. Cattaneo, Broadband measurements of the sources of explosions at Stromboli Volcano, Italy, *Geophys. Res. Lett.*, **26**, 1937–1940, 1999.
- Dawson, P. B., C. Dietel, B. A. Chouet, K. Honma, T. Ohminato and P. Okubo. A digitally telemetered broadband seismic network at Kilauea volcano, Hawaii, *U.S. Geol. Surv. Open File Rep.*, **98-108**, 122 pp., 1998.
- Kaneshima S., H. Kawakatsu, H. Matsubayashi, Y. Sudo, T. Tsutsui, T. Ohminato, H. Ito, K. Uhira, H. Yamasato, J. Oikawa, M. Takeo and T. Iidaka. Mechanism of phreatic eruptions at Aso volcano inferred from near-field broadband seismic observations, *Science*, **273**, 642–645, 1996.
- Kawakatsu, H., S., T. Ohminato , H. Ito and Y. Kuwahara. Broadband seismic observation at Sakurajima Volcano, Japan, *Geophys. Res. Lett.*, **19**, 1959–1962, 1992.
- Kawakatsu, H., S., T. Ohminato and H. Ito. 10s-Period volcanic tremors observed over a wide area in southwestern Japan, *Geophys. Res. Lett.*, **21**, 1963–1966, 1994.
- Longuet-Higgins, M. S. A theory of the origin of microseism. *Philos. Trans. R. Soc. London, Ser. A*, **423**, 1–35, 1950.
- Neuberg, J., R. Luckett, M. Ripepe and T. Braun, Highlights from a seismic broadband array on Stromboli volcano. *Geophys. Res. Lett.*, **21**, 749–752, 1994.
- Ohminato T. and B. A. Chouet. A free-surface boundary condition for including 3D topography in the finite difference method. *Bull. Seismol. Soc. Am.*, **87**, 494–515, 1997.
- Ominato, T. and D. Ereditato. Broadband seismic observations at Satsuma-Iwojima volcano, Japan. *Geophys. Res. Lett.*, **24**, 2845–2848, 1997.
- Ohminato T., B. A. Chouet, P. Dawson and S Kedar. Waveform inversion of very long period impulsive signals associated with magmatic injection beneath Kilauea Volcano, Hawaii. *J. Geophys. Res.*, **103**, 23,839–23,862, 1998.
- Ohminato, T., Broadband analysis of seismic signals observed in and around active volcanoes, Ph. D. Thesis, University of Tokyo, Tokyo, Japan, 1998.
- Rowe, C. A., R. C. Aster, P. R. Kyle, J. W. Schlue, and R. R. Dibble, Broadband recording of Strombolian explosions and associated very-long-period seismic signals on Mount Erebus Volcano, Ross Island, Antarctica, *Geophys. Res. Lett.*, **25**, 2297–2300, 1998.
- Siebe C., M. Abrams, J.L. Macias, and J. Obenholzner. Repeated volcanic disasters in Prehispanic time at Popocatepetl central Mexico; Past key to the future ?. *Geology*, **24**, 399–402, 1996.
- Uhira, K., and M. Takeo, The source of explosive eruptions at Sakurajima Volcano, Japan, *J. Geophys. Res.*, **99**, 17,775–17,789, 1994.

TESIS CON  
FALLA DE ORIGEN

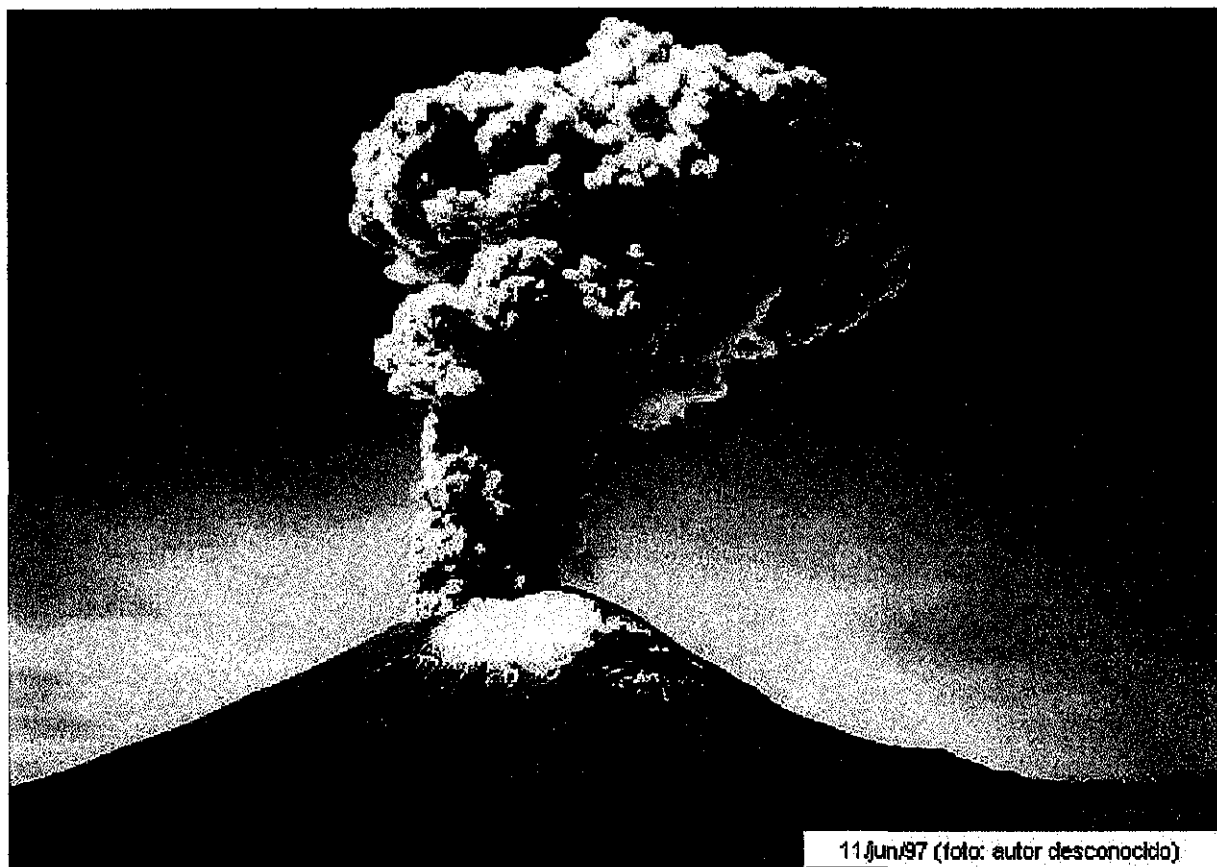


Foto. 4.1 Ejemplo de actividad eruptiva asociada a eventos explosivos.

## Capítulo V

# Experimento Sísmico de Banda Ancha en el Volcán Popocatépetl

### Introduction

Seismic monitoring of active volcanoes has relied on observations with short-period instruments. In recent years, broadband seismometers have been increasingly used, and in combination with a wide range of geophysical methods, have significantly expanded our understanding of volcanic processes [Chouet, 1996 a,b]. Broadband seismic arrays have demonstrated their usefulness to quantify mass transfer processes in active volcanoes and have opened a new window into quantitative analyses of complex dynamic volcanic systems [e.g., Kawakatsu et al., 1992; Neuberg et al., 1994; Chouet, 1996 a,b].

Popocatepetl volcano is located close to major population centers, and its present erup-

tive episodes have therefore attracted considerable interest. Popocatepetl is a large, partly glacier-clad, composite andesitic volcano, with a summit elevation of 5452 m. Since December 1994, eruptive activity at Popocatepetl has been dominated by passive fumarolic emissions interrupted by more energetic emissions of ash and gas through vents in the summit crater, and passive lava effusion leading to the formation of lava domes within the crater. The first dome associated with the current eruptive phase was observed in March 1996. This dome was subsequently destroyed in a vulcanian explosion on April 30, 1996. Since then, eruptive activity has been marked by a sequence of repetitive dome-building and dome-destroying episodes that is still ongoing today.

The most common eruptive activity consists in emissions of steam, ash and large quantities of  $SO_2$  and  $CO_2$  including both old and juvenile materials. These emissions range in intensity from small short-lived plumes rising a few hundred meters above the crater rim, to larger events producing plumes that may reach up to 5 km above the crater and blanket the entire summit area with ejecta. These emissions are related to seismic signals that may occur as isolated events or as sequences of discrete events with overall durations comparable to those of venting. As well as with episodes of tremor.

We classify the seismic signals observed at Popocatepetl accordingly to the scheme first proposed by Lahr *et al.* (1994) and Chouet (1996a). This scheme is based on the physics of the source process and includes two fundamental families of events. The first family includes volcano-tectonic (VT) earthquakes, which represent the brittle response of volcanic rocks to stresses induced by fluid movements within the volcanic edifice. The second family includes long-period (LP) events and tremor, collectively grouped under the common appellation of long-period seismicity and representing volumetric sources driven by pressure disturbances associated with the flow of magmatic and/or hydrothermal fluids [Chouet, 1996b]. LP seismicity has typical periods in the range 0.2-2s [Chouet, 1996a].

The LP events and tremor episodes recorded at Popocatepetl, are observed to correlate in time with degassing and the emplacement of lava domes, and are usually characterized by very emergent onsets. While individual LP event durations never exceed 3 min, tremor may last from 3-15 min to days. Different characteristics of tremor are commonly associated with different types of volcanic activities [e.g., McNutt, 1992]. Three distinct types of tremor have been observed during several episodes of activity over the past five years, namely persistent tremor lasting weeks, intermittent discrete tremor episodes with a wide range of durations, and swarms of LP events merging into sustained tremor. Those three types of tremor were most conspicuous during the emplacement of lava domes in March 1996 and February 2000 [Arciniega *et al.*, 2001].

Recent broadband observations at Sakurajima and Aso Volcanoes, Japan [Kawakatsu *et al.*, 1992, 1994, 2000; Kaneshima *et al.*, 1996; Legrand *et al.*, 2000], Satsuma-Iwojima Volcano, Japan [Ohminato and Ereditato, 1997; Ohminato, 1998], Iwate Volcano, Japan [Nishimura *et al.*, 2000], Miyake Island, Japan [Kumagai *et al.*, 2001], Stromboli Volcano, Italy [Neuberg *et al.*, 1994; Chouet *et al.*, 1999], Merapi Volcano, Indonesia [Hidayat *et al.*, 2001], Kilauea Volcano, Hawaii [Dawson *et al.*, 1998; Ohminato *et al.*, 1998], and Mount Erebus Volcano, Antarctica [Rowe *et al.*, 1998], demonstrate the ubiquitous nature of VLP signals under a variety of volcanic conditions. Put together, LP and VLP seismicities provide the most accurate and complete view of mass transport dynamics under a volcano.

At Popocatepetl, VLP signals have been observed to systematically accompany vulcanian explosions [Arciniega *et al.*, 1999]. A detailed description of the temporal sequence of LP events, tremor episodes, and other relevant signals accompanying volcanic phenomena observed at Popocatepetl since 1994 can be found in Arciniega (2001).

From November 1999 to September 2000, a broadband seismic experiment was carried out at Popocatepetl Volcano as part of an international cooperation program recently established between the GeoForschungsZentrum in Potsdam Germany (GFZ-Potsdam), the U.S. Geological Survey (USGS) in Menlo Park, California, and the Institute of Geophysics at UNAM, Mexico City (IGF-UNAM). The main goal of this experiment was to record seismic activity around the volcano over a wider range of frequencies. The broadband experiment increased the number of receivers from a single broadband instrument (PPIG station) located on the North flank 5 km away from the crater, to 22 instruments surrounding the volcano. The broadband network recorded a wide variety of seismic signals in the period range 0.04-100 s at different altitudes and at various distances from the crater, allowing the observation of seismic energy propagating through various sections of the volcanic edifice. Those data will be used to perform quantitative analyses of VLP signals associated with volcanic eruptive activity.

During the course of our experiment the eruptive behavior was dominated by emissions of water vapor, gas and ash, and the extrusion of a lava dome within the crater. This lava dome was subsequently destroyed on April 19, 2000. The data base recorded during the time span of the experiment provides the means for a better understanding of how Popocatepetl Volcano operates.

This chapter consists of two parts. First, we give a preliminary account of the seismicity of Popocatepetl Volcano observed in the short-period band during our experiment. This account focuses on LP activity associated with degassing. We demonstrate that the spectral characteristics of LP events are compatible with the modes of resonance of a fluid-filled crack [Chouet 1988, 1992, 1996]. We estimate the geometrical dimensions of the crack-like conduit at the source of the LP events following Chouet *et al.* (1994) and Gil-Cruz and Chouet (1997).

The second part of the chapter focuses on broadband observations made at periods larger than 5 s. We consider two period ranges, namely the so-called microseismic band between 5 and 12.5 s, and the VLP band at periods longer than 12.5 s. We first briefly discuss the contribution of Popocatepetl eruptive activity in the microseismic band (5–12.5 s). Within that band, the energy from Popocatepetl decays as the distance from the volcano increase. When such signal appears and persists with modulated amplitudes that dominate the seismogram, we identified it as VLP tremor. We proceed with a presentation of the broadband characteristics of the VLP signals recorded by the network. The similarities of VLP waveforms recorded around the volcano suggest the presence of a shallow repeatedly activated source. VLP pulses and VLP wave train packets, accompanied by LP seismicity, correlate with degassing activity and the extrusion of a lava dome in February, 2000.

## Instrumentation

The broadband experiment involved the deployment of 15 seismometers on the flanks of Popocatepetl. The seismometers were distributed in concentric rings around the volcano summit at altitudes ranging from 3300 to 4470 m, providing an azimuthal coverage between 56 and 309 degrees, and covering a distance range of 1.58 to 5.38 km from the crater (Fig 5.1). Station elevation and proximity to the crater were mainly controlled by the difficulties of access and logistics involved. Ten sites were equipped with Guralps CMG-3ESP instruments, three sites featured Guralps CMG-3T seismometers, and two featured Strekeisen STS-2 sensors. An additional 7 Guralp CMG-40T seismometers were also operated during the first two months of the experiment. These seismometers were installed on the north flank of the volcano in the towns of Amecameca and San Pedro Nexapa (Fig 5.1).

Each broadband sensor was placed on a concrete pad, oriented to geographic north (with exception of PPQ2, PPJ4, PPX3 which were oriented to magnetic north), leveled and mass centered after unlocking. With the exception of sites PPP2, PPX3 and PPQ5, all sensors were installed in a 90 cm deep hole excavated in the pyroclastic materials, covered by a 5 cm thick Styrofoam box, and buried in sand to insulate the sensor from extreme temperatures variations. Stations PPP2, PPX3 and PPQ5 were operated inside brick buildings already built for the permanent short-period network. These sensors were also insulated with Styrofoam boxes.

Data were collected in three different types of recorders, namely SAM data loggers for Guralp CMG-3ESP sensors, Orion data loggers for Guralp 3T sensors, and 24-bit Reftek DAS data loggers for STS-2 sensors. All the stations operated autonomously with solar

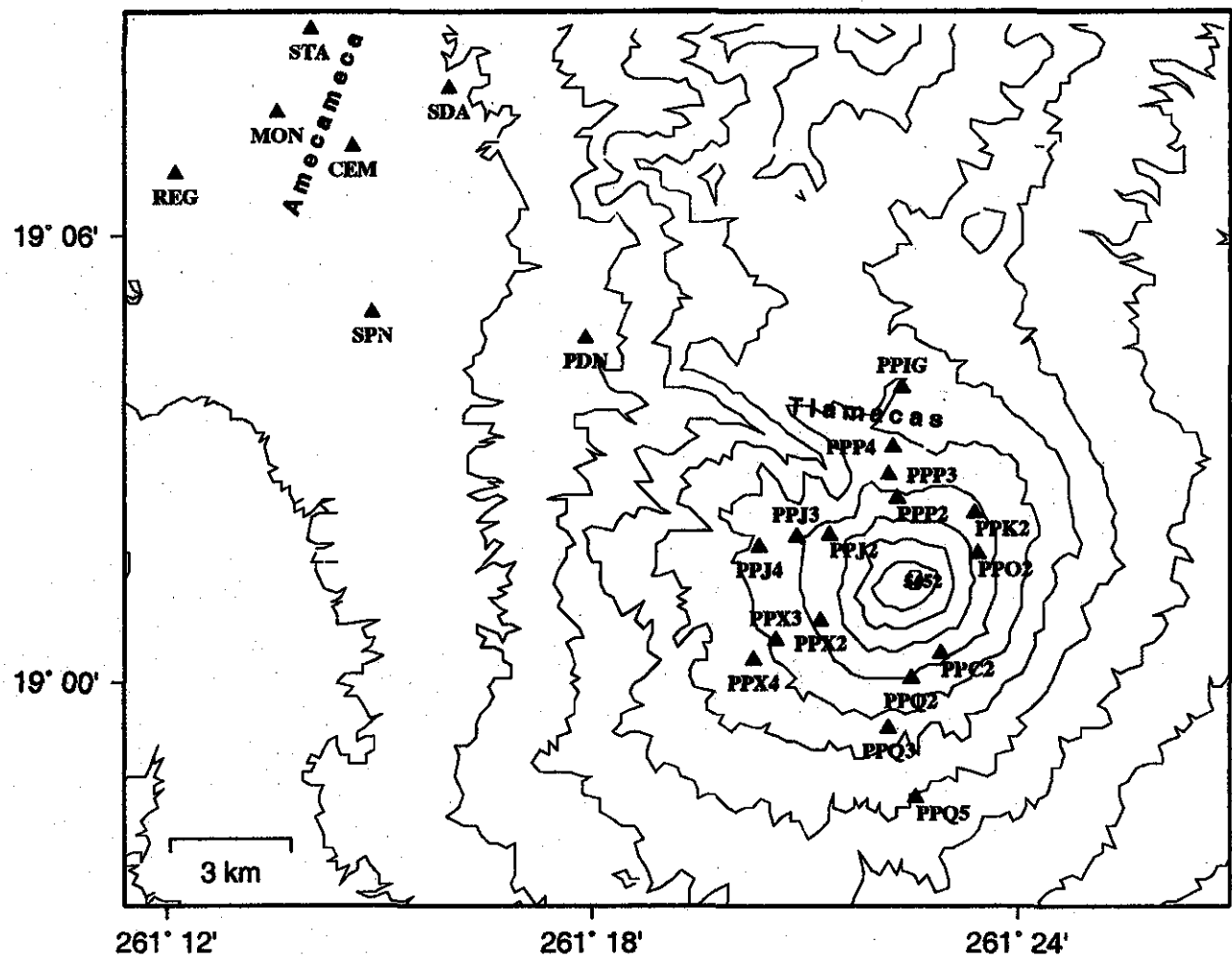


Fig. 5.1 Map of the broadband seismic network at Popocatepetl Volcano, Mexico. Solid triangles indicate broadband stations. Contour lines represent 300 m elevation intervals.

panels and batteries. Data were recorded on portable hard disks with capacities between 1.2 and 4.2 Gb depending on the site and type of recorder. All the data were recorded in continuous mode at a sampling rate of 100 samples/s, except for data from sites located in Amecameca and San Pedro Nexapa, which were sampled at 50 samples/s.

All seismic traces in the following study, have been corrected for instrument response. We use records selected from these twenty-two stations, supplemented by records from stations SDA and PDN located in the north flank of the volcano.

## **Short-period seismicity and eruptive behavior**

Two distinct types of volcanic activities associated with LP signals have been observed, namely emplacement of lava domes within the crater, and degassing. The first evidence of a connection between LP activity and lava dome formation was obtained for the dome extruded in March 1996. This was the first dome identified since the reawakening of the volcano on December 21 1994 and its formation was accompanied by LP swarms, which peaked at more than 220 events per day.

The broadband experiment was carried out from November, 1999 through September 2000, and we report here on data recorded between November, 1999 and May, 2000. During this period, the character of seismicity was marked by a predominance of LP events and volcanic tremor over volcano-tectonic events. A lava dome was extruded within the crater, and was visually observed during a helicopter flight on February 25, 2000. The seismicity accompanying the emplacement of the lava dome was dominated by both LP events and tremor. Fig 5.2 shows daily counts of LP events (in blue) and total

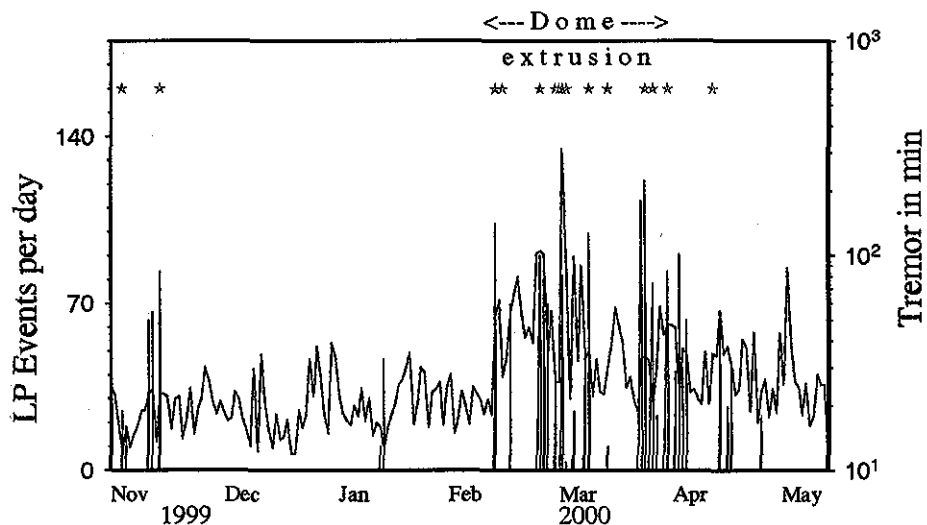


**Fig. 5.2** Seismicity observed at Popocatepetl between November 1999 and May 2000, showing the number of LP events per day (in blue) and total duration of tremor episodes per day (in red). Green stars indicate the presence of monochromatic tremor episodes. The inferred time interval of dome extrusion is indicated at the top of the plot.

duration of tremor per day (in red) based on horizontal-component records obtained at PPIG. Episodes of harmonic tremor are indicated by green stars. More than 7200 LP events with daily occurrence peaking at 145 LP events on March 01, 2000, and 40 tremor episodes lasting a minimum of 10 minutes, were recorded between November 10, 1999 and May 2000.

Figs 5.3 (a), 5.3 (b) and 5.3 (c) provide an overview of the seismicity recorded on 12/31/99 at PPO2, 02/26/00 at PPC2 and 01/03/00 at PPQ2 (see Fig 5.2). The time series in Fig 5.3 represent 6 hours of continuous data for the vertical component of velocity in units of  $\mu\text{m/s}$ . The traces are corrected for instrument response and filtered in the 0.8-20 Hz band to provide a record of signals in the short-period band.

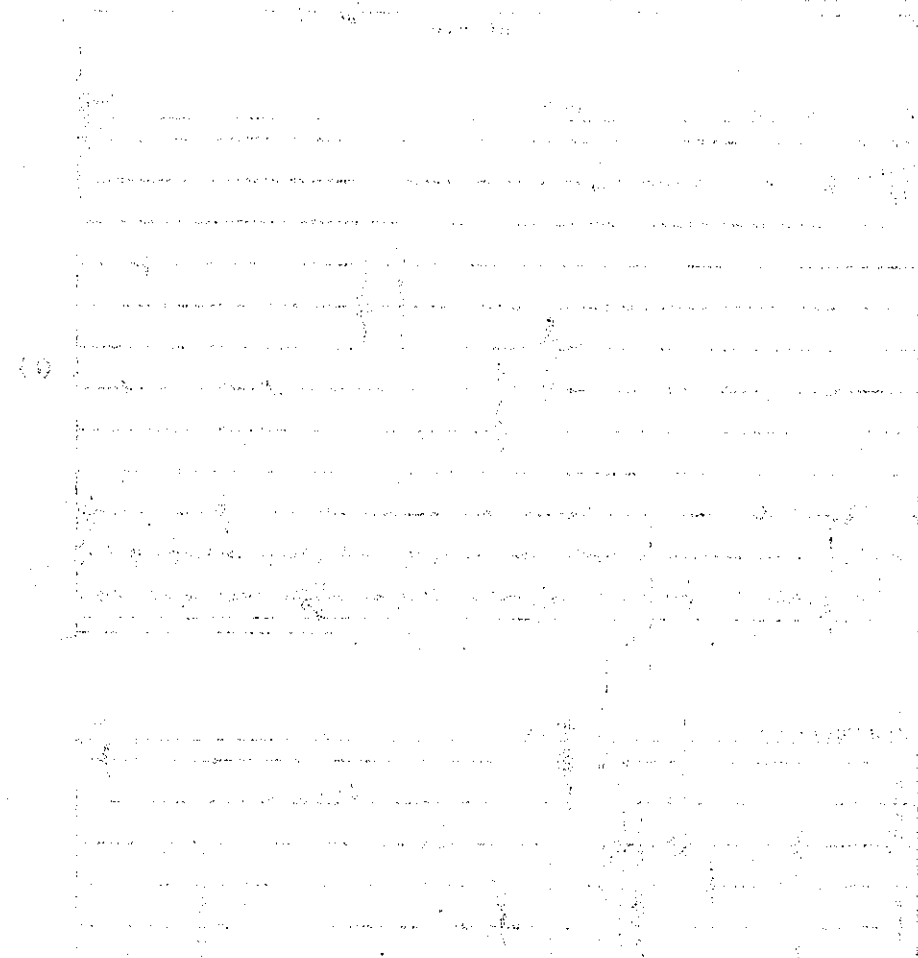


**Fig. 5.3** Broadband records of the vertical component of velocity at stations PPO2 on December 31, 1999 (*a*), PPC2 on February 26, 2000 (*b*), and PPQ2 on March 1, 2000 (*c*). Each line is 30 minutes in duration and the total time displayed is 6 hours. Date and beginning time of the record are indicated at the upper left. Vertical scale in  $\mu\text{m}/\text{s}$  is indicated at the upper-right of each plot.

Fig 5.3 illustrates changes in activity, and demonstrates the wide variety of signals produced within periods as short as a few hours. The variations in the amplitude and frequency of occurrence of LP events correlate with changes in eruptive activity. By the end of February, tremor episodes and LP events increase in number and intensity (Figs 5.3 *b*, *c*) in coincidence with visual observations of emplacement of the lava dome. At all the receivers located at distances less than 2500 m from the crater, the LP events dominate the seismograms. Tremor shows smaller amplitudes compared to LP events, and appears as a persistent background signal in the seismogram. This small amplitude high-frequency tremor correlates with VLP tremor as we will demonstrate in the next section.

Samples of LP events recorded on the network are shown in Figs 5.4-5.7, together with their associated power spectra. Power spectra were calculated by sampling each event with a 60-s window spanning the entire record. Comparing the spectral peaks obtained at different stations for a given event, we find that different sites share common peaks at several frequencies within the 0.5-5 Hz band. Variations in the amplitudes of common spectral peaks among stations may indicate path effects. Furthermore, comparing the spectral peaks obtained for different events at the same station, we find that common spectral peaks are shared for different events. The alignment of spectral peaks observed for different events and for different stations indicates that these events share a similar source geometry. Differences in the spectral amplitudes among different events are further suggestive of different excitations of a fixed source. Such differences may also be indicative of changes in fluid properties [Chouet *et al.*, 1994, 2000, 2001; Nakano *et al.*, 1998; Kumagai *et al.*, 2001].

Some LP events show a dominant peak around 1 Hz and are more depleted in higher frequencies than others. This is the case, for example, of event 122499 (Fig 5.4) and

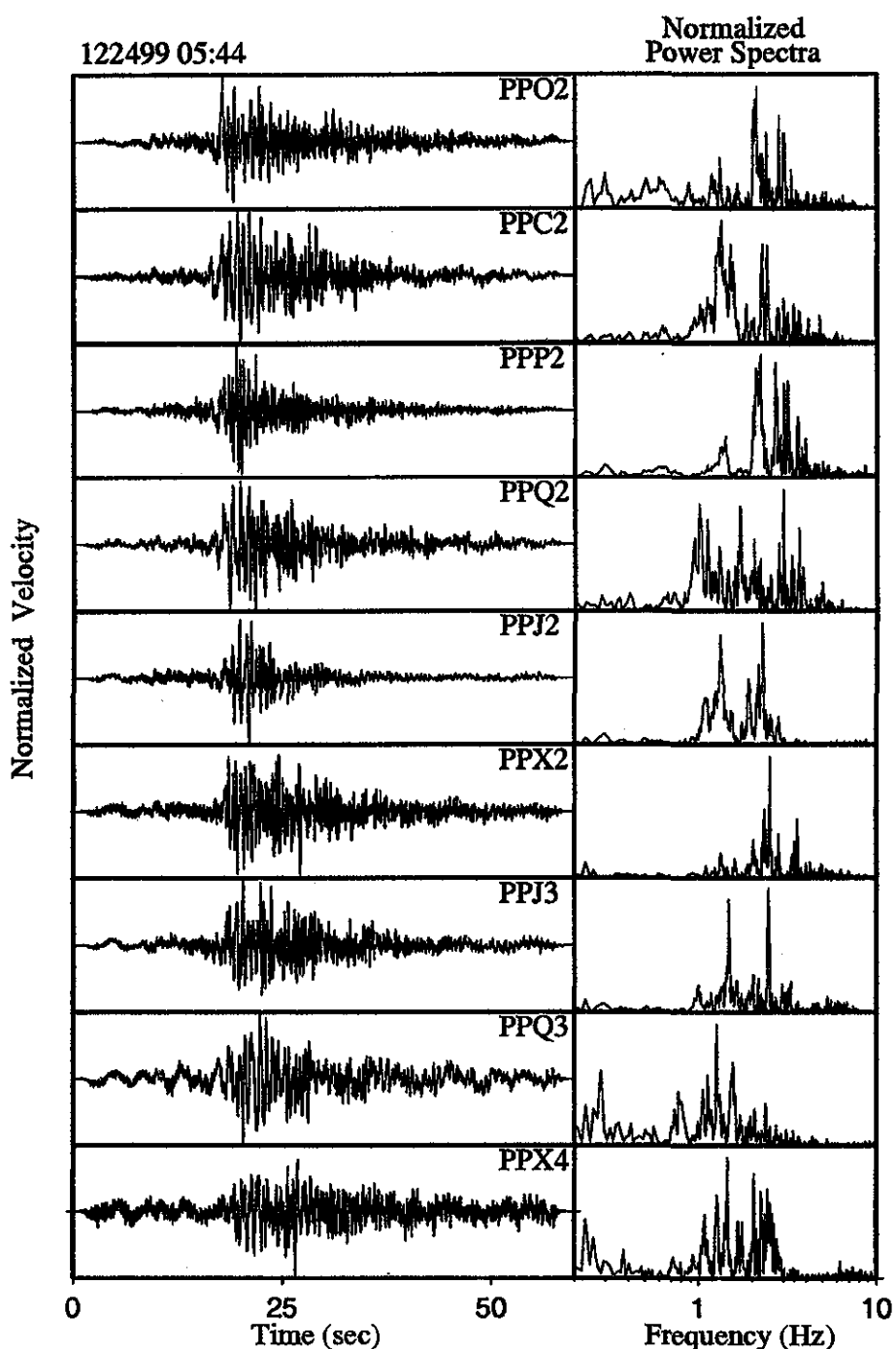


**Fig. 5.4** Examples of LP signatures recorded at nine stations on December 24, 1999, and corresponding normalized power spectra calculated over the same time window. The date and beginning time of the record indicated at the upper left. The station name is indicated at the upper right corner of each record. This LP event was associated with an emission of ash and gas.

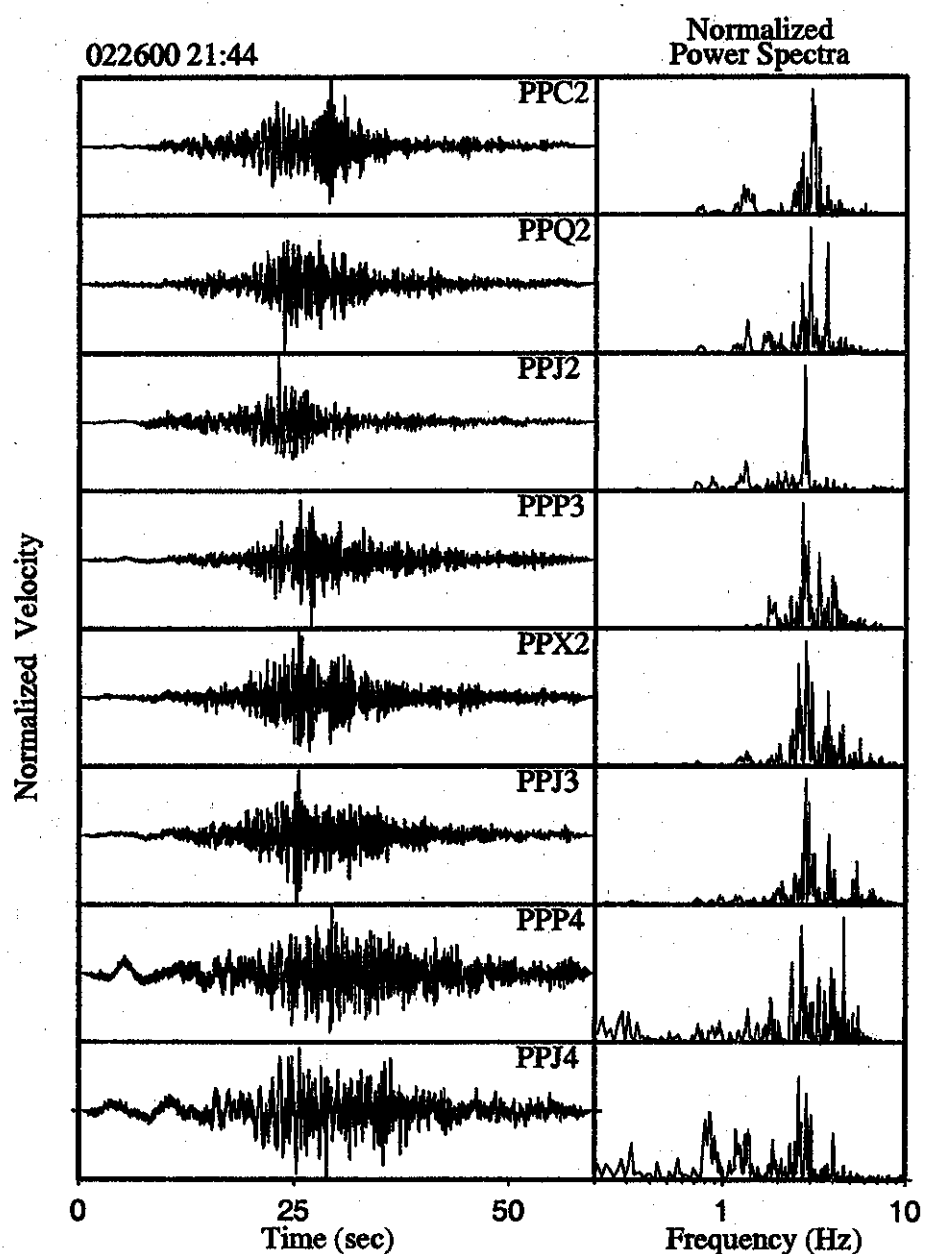


Fig. 5.5 Same as in Fig. 5.4 for an LP event at 21:44 on February 26, 2000.

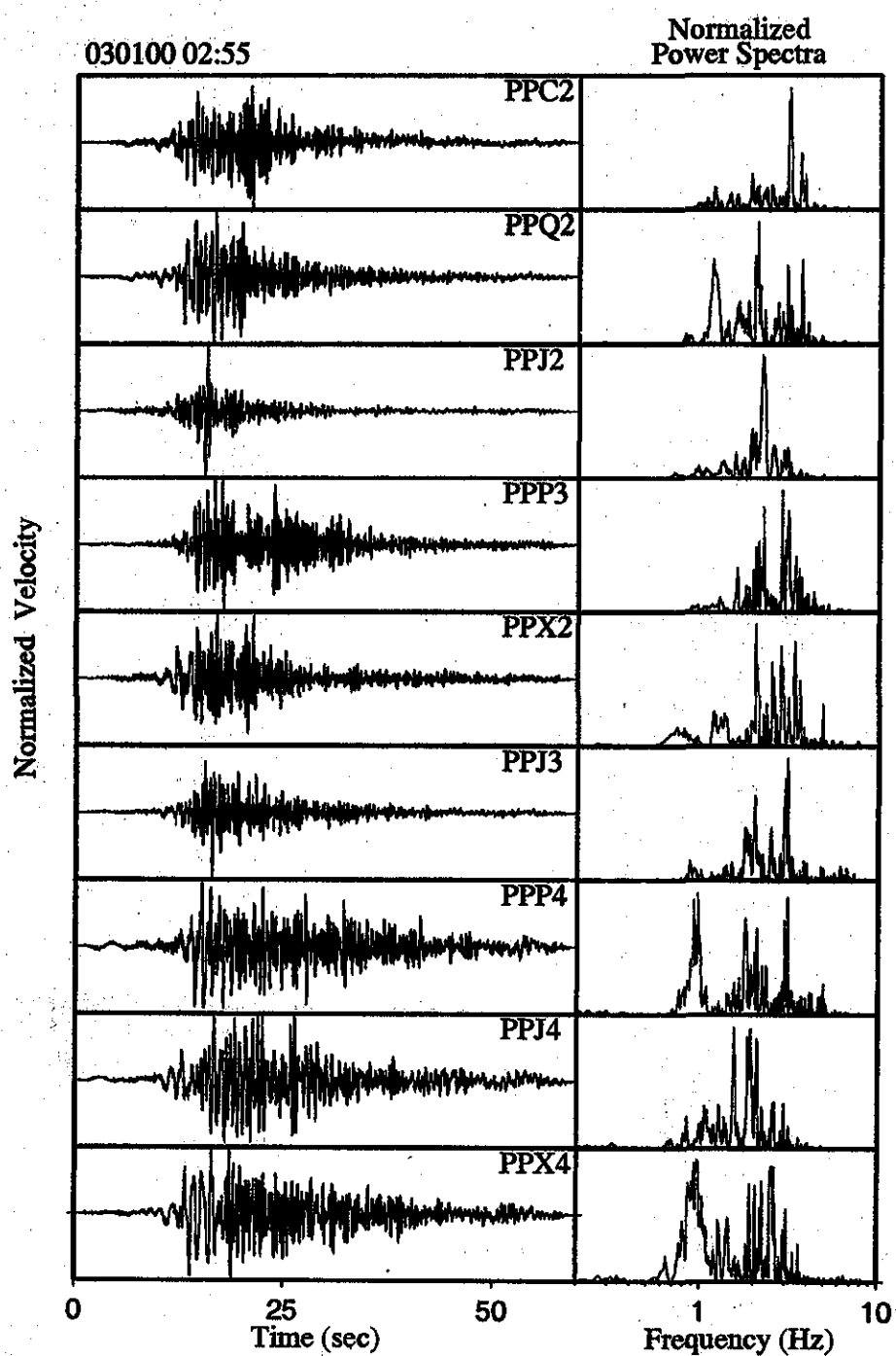


Fig. 5.6 Same as in Fig. 5.4 for an LP event at 02:55 on March 01, 2000.

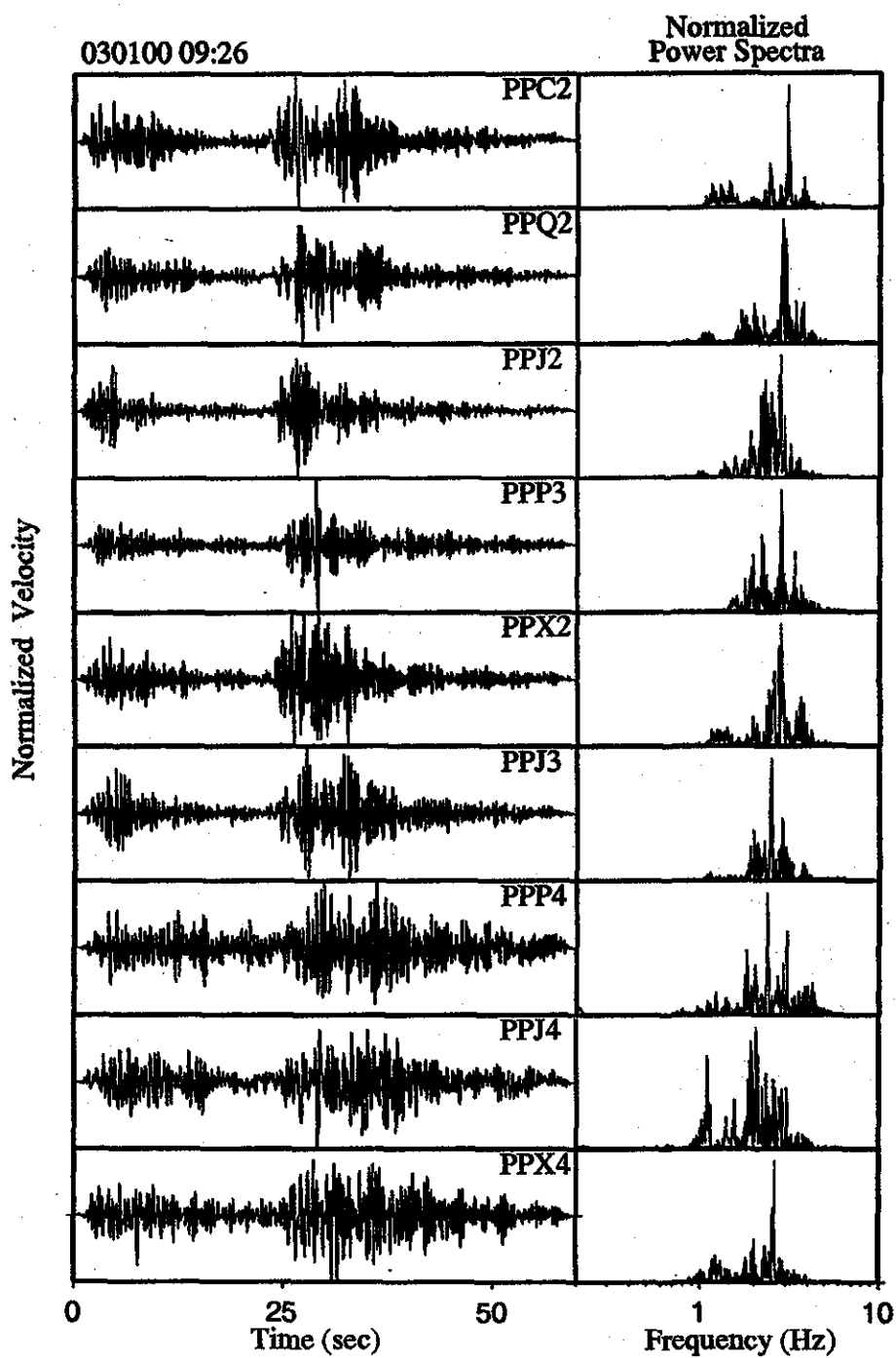


Fig. 5.7 Same as in Fig. 5.4 for an LP event at 09:26 on March 01, 2000.

event 030100 (Fig 5.7). Those temporal changes in frequency content suggest that the fluid mixtures may not remain the same within the same source. Recent investigations of the complex frequencies of the LP events demonstrate that the frequency content of LP events may be used to constrain the fluid composition beneath volcanoes [Kumagai and Chouet, 1999, 2000].

## Crack model

To study the modes of resonance and elastic radiation of a fluid-filled body in a volcano three geometries have been proposed: the fluid-filled sphere [Crosson and Bame, 1985], the fluid-filled pipe [Chouet, 1985] and the fluid-filled crack [Aki *et al.*, 1997; Chouet, 1986, 1988, 1992]. To model the frequencies of LP events, we use the fluid-filled crack model which has been extensively studied by Chouet [1986, 1988, 1992] using the finite difference method (a review of the fluid-filled crack model is presented in Appendix B). This model is appropriate for mass transport conditions beneath volcanoes. In Chouet's model the observed spectral peaks represent the resonance modes of the fluid-filled crack. Chouet's model has been used to fit the distribution of spectral peaks of LP events at Redoubt, Galeras and Kilauea volcanoes [Chouet *et al.*, 1994; Gil-Cruz and Chouet, 1997; Dawson *et al.*, 1998; Saccorotti *et al.*, 2001] and to account for the repetitive behavior of LP events observed at Redoubt [Morrissey and Chouet, 1997; Stephens and Chouet, 2001]. The dynamic of motion of the walls of the fluid-filled crack is determined by solving simultaneously the equations of elastodynamics in the solid and the equations for mass and momentum transfer in the fluid. The frequencies of the wave modes of the crack are fixed by the crack geometry and physical properties of the fluid and solid. The relative excitation of the modes depends on the position of pressure transient on the crack wall, the area over which this transient is applied, the time history of transient, and the boundary

conditions for the fluid flow at the crack perimeter. The spectra calculated from this model represent the combined contributions of the longitudinal and lateral modes of resonance of the fluid-filled crack. Chouet studies show that the resonance of the fluid-filled crack is sustained by a very slow wave he called the crack wave. The slow speed of the crack wave leads to more realistic estimates of the size of the resonator because the resonant periods of the fluid-filled crack are much longer than those expected from acoustic resonance. The crack wave is always slower than the acoustic speed of the fluid and inversely dispersive, showing a strong decrease in wave speed with increasing wavelengths. An important parameter controlling the speed of the crack wave is the crack stiffness,  $C$ , defined as [Aki *et al.*, 1977; Chouet, 1986]:

$$C = \frac{b L}{\mu d} , \quad (1)$$

where  $b$  is the bulk modulus of the fluid,  $\mu$  is the rigidity of the solid, and  $L$  and  $d$  are the length and aperture of the crack, respectively. Denoting the compressional wave velocity in the solid by  $\alpha = [(\lambda + 2\mu)/\rho_s]^{1/2}$ , in which  $\lambda$  and  $\mu$  are the Lamé constants, and denoting the acoustic speed in the fluid by  $a = (b/\rho_f)^{1/2}$  and assuming  $\lambda = \mu$ , we obtain the stiffness as:

$$C = 3 \frac{a^2 \rho_f}{\alpha^2 \rho_s} \frac{L}{d} , \quad (2)$$

where  $\rho_s$  and  $\rho_f$  denote density of the solid and fluid, respectively.

The dispersion characteristics of the crack wave represented by the dimensionless ratio

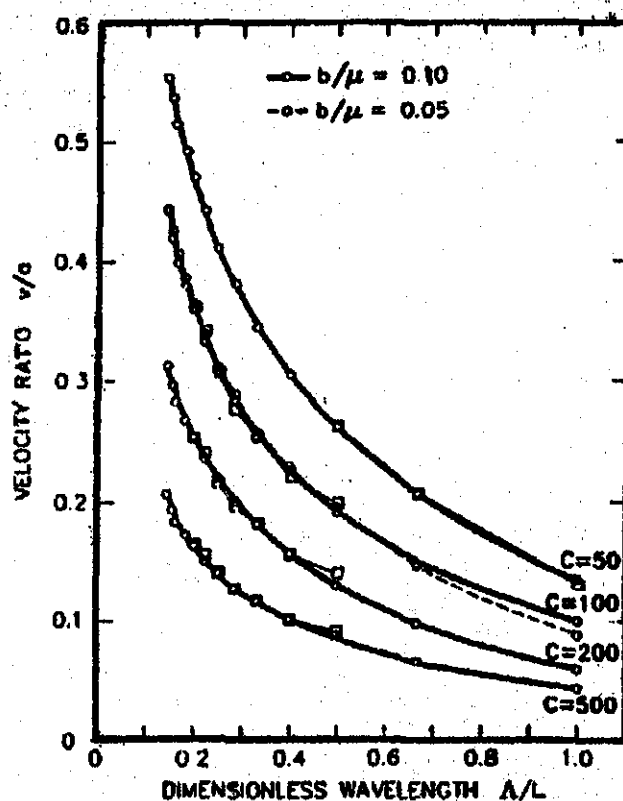


**Fig. 5.8** Ratio  $v/a$  of the phase velocity of the crack wave to the acoustic speed of the fluid plotted as a function of dimensionless wavelength  $\Lambda/L$ . Reproduced from Chouet *et al.* (1994).

$v/a$  of the phase velocity of the crack wave to acoustic velocity in the fluid plotted as a function of the dimensionless wavelength  $\Lambda/L$  for values of crack stiffness ranging from 50 to 500 and for two values of the ratio  $b/\mu$ , are shown in Fig 5.8. Ferrazzini *et al.* (1990) demonstrated that the dependence of the dispersion characteristics on the value of the ratio of the crack width to crack length,  $W/L$ , is small, and will not be considered in our discussion. As a first step in modeling our data, we assume here a width-to-length ratio  $W/L = 0.5$  and follow the same procedure as in Chouet *et al.* (1994) for Redoubt Volcano, or Gil and Chouet (1977) for Galeras Volcano.

## Spectral peaks and crack dimensions

LP events with common spectral characteristics occur synchronously with emissions of steam and gases. This close relationship between LP event production and eruptive activity has been observed since the reactivation of Popocatepetl in December 1994 [Arciniega *et al.*, 2000]. The same correlation of LP activity with eruptive activity was observed during the time span reported in this work. The similar spectral characteristics of LP events and tremor have been observed at several volcanoes including Redoubt, Kilauea, Stromboli, Galeras, Kusatsu-Shirane and Aso Volcanoes, to name a few. This repetitive behaviour of LP events may be explained by considering a generating system acting continuously in response to a repeated excitation of the source. Changes in the intensity of activity depend on the pressure conditions in the system. Although it does not provide a physical explanation for the origin of the pressure transient the fluid-filled crack model is useful for a separation of source, path and site effect [Chouet, 1992]. Based on our assumption that common spectral peaks in the LP events illustrated in Figs 5.4-5.7 represent a source effect, we use these spectral peaks to model the geometry of the LP source.

To assess source effects, we compare the power spectra of LP events recorded at 7 receivers near the crater (PPO2, PPC2, PPP2, PPQ2, PPJ2, PPP3 and PPX2). The dominant spectral features of the source are emphasized by stacking the power spectra of 55 LP signals, followed by smoothing and normalizing the resulting power spectra (Fig 5.9). Each spectrum is calculated over a 60 s window bracketing the entire record of a LP event.

Fig 5.9 shows the stacked spectra obtained at the 7 receivers. Each spectrum is marked

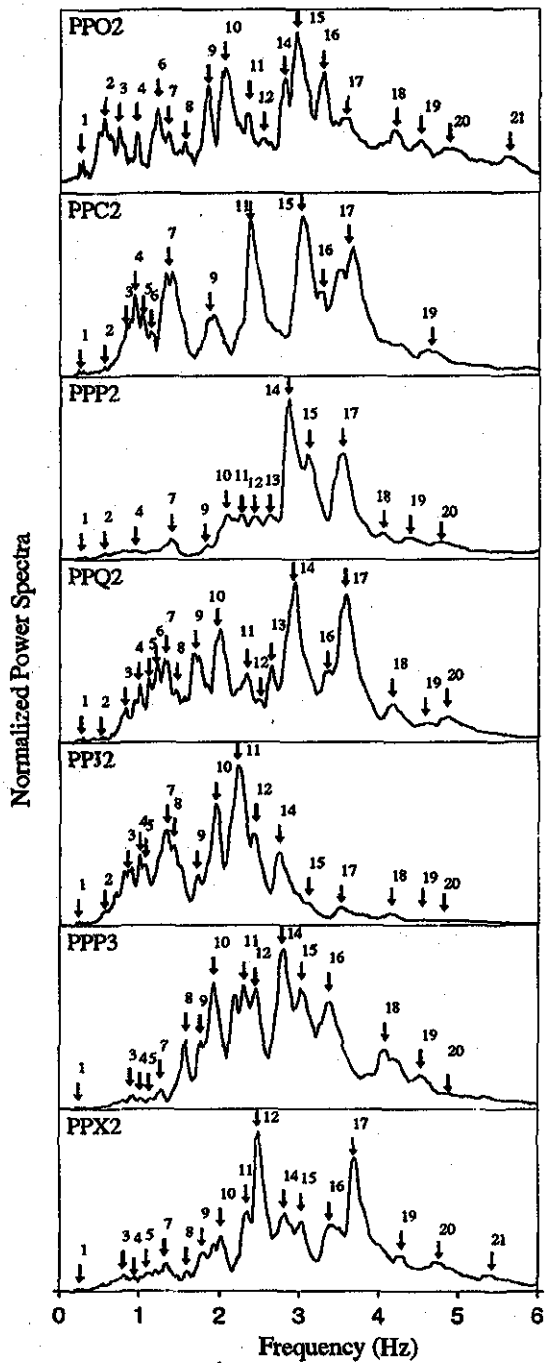


**Fig. 5.9** Normalized power spectra of the vertical component of ground velocity obtained at the seven stations nearest to the crater for LP events associated with degassing. The power spectra were obtained by stacking individual spectra for 55 LP events and smoothing and normalizing the resulting power spectra. Each spectrum was calculated over a 60 s window spanning the entire record of the event. Common spectral peaks observed in at least two stations are identified by numbers (see Table 5.1).

by several dominant and subdominant peaks. Individual spectral peaks are shared by at least two receivers within a maximum standard deviation of  $\pm 0.06$  Hz. We identified 21 common peaks which are marked by numbered arrows in the figure (their corresponding frequencies are listed in Table 5.1). As stated in Chouet *et al.* (1994), the stability of the individual spectral peaks observed at widely separated stations (Fig 5.1) for which the wave-fields are obviously uncorrelated, is strongly suggestive that the common spectral peaks represent a source effect. The amplitude of spectral peaks vary from site to site, possibly related to the radiation pattern of the source [Chouet, 1988] and/or path and site effects. Such source could be a resonator with characteristics as described in the previous section for a fluid-filled crack.

To estimate the geometrical parameters of the fluid-filled crack we first check if the observed frequencies listed in Table 5.1 are compatible with the dispersion curves of Fig 5.8. First, we calculate the dimensionless frequency  $\nu'$  using the formula  $\nu' = (v/a)/[(\alpha/a)(\Lambda/L)]$ , in which we take  $(v/a)$  from the dispersion curve (Fig 5.8). We assume the mode associated with a particular spectral peak and use the wavelength  $\Lambda$  of the mode given by the model ( $\Lambda = 2L/n, n = 2, 3, 4, \dots$ ). Then, the crack length is calculated from the relation  $L = \alpha\nu'/\nu$  where  $\nu$  is the observed frequency assuming that the sequence of frequencies in Table 5.1 represent longitudinal modes of resonance. After several trial and error iterations a suitable length of the crack is considered when each of the observed spectral peaks in Table 5.1 correlate with one resonance mode of the crack model, and the variation in crack length associated with each peak does not exceed 10% of the average  $L$  estimated for all peaks. Estimations are improved when the differences in the frequencies of a particular peak are negligible at different sites (see, for example peak number 7 in Table 5.1). We used the same procedure as outlined above in our treatment of the lateral modes of resonance. In this case, we use the transverse crack stiffness  $C_t = (b/\mu)(W/d)$  which is fixed from  $C$  in eq. (1) through the ratio  $W/L = 0.5$ .

Peak #	PPO2	PPC2	PPP2	PPQ2	PPJ2	PPP3	PPX2	$\lambda_2$	$\lambda_4$
1	<b>0.25</b>	<b>0.25</b>	<b>0.25</b>	0.26	0.23	<b>0.24</b>	<b>0.25</b>	L	L
2	<b>0.55</b>	<b>0.55</b>	0.54	0.52	<b>0.55</b>	—	0.52	2L/3	2L/3
3	0.73	0.80	—	0.80	0.84	0.79	0.79	—	L/2
4	0.95	0.92	<b>0.93</b>	<b>0.94</b>	0.99	0.89	0.92	L/2	—
5	—	<b>1.03</b>	—	0.98	1.07	1.00	1.08	2W/3	2W/3
6	1.20	1.12	—	1.19	—	—	—	—	—
7	1.35	1.35	1.38	<b>1.32</b>	<b>1.33</b>	1.26	1.30	2L/5	2L/5
8	1.56	—	1.56	1.54	1.52	1.56	1.57	—	—
9	<b>1.83</b>	1.86	1.80	1.85	1.71	—	1.88	W/2	W/2
10	<b>2.04</b>	—	2.06	1.96	1.93	2.06	<b>2.00</b>	L/3	—
11	2.34	2.37	2.26	2.33	2.22	<b>2.29</b>	2.32	—	2L/7
12	2.54	—	<b>2.41</b>	2.50	2.44	2.44	<b>2.47</b>	—	2W/5
13	—	—	2.61	2.64	—	—	2.79	2W/5	—
14	2.80	—	<b>2.84</b>	2.91	2.75	2.77	2.92	2L/7	L/4
15	2.95	<b>3.02</b>	3.11	—	3.11	<b>3.03</b>	3.02	L/4	—
16	3.28	3.28	—	3.34	—	3.28	—	—	W/3
17	3.58	3.48	<b>3.52</b>	3.56	3.51	—	3.38	2L/9	2L/9
18	4.04	4.13	4.04	4.16	4.15	<b>4.06</b>	4.02	W/3	L/5
19	4.52	<b>4.58</b>	—	<b>4.58</b>	4.54	4.53	4.59	L/5	2L/11
20	4.88	—	4.76	4.85	<b>4.81</b>	4.88	4.75	2W/7	2W/7
21	5.63	<b>5.61</b>	—	—	—	—	5.60	2L/11	L/6

**Table 5.1** Frequencies of spectral peaks shown in Fig 5.9, for common frequencies observed in at least three stations within ( $\pm 0.06$ ) Hz. Bold numbers denote frequencies that match the modes of resonance of a fluid-filled rectangular crack. Their associated wavelengths  $\lambda_2$  and  $\lambda_4$  correspond to models 2 and 4, respectively.

We consider three different values of sound speed in the fluid for our calculations, namely  $a = 400, 600$ , and  $800$  m/s. These values are consistent with acoustic speeds measured in gas mixtures and gas-ash mixtures [Morrissey and Chouet, 2001]. Measurements of  $SO_2$  and  $CO_2$  fluxes in Popocatepetl plumes indicate levels up to 60,000 t/day, while during quiescent periods the estimated levels are around 9000 t/day [Love *et al.*, 1998, Gerlach *et al.*, 1998], recent results report 5000 t/day [Delgado *et al.*, 2001]. The  $CO_2/SO_2$  ratios between 2 and 6 measured by Goff *et al.* (1998) represent the highest values of such ratio measured for any volcano. Morrissey and Chouet (2001) followed the study made by Kieffer (1977) and investigated the sound speeds of different types of fluids, including gas mixtures, ash-gas mixtures, and liquid-gas mixtures with gas-volume fractions  $< 10\%$ . Based on the content of  $SO_2$  and  $CO_2$  in volcanic emissions at Popocatepetl we assume that a crack filled with either gas mixtures or an ash-gas mixture, or steam.

For pure  $H_2O$ , the sound velocity ranges from 695 to 940 m/s at temperatures between 800 and 1600 K [Kieffer, 1977]. For a gas mixture of  $H_2O - CO_2$  or  $H_2O - SO_2$  within the same range of temperatures, and for a 50%/50% mixture of gases the sound speed varies from 550 to 750 m/s for  $H_2O - SO_2$ , and from 560 to 780 m/s for  $H_2O - CO_2$ . For an ash-gas mixture within the same range of temperatures, for a density of ash of  $2200 \text{ kg/m}^3$  and for a 50% weight fraction of ash, the sound speeds are between 470 and 695 m/s for an  $H_2O - \text{ash}$  mixture, and between 285 and 415 m/s for a  $CO_2 - \text{ash}$  mixture [Morrissey and Chouet, 2001]. In our calculations we use  $a = 800$  m/s for pure  $H_2O$ ,  $a = 600$  m/s for  $H_2O - CO_2$  or  $H_2O - SO_2$  mixtures and,  $a = 400$  m/s for gas-ash mixture.

Values of the compressional wave speed of the solid,  $\alpha$ , and the fluid density ratio,  $\rho_f/\rho_s$ , are both required for our calculations. For a volcano with andesitic composition such as Mt Hood, a compressional wave velocity of 5500 m/s was determined by Murase and Mc Birney (1973). Popocatepetl also has an andesitic composition, however, this

Model	C	L(m)	W(m)	d (m)	$\alpha/a$	$\rho_f/\rho_s$	$b/\mu$	$\Delta P$ (MPa)
1	200	108	56	0.009	8.0	0.37	0.017	0.008-0.81
2	500	106	54	0.008	5.3	0.37	0.040	0.085-1.14
3	200	215	110	0.075	4.0	0.37	0.069	0.008-0.26
4	100	266	132	0.104	5.3	0.37	0.040	0.064-0.14
5	100	323	166	0.224	4.0	0.37	0.069	0.008-0.10

**Table 5.2** Source parameters of the fluid-filled crack models estimated for LP events recorded at the seven sites closest to the crater.

edifice is composed of alternating layers of ash and vesiculated lava which result in a lower compressional wave velocity. In this work,  $\alpha$  is arbitrarily fixed to 3200 m/s taking into account that within the crater the material is partially molten, vesiculated and micro fractured. We assume the ratio  $\rho_f/\rho_s = 0.37$ . Although this represents a rough approximation, this ratio is compatible with magmatic and hydrothermal fluids containing void fractions of gas ranging up to a few percent [Kieffer, 1977; Aki *et al.*, 1978; Chouet *et al.*, 1994].

We considered three values of crack stiffness  $C = 100, 200$  and  $500$ , and tried several combinations of modes of resonance in which we used most of the peaks listed in Table 5.1. Five different geometries of the fluid-filled crack were found to be compatible with seismic data, yielding the following parameters:  $106 < L < 323$  m,  $54 < W < 166$  m, and  $0.009 < d < 0.224$  m. Table 5.2 lists the geometrical source parameters and ratios  $\alpha/a$  and  $\rho_f/\rho_s$  used in our calculations. The best match between data and model are obtained for models 2 and 4 in which fifteen frequencies are fitted, including the dominant peak of each spectrum. Frequencies appearing in bold in Table 5.1 correspond to the best fit obtained for the longitudinal or lateral modes of resonance for a fluid-filled rectangular crack. Their associated wavelengths are also listed in Table 5.1.

## Far-field radiation patterns

In this work, the term source refers to the composite source formed by the resonator and the triggering element (the energy source) as defined in Chouet (1988, 1992, 1996). In our first step in modeling the seismic data, we demonstrated in the previous section that the spectral characteristics of LP events associated with fumarolic activity and/or emissions of gas and ash, are compatible with the modes of resonance of a fluid-filled crack. Accordingly, the resonator involved at the source of LP events is represented by a crack-like conduit whose geometrical dimensions are estimated following the procedure of Chouet *et al.* (1994). The geometrical parameters we obtained are as follow: crack length 106-323 m; crack width 54-166 m; crack aperture 9-224 mm; sound speed of fluid, 400-800 m/s; and compressional wave speed in the rock, 3200 m/s.

To investigate the radiation patterns we assume two orientations (N45E and N120E) for a vertical crack located beneath the crater. Quantitative estimates of the reduced displacement and excess pressure associated with individual LP events may be obtained for different wave types composing the seismograms. From the calculated ratios of crack length to hypocentral distance (ranging from 1.58 to 2.670 km), we infer that the seismometers are recording the far-field from the sources. Accordingly, the observed vertical components of motion must consist of a mix of P, SV, and Rayleigh waves. Assuming  $\lambda = \mu$ , the Fourier transforms of the far-field P and SV displacements  $u^R$  and  $u^\theta$  radiated by the crack are given by Chouet, 1988 and Chouet *et al.* (1994):

$$u^R(\vec{R}, \omega) = \frac{1}{12\pi\alpha R} (1 + 2\sin^2\theta \sin^2\phi) \Delta\dot{v}(k_z, w, \phi) , \quad (3)$$

$$u^\theta(\vec{R}, \omega) = \frac{1}{4\pi\beta R} \sin 2\theta \sin^2\phi \Delta\dot{v}(k_z, w, \phi) ,$$

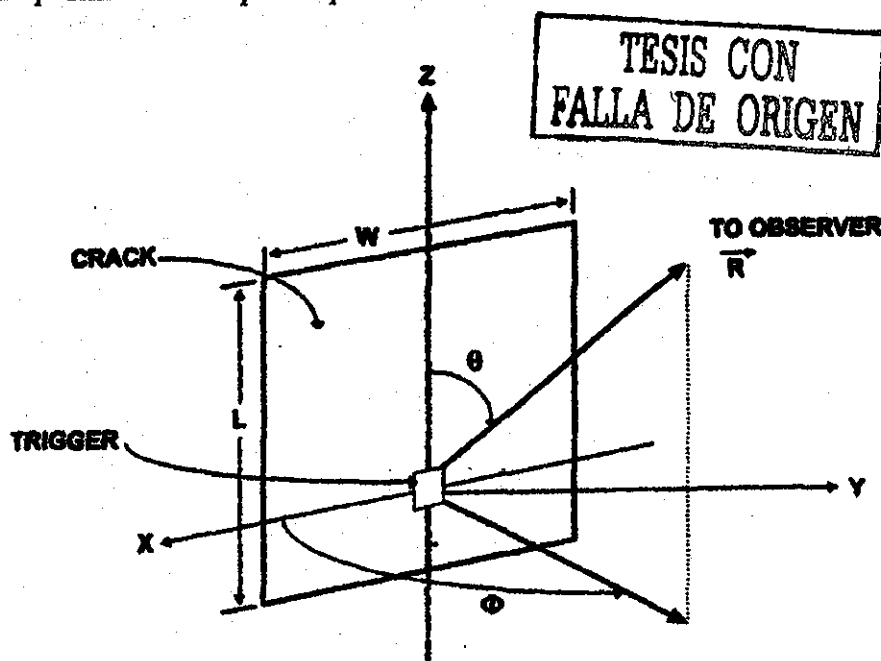


**Fig. 5.10** Crack geometry and coordinate system used in the calculations of the far field radiation from the fluid-filled crack. Reproduced from Gil-Cruz and Chouet (1997).

where  $\vec{R}$  is the position vector of the observer  $R = |\vec{R}|$ ,  $\alpha$  is the compressional velocity,  $\beta$  is the shear velocity,  $\theta$  and  $\phi$  are the polar and azimuth angles under which the source is observed (Fig 5.10),  $k_z$  is the wavenumber in the  $z$  direction,  $\omega$  is the radial frequency, and the quantity  $\Delta\nu$  is the source opening-velocity function.

To investigate the Rayleigh wave spectrum generated by the crack oscillation, we assume a cylindrical coordinate system  $(x, \phi, z)$  and Cartesian coordinate system  $(x, y, z)$ , in which the  $z$  axis is taken positive downward and where  $x = r\cos\phi$  and  $y = r\sin\phi$ , and consider a vertical crack located at  $r = 0$  in the plane  $y = 0$ , with a trigger positioned at depth  $h$ . The vertical component of displacement of  $n$ th mode Rayleigh waves radiated by the point source with moment tensor corresponding to a tensile crack with this geometry can be written as [Chouet *et al.*, 1994]:

$$|u_z^R| = \frac{1}{\beta\mu} \left( \frac{1}{\Lambda r} \right)^{1/2} (p + q \sin^2 \phi) L^3 \Delta P |\Delta \dot{v}'| , \quad (4)$$

where  $\Delta \dot{v}'$  is the dimensionless quantity  $(\mu/\Delta P)(1/L^3)\Delta \dot{v}$ ,  $\Delta P$  is the excess pressure at the source,  $L$  is the crack length,  $\Lambda$  is the wavelength,  $r$  is the epicentral distance, and  $p$  and  $q$  are given by:

$$p = 0.5527 e^{-0.8475 k_n h} - 0.3714 e^{-0.3933 k_n h} , \quad (5)$$

$$q = 0.9650 e^{-0.8475 k_n h} - 0.5571 e^{-0.3933 k_n h} ,$$

where  $k_n$  is the wavenumber of  $n$ th mode in the ground, and  $h$  is the focal depth. Using the above relations we obtain the ratios of amplitudes of P, SV and Rayleigh waves as:

$$\frac{|u^\theta|}{|u_z^R|} = \frac{\sin 2\theta \sin^2 \phi}{4\pi(p + q \sin^2 \phi)} \sqrt{\frac{\Lambda}{r}} ,$$

$$\frac{|u^R|}{|u_z^R|} = \frac{1 + 2\sin^2 \theta \sin^2 \phi}{12\pi\sqrt{3}(p + q \sin^2 \phi)} \sqrt{\frac{\Lambda}{r}} , \quad (6)$$

$$\frac{|u^\theta|}{|u^R|} = \frac{3\sqrt{3}(\sin 2\theta \sin^2 \phi)}{1 + 2\sin^2 \theta \sin^2 \phi}$$

To infer the types of waves in the vertical component seismograms of LP events, we estimate the above ratios at stations PPO2, PPC2, PPP2 and PPJ2, in which we use the appropriate angles  $\theta$  and  $\phi$  for the selected crack orientations. We assume a depth range of 0-1.2 km, consistent with our assumed acoustic properties for LP events and with locations obtained earlier for LP events (see Chapter 3). The frequencies ( $\nu$ ) we select are those of the dominant spectral peaks observed at sites PPO2, PPC2, PPP2 and PPJ2 (see Fig 5.1 and Table 5.1). Data pertaining to each site are listed in Table 5.3. We used  $\Lambda = 5.80$  km ( $\nu = 2.95$  Hz) at  $r = 1.5$  km for PPO2,  $\Lambda = 5.60$  km ( $\nu = 3.02$  Hz) at  $r = 1.8$  km for PPC2,  $\Lambda = 6.00$  km ( $\nu = 2.84$  Hz) at  $r = 2.1$  km for PPP2,  $\Lambda = 7.80$  km ( $\nu = 2.22$  Hz) at  $r = 2.6$  km for PPJ2, with  $\beta = 1.85$  km/s. From the spectral ratios and depth range 0-1.2 km, the SV-wave amplitudes are 1.3 times larger than P-wave amplitudes, and Rayleigh-wave amplitudes are 20-70 times larger than the SV-wave amplitudes. Therefore, the dominant amplitudes observed in the seismograms recorded on broadband stations around the crater consist mainly of Rayleigh waves.

### Estimates of pressure

Pressure fluctuations causing LP seismicity may be of any origin. For example, pressure transients associated with mass transport may trigger the acoustic vibrations of the fluid, thus generating LP events and/or tremor [Chouet, 1996]. Crack resonance is triggered by a pressure-transient and the location and spatial extent of the transient determines which modes of resonance are excited [Chouet, 1992].

The excess pressure  $\Delta P$  at the LP source can be obtained from the expression for Rayleigh and body waves given by Aki (1984):

$$RMS(\Delta P) = \frac{2\pi RMS(u^R)\sqrt{\Lambda r}}{(1/Q_r)^{1/2}[V/(\delta\nu\rho_sbc)]^{1/2}}, \quad (7)$$

$$RMS(\Delta P) = \frac{2\pi RMS(u^{R,\theta})R}{(1/Q_r)^{1/2}[V/(2\nu\rho_sbc)]^{1/2}},$$

where  $RMS(u^R)\sqrt{\Lambda r}$  and  $RMS(u^{R,\theta})R$  are the reduced displacements for Rayleigh and body waves, respectively,  $V$  is the volume of the crack,  $\nu$  is the dominant frequency of the seismic event,  $c$  the wave velocity,  $\rho_s$  is the density of the solid,  $b$  the bulk modulus of the fluid,  $\delta$  is a factor characterizing the effective depth of penetration of surface waves, and  $Q_r$  is the quality factor defining the radiation loss. From the assumption  $\lambda = \mu$ , the ratio  $(b/\mu) = 3(\rho_f/\rho_s)/(\alpha/a)^2$ , and using values in Table 5.2 for the density and velocity ratios, we obtain the ratio  $b/\mu$  in the range 0.017-0.069 for our models. The factor  $Q^{-1}$  of the LP event can be expressed as  $Q^{-1} = Q_r^{-1} + Q_i^{-1}$ , where  $Q_r^{-1}$  and  $Q_i^{-1}$  represent the radiation and intrinsic losses, respectively [Aki, 1984]. Intrinsic losses include viscous, thermal, and acoustic damping in bubbly liquids, or other phase interactions such as momentum transfer and phase changes in ash-gas mixtures and other multiphase fluids. In this work, the values for fluid properties are consistent with an inviscid fluid and we neglect interactions between phases [Kumagai and Chouet, 2001]. Accordingly,  $Q^{-1} \approx Q_r^{-1}$ , which can be estimated from the bandwidth of the dominant peak observed in the spectrum using the relation  $Q = \nu/\Delta\nu$  [Aki and Richards, 1980], in which  $\Delta\nu$  is the bandwidth of the spectral peak measured at one half of its amplitude. The quality factor for LP events recorded during the broadband experiment yield an average value  $Q = 22$ .

To estimate the excess pressure  $\Delta P$  that triggers the crack oscillations we used maximum and minimum values of reduced displacements for LP events recorded at PPO2 at  $\nu = 2.95$  Hz and in PPC2 at  $\nu = 3.02$  Hz. These values range from  $2.4 \text{ cm}^2$  to  $27 \text{ cm}^2$ .

Station	Epicentral distance (km)	Elevation (km)	Hypocentral distance (km)	Earthquake elevation (km)	Elevation difference (km)
PPO2	1.58	4.47	1.61	4.15	0.32
PPC2	1.87	4.30	1.87	4.15	0.15
PPP2	2.15	4.24	2.15	4.15	0.09
PPJ2	2.67	4.34	2.68	4.15	0.19

**Table 5.3** Station parameters

The values of  $\Delta P$  obtained for the different models range from 0.008 MPa to 1.14 MPa and are listed in Table 5.2.

## Discussion

Degassing is the most characteristic eruptive behaviour observed at Popocatepetl since the reactivation of the volcano in December 1994 [Arciniega *et al.*, 2000]. The seismicity is dominated by LP signals and tremor reflecting degassing activity mainly in the form of steam and larger emissions of  $SO_2$  and  $CO_2$ . The seismicity observed in the short-period frequency band (1-10 Hz) reported in this section correlates with the emplacement of a lava dome within the crater. During dome growth, LP seismicity increases in amplitude and daily rate of event production. Both individual LP events and tremor characterized by a persistent low-amplitude signal, are observed to occur simultaneously.

A wider coverage of the volcano with broadband instruments allowed us to investigate the characteristics of LP events in space and time. The spectra of LP events display common peaks for different events recorded over the network, strongly suggesting these

spectral features reflect source effects. The relative amplitudes of the spectral peaks vary from event to event, suggesting different non-destructive excitation of a common source. We have modelled this LP seismicity using a fluid-filled crack [Chouet 1988, 1992, 1996] as this geometry is the most appropriate for mass transport conditions beneath volcanoes. Moreover, Chouet's model has been successfully used to fit the distributions of spectral peaks observed at other volcanoes, and to account for the repetitive behavior of LP events. The fluid-filled crack model represents an idealization of a volcanic source in view of the complexities of volcanic media. Nevertheless, this model has shown that observed LP events and tremor episodes are consistent with the crack geometry [Chouet *et al.*, 1994; Gil-Cruz and Chouet, 1997]. We have demonstrated that the distribution of dominant spectral peaks in LP events at Popocatepetl are compatible with the modes of resonance of the fluid-filled crack model. The results of our analyses of LP events suggest that LP seismicity of Popocatepetl can be explained by a shallow crack-like fluid-filled conduit with crack length ranging from 106 to 323 m, crack width of 54 to 166 m, and crack aperture ranging from 9 to 224 mm, assuming a sound speed of the fluid between 400 and 800 m/s and compressional wave speed in the rock of 3200 m/s. The excess pressure  $\Delta P$  triggering the conduit resonance ranges from 0.008 to 1.14 MPa (0.08-11.4 bar). These estimates may be improved by matching the observed spectra with synthetics. For such purpose, however, better knowledge of the velocity structure is required, and the fulfillment of such objective is left for future studies.

## Very-long period seismic observations

Mass transport under volcanoes may produce seismic signals extending to periods much longer than 2 s. This type of signals falls under the appellation of very-long-period (VLP) seismicity. Previous studies of the VLP signals at Popocatepetl were based on data from a single broadband station located at a distance 5 km from the summit crater [Arciniega *et al.*, 1999; chapter III of this work]. Those studies demonstrated that a good correlation exists between LP activity and VLP signals occurring within a source region in the top 1.5 km beneath the crater floor. The observed repetitive occurrence of VLP signals with closely matched waveform characteristics is consistent with a non-destructive reactivation of at least two sources. One source appears to coincide with the main source region of LP seismicity, while the second is a deeper source whose activity appears to be intimately linked with episodes of monochromatic tremor. Another type of VLP signals was found to be associated with vulcanian explosions. These signals point to a mechanism involving the repetitive non-destructive activation of a fixed source located at a depth of approximately 2.8 km beneath the crater floor, and suggest a sequence of pressurization-depressurization-repressurization of the conduit.

We report results from initial analyses of continuous VLP data recorded at periods longer than 3 s. Our seismic observations focus on VLP characteristics recorded in two periods ranges, namely 2-12.5 s and 12.5-100 s. The first band contains a modulated persistent signal of volcanic origin, and microseismic oceanic noise. The second band includes signals exclusively of volcanic origin.

Figs 5.11 and 5.12 show a six-hour interval of continuous vertical-component velocity at station PPO2 on December 31, 1999 and January 7, 2000, respectively. Velocity traces

are shown in three different periods ranges, namely, 0.04-1 s (Figs 5.11 *a* and 5.12 *a*), 2-12.5 s (Figs 5.11 *b* and 5.12 *b*), and 12.5-100 s (Figs 5.11 *c* and 5.12 *c*). The seismograms are individually normalized by their maximum amplitude to facilitate comparison. The scale factor in  $\mu\text{m}/\text{s}$  is indicated at the upper right corner in each plot.

The correspondence between events in the 0.04-1 s band and VLP signals in the 12.5-100 s band is clear. Each strong VLP pulse in Figs 5.11 (*c*) and 5.12 (*c*) correlates with an energetic LP event in Figs 5.11 (*a*) and 5.12 (*a*), respectively. The VLP signals contain periods between 15 and 28 s and these are discussed in more detail in the next section.

Although, the 2-12.5 s band in Figs 5.11 (*b*) and 5.12 (*b*) includes the ocean microseismic noise with energy mainly concentrated in the 3-10 s band, detailed analyses of the spatial distribution of seismic amplitudes across our network suggest that the contribution from microseismicity is weak compared to the contribution from volcanic sources.

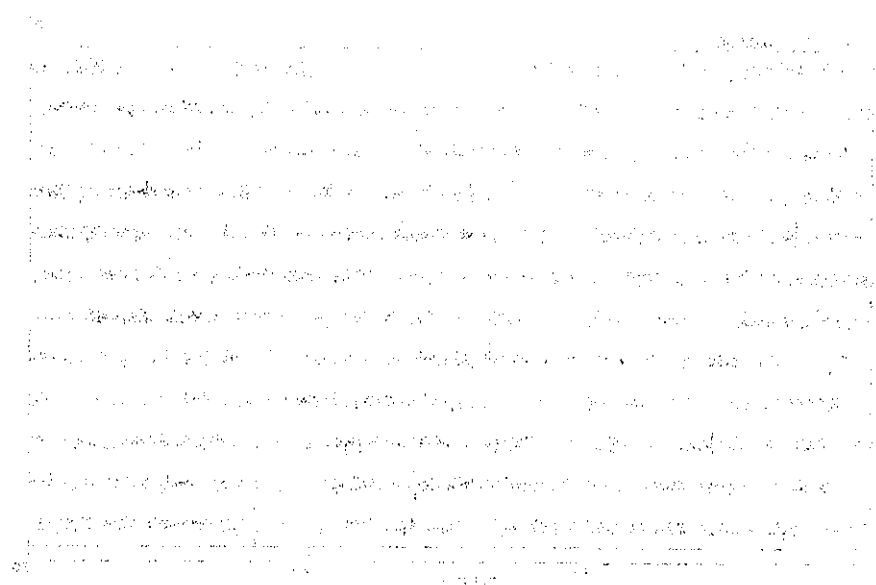


**Fig. 5.11** Bandpass filtered records of the vertical component of velocity at station PPO2 on December 31, 1999. (a) Record filtered in the 0.04-1 s band. (b) Record filtered in the 2-12.5 s band. (c) Record filtered in the 12.5-100 s band. Notice the correspondence between LP events and VLP pulses, and notice also the VLP tremor in the background. The total time shown is 6 hours and each line is 30 minutes in duration. The date and beginning time of the record are indicated at the upper left. Vertical scale in  $\mu\text{m}/\text{s}$  is indicated at the upper right, of each panel.

200 GRSI  
WAVEFORMS 2000

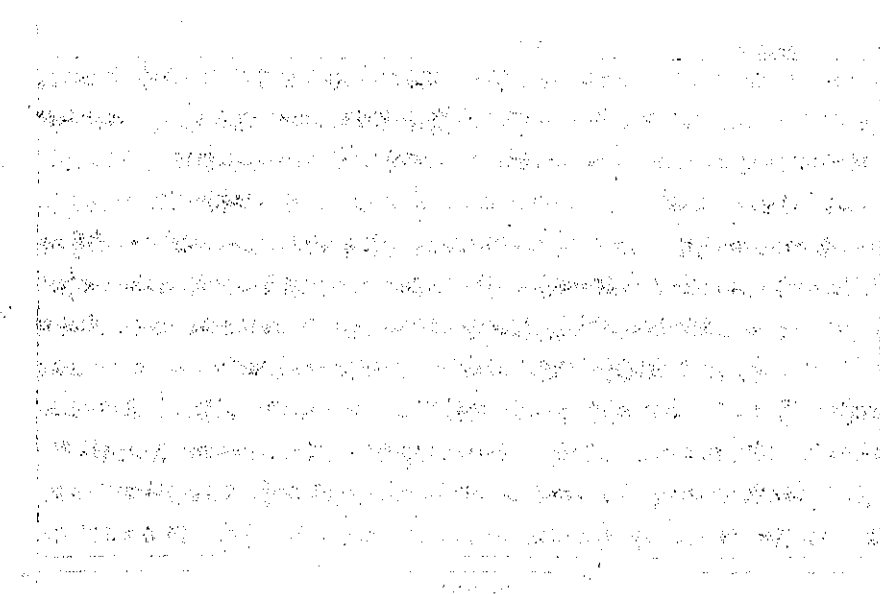


Fig. 5.11 Velocity record on January 7, 2000. The record shows the ground motion velocity over time. The vertical axis is labeled "VELOCITY" and has a scale bar from 0 to 10. The horizontal axis is labeled "TIME" and has a scale bar from 0 to 100. The plot shows several distinct seismic waves, with a prominent initial pulse followed by smaller, more frequent oscillations.

Fig. 5.12 Same as Fig 5.11 for velocity record on January 7, 2000.

Some of the background energy in the 12.5-100 s band in Figs 5.11 (c) and 5.12 (c) may be oceanic microseismic noise. Considering the large distances from the coastlines of Mexico to Popocatepetl of around 300 km, oceanic noise may contain some energy up to 20 s [Babcock *et al.*, 1994].

Our data suggest that Popocatepetl is generating energy in the 2-12.5 s band. Comparing time series and amplitude spectra obtained at stations located at different distances from the crater, we notice a clear attenuation of seismic energy with increasing distance from the crater. To demonstrate these feature of data we follow three steps. First, the spectral structure of the signals recorded in the different bands shown in Figs 5.11 and 5.12 is quantified by stacking individual amplitude spectra in these records. Second, using data from the seismic array located near Amecameca at a distance of more than 10 km from the crater (Fig 5.1), we compare peak-to-peak ground velocities measured at sites located at distances of 1.6 km to 17 km from the crater. Third, we compare the velocity amplitude spectra at stations located on the volcano with the corresponding spectra obtained at stations located at least 10 km away from the crater.

Stacked spectral records obtained at PPO2, PPC2, PPP2, PPQ2 and PPJ2 are shown in Fig 5.13. Each spectrum is obtained by calculating spectra in twenty-four 5-min-long windows spanning LP events. These spectra are stacked at each site. Our selection of sites was made to provide the best azimuthal coverage of sources below the crater. The spectra contain three bands; short-period < 2 s, noise band 2-12.5 s, and VLP band > 12.5 s. The peaks at periods longer than 10 s are due to VLP pulses, while the energy at periods shorter than 2.5 s belongs to the short-period band.

To assess whether the volcano is also contributing energy to the microseismic band we compare velocity traces obtained for sections of data that include LP events with

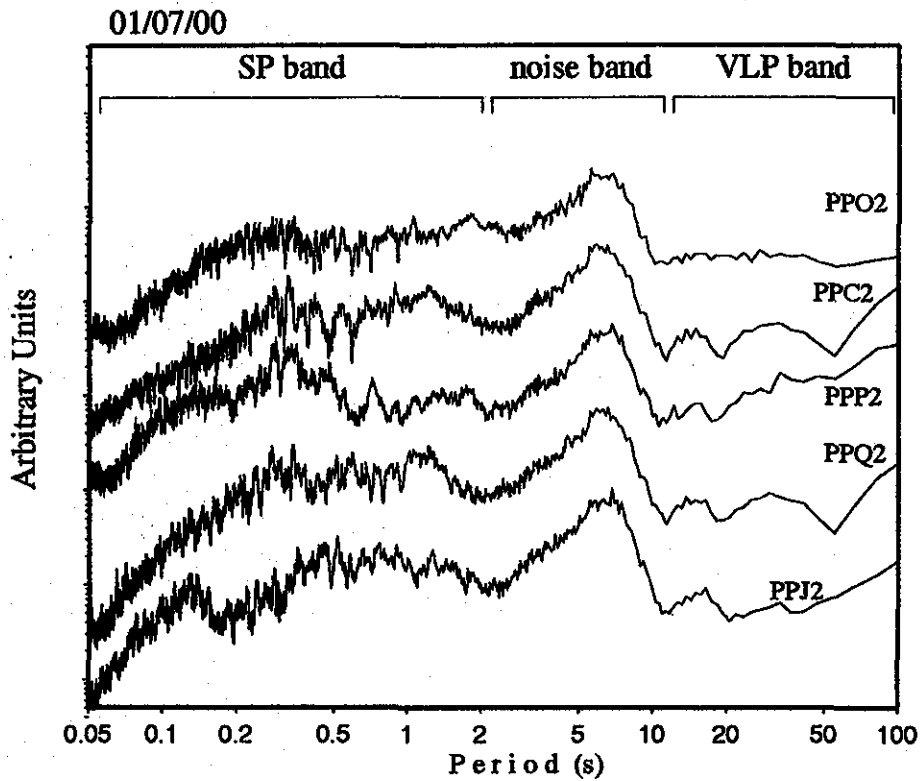


**Fig. 5.13** Amplitude spectra of the vertical component of velocity calculated at stations PPO2, PPC2, PPP2, PPQ2, and PPJ2. Each spectrum was obtained by calculating spectra for twenty four 5-min-long windows spanning the individual LP events and stacking these spectra to produce an average spectrum at each site. The spectra are representative of data recorded on January 1, 2000. Three frequency bands are indicated by brackets above the spectra, namely, the short-period band, the noise band, which includes oceanic microseismicity and VLP tremor, and the VLP band.

those obtained for sections of data lasting 600 s, in which the energy is not attributable to LP events or high-frequency tremor. Figs 5.14 and 5.15 show examples of amplitude attenuation of energy in raw traces and in the 5-12.5 s band as a function of distance from the summit crater. Fig 5.14 shows the vertical component of velocity for a LP event recorded on 11 stations. Traces are plotted from top to bottom as a function of the crater-receiver distance, starting with the closest station PPO2. The last two stations PDN and SDA are located at 10 km and 17 km from the crater, respectively (see Fig 5.1). In Fig 5.14 (*a*), we compare the difference in peak-to-peak amplitude of ground velocity measured at PDN and SDA with respect to the maximum and minimum peak-to-peak amplitudes of ground velocity measured at stations located on the volcano. The maximum peak-to-peak amplitude recorded at stations on the volcano is  $45.0 \mu\text{m/s}$  and the minimum is  $5.8 \mu\text{m/s}$  at stations PPP2 and PPJ4, respectively. The peak-to-peak amplitude of ground velocity measured at PDN ( $1.14 \mu\text{m/s}$ ) is 39 times smaller than that measured at PPP2. At SDA the peak-to-peak amplitude ( $0.64 \mu\text{m/s}$ ) is 70 times smaller compared to that at PPP2. Larger differences in peak-to-peak amplitudes were found in larger LP events, for which the amplitudes were up to 50-80 times larger at receiver sites on the volcano compared to PDN or SDA.

The LP records shown in Fig 5.14 (*a*) were filtered in the 5-12.5 s band to emphasize energy at longer periods (Fig 5.14 *b*). The traces in Fig 5.14 (*b*) show distinct wave packets, which appear to be closely linked to the spatial distribution of receivers around the crater. For example, a comparison of the traces obtained at receivers PPC2 and PPQ2 on the south flank of the volcano with the traces obtained at receivers PPJ3 and PPJ4 on the northwest flank show common wave packets at each receiver pair but with distinct temporal occurrence on the south versus northwest flanks. Again, the peak-to-peak amplitude of ground velocity at PDN and SDA are found to be 1.3 to 4 times smaller than the maximum ( $1.46 \mu\text{m/s}$ ) and minimum ( $0.45 \mu\text{m/s}$ ) amplitude values measured

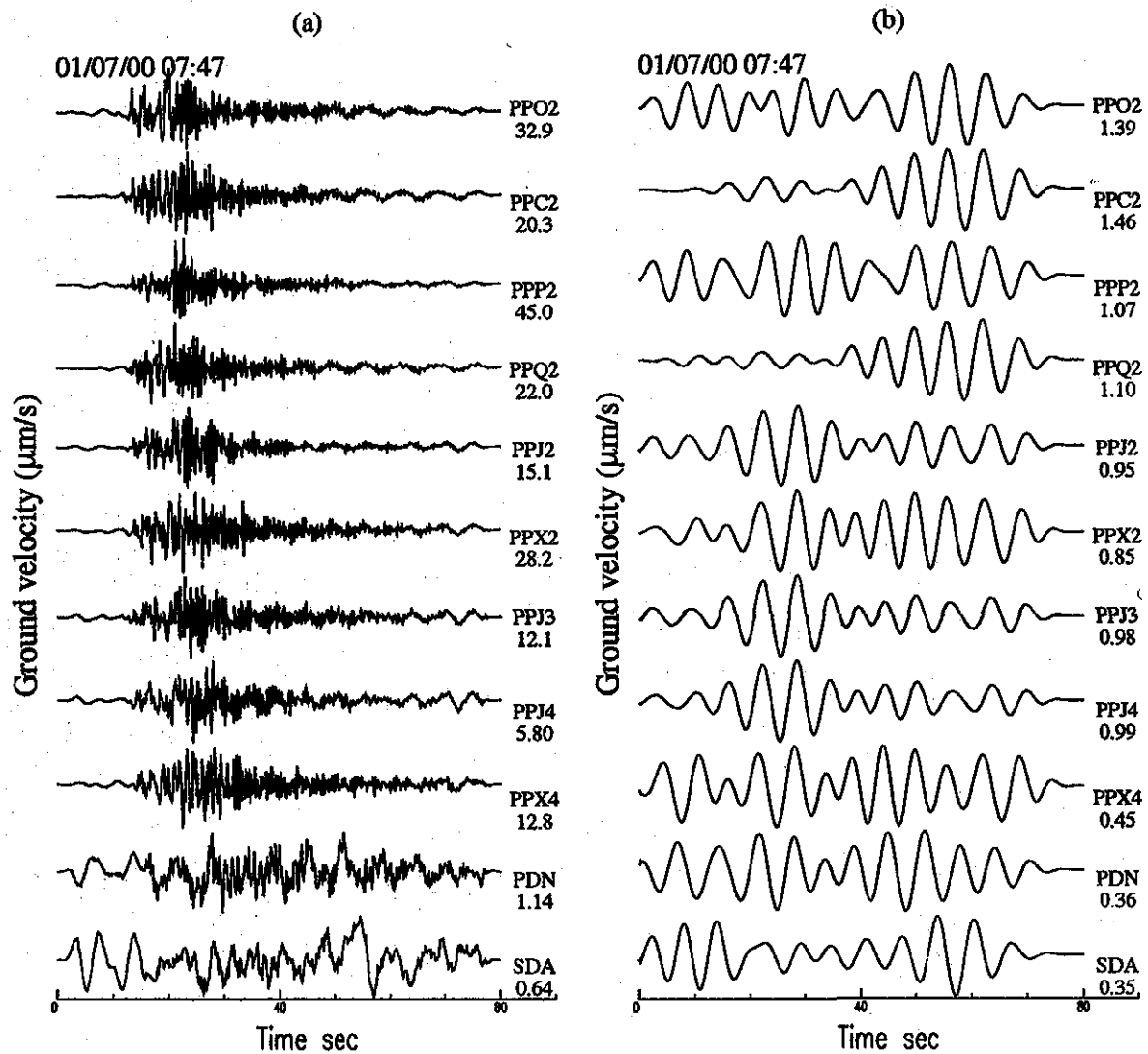


Fig. 5.14 Vertical velocity records at stations of the network for one LP event. (a) Raw data. (b) Records in (a) after filtering in the 5-12.5 s band. The station code and maximum peak-to-peak amplitude of ground velocity recorded at the station are indicated at the end of each trace. The date and time at the beginning of the record are shown at the upper left. Traces are ordered from top to bottom with increasing distance from the crater.

at PPC2 and PPX4, respectively.

Following the same criteria we select a 600 s-long section of seismogram in Fig 5.12 in which no LP events or high-frequency tremor are present. Fig 5.15 (*a*) shows the vertical component of ground velocity in the raw data recorded at the same 11 receivers, plotted in the same order as in Fig 5.14. Peak-to-peak amplitudes of ground velocity with respect to the maximum ( $1.95 \mu\text{m/s}$ ) and minimum values ( $1.17 \mu\text{m/s}$ ) obtained at PPX2 and PPJ3, respectively, are 13 and 22 times smaller at PDN and SDA sites (Fig 5.15 *a*). The same seismic traces recorded in the 5-12.5 s band are shown in Fig 5.15 (*b*). The peak-to-peak amplitudes recorded at PDN and SDA are 19-30 times smaller than the maximum peak-to-peak amplitude ( $1.45 \mu\text{m/s}$ ) or minimum peak-to-peak amplitude ( $0.96 \mu\text{m/s}$ ) recorded at PPX2 and PPX4, respectively.

Some interesting features are emphasized by filtering. Comparing Figs 5.15 (*b*), 5.14 (*a*) and 5.14 (*b*) we observe no significant changes in peak-to-peak amplitudes for a given receiver located on the volcano. In contrast, the amplitudes obtained at PDN and SDA after filtering are up to 5 times larger (Fig 5.14 *b*). This suggests that the differences in amplitudes detected at PDN and SDA in the 5-12.5 s band are attributable to LP activity. Furthermore, after filtering the waveform coherence increases at PDN and SDA, while the waveforms are different at the other receivers. Figs 5.14 and 5.15 clearly illustrate that seismic amplitudes attenuate with distance with higher values measured at stations located on the volcano.

Our comparisons of peak-to-peak amplitudes of ground velocity become more convincing if we consider the differences in amplitude spectra. Considering the same 600-s-long sections we show in Fig 5.16 the amplitude spectra of ground velocity calculated for stations located on the volcano and stations PDN and SDA. As the signals recorded at PDN

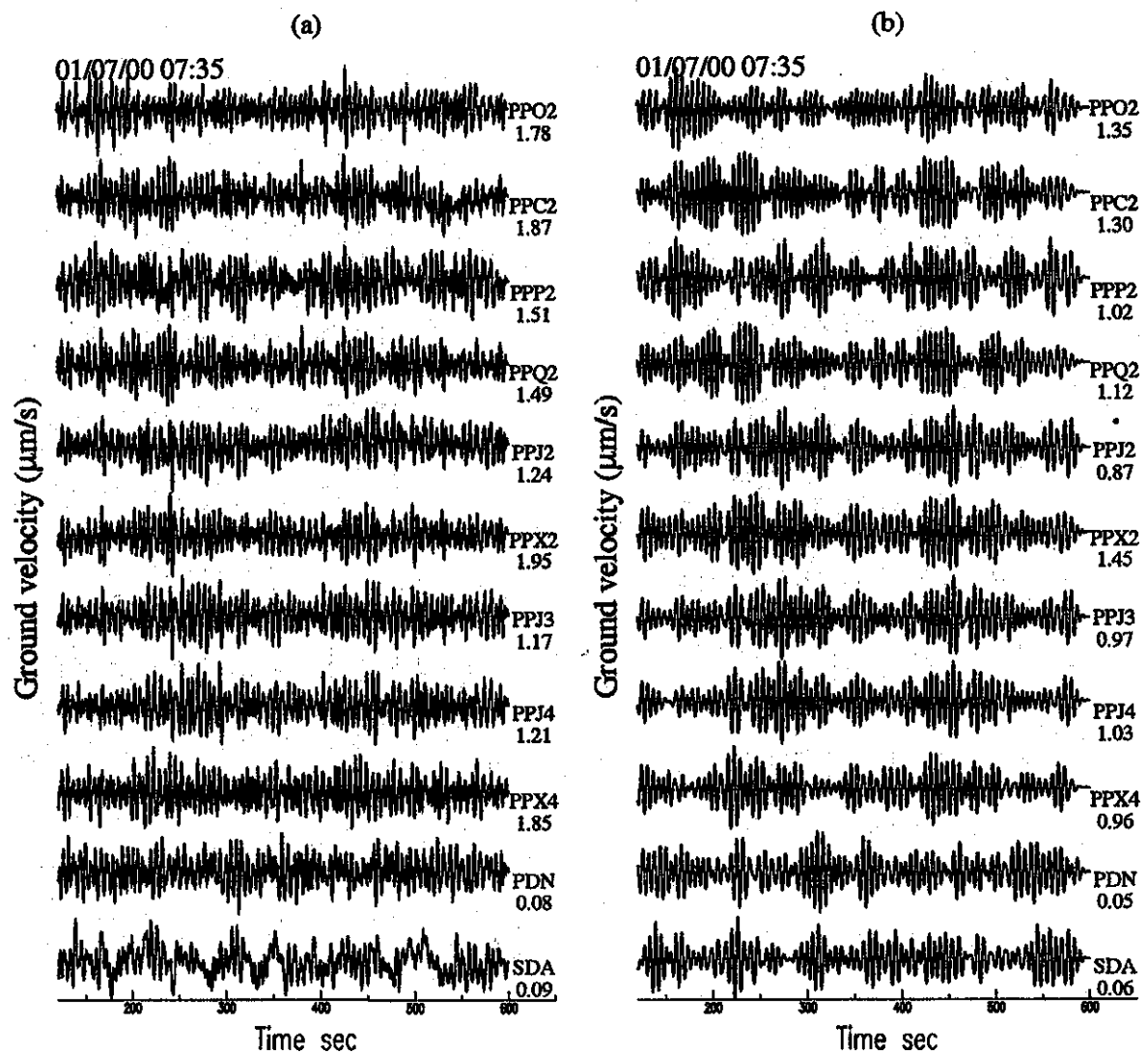


**Fig. 5.15** Same as Fig 5.14 for an 8-min-long record of vertical ground velocity obtained during a period with no LP events and no high-frequency tremor. (a) Raw data. (b) Records in (a) after filtering in the 5-12.5 s band.

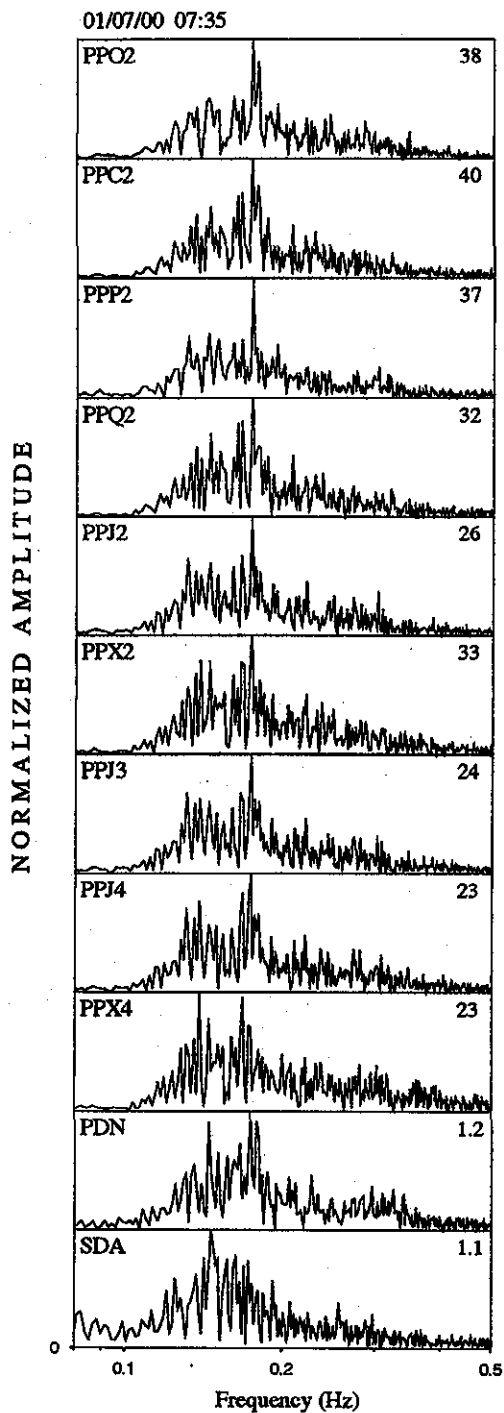


**Fig. 5.16** Amplitude spectra of the records shown in Fig. 5.15 (a). Each spectrum has been normalized to a peak spectral amplitude of 1 to facilitate the comparison. The spectra are ordered from top to bottom with increasing distance from the crater. The station code is indicated at the upper left corner of each panel. Maximum amplitude of each spectrum is indicated at the right corner of each panel.

and SDA are at 50 samples/s, the signals recorded at the receivers on the volcano have been decimated and high-pass filtered at 30 s prior to computing the spectra. The amplitude spectra present similar shapes at all sites, however, the spectral peaks at PDN and SDA differ in amplitudes by up to 40 times with respect to PPO2 and 10 times with respect to PPX4.

From this simple comparison, there is clear evidence that the volcano is adding energy to the microseismic band. This suggests that what we observe in the background signals in Figs 5.11 (b) and 5.12 (b) may include VLP tremor of volcanic origin. Such tremor may represent the response of the volcanic system to the slow movements of fluids under pressure. Another possible explanation that must be investigated is that the observed amplitude pattern is related to the steep topography of the volcano, which may trap the energy from ocean microseismicity and produce the observed amplification effect. Further investigations of the spatial amplitude patterns will be performed using the data from the small aperture array set up in Amecameca to quantify the direction of wave propagation.

### Very-long period signals

A 40-min-long record section starting at 22:44 on 02/26/00, and sampling a swarm of LP events recorded during the emplacement of a lava dome, is shown in the two bands 5-12.5 s and 12.5-100 s at the four stations closest to the crater (Fig 5.17). The upper traces show the raw velocity data recorded at PPQ2. Each seismogram is normalized by its maximum amplitude to emphasize the similarities between filtered signals. A 10-min-long window in the left panel shows wave packets of VLP tremor with typical periods of 6-10 s, which correlate with the short-period signals. During that time, the VLP tremor

amplitude increases in a response to the increasing activity of the volcano associated with the dome extrusion. The right panel shows an 18-min-long record of velocity filtered in the 12.5-100 s band. Very clear VLP pulses are observed to be correlated with LP events in this band. These VLP pulses display a strong amplitude decay with distance and are usually masked by VLP tremor as the distance from the crater increases. In Fig 5.17, station PPC2 appears to be the closest site to the source, and each pulse in this record shows a one-to-one correspondence with each event in the short-period band. At PPJ2 the amplitude of the main pulses dominates the record and smaller pulses are not clearly observed in this plot. PPQ2 is dominated by VLP tremor, and PPX2 presents almost the same VLP amplitude for each of the three largest events seen in the short-period band.

VLP signals have been identified at Popocatepetl since August 1996, and are related to slower processes associated with transport of fluids. The fluid moving through cracks and/or pipes will inflate and deflate the segments of the conduit. Therefore the inertia of the fluid are the origin of the elastic deformation of the conduit walls and VLP seismic signals observed. In Fig 5.18 we show an example of VLP signals recorded at 10 stations located at increasing distances from the crater, with the closest station at the top and farthest at the bottom. The PPO2 trace in the short-period band is used as reference (see top trace). All the seismograms represent the vertical component of velocity band-pass filtered in the 12.5-100 s band and plotted with an arbitrary amplitude scale. All the traces show VLP pulses and wave packets correlated with LP events in the short-period band. The most energetic VLP pulse does not necessarily correspond to the largest LP event. Tremor-like VLP wave packets dominate the seismograms as the distance from the crater increases.

The VLP signals display two basic types of waveforms: a pulse-like waveform with periods of 20-47 s, and wave packets with periods of 15-22 s. Figs 5.19-5.21 show examples

02/26/00 22:44 PPQ2

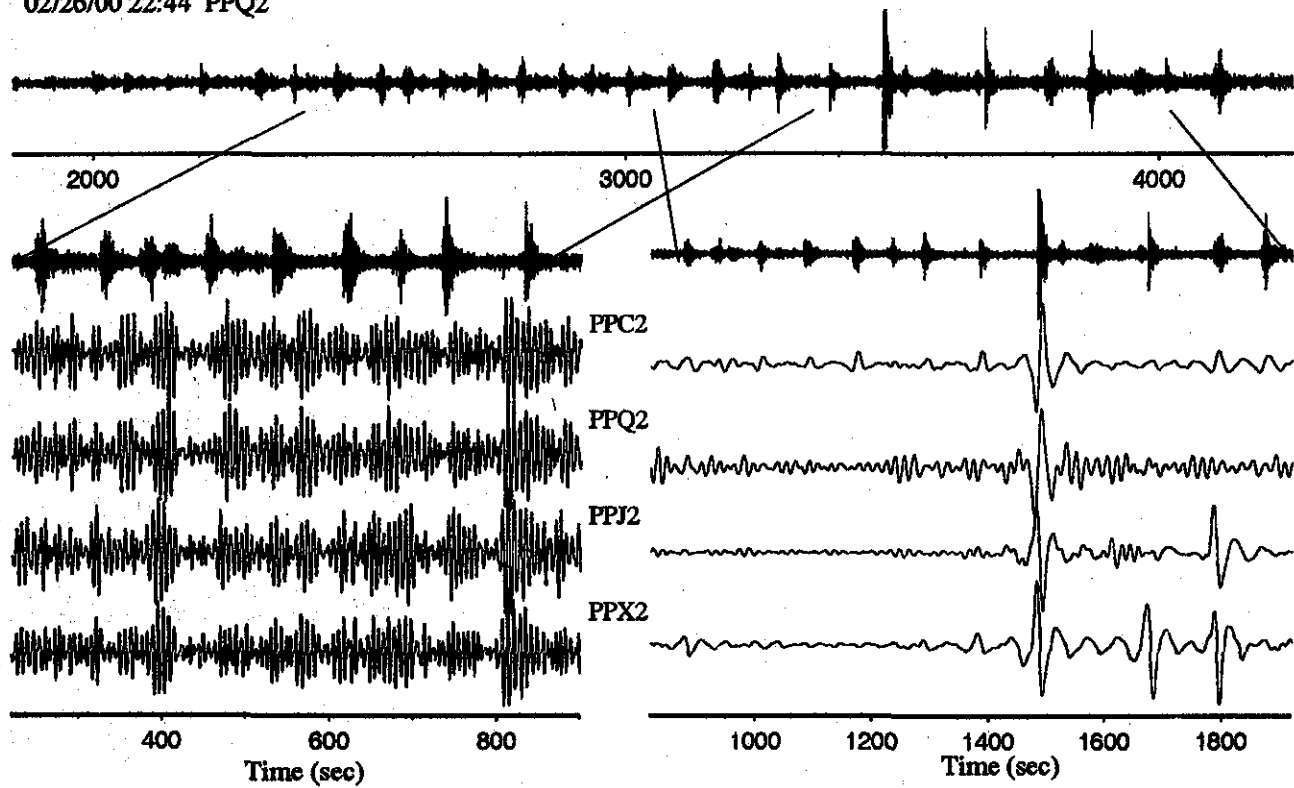


**Fig. 5.17** Vertical velocity record obtained at PPQ2 during a 40-min-long showing a swarm of LP events recorded during the emplacement of a lava dome (top trace). The left panel displays a 10-min-long window extracted from the 40-min-long record at the top, with the top trace representing the raw data at PPQ2, and the next four traces representing data at PPC2, PPQ2, PPJ2 and PPX2 filtered in the 5-12.5 s band. The right panel displays an 18-min-long window extracted from the 40-min-long record at the top, with the top trace representing the raw data at PPQ2, and the next four traces representing data at PPC2, PPQ2, PPJ2 and PPX2, filtered in the 12.5-100 s band. Each seismogram is normalized by its maximum amplitude to emphasize the similarities between traces.

TESIS CON  
FALLA DE ORIGEN

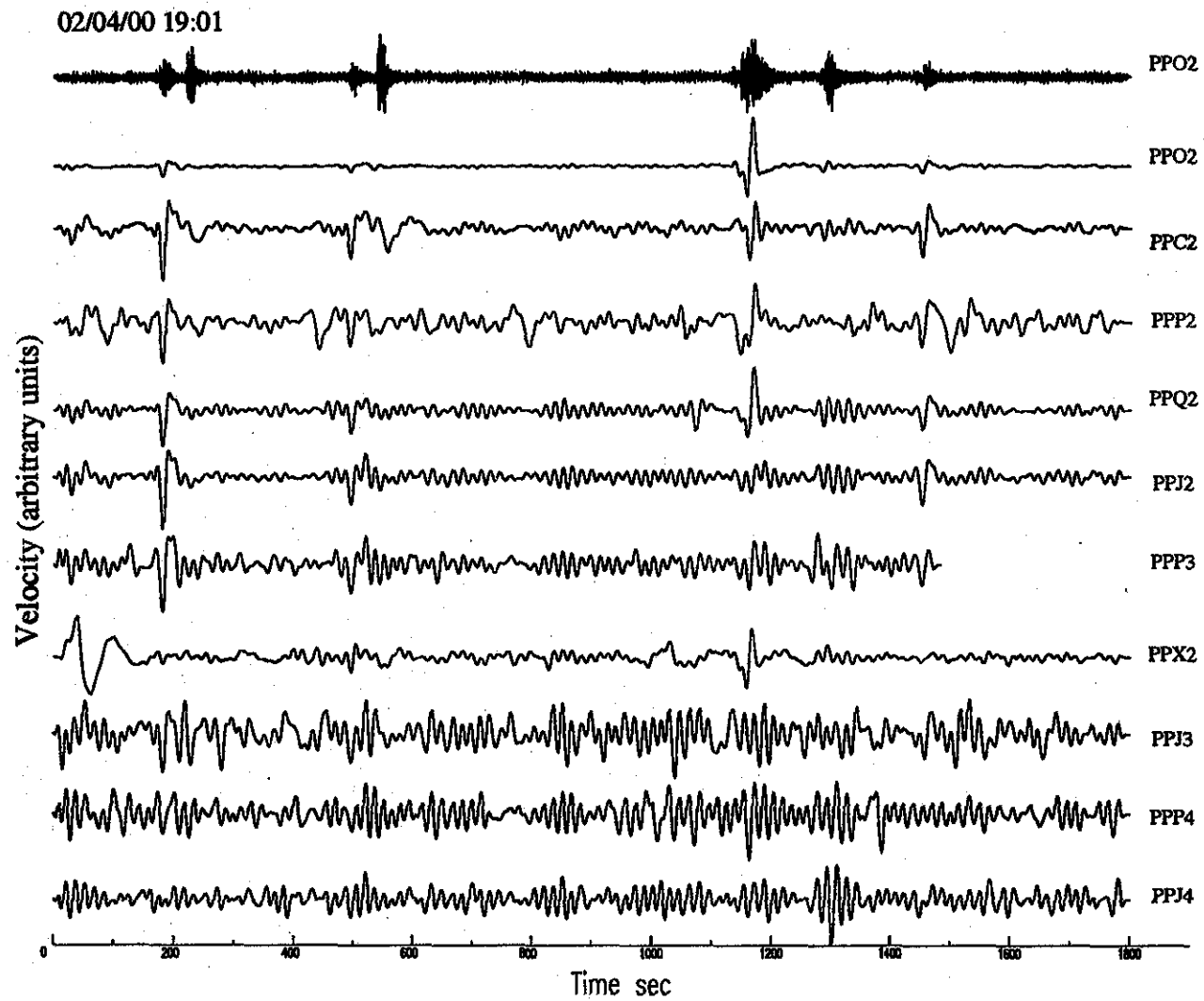


**Fig. 5.18** Vertical velocity records observed at different stations at 19:01 02/04/00. The short-period (0.04-1 s) trace obtained at PPO2 is shown at the top for reference. The other records have been band-pass filtered in the 12.5-100 s band. All traces are normalized by their maximum amplitude to facilitate the comparison of waveforms. The traces are plotted from top to bottom with increasing distance from the crater. Each trace is 30-min-long. The date and beginning time of the records are indicated at the upper left.

of filtered velocities and displacements in the band 12.5-100 s for events recorded on 122499, 020400 and 022500 at the same 10 sites. Each seismogram is normalized by its maximum amplitude to facilitate the comparison between waveforms. Figs 5.19 and 5.21 show seismograms containing similar-looking wave packets. VLP signals in Fig 5.20 also show similar-looking pulse-like waveforms. Wave packets were observed more frequently during the emplacement of the lava dome. The similar waveforms observed across the network suggest we are observing the near-field component of a source located below the crater. If true, these waveforms can be interpreted as representing a source-time function consisting of a compression-dilatation-compression sequence.

The peak-to-peak amplitudes of ground displacement for pulses with periods of 18-28 s recorded at all the stations are plotted versus time in Fig 5.22 (a). The maximum values of displacements coincide with the dome extrusion in late February. Amplitude ratios between small and large events range up to 14. In Fig 5.22 (b) the same values of peak-to-peak ground displacements are plotted versus distance to the crater. These values can be compared with the peak-to-peak ground displacements produced by vulcanian explosions that occurred between April 1997 and January 1999 [Arciniega *et al.*, 1999]. The latter data marked by crosses in Fig 5.22 (b), are from station PPIG located at a range of 4859 m (see Fig 5.1). The displacement amplitude decays with distance from the crater according to the empirical relation

$$A(x) = A_0 e^{-0.0123 \frac{x}{T}}$$

where  $A(x)$  is peak-to-peak amplitude of displacement measured at distance  $x$  from the crater,  $T$  is the period of the signal, and  $A_0$  is the displacement at the source, which is determined by fitting the data of Fig 5.22 (b) to the above relation. The amplitudes of events observed during the time reported in this work are 3-10 smaller than those associated with vulcanian explosions recorded at PPIG.

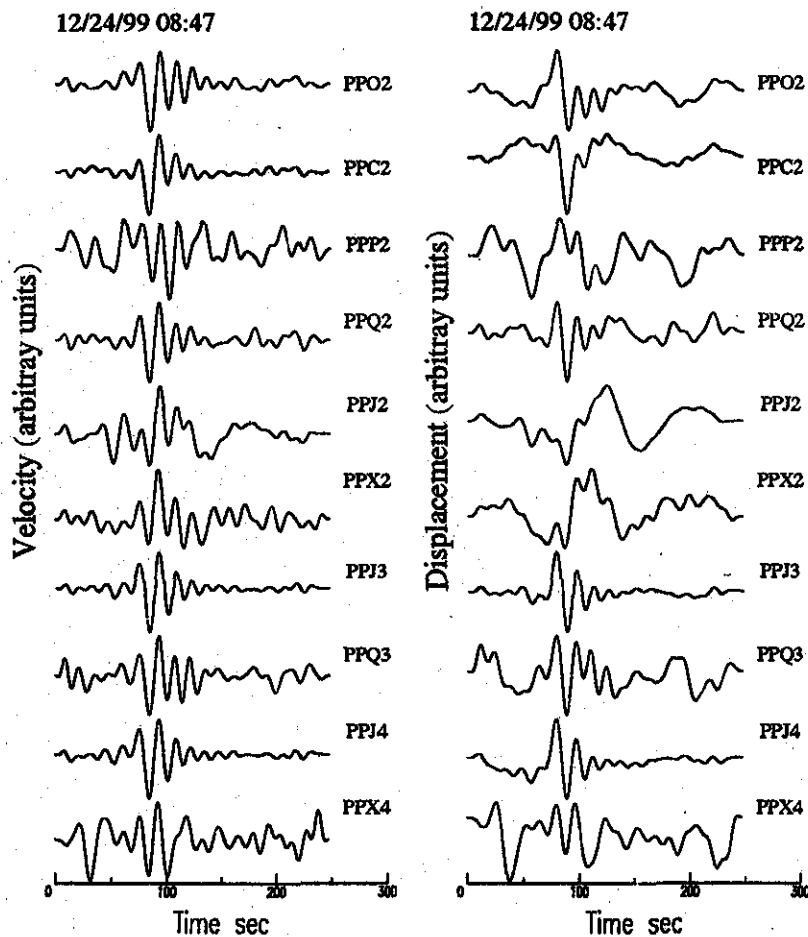


**Fig. 5.19** Band-pass filtered (12.5-100 s) 250-s-long records of velocity and displacement obtained at different stations on December 24, 1999 are plotted in the left and right panels, respectively. The amplitudes have been normalized by their maximum to ease the comparison of waveforms.

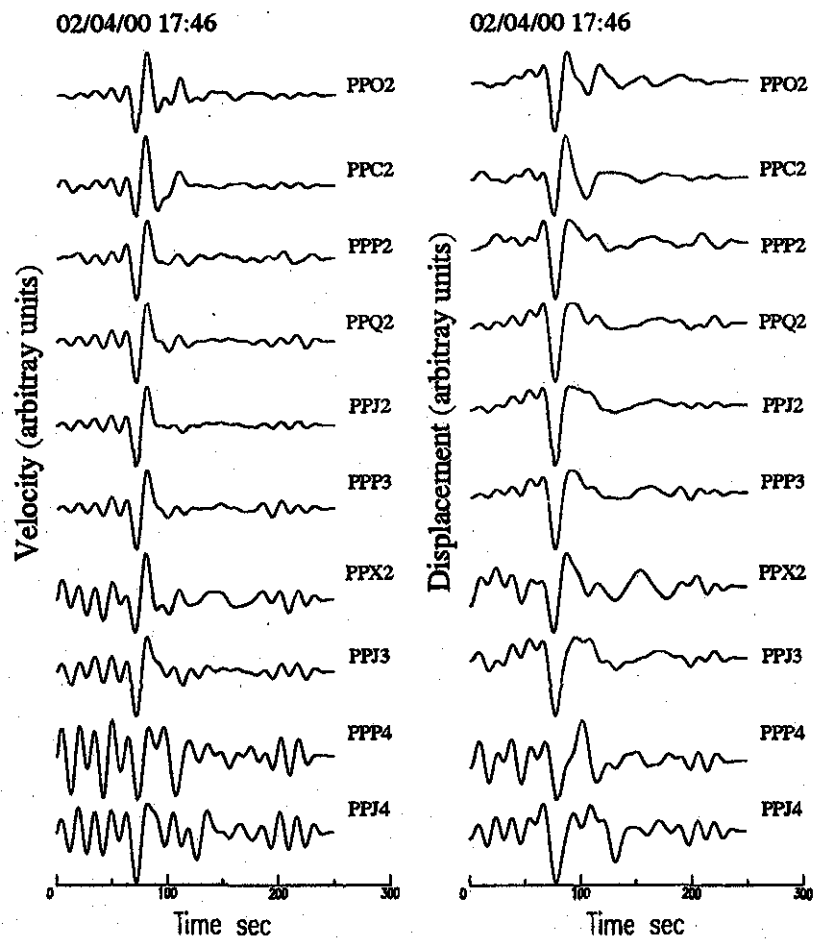


Fig. 5.20 Same as in Fig. 5.19 for records obtained at different stations on February 04, 1999.

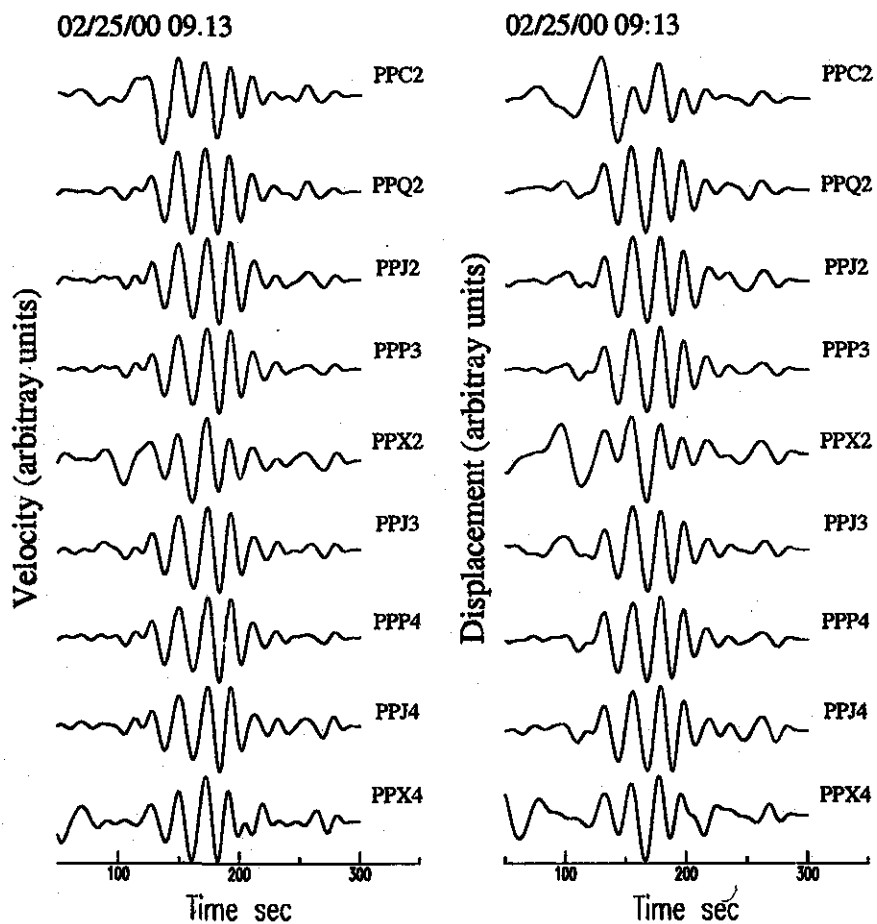
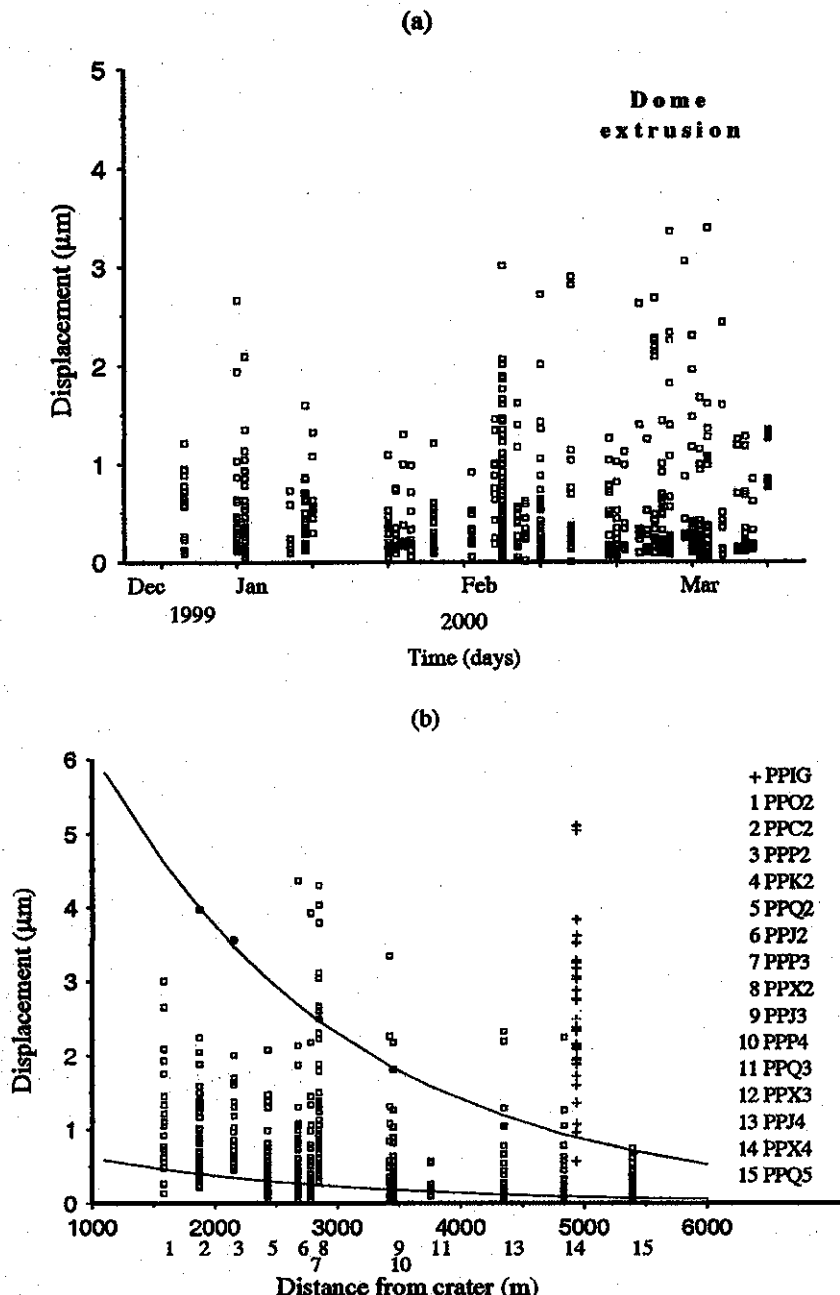


Fig. 5.21 Same as in Fig. 5.19 for records obtained at different stations on February 25, 1999.



**Fig. 5.22** Displacement amplitudes of VLP events with periods 18-28 s plotted as a function of time and distance. The open squares denote peak-to-peak ground displacements for individual events recorded at different stations versus time (a) and versus distance to the crater (b). The station code is identified by a number in (b). A cross identifies data from PPIG (see Fig 5.1) during the explosive crisis in 1997-1999. The solid lines denote the amplitude decay function fitted using data indicated by solid squares (see text for details).

The VLP displacement records obtained at PPO2 for 32 events are shown in Fig 5.23. PPO2 is located at a distance of 1583 m from the crater and is the nearest station to the crater. The VLP waveforms, recorded between December 1999 and February 2000, exhibit quasi-identical pulse shapes with periods near 25 s. The traces have been band-pass filtered between 12.5 and 100 s to emphasize the VLP components of the signals. This repetitive behavior of VLP pulses has been observed at Popocatepetl since August, 1996 (reported in chapter III), and is a clear indication of the repetitive non-destructive excitation of a source associated with the unsteady transport of fluids beneath the volcano.

Particle motions of VLP displacements in the horizontal and vertical-radial planes obtained in the band 15-50 s, are shown in Figs 5.24 and 5.25, respectively. Figs 5.24 (*a-c*) show examples of particle motion trajectories in the horizontal plane recorded at a minimum of 10 stations for events that occurred on 12/31/99 (*a*), 01/20/00 (*b*) and 02/04/00 (*c*). The horizontal particle motions are dominated by nearly linear motion except for a few sites located at crater distances greater than 3 km from the crater.

The radial component of displacement was obtained by rotating the horizontal components to the azimuth of dominant motion measured in the horizontal particle motion plot. The depth of the source can be roughly estimated from the particle motions in the vertical-radial plane. Fig 5.25 exhibit particle motion trajectories for the three events shown in Fig 5.24. In Figs 5.25 (*a-c*) the major axes of the particle motion trajectories at stations PPO2, PPC2, PPX2, PPJ2, PPP2, PPP3 and PPQ2 point to the same region. The projections of those major axes point to a source region located slightly east of the crater. Rough bounds on the source depth, obtained from the projections of the dip angles, suggest that the source is located at depths between 0.3 and 2 km beneath the eastern edge of the crater.

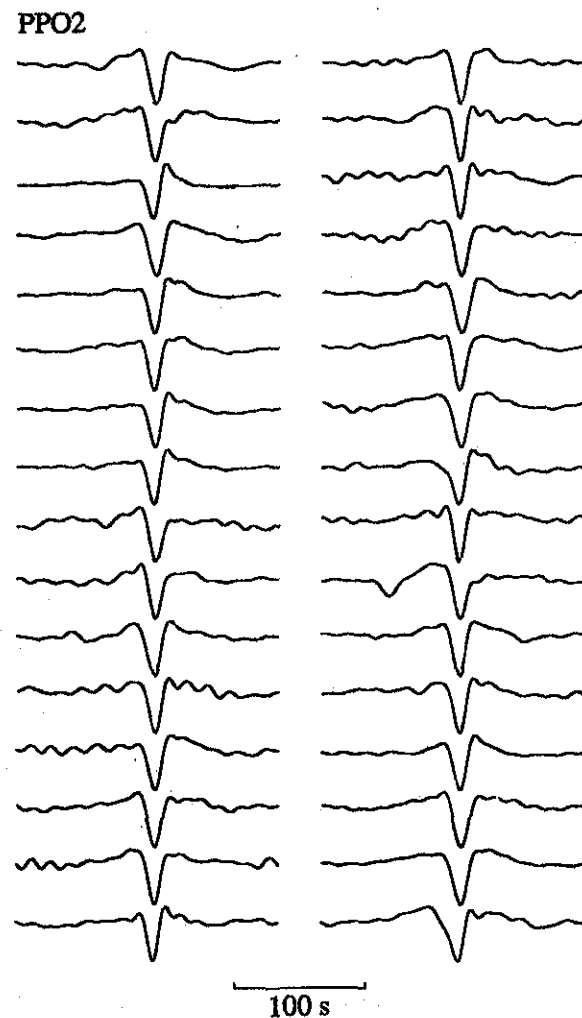


**Fig. 5.23** Band-pass filtered (12.5-100 s) VLP displacement records from station PPO2, located 1.58 km from the crater. The 32 VLP signals have been aligned to illustrate the repeatability of the signal from event to event. The amplitudes have been normalized by their maximum to facilitate the comparison of traces.

TESIS CON  
FALLA DE ORIGEN

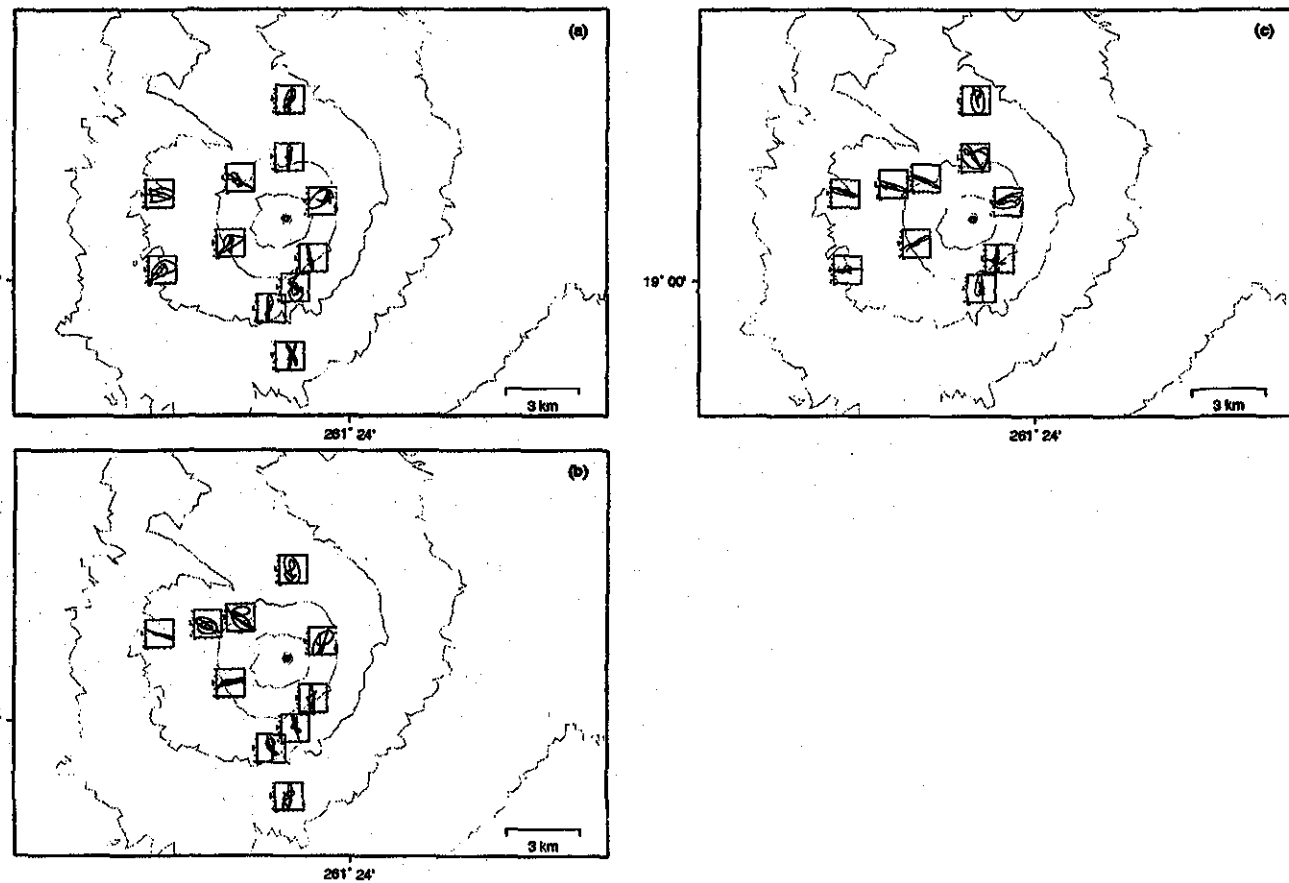


**Fig. 5.24** Displacement particle trajectories obtained in the horizontal plane at a minimum of 10 stations for events on (a) 12/31/99, (b) 01/20/00 and (c) 02/04/00. Note the quasi-linear motion of the VLP signals at sites near the crater and the general trend of particle motions toward the crater of Popocatepetl.

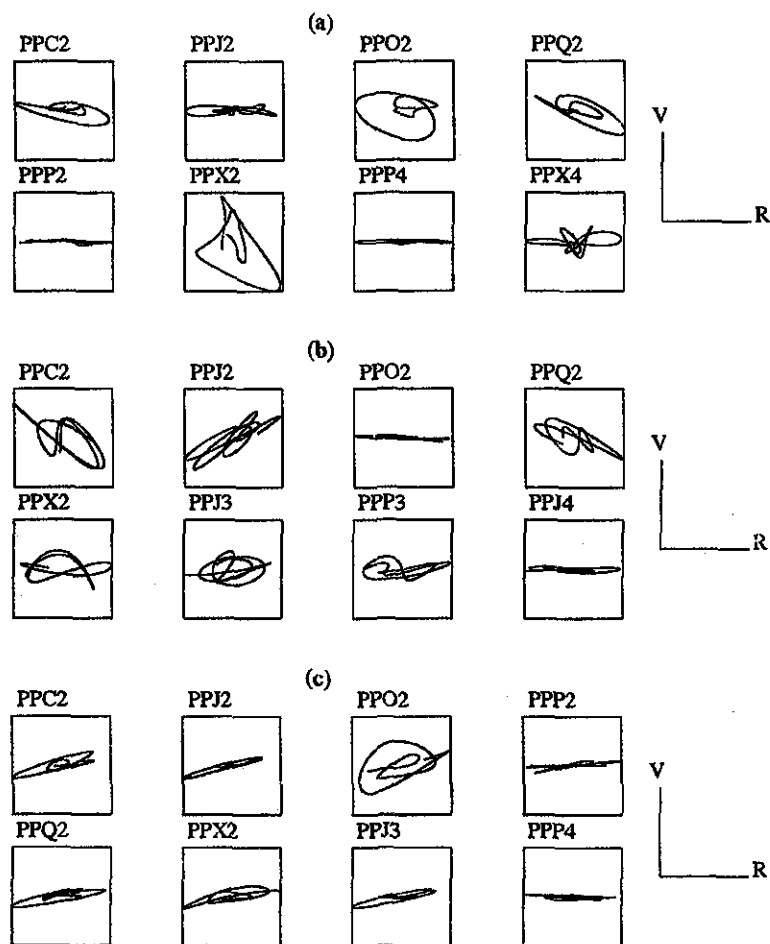


**Fig. 5.25** Displacement particle trajectories in the vertical-radial plane for the three events shown in Fig 5.24. The positive radial direction is away from the crater.

Phase pick locations obtained for LP events recorded in the short-period band provide good estimates of the hypocentral locations of LP seismicity, which can be compared with the locations of the VLP signals based on particle motions (Figs 5.24 and 5.25).

Among the hundreds of events recorded by our network, we selected a subset of 79 LP signals with good signal-to-noise ratios to determine their source locations using a standard phase pick procedure and location routine *gloc* [Julian, 2001]. Figure 5.26 shows the hypocentral locations determined with a velocity model consisting of five horizontal layers with compressional wave velocities and thicknesses of 3.2 km/s and 1.5 km; 3.5 km/s and 3.5 km; 4.0 km/s and 0.5 km; 4.5 km/s and 0.5 km; and 5.0 km/s and 6.0 km, from top to bottom respectively. The scatter in individual event locations is the result of uncertainties in the velocity structure, and emergent characteristics of first arrivals detected by the receivers. Location errors are on the order of  $\pm 0.2$  km. Each event was located using at least 6 stations. The source region outlined by hypocenters is confined within a restricted zone at shallow depths beneath the crater of Popocatepetl with a majority of hypocenters occurring in the depth range 0.3-2 km below the crater floor. Taking into account the uncertainty in event locations, it is reasonable to view these LP events as representative of the shallow seismicity associated with degassing activity and extrusion of lava dome in the crater. These events have signatures exhibiting a broad range of frequencies similar to the signatures illustrated in Figures 5.4-5.7. These LP events depths are comparable to those of VLP sources inferred from particle motions (see Fig. 5.25).

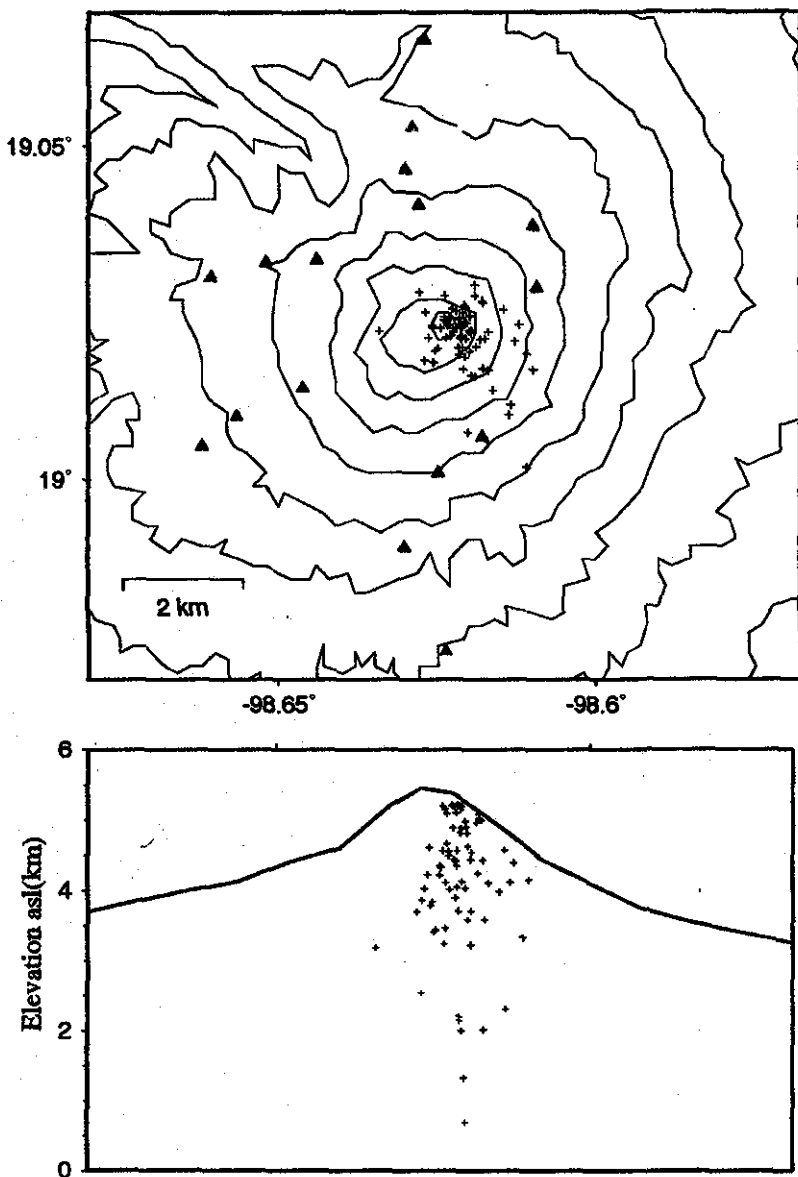


**Fig. 5.26** Hypocentral distribution (crosses) of 79 LP events recorded by the broadband seismic network (triangles). East-west cross section passing through the summit. Contour lines represent 300 m elevation intervals.

## Discussion and conclusions

This work describes the deployment of a broadband digital seismic network on Popocatepetl and presents preliminary analyses of the seismic data recorded by the network. Seismic data were analyzed in the three bands, 0.04-2 s, 2-12.5 s and 12.5-100 s.

The observed stationarity with time in the waveform features of LP events and VLP pulses suggests that a repetitive source process is involved. The only viable mechanism that can explain such a repeating non-destructive source process is a mechanism involving the active participation of fluids [Chouet, 1996]. The acoustic resonance of a crack-like conduit containing magmatic and/or hydrothermal fluids provides a reasonable mechanism that can naturally explain the common properties observed in LP events [Chouet *et al.*, 1994; Morrissey and Chouet, 1997; Gil Cruz and Chouet, 1997]. We demonstrated that the spectral characteristics of the LP events are compatible with the resonance of a fluid-filled crack in which short-term pressure disturbances associated with the transport process provide the required trigger for the generation of LP seismicity [Chouet, 1996].

Observations made in the 2-12.5 s band suggest that a significant part of this energy may be of volcanic origin. This conclusion is based on the spatial pattern of amplitudes recorded by the network, which shows a strong attenuation of seismic amplitudes as distance from the crater increases. Although, this attenuation pattern could possibly reflect a topography effect on the background microseismic noise, we favor the former explanation based on our observations of distinct spectral peaks which are common to all the stations of our network and are suggestive of a source of volcanic origin. VLP tremor correlates with the emplacement of a lava dome within the crater. This observation suggests that the volcano is continuously producing VLP tremor in response to the slow

unsteady movements of fluids under pressure. The origin of the radiated wavefield can be further quantified by particle motion analyses.

The lithology of the volcano and magma interactions with this lithology may shed additional light on the origin of VLP tremor. Several outcrops of Cretaceous limestone rocks are observed between sea level and 1.0 km a.s.l. [PEMEX 1988; Perez-Cruz, 1988; Urrutia-Fucugauchi, 1992] beneath the Popocatepetl volcanic edifice. The contact between the limestone and the volcanic rocks lies near  $1.00 \pm 0.5$  km a.s.l. beneath the volcano [Arciniega *et al.*, 2000]. Magmatic fluids pass through carbonate rocks on their way to the surface, resulting in a high quantities of  $SO_2$  and  $CO_2$  and a sustained production of gas bubbles which may be at the origin of the VLP tremor. Goff *et al.* (2001) reported that high  $CO_2$  discharges are caused by occasional assimilation of limestone blocks into the magma at shallow levels beneath the summit of the volcano (at depths of 3.5 to 7 km deep). According to this interpretation, once the fluids reach shallower depths (0.3-2 km beneath the crater), excess pressures associated with the collapses of foam rafts into large slugs of gas may trigger the resonance of a crack-like conduit, thereby producing LP events and associated gas emissions.

Correlations between VLP tremor and/or VLP transients with short-period activity confirm that the movement of magmatic fluids produce a wide variety of signals. Inertial forces associated with unsteady mass transport provide a natural source of VLP signals [Chouet, 1996; Dawson *et al.*, 1998]. The VLP displacement waveforms display almost identical shapes from event to event for a given eruption, pointing to a process involving the repeated activation of a fixed non-destructive source. The VLP waveforms observed at different stations share a similar shape, which differs only in relative amplitude among stations, indicating that the seismograms are source-dominated. The characteristic compression-dilatation-compression sequence in VLP waveforms is described in Chouet

*et al.* (1999, 2001) for Strombolian eruptions by the following processes; (1) pressurization and dilatation of the conduit associated with the collapse of a foam raft and formation of a large slug of gas; (2) depressurization and deflation of the conduit in response to mass ejection from the conduit; and (3) repressurization and dilation of the conduit in response to the source replenishment with fluid. VLP signals observed at Popocatepetl show waveforms similar to those observed at Stromboli and may be qualitatively accounted for by considering a similar sequence of pressurization-depressurization-repressurization of the conduit. Ohminato *et al.* (1998) investigated the source mechanism of VLP signals at Kilauea Volcano, Hawaii, and showed these signals are well explained by a source mechanism involving a pulsating transport mechanism operating on a fluid-filled crack. The crack acts like a buffer in which a batch of fluid (magma and/or gas) accumulates before being ejected.

The shallowness of the source region some 0.3-2 km beneath the eastern region of the crater, suggested by the LP and VLP signals, and close relationship observed between LP and VLP seismicity and steam and ash emissions, provide strong qualitative evidence of a hydrothermal origin for most of this seismicity. Future analyses to better constrain the source location can be carried out by applying the semblance method [Almendros, 2001] since particle motions at the stations near the crater are almost linear and point toward a common intersection. Results from our preliminary analyses indicate that the deployment of our network, and lessons learned from this deployment should have a direct and positive influence on future analyses of the seismicity of Popocatepetl Volcano.

## References

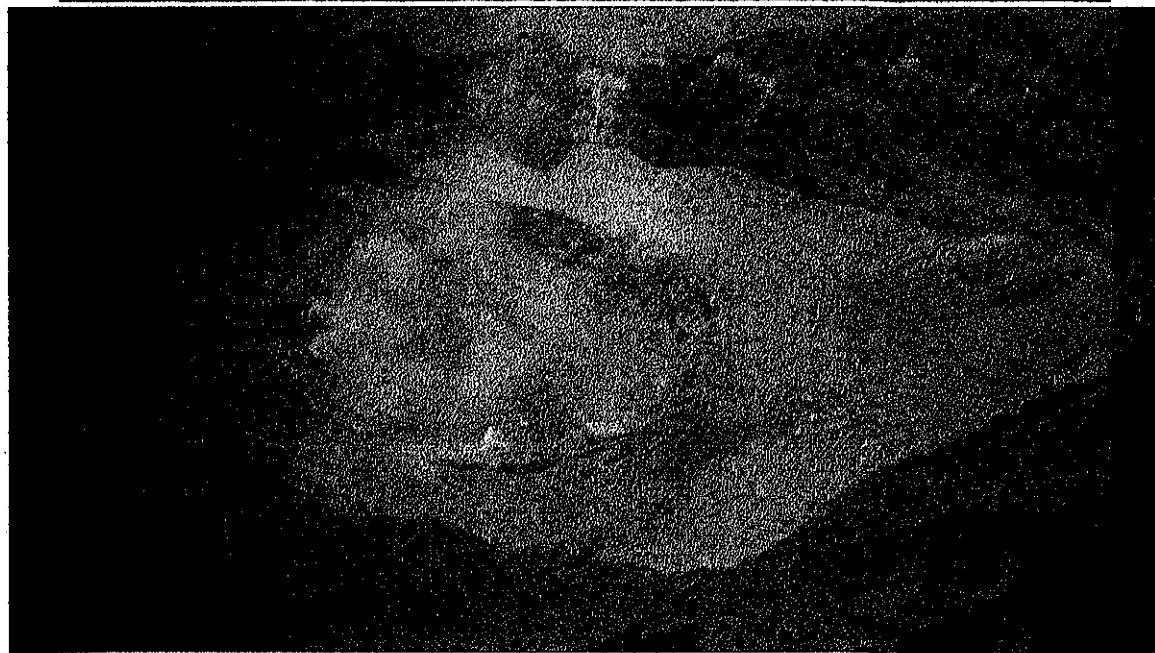
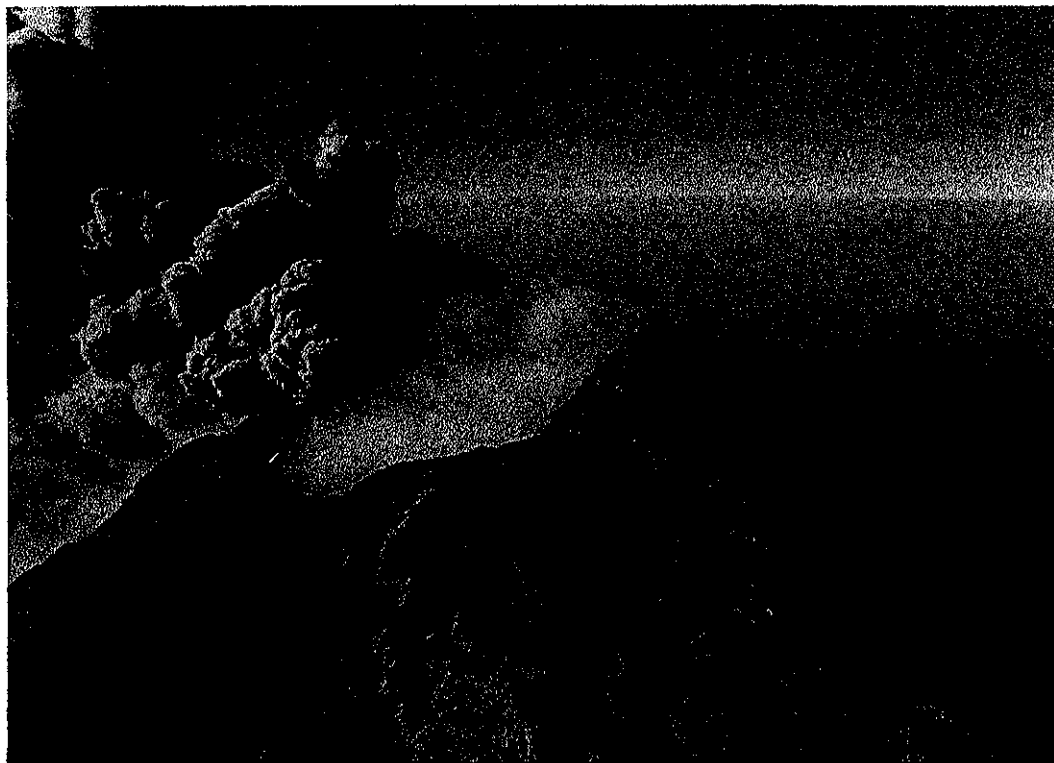
- Aki K., Fehler M. and Das S. (1977). Source mechanism of volcanic tremor: fluid-driven crack models and their application to the 1963 Kilauea eruption. *J. Volcanol. Geotherm. Res.* 2, 259-287.
- Aki K. and P. Richards. (1980) *Quantitative Seismology*. Freeman San Francisco, CA.
- Aki K. and Koyanagi (1981). Deep volcanic tremor and magma ascent mechanism under Kilauea, Hawaii. *J. Geophys. Res.* 86:7095-7109.
- Aki K. (1984). Evidence for magma intrusion during the Mammoth Lakes earthquakes of May 1980 and implications of the absence of volcanic (harmonic) tremor. *J. Geophys. Res.* 89: 7689-7696.
- Almendros J., B. Chouet, P Dawson. (2001) Hawaii. Spatial extent of a hydrothermal system at Kilauea Volcano, Hawaii, determined from array analyses of shallow long-period seismicity 1; Results *J. Geophys. Res.* 106, 7 13581-13597.
- Arciniega-Ceballos A, Chouet BA, Dawson P (1999) Very long-period signals associated with vulcanian explosions at Popocatepetl Volcano, Mexico. *Geophys. Res. Lett.* 26:3013-3016
- Arciniega-Ceballos A, Chouet B, Dawson P, Asch G, Kind R. (2001). Broadband seismic experiment at Popocatepetl Volcano in Central Mexico. *Proceedings Geol. Soc. Am.* 32-7, Reno, Nov 13-16.
- Arciniega-Ceballos A, Valdes C, Dawson P (2000) Temporal and spectral characteristics of seismicity observed at Popocatepetl volcano, central Mexico. *J. Volcanol. Geotherm. Res.* 102:207-216
- Babcock, J. M., B. A. Kirkendall, and J. A. Orcutt, Relationships between ocean bottom noise and the environment, *Bull. Seismol. Soc. Am.*, 84, 1991-2007, 1994.
- Chouet B (1985) Excitation of a buried magmatic pipe: A seismic source model for volcanic tremor. *J. Geophys. Res.* 90:1881-1893
- Chouet B (1986) Dynamics of a fluid-driven crack in three dimensions by the finite difference method. *J. Geophys. Res.* 91:13967-13992
- Chouet B (1988) Resonance of a fluid-driven crack: Radiation properties and implications for the source of long-period events and harmonic tremor. *J. Geophys. Res.* 93:4375-4400
- Chouet B (1992) A seismic model for the source of long-period events and harmonic tremor. In: *Volcanic Seismology*, Gasparini P, Scarpa R, Aki K (eds) Springer-Verlag, New York, pp. 133-156
- Chouet BA, Page RA, Stephens CD, Lahr JC, Power JA (1994) Precursory swarms of long-period events at Redoubt Volcano (1989-1990), Alaska: Their origin and use as a forecasting tool. *J. Volcanol. Geotherm. Res.* 62:95-135
- Chouet B (1996a) Long-period volcano seismicity: its source and use in eruption forecasting. *Nature* 380:309-316
- Chouet B (1996b) New methods and future trends in seismological volcano monitoring. In: *Monitoring and Mitigation of Volcano Hazards*, R Scarpa and R Tilling (Eds)

Springer-Verlag, New York, pp. 23-97

- Chouet B, Saccorotti G, Martini M, Dawson P, De Luca G, Milana G, Scarpa R (1997) Source and path effects in the wave fields of tremor and explosions at Stromboli Volcano, Italy. *J. Geophys. Res.* 102:15129-15150
- Chouet B, Saccorotti G, Dawson P, Martini M, Scarpa R, De Luca G, Milana G, Cattaneo M (1999) Broadband measurements of the sources of explosions at Stromboli Volcano, Italy. *Geophys. Res. Lett.* 26:1937-1940
- Commander K. W. and Prosperetti A. (1989). Linear pressure waves in bubbly liquids; comparison between theory and experiments. *J. Acoust. Soc. Am.* 85: 732-746.
- Crosson R. S. and Bame D. A. (1985). A spherical source model for low-frequency volcanic earthquakes. *J. Geophys. Res.* 90:10237-10247.
- Dawson PB, Dietel C, Chouet BA, Honma K, Ohminato T, Okubo P (1998) A digitally telemetered broadband seismic network at Kilauea Volcano, Hawaii. U.S. Geol. Surv. Open-File Rep. 98-108 pp. 121
- Delgado H. L Cárdenas, N Piedad (2001). Sulfur dioxide emissions from Popocatépetl volcano (Mexico): cas study of a high-emission rate, passively degassing erupting. *J. Volcanol. Geotherm. Res.*, 108, 107-120
- Fehler M. (1983). Observations of volcanic tremor at mount St. Helens Volcano. *J. Geophys. Res.* 88:3476-3484.
- Gil Cruz F, Chouet BA (1997) Long-Period events, the most characteristic seismicity accompanying the emplacement and extrusion of a lava dome in Galeras Volcano, Colombia, in 1991. *J. Volcanol. Geotherm. Res.* 77:121-158
- Gerlach T, Delgado H, McGee K, Doukas M, Venegas Jm Cardenas L. (1998) Applications of the LI COR  $CO_2$  analyzer to volcanic plumes: a case study, volcan Popocatepetl Mexico. *J. Geophys. Res.* 102,8005-8019.
- Goff F, Janik C, Delgado H, Werner C, Counce D, Stimac JA, Siebe C, Love S, Williams S, Fisher T, Johnson L. (1998) Geochemical surveillance of magmatic volatiles at Popocatepetl volcano, Mexico. *Geol. Soc. Am. Bull.* 110(6), 695-710.
- Hidayat D, Chouet BA, Voight B, Dawson P, Ratdomopurbo A (2001) Source mechanism of very-long-period signals accompanying dome growth activity at Merapi Volcano, Indonesia. *Geophys. Res. Lett.* submitted
- Julian B (2001) *qloc*, a general earthquake location computer program. U S Geol Surv Open-File Rep in preparation.
- Kaneshima S, Kawakatsu H, Matsubayashi H, Sudo Y, Tsutsui T, Ohminato T, Ito H, Uhira K, Yamasato H, Oikawa J, Takeo M, Iidaka T (1996) Mechanism of phreatic eruptions at Aso volcano inferred from near-field broadband seismic observations. *Science* 273:642-645
- Kawakatsu H, Ohminato T, Ito H, Kuwahara Y (1992) Broadband seismic observation at Sakurajima Volcano, Japan. *Geophys. Res. Lett.* 19:1959-1962
- Kawakatsu H, Ohminato T, Ito H (1994) 10-s-period volcanic tremors observed over a wide area in southwestern Japan. *Geophys. Res. Lett.* 21:1963-1966

- Kawakatsu H, Kaneshima S, Matsubayashi H, Ohminato T, Sudo Y, Tsutsui T, Uhira K, Yamasato H, Ito H, Legrand D (2000) Aso94: Aso seismic observation with broadband instruments. *J. Volcanol. Geotherm. Res.* 101:129-154
- Kieffer S. W. (1977). Sound speed in liquid-gas mixtures: water-air and water-steam. *J. Geophys. Res.* 82:2895-2904.
- Kumagai H, Chouet BA (1999) The complex frequencies of long-period events as probes of fluid compositions beneath volcanoes. *Geophys. J. Int.* 138:F7-F12
- Kumagai H, Chouet BA (2000) Acoustic properties of a crack containing magmatic or hydrothermal fluids. *J. Geophys. Res.* 105:25493-25512
- Kumagai H, Chouet BA (2001). The dependence of acoustic properties of a crack on the resonance mode and geometry. *Geophys. Res. Lett.* 28:3325-3328
- Kumagai H, Ohminato T, Nakano M, Ooi M, Kubo A, Inoue H (2001) Very-long-period seismic signals and the caldera formation at Miyake Island, Japan. *J. Volcanol. Geotherm. Res.* submitted
- Lahr JC, Chouet BA, Stephens CD, Power JA, Page RA (1994) Earthquake classification, location, and error analysis in a volcanic environment: Implications for the magmatic system of the 1989-1990 eruptions at Redoubt Volcano, Alaska. *J. Volcanol. Geotherm. Res.* 62:137-151
- Legrand D, Kaneshima S, Kawakatsu H (2000) Moment tensor analysis of broadband waveforms observed at Aso Volcano, Japan. *J. Volcanol. Geotherm. Res.* 101: 155-169
- Longuet-Higgins MS (1950) A theory of the origin of microseism. *Philos Trans R Soc London Ser A* 423:1-35
- Love S, Goff F, Counce D, Siebe C, Delgado H. (1998) Passive infrared spectroscopy of the eruption plume at Popocatepetl volcano, Mexico. *Nature* 396, 563-567.
- Matsubayashi, H. (1995) The source of the long period tremor and the very-long period events preceding the mud eruption at Aso Volcano, Japan (in Japanese with English abstract) M.A.Thesis, Tokyo Univ.
- Mc Nutt SR (1992) Title of paper, Encyclopedia of Earth System Science. Academic Press, San Diego, v. 4 pp. 417-425.
- Morrissey MM, Chouet BA (1997) A numerical investigation of choked flow dynamics and its application to the triggering mechanism of long-period events at Redoubt Volcano, Alaska. *J. Geophys. Res.* 102:7965-7983
- Morrissey MM, Chouet BA (2001). Trends in long-period seismicity related to magmatic fluid compositions. *J. Volcanol. Geotherm. Res.* 108:265-281
- Murase T. and Mc Birney A. (1973). Properties of some common igneous rocks and their melts at high temperatures. *Bull. Geol. Soc. Am.* 84: 3563-3592.
- Neuberg J, Luckett R, Ripepe M, Braun T (1994) Highlights from a seismic broadband array on Stromboli volcano. *Geophys. Res. Lett.* 21:749-752
- Nishimura T (2000) Source process of very long period seismic events associated with the 1998 activity of Iwate Volcano, northeastern Japan. *J. Geophys. Res.* 105:19135-19145

- Nuttli O (1961) The effect of the Earth's surface on the S wave particle motion, Bull. Seismol. Soc. Am. 51:237-246
- Ohminato T, Ereditato D (1997) Broadband seismic observations at Satsuma-Iwojima Volcano, Japan. Geophys. Res. Lett. 24:2845-2848
- Ohminato T, Chouet BA, Dawson P, Kedar S (1998) Waveform inversion of very-long-period impulsive signals associated with magmatic injection beneath Kilauea Volcano, Hawaii. J. Geophys. Res. 103:23839-23862
- Ohminato T (1998) Broadband analysis of seismic signals observed in and around active volcanoes. Ph. D. Thesis, University of Tokyo, Japan. pp. 114
- PEMEX (1988). Cortes litológicos y registros geofísicos de los pozos profundos exploratorios Roma-1, Mixhuca-1, Tulyehualco-1 y Copilco-1. Fundación Barros Sierra. A.C.
- Perez-Cruz G. (1988). Estudio sismológico de reflexión del subsuelo de la Ciudad de México. M.A. Thesis Facultad de Ingeniería U.N.A.M.
- Rowe CA, Aster RC, Kyle PR, Schlue JW, Dibble RR (1998) Broadband recording of Strombolian explosions and associated very-long-period seismic signals on Mount Erebus Volcano, Ross Island, Antarctica. Geophys. Res. Lett. 25:2297-2300
- Rowe CA, Aster RC, Kyle PR, Schlue JW, Dibble RR (2000). Seismic and acoustic observations at Mount Erebus Volcano, Ross Island, Antarctica, 1994-1998. J. Volcanol. Geotherm. Res. 101:105-128.
- Saccorotti *et al.*, 2001.
- Seidl S, Kirbani SB, Brustle W (1990) Maximum entropy spectral analysis of volcanic tremor using data from Etna (Sicily) and Merapi (central Java). Bull Volcanol 52:460-474.
- Urrutia-Fucugauchi, J. (1992). Reconnaissance electrical resistivity and self-potential studies of Atotonilco-Jonacatepec region, Morelos State, Mexico. Geof. Int., 31-4, pp 341-358.
- Wessel P, Smith WHF (1995) New version of the Generic Mapping Tools released (abstract). Eos Trans AGU 76(33)-329



**Fotos 5.1 y 5.2** Ejemplo del tipo de emisiones observadas durante el experimento sísmico de banda ancha noviembre 1999 - agosto 2000 (arriba). Condiciones del cráter en abril del 2000 (abajo). (fotos A. Arciniega)

## Agradecimientos

*Muy especialmente agradezco al Dr Bernard Chouet por su interés, asesoría y constante estímulo durante el desarrollo del presente trabajo. Igualmente mil gracias al Dr Phil Dawson por su entusiasta colaboración y asesoría en diferentes etapas de mis estudios.*

*También deseo expresar mi gratitud al Dr Servando de la Cruz por la detallada revisión de este trabajo su interés y recomendaciones, a los doctores Ramón Zuñiga y Enrique Cabral por sus correcciones y sugerencias, igualmente agradezco al Dr Hugo Delgado. A los doctores Takeshi Mikumo y Francisco Sánchez Sesma les agradezco la gentileza y dedicación a la lectura de este trabajo así como sus comentarios y recomendaciones.*

*Gracias al Centro de Geociencias de Potsdam, Alemania por facilitar el equipo de banda ancha para la realización del experimento sísmico y en particular al Dr Guenter Asch por su colaboración y asesoría técnica en la operación y mantenimiento de la red instrumental así como en la construcción de la base de datos. Se reconoce la participación del Servicio Sismológico Nacional y del Centro Nacional de Prevención de Desastres durante la fase de instalación de los equipos.*

*Un reconocimiento al Sr Marcos Galicia y su equipo de rescate por el apoyo recibido durante el trabajo de campo que requirió el experimento de banda ancha. A P Chouet, C Dietel, D Escobedo, J Estrada, F Lizarraga, H López-Loera, J Méndez, J Pérez, a todos ellos mil gracias.*

*Gracias al Dr Campos, Araceli y Mónica del Posgrado en Ciencias de la Tierra, a E Cabral, F Correa M García y A Soler por facilitarme el uso de las computadoras y a R Colín por su ayuda con los trámites aduanales. Mis estudios fueron apoyados por CONACYT, DGAPA y PADEP.*

*Especialmente GRACIAS a Alex y Jaime por su paciencia, cariño y apoyo durante todo este tiempo. A Javier por su ayuda y compañía durante el trabajo de campo en el volcán. Y a mi familia por todo el apoyo, gracias.*

## Apéndice A. Semblance

El método de semblance es un procedimiento alternativo para localizar eventos sísmicos. Esta técnica se basa en la medida de coherencia que tienen las señales y por lo tanto no hace uso del arribo de las fases. El método es una medida de la coherencia existente entre las señales que se registran en multicanal [Neidell and Tarner, 1971; Furomoto *et al.*, 1990; Almendros, 2002]. Este método es útil en el caso de señales de periodo muy largo que presentan arribos emergentes.

El coeficiente de Semblance  $S$  está definido como sigue:

$$S = \frac{\sum_{j=s(i)}^{e(i)} (\sum_{i=1}^M u_{ij(i)})^2}{M \sum_{j=s(i)}^{e(i)} \sum_{i=1}^M u_{ij(i)}}$$

donde  $M$  es el número de estaciones de la red;  $u_{ij(i)}$  es la  $j(i)$ -esima muestra en la estación  $i$ -esima, y  $s(i)$  y  $e(i)$  son la primera y la última muestras en la ventana de tiempo de la  $i$ -esima estación usada para calcular semblance. En este caso se usa la componente vertical de velocidad de cada estación para el calculo del coeficiente. El coeficiente de semblance se puede describir como la razón de energía normalizada de entrada y salida de los datos del multicanal, donde la salida es simplemente la suma de las trazas que entraron. Para una ventana de tiempo dada el cociente entre las potencias entre la señal sumada y el total de la potencia provee los valores de semblance, que están en el rango entre 0 y 1. Si las señales de las diferentes estaciones son coherentes en esa ventana de tiempo, la suma en el numerador de la ecuación anterior (lo que es escencialmente el apilamiento de las señales) es grande y por lo tanto el cociente se acerca a uno. Si las señales son incoherentes en esa ventana de tiempo la suma en el numerador es pequeña y por lo tanto el cociente se aproxima a cero.

Siguiendo la descripción anterior y la definición original de semblance para una componente se desarrolló el método para tres componentes como sigue:

$$S = \frac{\sum_{j=s(i)}^{e(i)} (\sum_{i=1}^M u_{ij(i)}^r)^2}{M \sum_{j=s(i)}^{e(i)} \sum_{i=1}^M u_{ij(i)}^r}$$

en donde  $u_{ij(i)}^r$  es la componente radial de la señal.

Una modificación al método, es una extensión de la definición anterior, incluye la componente transversal y una función de penalización que se origina en la componente transversal y la cual debe ser cero en condiciones sin ruido [Matsubayashi, 1995].

$$S_M = \sum_{j=s(i)}^{e(i)} \left( \sum_{i=1}^M u_{ij(i)}^r \right)^2 - M \left( \sum_{i=1}^M u_{ij(i)}^{tv} \right)^2 - M \left( \sum_{i=1}^M u_{ij(i)}^{th} \right)^2 / M \sum_{j=s(i)}^{e(i)} \sum_{i=1}^M u_{ij(i)}^r$$

donde  $u_{ij(i)}^{th}$  representa la componente transversal del movimiento en el plano vertical incluyendo la fuente y el receptor y  $u_{ij(i)}^{th}$  representa la componente horizontal en el plano horizontal. Esta es la expresión que se usó para localizar eventos VLP en el volcán Aso [Kaneshima *et al.*, 1996] y el Kilauea [Ohminato *et al.*, 1998; Dawson *et al.* 1997]. El significado de la definición anterior puede ser entendida si consideramos lo siguiente. Asumamos que la fuente es isotrópica y que se aproxima a una señal sin ruido que se expresa como:

$$\tilde{u}_{ij}^r = \frac{1}{M} \sum_{i=1}^M u_{ij}^r \quad \tilde{u}_{ij}^{tv} = \tilde{u}_{ij}^{th} = 0$$

por lo que la definición de Matsubayashi puede ser representada como:  $S_M = 1 - \sigma^2$   
donde:

$$\sigma^2 = \sum_{j=s(i)}^{e(i)} \left( \sum_{i=1}^M [(u_{ij(i)}^r - \tilde{u}_{ij}^r)^2 + (u_{ij(i)}^{tv} - \tilde{u}_{ij}^{tv})^2 + (u_{ij(i)}^{th} - \tilde{u}_{ij}^{th})^2] / M \sum_{j=s(i)}^{e(i)} \sum_{i=1}^M u_{ij(i)}^r \right)$$

representa el error cuadrático normalizado respecto a la componente radial. De tal manera que se tiene una función de penalización que debe ser cero en condiciones ideales sin ruido.

Según la definición, semblance tiene valores entre 0 y 1 que se obtienen de la desigualdad de Schwartz:

$$\left(\sum_{i=1}^M u_{ij}\right)^2 \leq M \sum_{i=1}^M u_{ij}^2$$

donde  $u_{1j} = u_{2j} = \dots = u_{Mj} = 0$ . Sumando ambos lados se obtiene:

$$\sum_{j=s(i)}^{e(i)} \left[ \sum_{i=1}^M u_{ij}(i) \right]^2 \leq M \sum_{j=s(i)}^{e(i)} \sum_{i=1}^M u_{ij}(i)^2$$

Por lo tanto el lado izquierdo es trivial y la condición  $0 < S < 1$  se satisface.

Para encontrar un hipocentro se toman los coeficientes de semblance que indiquen mayor coherencia. La coherencia para todas las señales en una misma ventana de tiempo, si hay buena coherencia entonces se calculan los tiempos de arribo en un volumen definido por una malla entre nodos. Para esto, lo ideal es conocer el modelo de velocidad sino se asume un semiespacio con una determinada velocidad. Las diferencias en tiempos de viaje de cada nodo a cada estación determinan el tiempo de inicio de la ventana de tiempo que se analizó y se obtiene la localización en la malla.

## Apéndice B. Modelo de fractura

### Antecedentes

Para explicar el mecanismo involucrado en la generación de eventos LP y tremor en volcanes se ha incursionado en diferentes modelos; los principales están enfocados hacia el análisis de los efectos sísmicos producidos por cavidades llenas de fluidos y excitadas por varios procesos en los que la presión es determinante. El modelo de Aki *et al.* (1977) explica las causas de tremor superficial observado en el volcán Kilauea, Hawaii. En el modelo se considera el tremor como resultado de la excitación de fracturas y se asume que la excitación es causada por apertura espasmódica de canales que responden al exceso de presión magmática. En este modelo la respuesta de los fluidos a la vibración de las paredes se considera pasiva y el comportamiento de la fuente se describe sólo con un parámetro llamado factor de rigidez de la fractura. Estas características son un limitante del modelo de Aki *et al.*, porque como demostró Chouet (1981) la vibración por apertura de canales sólo alcanza unos cuantos ciclos de duración. Por ello la duración del tremor implica que la generación de tremor debe estar asociada al comportamiento activo de los fluidos. A partir de estos trabajos se incursionó en modelos hidráulicos basados en resonancia acústica [St Lawrence and Qamar, 1979; Ferrick *et al.*, 1982]. Ferrick *et al.* (1982) desarrollaron las ecuaciones que describen el movimiento del fluido a partir de las leyes físicas de conservación de la masa y conservación de momentum. La fuente modelada describe la estructura de multi-picos que presenta el espectro del tremor. Aunque en estos modelos el mecanismo de excitación que genera esta resonancia no es identificado.

En 1982, Chouet sugirió que dadas las profundidades someras a las cuales se originan los LP y sus características espectrales, todos los procesos deben ocurrir en la región donde el magma está almacenado y esto es justo debajo del volcán. Su hipótesis se basa en que los LP representan la excitación de los conductos del volcán y que la excitación se debe a algún mecanismo, el cual no está necesariamente relacionado con fracturamiento de rocas pero si con mecanismos de origen térmico, químico o de naturaleza hidráulica. Como ejemplo de estos mecanismos podrían ser la exolución de gases a partir de cambios de fases durante el transporte de magma o la interacción de magma con agua subterránea a profundidades someras. Posteriormente, Chouet apoyándose en los trabajos de Fehler y Chouet (1982) y Fehler (1983) y en los datos de LP y de tremor registrados en el Mt St Helens, observó que el tamaño de la región de la fuente se mantiene invariante de un evento a otro y que no hay correlación entre la ocurrencia de los eventos LP y los cambios

ocurridos dentro del cráter del St Helens de los cuales se tiene evidencia visual [Chouet, 1985].

Chouet (1986) aplicó la técnica de diferencias finitas a la dinámica de una fractura rellena de fluido en un medio elástico lineal con un espesor mucho menor que la longitud de onda sísmica de interés. La fractura entra en resonancia debido a la duración del proceso de apertura de la grieta rellena de fluidos. La forma en que lo relaciona con el tremor es considerando un mecanismo arbitrario que relaciona los cambios de presión en el fluido y las fluctuaciones en la velocidad del fluido, ambos cambios los relaciona con la inyección de magma. En 1988, Chouet desarrolló un modelo dinámico en 3 dimensiones en el que representa a la fuente generadora del tremor con fracturas llenas de fluido compresible y viscoso el cual al ser excitado por pulsos de presión intermitentes aplicados a una pequeña área de la superficie de la fractura provocan la resonancia del fluido en la fractura y se origina el tremor. La excitación depende de dos parámetros críticos que son la rigidez de la fractura, la cual caracteriza la habilidad de la fractura para vibrar, y la pérdida de amortiguamiento viscoso el cual ejerce un efecto en la duración de la resonancia.

En 1994 Chouet *et al.*, aplicaron el modelo tridimensional de una fractura rellena de fluido desarrollado por Chouet en 1992 a los datos generados por el volcán Redoubt. Con ello y a partir de las características de los eventos de LP determinaron parámetros como longitud (280 - 380 m) y ancho de fractura (140 - 190 m), espesor (0.05 - 0.20 m), rigidez (100 -200), velocidad del sonido en el fluido (0.8 -1.3 km/s), velocidad de ondas compresionales en la roca (5.1 km/s), la relación de densidades entre la roca y el fluido (aprox. 0.4) y la relación de módulo volumétrico del fluido y la rigidez de la roca (0.03-0.07). Para este modelo usaron los resultados de 18 explosiones de cargas de 450 kg de dinamita detectados por un arreglo de 20 estaciones tipo Ref-Tek alrededor del volcán. Esto les permitió tener un mayor control sobre los parámetros de velocidad y estratificación en el lugar.

Chouet (1992) expuso que existe una clara asociación entre la resonancia de la fractura y los parámetros de la fuente. Analizó efectos de fuente y trayecto usando sismogramas sintéticos y aplicó su modelo a los datos del Redoubt para estimar los parámetros de fuente. También discute las propiedades acústicas de los fluidos burbujeantes, donde la vesiculación y desgasificación juegan un papel relevante en la dinámica de la erupción y comenta que en estudios recientes se ha involucrado la teoría de burbujas en líquidos (Commander y Prosperetti, 1989) con la cual se han revelado características de la física de los fluidos volcánicos. Encuentra que hay dos tendencias para explicar la actividad de los LP; la primera se basa en la conexión directa entre la actividad superficial ( a

menos de 2 km) de eventos LP y las erupciones, la cual, ha sido observada sólo en algunos cuantos volcanes como reporta el Pinatubo Volcano Observatory Team (1991), Chouet *et al.* (1994) y Fischer *et al.* (1994); y la segunda, asocia la actividad de los eventos LP, localizados a profundidades mayores de 10 km, directamente con la dinámica profunda del abastecimiento de magma Koyanagi *et al.* (1987), Shaw y Chouet (1991) y Pitt y Hill (1994).

Por el momento no se ha desarrollado un modelo que explique completamente los procesos de generación del tremor y de los eventos LP. Uno de los obstáculos más importantes a comprender es el acoplamiento de la dinámica del fluido y la elastodinámica. En esta sección se han mencionado sólo algunas características de los modelos de mayor interés para sentar los antecedentes en esta materia puesto que el camino por recorrer es largo dada la complejidad de los procesos volcánicos y el alcance de los modelos para explicarlos.

## Dinámica de una grieta rellena de fluido en tres dimensiones por el método de diferencias finitas

En este modelo se acepta que el tremor y los eventos LP comparten el mismo origen y son el resultado de la excitación de un conducto por flujo de magma o algún otro tipo de inestabilidad magmática de naturaleza térmica, química o hidráulica.

El tremor se considera como el resultado de la ocurrencia aleatoria y sostenida de eventos LP, es decir que los eventos LP se pueden ver como el proceso elemental de tremor e interpretarlos como la respuesta al impulso del sistema generador de tremor.

El objetivo del trabajo de Chouet (1986) es analizar la dinámica de la fuente de hidrofracturas y su radiación elástica con base en el estudio del movimiento en tres dimensiones de fracturas llenas de fluido en resonancia. Estas fracturas son excitadas subitamente por la falla de una pequeña barrera de área  $\Delta S$  sobre su superficie. La suposición básica en este modelo es que la falla es instantánea por lo que la emisión acústica es posible. Como se asume que la fractura está llena de fluido un exceso de presión  $\Delta P$  simula la falla de la barrera al ser aplicado  $\Delta P$  sobre el área  $\Delta S$ . El modelo explica la

penetración del fluido en la grieta suponiendo que se puede describir el flujo en la cavidad por la relación de continuidad que establece que la tasa de volumen del fluido que entra a la cavidad es igual a la tasa de incremento de la cavidad. Se asume que el frente de propagación de la fractura tiene velocidad infinita y que la presión  $\Delta P$  es aplicada instantáneamente sobre  $\Delta S$ . Otras idealizaciones incluidas en este modelo son: a) el fluido en la fractura se comporta como un líquido viscoso, b) el líquido se trata como un medio continuo de dos dimensiones, se trata al fluido como un sólido elástico con rigidez cero, c) el incremento en la extensión de la fractura y las velocidades resultantes del flujo en la fractura son tan pequeñas que en cualquier lugar de la fractura el flujo es laminar y d) la roca que rodea la fractura es perfectamente elástica, homogénea, isotrópica e impermeable. La consideración b) permite aplicar la ecuación acústica dentro del fluido de tal manera que se evita el problema de acoplar la fase líquida y la sólida en una interfase.

La técnica de diferencias finitas no es directamente aplicable a este tipo de fracturas porque éstas requieren de la formulación de la ecuación de la dinámica de fluidos. Entonces, es necesario incluir las ecuaciones de transferencia de masa y momento en el fluido para especificar las condiciones apropiadas para un flujo de fluidos dentro de un volumen que se expande en una fractura. Por esto, se analiza el comportamiento de la fuente en términos de la rigidez de la fractura y de la pérdida de amortiguamiento viscoso, ambos parámetros son adimensionales y cuantifican la dinámica del comportamiento de la fractura y el efecto de la viscosidad del fluido sobre las características de la resonancia inducida por la falla de la barrera.

## Formulación del problema

Considerese un medio lineal, infinito y elástico. Una área de fractura de espesor mucho menor a la longitud de onda de interés con longitud  $L$  según el croquis (Fig B-1), y ancho desde  $-w/2$  a  $w/2$  que se extiende en el eje  $x$ . La barrera de área  $\Delta S$  está en  $z=0$ . La falla de esta pequeña área es la que produce el disparo que genera la resonancia en la fractura, la cual está rellena de fluido. Este fluido está a una presión que excede el esfuerzo en la dirección  $\sigma_{zz}$ .

Lo que se pretende es calcular el movimiento de la superficie de la fractura (Fig B-1) cuando en un tiempo  $t=0$  la barrera de área  $\Delta S$  falla, de tal manera que la fractura subitamente se expande un  $\Delta V$  y el fluido fluye hacia la cavidad abierta. Para hacer

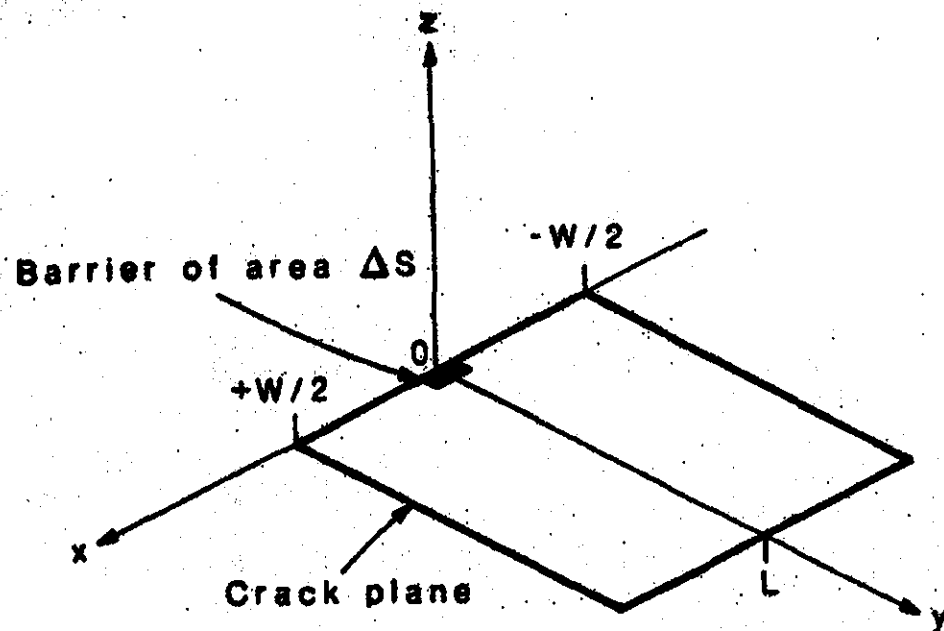


Fig B-1 Croquis del modelo.

una evaluación se requieren de ciertas condiciones iniciales sobre  $\Delta S$ , que involucran el estado de esfuerzos  $\sigma_{xx}, \sigma_{yy}, \sigma_{zz}, \sigma_{xy}, \sigma_{xz}, \sigma_{yz}$  y desplazamientos  $u, v, w$  en función de las constantes de Lamé  $\lambda$  y  $\mu$ , la densidad del sólido  $\rho_1$ , las ecuaciones son las siguientes:

$$\frac{\partial \sigma_{xx}}{\partial t} = \lambda \left( \frac{\partial u}{\partial x} + \frac{\partial v}{\partial y} + \frac{\partial w}{\partial z} \right) + 2\mu \frac{\partial u}{\partial x}$$

$$\frac{\partial \sigma_{yy}}{\partial t} = \lambda \left( \frac{\partial u}{\partial x} + \frac{\partial v}{\partial y} + \frac{\partial w}{\partial z} \right) + 2\mu \frac{\partial v}{\partial y}$$

$$\frac{\partial \sigma_{zz}}{\partial t} = \lambda \left( \frac{\partial u}{\partial x} + \frac{\partial v}{\partial y} + \frac{\partial w}{\partial z} \right) + 2\mu \frac{\partial w}{\partial z}$$

$$\frac{\partial \sigma_{xy}}{\partial t} = \mu \left( \frac{\partial u}{\partial y} + \frac{\partial v}{\partial x} \right)$$

$$\frac{\partial \sigma_{xz}}{\partial t} = \mu \left( \frac{\partial u}{\partial z} + \frac{\partial w}{\partial x} \right)$$

$$\frac{\partial \sigma_{yz}}{\partial t} = \mu \left( \frac{\partial v}{\partial z} + \frac{\partial w}{\partial y} \right)$$

$$\begin{aligned}\frac{\partial u}{\partial t} &= \frac{1}{\rho_1} \left( \frac{\partial \sigma_{xx}}{\partial x} + \frac{\partial \sigma_{xy}}{\partial y} + \frac{\partial \sigma_{xz}}{\partial z} \right) \\ \frac{\partial v}{\partial t} &= \frac{1}{\rho_1} \left( \frac{\partial \sigma_{xy}}{\partial x} + \frac{\partial \sigma_{yy}}{\partial y} + \frac{\partial \sigma_{yz}}{\partial z} \right) \\ \frac{\partial w}{\partial t} &= \frac{1}{\rho_1} \left( \frac{\partial \sigma_{xz}}{\partial x} + \frac{\partial \sigma_{yz}}{\partial y} + \frac{\partial \sigma_{zz}}{\partial z} \right)\end{aligned}$$

Para el caso en que  $\lambda$  es grande el movimiento del fluido está predominantemente en el plano de la fractura (Fig B-1) y por lo tanto la aparente tercera dimensión del flujo se puede simplificar y entonces la dinámica del fluido se trata en 2 dimensiones. La descripción de la dinámica del fluido en la fractura se obtiene integrando las ecuaciones que gobiernan la apertura de la fractura. Siguiendo a Lamb (1932) y a Wooding (1960), la componente de velocidad del flujo paralela a la apertura es igual a cero. Las otras componentes de velocidad paralelas al plano de la fractura tienen un perfil parabólico transversal a la apertura a un número de Reynolds bajo. Es decir los flujos son laminares, no hay turbulencia. Después de la integración y de promediar sobre el perfil parabólico de la velocidad del flujo se obtienen las ecuaciones de conservación del momentum en las direcciones  $x$  e  $y$  como:

$$\begin{aligned}\frac{1}{\rho_2} \frac{\partial p}{\partial x} + \frac{\partial U}{\partial t} + \frac{12\eta}{\rho_2 d^2} U &= 0 \\ \frac{1}{\rho_2} \frac{\partial p}{\partial y} + \frac{\partial V}{\partial t} + \frac{12\eta}{\rho_2 d^2} V &= 0\end{aligned}$$

y la ecuación de continuidad queda como:

$$\frac{1}{b} \frac{\partial p}{\partial t} + \frac{2}{d} \frac{\partial w_d}{\partial t} + \frac{\partial U}{\partial x} + \frac{\partial V}{\partial y} = 0$$

en estas ecuaciones  $\rho_2$  es la densidad,  $\eta$  es la viscosidad y  $b$  es el modulo volumétrico del fluido;  $w_d$  es la normal del desplazamiento de la pared de la fractura;  $p$  es la presión en el fluido y  $U$  y  $V$  son las componentes  $x$  e  $y$  de la velocidad del fluido promediadas

sobre el perfil del fluido. En estas ecuaciones las componentes térmicas se han despreciado por considerarse muy pequeñas respecto a las derivadas contra el tiempo de presión y velocidad de flujo. Los esfuerzos cortantes se relacionan con la velocidad del flujo promedio a través de:

$$\tau_x = \frac{6\eta}{d} U$$

$$\tau_y = \frac{6\eta}{d} V$$

donde  $\tau_x$  y  $\tau_y$  representan las componentes  $x$  e  $y$  de los esfuerzos. Por otro lado, si se considera que las paredes de la fractura son perfectamente rígidas  $w_d = 0$  y se combinan las ecs anteriores, se obtiene la ecuación de onda en dos dimensiones en términos de la presión para un fluido no viscoso como:

$$\frac{\partial^2 p}{\partial t^2} = a^2 \left( \frac{\partial^2 p}{\partial x^2} + \frac{\partial^2 p}{\partial y^2} \right)$$

donde  $a^2 = \frac{b}{\rho_2}$  es la velocidad del sonido en el fluido. El comportamiento elástico de la pared tiene el efecto de alentar la velocidad acústica por lo que la relación ( $v/a$ ) velocidad de la onda en la fractura y velocidad acústica en el fluido generalmente es menor de uno. La velocidad de la onda en la fractura es típicamente ordenes de magnitud más grande que la velocidad del fluido  $U$  y  $V$ .

Las condiciones de frontera para el problema planteado (fluido viscoso) suponen propiedades simétricas en el plano de la fractura. En el sólido los esfuerzos  $\sigma_{xz}$ ,  $\sigma_{yz}$  y el desplazamiento normal  $w$  son funciones impares de  $z$  por lo que desaparecen de la superficie del plano de fractura que está afuera de la fractura. Las condiciones del sólido para una fractura en tensión son:

- 1) sobre la superficie de la fractura  $S_1$

$$\sigma_{zz} = -p, \sigma_{xz} = -\tau_x, \sigma_{yz} = -\tau_y$$

y 2) sobre la superficie fuera de la fractura  $S_2$

$$w = 0, \sigma_{xz} = 0 \text{ y } \sigma_{yz} = 0$$

Las condiciones del fluido en el perímetro de la fractura están dados por:

$$U = \dot{u} \text{ a lo largo del eje } x = W/2 \text{ para } 0 \leq y \leq L$$

y por

$$V + \dot{v} \text{ a lo largo de } -w/2 \leq x \leq W/2, y = 0 \text{ y } y = L$$

Con estas condiciones queda establecida la continuidad entre la componente de velocidad del fluido en la periferia y la componente de velocidad de la partícula en el sólido en las orillas de la fractura. Nótese que no hay límites entre la velocidad el fluido  $U$  y  $V$  y las velocidades de la partícula  $\dot{u}$  y  $\dot{v}$  sobre la superficie de la fractura. En el caso particular en que supongamos que el fluido no es viscoso se entiende que la superficie de la fractura es una frontera sin fricción, y el fluido se puede deslizar sobre la superficie por lo tanto  $U \neq \dot{u}$  y  $V \neq \dot{v}$  sobre la superficie  $S_1$ .

En este modelo se está considerando que la respuesta de la fractura a la excitación es  $\sigma_{zz}$  o su equivalente en presión de amplitud  $\Delta P$  aplicada en el área  $\Delta S$ . Como se está asumiendo que el fluido penetra toda la fractura, la condición inicial para el flujo se idealiza por la ecuación de continuidad igual a:

$$2\Delta S \dot{w}_d = \dot{Q}_x + \dot{Q}_y$$

donde  $\dot{Q}_x$  y  $\dot{Q}_y$  representan la tasa de flujo en las direcciones  $x$  e  $y$ . Entonces representa la igualdad entre el incremento de volumen y el flujo que entra. De tal manera que una vez llena la cavidad se resuelven las ecuaciones del movimiento y continuidad como para el resto de la fuente. Por lo tanto esta ecuación es sólo una condición inicial.

## Solución Numérica

Las ecuaciones se resuelven por el método de diferencias finitas, simulando un cambio de presión  $\Delta P$  en una localidad de la rejilla. Con este método se calculan velocidades de partícula y derivadas con respecto al tiempo de los esfuerzos, de las cuales es obtenido el desplazamiento y esfuerzos por integración. El error obtenido en la solución es del orden de 10% en la velocidad de fase para una longitud de onda  $\lambda > 5L/n$ , donde  $n$  es el número de celdas en la longitud  $L$  de la fractura.

Los resultados numéricos están expresados como funciones adimensionales de la fractura y de los parámetros del medio según lo siguiente:

Longitud

$$r' = r/L$$

tiempo

$$t' = \alpha t/L$$

esfuerzo

$$\sigma_{ij'} = \sigma_{ij}/\sigma_0$$

desplazamiento

$$u'_i = u_i \mu / (L \sigma_0)$$

velocidad

$$u'_{i'} = u_{i'} \mu / (\alpha \sigma_0)$$

donde las variables con prima son adimensionales. Las variables físicas son la longitud  $L$ , el esfuerzo efectivo  $\sigma_0$ , la velocidad compresional  $\alpha$  y la rigidez del sólido  $\mu$ .

En este modelo se consideró simetría respecto al eje  $y$ , con la idea de evitar problemas con la capacidad de memoria de la máquina. Además debido a las condiciones iniciales que se aplican simétricamente sobre dos rejillas alrededor del eje  $y$ , el problema tiene simetría en el plano  $x = 0$ , y la solución se reduce al cálculo en un sólo cuarto del espacio en  $x \geq 0$ ,  $-\infty \leq y \leq +\infty$  y  $z \geq 0$ . El número de rejillas usado es de  $20 \times 20$  donde  $(W/L) = 1$  y la fractura se supone es de longitud igual a dos rejillas en el eje  $x$  y una en el eje  $y$ , localizada en la mitad en  $|x| \leq W/2$  y  $y = 0$ , en una fractura de longitud  $L$  y ancho  $W$  (Fig B-1).

Los resultados obtenidos se fijaron para una relación de Poisson de  $1/4(\lambda + \mu)$  para el sólido. Criticamente la solución queda en función de un parámetro adimensional llamado rigidez de la fractura y está definido por

$$C = \frac{bL}{\mu d}$$

esta ecuación caracteriza la dinámica del comportamiento de la fractura. Otro parámetro adimensional es la perdida de amortiguamiento viscoso debido a la viscosidad del fluido, definido como:

$$F = \frac{12\eta L}{\rho_2 d^2 \alpha}$$

Estas ecuaciones se resuelven para diferentes valores de C y se obtienen los parámetros físicos de la fractura. Con este modelo se demostró que el mayor contenido de ondas son de tipo superficiales predominantemente Rayleigh.

Las características de dispersión fueron definidas por el modelo de diferencias finitas, en él se representan las relaciones de velocidad de fase respecto de la velocidad acústica y se grafican en función de la longitud de onda  $\Lambda/L$ , cantidad adimensional (ver Fig B-2).

La impedancia entre el sólido y el fluido se expresa  $Z = \rho_s \alpha / \rho_f a$ . Esta definición afecta tanto la frecuencia como la duración de la señal radiada por la fractura. La presencia de burbujas de gas puede reducir drásticamente la velocidad del sonido en el fluido, por lo que la resonancia de grandes periodos es posible en fracturas pequeñas. La presencia de burbujas incrementa el contraste de impedancia el cual incrementa la duración de la resonancia debido a energía acústica atrapada dentro de la fractura. Esta característica de cómo afecta la impedancia en la duración está bien ejemplificada en el volcán Galeras, Colombia. En este volcán las distribución de estaciones e hipocentros permitieron notar que la resonancia sostenida de la fuente asociada con el fuerte contraste de impedancias agudiza la definición de picos espectrales haciendo más fácil la identificación. El problema es más complicado cuando la fuente se encuentra en capas suaves y superficiales (menos de 1 km) y el contraste de impedancias es débil.

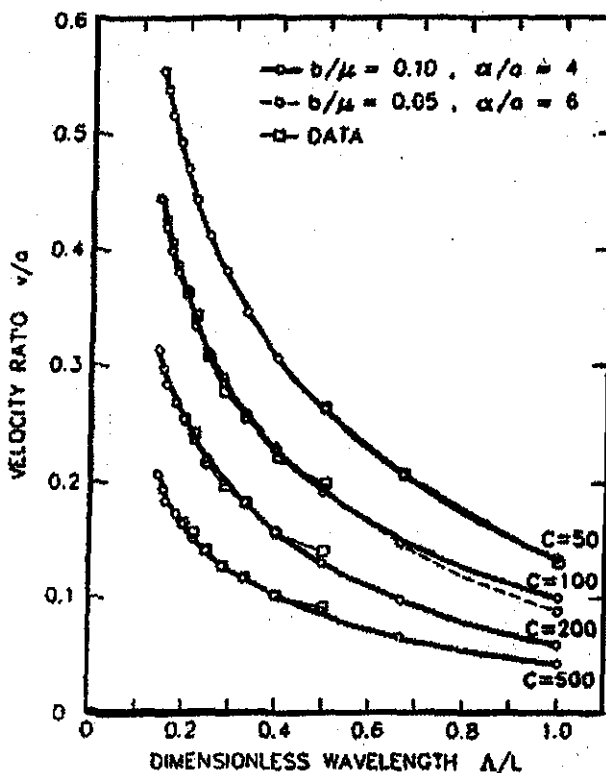


Fig B-2. Curvas de dispersión.

El espectro de frecuencias de los eventos LP registrados en el volcán Redoubt son compatibles con las características del modelo de fractura rellenas de fluido. Chouet *et al.* (1994) obtuvieron los parámetros de la fuente como la longitud de la fractura de entre 280-380 m; ancho de la fractura entre 140-190 m; apertura de la fractura entre 0.05-0.20 m; rigidez de la fractura entre 100 y 200; velocidad del sonido en el fluido entre 0.8 y 1.3 km/s; velocidad de la onda compresional en la roca de 5.1 km/s; relación de densidades entre el fluido y la roca de aprox 0.4; y relación del módulo volumétrico del fluido y rigidez de la roca de 0.03 a 0.07. La excitación de la fractura la suponen por una caída de presión de entre 0.4 y 40 bares.

El modelo expuesto predice satisfactoriamente los datos LP y de tremor analizados en los capítulos II y V de este trabajo debido a que los espectros de los eventos LP presentan las características de picos bien definidos. Para ello se utilizaron las curvas de dispersión calculadas para diferentes rigideces mostradas en la Fig B-2.

En el modelo del 'fluid-driven crack' el contraste de impedancias tiene importantes implicaciones en la duración y amplitud de las señales (Chouet, 1992). Para ejemplificar, definiremos los siguientes parámetros: el parámetro adimensional llamado rigidez de la fractura definido por  $C = bL/\mu d$  y la impedancia entre el sólido y el fluido que se expresa

como:  $Z = \rho_s \alpha / \rho_f a$ . Se muestra en la Fig B-3 el espectro radiado por la excitación de un "fluid-filled crack" y el sismograma asociado para una incidencia de un tren de ondas compresional. La resonancia en la fractura es enormemente mejorada cuando existe un incremento en el contraste de impedancias.

Las soluciones mostradas en la Fig B-3 están calculadas para relaciones fijas de  $W/L = 0.5$ ,  $L/d = 200$  y un contraste de impedancias en el rango entre 3 y 37.5. El incremento en la relación  $\alpha/a$  mostrado en las Figs B-3 a, c, e implica un decremento en las frecuencias de los picos espectrales, aunque este efecto se compensa por el decremento asociado del factor de rigidez de la fractura  $C$ , el cual provoca un incremento en la relación  $v/a$  donde  $v$  es la frecuencia. Lo anterior explica porqué los picos dominantes se mantienen en las Figs B-3 a, c y cambian para la Fig B-3 e, hay un efecto opuesto entre estos factores y por lo tanto se cancelan. Obsérvese los cambios en la amplitud y el decremento en el ancho de banda, produciéndose un aumento en el contenido de bajas frecuencias cuando los valores de rigidez de la fractura son bajos. Los sismogramas sintéticos correspondientes a los espectros muestran esas características. Basicamente muestran como tanto la frecuencia como la duración de la señal radiada por la fractura se incrementa con el contraste de impedancia, y tambien es indicativo de que la forma y la envolvente de la coda es dependiente de la rigidez de la fractura.

Por lo anterior es importante señalar tambien que existe dependencia de la rigidez de la fractura  $C$  con el contraste de impedancia. Al incrementarse  $Z$  se incrementa tambien la excitación de los modos subdominantes al modo principal. Estas variaciones en los modos de vibrar estas relacionadas con el factor de atenuación  $Q$  de cada modo por lo que el contraste de impedancias tambien tiene implicaciones en la atenuación de las frecuencias. Y como se mencionó la presencia de burbujas en los fluidos que llenan la cavidad incrementan el contraste de impedancias aumentando la duración de la resonancia, debido a la energía acústica atrapada dentro de la fractura. Hay otros modelos en los que tratan las implicaciones del contraste de impedancias en la generación de energía radiada por un resonador (e.g. Garcés y Mc Nutt, 1997.), o en un sistema de magma-filled dike con geometría compleja (Dahm, 1991)

Para ejemplificar lo anterior se mostrará el campo radiado por modelo del "fluid-filled crack" el cual ha sido ampliamente explorado analíticamente y teóricamente con modelos sintéticos [Aki *et al.*, 1977; Chouet, 1986, 1988, 1994] y tambien ha sido aplicado a datos de otros volcanes como el Redoubt [Chouet *et al.*, 1994]; Galeras [Gil-Cruz y Chouet *et al.*, 1997] permitiendo conocer más acerca del sistema de generación de las señales tipo LP y tremor. El modelo del "fluid-filled crack" explica como el campo radiado de

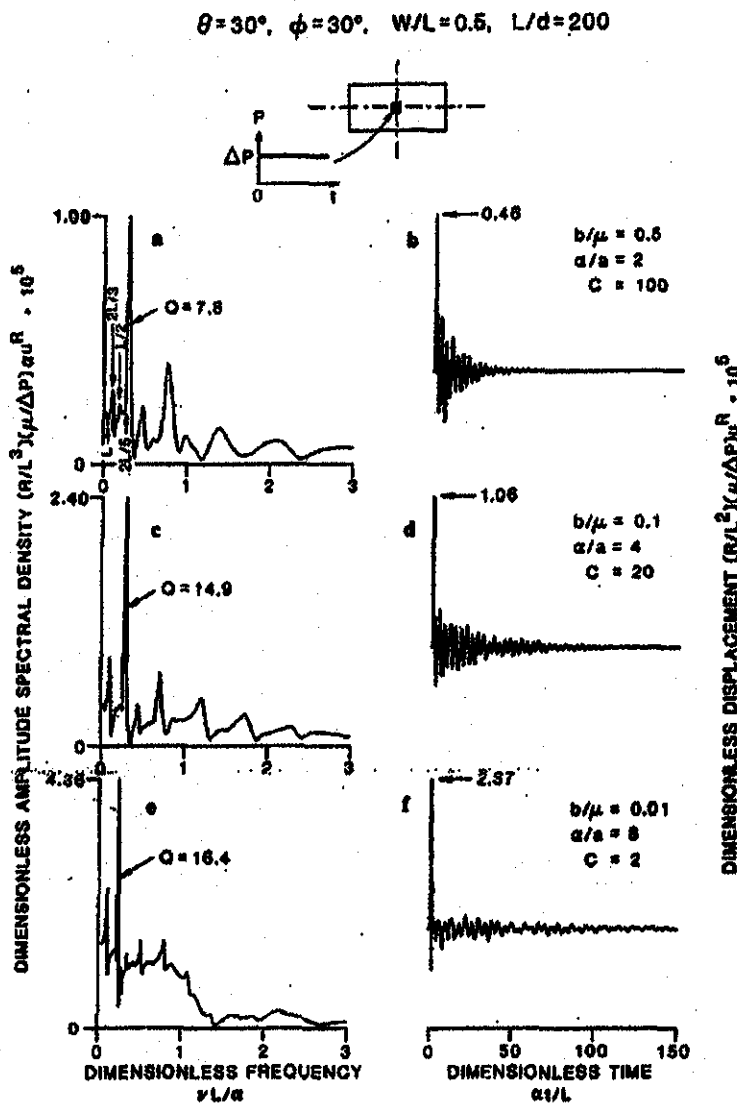


**Fig B-3** Ejemplo dados diferentes valores de  $Z$  y  $C$ . El espectro en el campo lejano y su asociado sismograma de un tren de ondas compresional radiado por la excitación del "fluid-filled-crack". Los cocientes  $W/L = 0.5$  y  $L/d = 200$  se mantienen constantes. El transitorio de presión es un esclón de amplitud  $\Delta P$  aplicado en el centro del "crack". Las amplitudes son adimensionales y están indicadas con flechas.

desplazamientos contiene ondas P, SV y Rayleigh y como la posición de la fuente tiene implicaciones en el campo radiado.

El campo de ondas elásticas radiado por el "fluid-filled crack" está en función de la geometría de la grieta, propiedades del fluido, del sólido y de las características espaciotemporales de los transitorios de presión y de los disparadores de la excitación de la grieta. Una grieta con geometría similar a un conducto es excelente para generar ondas P, SV y SH y si está rellena de fluidos generará ondas armónicas sostenidas [Chouet, 1986; 1988]. Para una grieta rectangular los parámetros adimensionales se expresan como  $L/d$  y  $W/L$ , donde  $L$  es la longitud de la grieta,  $W$  es el ancho y  $d$  es su espesor. Las propiedades del fluido se caracterizan por las relaciones adimensionales  $\alpha/a$  que es velocidad de la onda compresional en el sólido entre velocidad del sonido en el fluido,  $b/\mu$  que es el módulo volumétrico del fluido entre rigidez del sólido, y su relación de densidades  $\rho_s/\rho_f$ . De aquí se define el contraste de impedancias como:  $Z = \rho_s\alpha/\rho_f a$ . La influencia del contraste de impedancias se ve reflejado en el ancho de banda de los picos espectrales del espectro radiado. Las relaciones  $b/\mu$  y  $L/d$  definen las características de rigidez de la fractura y fijan las características de onda de la fractura. También se asume  $\lambda = \mu$  en la roca y  $\Delta S$  es el área dónde el transitorio de presión se aplicará. Se asume que el mecanismo disparador es una perturbación debido a cambios de presión o de cualquier origen y que provoca resonancia en la grieta rellena de fluidos. Estas condiciones de resonancia de conductos efectivamente rodian energía sísmica. Para exponer las relaciones de amplitudes del campo radiado en términos de ondas P, SV y Rayleigh se planteará el campo radiado de desplazamientos producido por el "fluid-filled crack", el cual cumple con las condiciones de frontera sólido-líquido. Los desplazamientos son:

$$u^R(R, \omega) = \frac{1}{12\pi\alpha R} (1 + 2\sin^2\theta\sin^2\phi) \Delta v(k_z, \omega)$$

$$u^\phi(R, \omega) = \frac{1}{4\pi\beta R} (\sin\theta\sin 2\phi) \Delta v(k_z, \omega)$$

$$u^\theta(R, \omega) = \frac{1}{4\pi\beta R} (\sin 2\theta\sin^2\phi) \Delta v(k_z, \omega)$$

donde  $R$  es el vector de posición del observador,  $\beta$  es la velocidad de cortante en la

roca,  $\omega$  es la frecuencia radial,  $\theta$  y  $\phi$  son los ángulos polar y azimutal (ver croquis del modelo Fig B-1). La cantidad  $\Delta\dot{v}$  es la función de velocidad de apertura de la grieta.

se trate de P o

Para investigar el campo radiado por el "crack" de ondas superficiales (sabemos que se generan por la interacción de ondas P y SV), se supondrá una geometría cilíndrica con  $z$  positivo hacia abajo y donde  $x = r\cos\psi$  y  $y = r\sin\psi$  y considera una grieta vertical localizada en  $r = 0$  en el plano  $y = 0$  con la fuente posicionada a una profundidad  $h$  (Aki y Richards, 1980). Como  $\psi = \theta$  y se asume un medio con relación de Poisson igual a 0.25 entonces las ondas Rayleigh no son dispersivas. De Aki y Richards (1980) y de Aki et al. (1977) se tiene que los desplazamientos para la componente vertical son:

$$u_z^R = \frac{1}{\beta\mu} \left( \frac{1}{\Lambda r} \right)^{(1/2)} (p + q\sin^2\psi) L^3 \Delta P |\Delta v'|$$

dónde  $\Delta v'$  es una cantidad adimensional igual a  $(\mu/\Delta P)(1/L^3)\Delta\dot{v}$ , y  $p$  y  $q$  están dados por valores que dependen del número de onda  $k_n$  y es la longitud de onda  $\Lambda$ . Usando las ecuaciones que describen los desplazamientos  $u^R, u^\phi, u^\theta$  y  $u_z^R$  se pueden estimar las relaciones de amplitud para las ondas P, SV y Rayleigh. Como ejemplos se aplicaron por Chouet et al. (1994) y Gil-Cruz y Chouet (1997) al volcán Redoubt y Galeras, respectivamente. En el caso de Redoubt la amplitud de los desplazamientos en promedio de las ondas SV es 1.4 veces más grande que la amplitud de las ondas P, y que las amplitudes de las ondas Rayleigh, considerando las distancias a las cuales se hicieron las observaciones sísmicas, son de 5 a 10 veces más grandes que las ondas SV. Esto para una fuente que se encuentre entre 0 y 1 km de profundidad. Para esta misma fuente y con estas mismas ecuaciones de desplazamientos encontraron valores de  $\Delta P$  para cada uno de sus puntos de observación. De tal manera que obtiene una estimación del decaimiento de presión  $\Delta P$  que inició la resonancia, según sus datos es del orden de 20 bars.

Finalmente se muestra como según la ubicación de la fuente de energía elástica hay variaciones en el campo radiado. En la Fig B-4 se muestra el campo radiado de un tren de ondas compresional para un modelo de fuente impulsiva de forma triangular de amplitud  $\Delta P$  y ancho  $2\tau$ . En los seis modelos se muestra como la onda radiada por fuentes con parámetros comunes ( $W/L = 0.5, b/\mu = 0.5, \alpha/a = 2$ ) depende de la rigidez de la fractura

y de las características de la función de disparo. Los tres sintéticos (a,b,c) se obtuvieron para una transitorio aplicado en el área  $\Delta S = L^2/800$  localizada en  $l = 0, w = W/2$  para grietas de diferentes rigideces  $C = 5, 50, 100$  Figs B-4 a,b y c, respectivamente. En la Fig B-4 d se aplicó un  $\Delta S = L^2/800$  centrado en el eje principal de la grieta en  $l = L/4$ ; para la Fig B-4 e se aumentó  $\Delta S = L^2/80$  extendido a todo lo ancho de la grieta en  $l = L/4$ , y para la Fig B-4 f se aplicó un  $\Delta S = L^2/800$  posicionado en el centro de la grieta.

La forma de onda de estos sintéticos reflejan la excitación y la interacción de los modos de resonancia del "crack", en los que resalta la dependencia con el tamaño y posición del transitorio. Por ejemplo, el modo longitudinal (señalado con una flecha) es minimizado (Figs B-4 a,b,c,f) cuando se posiciona el transitorio en un nodo, y es maximizado cuando la fuente de  $\Delta P$  es posicionado en un antinodo de ese modo. La máxima exitación de este modo se presenta en el caso donde  $\Delta S$  es más grande y está en un antinodo. El sintético de la Fig B-f muestra un evento quasi-monocromático. Este se obtuvo debido a que se escogió un  $\tau$  de tal manera que coincide con un pico espectral subdominante, por lo tanto este valor se elimina del espectro obteniéndose un pico angosto y bien definido, el cual define a la señal armónica. Por lo tanto este modelo refleja como la transmisión y partición de la energía es fuertemente dependiente del contraste de impedancias, las condiciones de frontera, y el tamaño y el lugar donde se ubica la fuente de disparo que genera la resonancia.

**TESIS CON  
FALLA DE ORIGEN**

$$\theta = 30^\circ, \phi = 30^\circ, W/L = 0.5, b/\mu = 0.5, a/a = 2$$

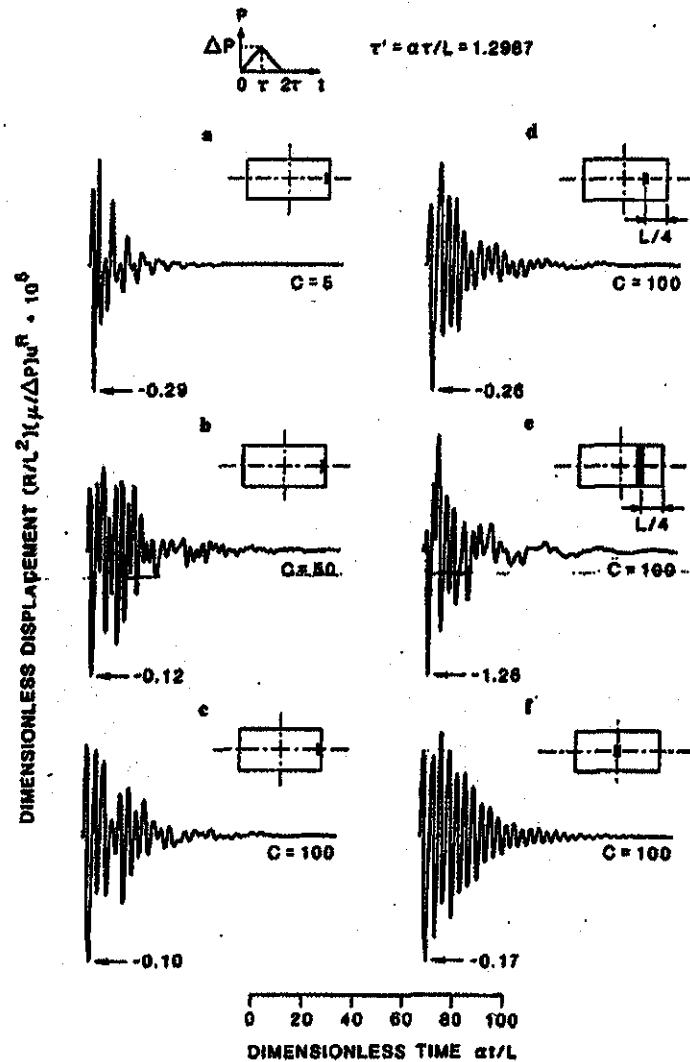


**Fig B-4** Variaciones con la posición de  $\Delta P$ . Los sintéticos de desplazamiento muestran diferencias en el campo lejano conforme varía la rigidez de la grieta, la posición de  $\Delta P$ , la forma del área donde se aplica y la duración.

## Referencias

- Aki K. and P. Richards. (1980) *Quantitative Seismology*. Freeman San Francisco, CA.
- Aki K., Fehler M. and Das S. (1977). Source mechanism of volcanic tremor: fluid-driven crack models and their application to the 1963 Kilauea eruption. *J. Volcanol. Geotherm. Res.* 2:259-287.
- Almendros J., B. Chouet, P Dawson. (2001) Hawaii. Spatial extent of a hydrothermal system at Kilauea Volcano, Hawaii, determined from array analyses of shallow long-period seismicity 1; Results *J. Geophys. Res.* 106, 7 13581-13597.
- Araña-Saavedra y Ortiz. (1984) *Vulcanología* Editorial Rueda, Madrid, España.
- Benoit, JP., Mc Nutt, SR., (1997). New constraints on source processes of volcanic tremor at arenal Volcano, Costa Rica, using broadband seismic data. *Geophys. Res. Lett.* 24:449-452.
- Biot, M.A., (1992). Propagation of elastic waves in a cylindrical bore containing a fluid. *J. Appl. Phys.*, 23, 997-1005.
- Carrasco G., S. Mora, H. Delgado, and J. Urrutia. (1986). *Geología y paleomagnetismo del Popocatépetl*. Serie de Investigación, Instituto de Geofísica, UNAM.
- Boudal C. and Robin C. (1988). Relations entre dynamismes éruptifs et réalimentations magmatiques d'origine profonde au Popocatépetl. *J. Earth. Sci.* 21: 955-971.
- Chouet B. (1981). Ground motion in the near field of a fluid-driven crack and its interpretation in the study of shallow volcanic tremor. *J. Geophys. Res.* 86: 5985-6016.
- Chouet B. (1982). Free surface displacements in the near field of a tensile crack expanding in three dimensions. *J. Geophys. Res.* 87: 3868-3872.
- Chouet B and Julian B. (1985). Dynamics of an expanding fluid-filled crack. *J. Geophys. Res.* 90: 11,187-11,198.
- Chouet B. (1985). Excitation of a buried magmatic pipe: a seismic source model for volcanic tremor. *J. Geophys. Res.* 90: 1881-1893.
- Chouet B. (1986). Dynamics of a fluid-driven crack in three dimensions by the finite difference method. *J. Geophys. Res.* 91:13967-13992.
- Chouet B. (1988). Resonance of a fluid-driven crack: radiation properties and implications for the source of long-period events and harmonic tremor. *J. Geophys. Res.* 93: 4375-4400.
- Chouet B. (1992). A seismic model for the source of the long-period events and harmonic tremor. In. Gasparini P, Scarpa R, Aki K (eds) *Volcanic seismology*. IAVCEI Proc. in Volcanology 3. Springer, Berlin Heidelberg New York, pp. 133-156.
- Chouet B., Page R. A., Stephens C. D., Lahr J. C. and Power J. A. (1994). Precursory swarms of long-period events at Redoubt Volcano (1989-1990), Alaska; their origin and use as a forecasting tool. In. T P Miller and Chouet B (edit). *The 1989-1990 eruptions of Redoubt Volcano, Alaska*. *J. Geophys. Res.* 62: 95-135.
- Chouet B. (1996a). Long-period volcano seismicity: its source and the use in eruption forecasting. *Nature* 380: 309-316.

- Chouet B. (1996b). New Methods and Future Trends in Seismological Volcano Monitoring. *Monitoring and Mitigation of Volcano Hazards*, Springer-Verlag, Berlin Heidelberg.
- Chouet, B., G. Saccorotti, P. Dawson, M. Martini, R. Scarpa, G. De Luca, G. Milana, and M. Cattaneo. (1999) Broadband measurements of the sources of explosions at Stromboli Volcano, Italy, *Geophys. Res. Lett.* 26:1937-1940.
- Commander K. W. and Prosperetti A. (1989). Linear pressure waves in bubbly liquids; comparison between theory and experiments. *J. Acoust. Soc. Am.* 85:732-746.
- Dawson, P. B., C. Dietel, B. A. Chouet, K. Honma, T. Ohminato and P. Okubo. A digitally telemetered broadband seismic network at Kilauea volcano, Hawaii. (1998). *U.S. Geol. Surv. Open File Rep.*, 98-108, 122.
- De la Cruz S, Quezada, J. L., Peña C., Zepeda, O. Sánchez, T. (1995). Historia de la Actividad Reciente del Popocatépetl (1354-1995). In: Volcán Popocatépetl, estudios realizados durante la crisis de 1994-1995, CENAPRED and UNAM, pp 3-22.
- Delgado H. L Cárdenas, N Piedad (2001). Sulfur dioxide emissions from Popocatépetl volcano (Mexico): cas study of a high-emission rate, passively degassing erupting. *J. Volcanol. Geotherm. Res.* , 108, 107-120
- Fehler M. (1983). Observations of volcanic tremor at mount St. Helens Volcano. *J. Geophys. Res.* 88: 3476-3484.
- Fehler M. and Chouet B. (1982). Operation of a digital seismic network on Mount St Helens Volcano and observations of long-period seismic events the originate under the volcano. *Geophys. Res. Lett.* 9:1017-1020.
- Ferrick M., Qamar A. and St Lawrence W. (1982). Source mechanism of volcanic tremor. *J. Geophys. Res.* 87:8675-8683.
- Fischer T.P. et al. (1994). *Nature* 368: 135-137.
- Garcés, M. (2000). Theory of acoustic propagation in a multi-phase stratified liquid flowing within an elastic-walled conduit of varying cross-sectional area. *J. Volcanol. Geotherm. Res.* 101:1-17
- Garcés, M., S. Mc Nutt. (1997). Theory of the airborne sound field generated in a resonant magma conduit. *J. Volcanol. Geotherm. Res.* 78, 155-178.
- Gil-Cruz F., B. Chouet. (1997) Long-Period events, the most characteristic seismicity accompanying the emplacement and extrusion of a lava dome in Galeras Volcano, Colombia, in 1991. *J. Volcanol. Geotherm. Res.* 77: 121-128.
- Gil Cruz F., Meyer H. J., Chouet B. and Harlow D. (1987). Observations of long-period events at Nevado del Ruiz Volcano 1985-1986. *Hawaii symposium on How Volcanoes Work, Diamond Jubilee (1912-1987)*. Hawaiian Volcano Observatory, Hawaii, Abstr. Vol. p. 90.
- Hagerty, M., Schwartz, S.Y., Protti, M., Garcés, M., Dixon, T., (1997) Observations at Costa Rican volcano offer clues to causes of eruptions. *EOS Trans. Am Geophys. Union* 78 (49), 565-571.
- Hellweg, M. (2000). Physical models for the source of Lascar's harmonic tremor. *J.*

- Volcanol. Geotherm. Res. 101:183-198.
- Havskov, J., De la Cruz-Reyna, S., Singh, S.K., Medina, F., Gutierrez, C. (1983) Seismic activity related to the March-April, 1982 eruptions of el Chichon Volcano, Chiapas Mexico. *Geophys. Res. Lett.* 10:293-296.
- Hidayat D, Chouet BA, Voight B, Dawson P, Ratdomopurbo A (2001) Source mechanism of very-long-period signals accompanying dome growth activity at Merapi Volcano, Indonesia. *Geophys. Res. Lett.* submitted
- Julian, B. (1994). Volcanic tremor: nonlinear excitation by fluid flow. *J. Geophys. Res.* 99, 11859-11877.
- Kagiyama, T., Gyoda, N., Koyama, E., Tsuji, H. (1985). Geological meanings of minor eruptions of the volcano Asama and their precursory phenomena. In: Okada (Ed). Comparative studies of Physical Bachground of Volcanic Activity and its Relation to Eruption Disasters. Hokkaido Univ., 92-101.
- Kaneshima S., H. Kawakatsu, H. Matsubayashi, Y. Sudo, T. Tsutsui, T. Ohminato, H. Ito, K. Uhira, H. Yamasato, J.Oikawa, M Takeo and T. Iidaka. (1996). Mechanism of phreatic eruptions at Aso volcano inferred from near-field broadband seismic observations, *Science* 273, 642-645.
- Kawakatsu, H., S., T. Ohminato , H. Ito and Y. Kuwahara. (1992). Broadband seismic observation at Sakurajima Volcano, Japan. *Geophys. Res. Lett.* 19, 1959-1962.
- Kawakatsu H, Kaneshima S, Matsubayashi H, Ohminato T, Sudo Y, Tsutsui T, Uhira K, Yamasato H, Ito H, Legrand D (2000) Aso94: Aso seismic observation with broadband instruments. *J. Volcanol. Geotherm. Res.* 101:129-154
- Kawakatsu, H., S., T. Ohminato and H. Ito. (1994). 10s-Period volcanic tremors observed over a wide area in southwestern Japan, *Geophys. Res. Lett.* 21, 1963-1966.
- Koyanagi R. Y., Chouet B. and Aki K. (1987). Origin of volcanic tremor in Hawaii, Part I. Data from the Hawaiian Volcano Observatory 1969-1985. In R W Decker T L Wrigth and P H Stauffer (Eds), *Volcanism in Hawaii*. U. S. Geol. Surv. Prof. Paper. 1350: 1221-1257.
- Malone S. D. (1983). Volcanic earthquakes: Examples from Mt. St. Helens. In: Kanamori and Boschi (Eds.), *Earthquakes: Observations, Theory and Interpretation*. Elsevier, North-Holland, Amsterdam, 436-455.
- Lahr JC, Chouet BA, Stephens CD, Power JA, Page RA (1994) Earthquake classification, location, and error analysis in a volcanic environment: Implications for the magmatic system of the 1989-1990 eruptions at Redoubt Volcano, Alaska. *J. Volcanol. Geotherm. Res.* 62:137-151
- Lamb, H. (1932). *Hydrodynamics*, 6th ed. p582, Dover, New York.
- Legrand D, Kaneshima S, Kawakatsu H (2000) Moment tensor analysis of broadband waveforms observed at Aso Volcano, Japan. *J. Volcanol. Geotherm. Res.* 101: 155-169
- Lienert B., E. Berg and L. Frazer. (1986). HYPOCENTER an earthquake location method using centered, scaled and adaptively damped least squares. *Bull. Seism. Soc. Am.* 76, 771-783.
- Martinelli, B. (1990). Analysis of seismic patterns observed at Nevado del Ruiz, Colombia

- during August-September 1985. *J. Volcanol. Geotherm. Res.* 41:297-314
- Matsubayashi H.(1995). The source of the long period tremors and the very long-period events proceeding the mud eruption at Aso volcano, Japan. (in Japanese with English abstract), M.A. Thesis Tokyo Univ.
- Mc Nutt (1992). *Encyclopedia of Earth System Science*, Academic Press San Diego v. 4, p. 417-425.
- Minakami, t., (1974). Seismology of volcanoes in Japan. In: L.Civetta, P. Gasparini, G. Luongo and A. Rapolla (Eds). *Physical Volcanology*. Elsevier. Amsterdam-New York, 1-27.
- Mogi, K. (1958). Relations of the eruptions of various volcanoes and the deformations of the ground surfaces around them *Bull. Earthquake Res. Inst. Tokyo Univ.* 36, 99-134.
- Morrissey M., and B. Chouet. (1997) A numerical investigation of choked flow dynamics and its application to the triggering mechanism of long-period events at Redoubt Volcano, Alaska. *J. Geophys. Res.* 102, 7965-7983.
- Neuberg, J., R. Luckett, M. Ripepe and T. Braun. (1994). Highlights from a seismic broadband array on Stromboli volcano. *Geophys. Res. Lett.* 21, 749-752.
- Ohminato, T. and D. Eridato. (1997). Broadband seismic observations at Satsuma-Iwojima volcano, Japan. *Geophys. Res. Lett.* 24, 2845-2848.
- Ohminato T. and B. A. Chouet. (1997). A free-surface boundary condition for including 3D topography in the finite difference method. *Bull. Seism. Soc. Am.* 87, 494-515.
- Ohminato T. Broadband analysis of seismic signals observed in and around active volcanoes. (1998) Ph D Thesis, Geological Survey of Japan, Tsukuba, Japan.
- Ohminato T., B. A. Chouet, P. Dawson and S Kedar. (1998). Waveform inversion of very long period impulsive signals associated with magmatic injection beneath Kilauea Volcano, Hawaii. *J. Geophys. Res.* 103, 23,839-23,862.
- Okada, H., Nishimura, Y., Miyamachi, H., Mori, H., Ishihara, K. (1990). Geophysical significance of the 1988-1089 explosive eruptions of Mt Tokachi, Hokkaido, Japan. *Bull. Volcanol. Soc. Jap.*, Ser. 2, 35:175-203.
- Power, J., Lahr, J.C., Page, R.A., Chouet, B.A., Stephens, C.D., Harlow, D.H., Murray, T.L., Davies, J.N. (1994). Seismic evolution of the 1989-1990 eruption sequence of Redoubt Volcano, Alaska. *J. Volcanol. Geotherm. Res.* 62:69-94.
- Pinatubo Volcano Observatory Team (1991). Lessons from major eruption Mt. Pinatubo Philippines. *EOS, Trans. Am. Geophys. Un.* 72: 545-555.
- Pitt A.M., Hill, D.P. (1994). Long-period earthquakes in the Long Valley Caldera Region, Eastern California. *Geophys. Res. Lett.* 21: 1679-1682.
- Rowe, C. A., R. C. Aster, P. R. Kyle, J. W. Schlue, and R. R. Dibble, (1998). Broadband recording of Strombolian explosions and associated very-long-period seismic signals on Mount Erebus Volcano, Ross Island, Antarctica, *Geophys. Res. Lett.* , 25:2297-2300.
- Rowe C.A, Aster R.C, Kyle P.R, Schlue J.W, Dibble, R.R (2000). Seismic and acoustic observations at Mount Erebus Volcano, Ross Island, Antarctica, 1994-1998. *J. Volcanol.*

- Geotherm. Res. 101:105-128.
- Sassa, K., (1935). Volcanic micro-tremors and eruption-earthquakes. *Mem. Coll. Sci. Kyoto Univ.*, series A 18,225-293.
- Siebe C., M. Abrams, J.L. Macias, J. Obenholzner. (1996). Repeated volcanic disasters in Prehispanic time at Popocatepetl central Mexico; Past key to the future ?. *Geology*, 24:399-402.
- Seidl D., Schick R. and Riuscetti M. (1981). Volcanic tremors at Mt. Etna: A model for hidraulic origin. *Bull. Volcanol.* 44: 43-56.
- Shaw H. R., Chouet B. (1991). Fractal hierarchies of magma transport in Hawaii and critical self-organization of tremor. *J. Geophys. Res.* 96: 10191-10207.
- Shimozuru, D., Kagiyama, T., (1989) Some significant features of pre-eruption volcanicn earthquakes. In: J.H. Latter (ed) Volcanicn Hazards, IAVCEI Proc. in Volcanology, Springer-Verlag, Berlin, 1:504-512
- St Lawrence W., Qamar A. (1979). Hydraulic transients; a seismic source in volcanoes and glaciers. *Science* 203: 654-656.
- Swanson D.A., Casadevall, T.J., Dzurisin, D., Holcomb, R.T., Newhall, C.G., Malone, S.D. Weaver C.S. (1985) Forecasts and predictions of eruptive activity at Mount St Helens, USA: 1975-1984. *J.Geodyn.*, 3:397-423.
- Uhira, K., M. Takeo. The source of explosive eruptions at Sakurajima Volcano, Japan, *J. Geophys. Res.* , 99, 17,775-17,789, 1994.
- Usu Volcano Observatory, 19888. Observational report on the volcanic activities of Hakkaido (October 1987-April 1988). Committee on Prediction of volcanic Erup- tions, 41:64-77. Volcano, Japan, *J. Geophys. Res.* , 99, 17,775-17,789, 1994.
- Wegler U and Seidl D. (1997). Kinematic parameters of tremor wave field at Mt Etna (Sicily). *Geophys. Res. Lett.* 24: 759-762.
- Weaver, C.S., Grant, W.C., Malone, S.D., Endo, E.T., (1981). Post-May 18 seismicity: Volcanic and tectonic implications. The 1980 Eruptions of Mount St Helens. *U.S. Geological Surv. Prof Pap.*, 1250:109-121.
- Wolfe and Hoblitt. An overview. In: C.G.Newhall and R.S. Punongbayan (eds) Fire and Mud eruptions and lahars of Mount Pinatubo, Phillipines. *University of Washington Press*, p1126, 1996.
- Wooding, R.A., (1960). Inestability of a visous liquid of variable density in a vertical Hele-shaw cell, *J. Fluid Mech.*, 7:501-515.
- Yamamoto, M., H. Kawakatsu, S. Kaneshima, T. Mori, T. Tsutsui, Y Sudo, Y Morita. (1999). Detection of a crack-like conduit beneath the active crater at Aso volcano, Japan. *Geophys. Res. Lett.* 24:3677-3680.